NOVEMBER 2019 Ph.D. in Mechanical Engineering HATEM HASAN ISMAEEL

REPUBLIC OF TURKEY
GAZİANTEP UNIVERSITY
GRADUATE SCHOOL OF NATURAL & APPLIED SCIENCES

INVESTIGATION OF THERMAL PERFORMANCE OF A SOLAR-ASSISTED HEAT PUMP DRYING SYSTEM WITH UNDERGROUND THERMAL ENERGY STORAGE TANK AND HEAT RECOVERY UNIT

Ph.D. THESIS
IN
MECHANICAL ENGINEERING

BY
HATEM HASAN ISMAEEL
NOVEMBER 2019

INVESTIGATION OF THERMAL PERFORMANCE OF A SOLAR-ASSISTED HEAT PUMP DRYING SYSTEM WITH UNDERGROUND THERMAL ENERGY STORAGE TANK AND HEAT RECOVERY UNIT

Ph.D. Thesis
in
Mechanical Engineering
Gaziantep University

Supervisor
Prof. Dr. Recep YUMRUTAŞ

by
Hatem Hasan ISMAEEL
November 2019

REPUBLIC OF TURKEY
UNIVERSITY OF GANITEP
GRADUATE SCHOOL OF NATURAL & APPLIED SCIENCES
MECHANICAL ENGINEERING DEPARTMENT

Name of the thesis: Investigation of Thermal Performance of a Solar-Assisted Heat Pump Drying System with Underground Thermal Energy Storage Tank and Heat Recovery Unit

Name of the student: Hatem Hasan ISMAEEL

Exam date: 20.11.2019

Approval of the Graduate School of Natural and Applied Sciences

Prof. Dr. Ahmet Necmeddin YAZICI
Director

I certify that this thesis satisfies all the requirements as a thesis for the degree of Doctor of Philosophy.

Prof. Dr. Melda ÇARPINLIOĞLU
Head of Department

This is to certify that we have read this thesis and that in our consensus/majority opinion it is fully adequate, in scope and quality, as a thesis for the degree of Doctor of Philosophy.

Prof. Dr. Recep YUMRUTAŞ
Supervisor

Examining Committee Members:	Signature
Prof. Dr. Hüsamettin BULUT	....
Prof. Dr. Mehmet Sait SÖYLEMEZ	....
Prof. Dr. Recep YUMRUTAŞ	....
Assoc. Prof. Dr. Önder KAŞKA	....
Assoc. Prof. Dr. Adem ATMACA	....

I hereby declare that all information in this document has been obtained and presented in accordance with academic rules and ethical conduct. I also declare that, as required by these rules and conduct, I have fully cited and referenced all material and results that are not original to this work.

Hatem Hasan ISMAEEL

ABSTRACT

INVESTIGATION OF THERMAL PERFORMANCE OF A SOLAR-ASSISTED HEAT PUMP DRYING SYSTEM WITH UNDERGROUND THERMAL ENERGY STORAGE TANK AND HEAT RECOVERY UNIT

ISMAEEL, Hatem Hasan
Ph.D. in Mechanical Engineering
Supervisor: Prof. Dr. Recep YUMRUTAŞ
November 2019
174 pages

The conventional drying systems in the industrial applications have been used for decades, and consumed a great amount of energy. Since these systems have not been operated efficiently, they have lost great deal of energy, and cause environmental pollution. Therefore, innovative, efficient and environment friendly drying systems need to be developed and operated in these days. In this study, theoretical models for a Solar-Assisted Heat Pump (SAHP) drying system including underground Thermal Energy Storage (TES) tank with and without using Heat Recovery Unit (HRU) are developed, and thermal performance parameters for the drying systems are investigated. Two different analytical models are developed to find the thermal performance parameters for the drying system. In the first model, transient heat transfer problem around the TES tank is solved by using Duhamel's superposition and similarity transformation techniques to find hourly temperature variation of water in the TES tank and the other performance parameters. In the second model, the unsteady heat transfer problem for the TES tank is solved applying Complex Finite Fourier Transform (CFFT) Technique to find monthly periodic store temperature and the other performance parameters. These parameters are Coefficients of Performances for the heat pump (COP) and system (COPs), Specific Moisture Evaporation Rate (SMER), annual variation of water temperature in the TES tank, energy fractions for energy charging, and extraction from the system. MATLAB programs have been generated to build new models for the drying system. For the SAHP drying system with TES using the first model, when wheat mass flow rate and Carnot efficiency are selected as 50 kg/h and 40% respectively, the values of collector area, TES tank volume, COP, COPs and SMER are obtained as 70 m^2, 300 m^3, 4.2, 4.1 and 6 respectively when the system attains periodic operation time in fifth year. For SAHP drying system with TES tank and HRU using the first model, the results for COP, COPs and SMER are 5.55, 5.28 and 9.25 respectively, by using wheat mass flow rate of 100 kg/h, Carnot Efficiency (CE) for heat pump of 40%, collector area of 100 m^2 and TES tank volume of 300 m^3 when the system attains periodic operation duration from the fifth year onwards for ten selected years of operation. Annual energy saving is calculated to be 21.4% in comparison with the same system without using HRU for the same input data. For SAHP drying system including TES with and without HRU using the second model, the results reveal that moisture contents in wheat at initial and final states, and wheat mass flow rate have great effects on system performance parameters. Results also indicate that using of HRU increases the system performance parameters.

Key Words: Heat Pump Drying, Energy Storage, Solar Energy, Heat Recovery

ÖZET

YERALTI ENERJİ DEPOLU ISI GERİ KAZANIMLI VE GÜNEŞ ENERJİSİ DESTEKLİ ISI POMPALI KURUTMA SİSTEMİNİN PERFORMANSININ İNCELENMESİ

ISMAEEL, Hatem Hasan
Doktora Tezi, Makine Mühendisliği
Danışman: Prof. Dr. Recep YUMRUTAŞ
Kasım 2019
174 sayfa

Endüstriyel uygulamalardaki geleneksel kurutma sistemleri, onlarca yıldır kullanılmakta ve büyük miktarda enerji tüketmektedirler. Bu sistemler verimli bir şekilde çalıştırılamadığından, çok fazla enerji kaybedilmekte ve çevre kirliliği arttırılmaktadırlar. Bu nedenle, günümüzde yenilikçi ve çevre dostu kurutma sistemlerinin geliştirilmesi ve işletilmesi gerekmektedir. Bu çalışmada, ısı geri kazanım üniteli (HRU) ve ünitesiz, yeraltı ısıl enerji (TES) depolu ve Güneş Enerjisi destekli bir Isı Pompası (SAHP) ile kurutma sisteminin teorik modelleri geliştirilmiş ve kurutma sisteminin ısıl performans parametreleri incelenmiştir. SAHP kurutma sistemi; bir kurutma ünitesi, bir ısı pompası, düz plakalı güneş kollektörleri, bir yeraltı TES tankı ve bir HRU'dan oluşmaktadır. Kurutma sisteminin ısıl performans parametrelerini bulmak için iki farklı analitik model geliştirilmiştir. İlk modelde, TES tankındaki bulunan su sıcaklığı ile diğer performans parametrelerinin saatlik değişimini bulmak için, TES tankı etrafındaki geçici rejim ısı transferi problemi Duhamel'in süperpozisyon ve benzerlik dönüşüm teknikleri uygulanarak çözülmüştür. İkinci modelde ise, aylık periyodik depo sıcaklığı ve diğer performans parametrelerini bulmak için, TES tankı için kararsız ısı transferi problemi Karmaşık Sonlu Fourier Dönüşümü (CFFT) Tekniği uygulanarak çözülmüştür. Bu parametreler; ısı pompası (COP) ve sistem (COPs) için Performans Katsayıları, Özgül Nem Buharlaşma Oranı (SMER), TES tankındaki yıllık su sıcaklığının değişimi, sisteme aktarılan enerji oranları ile sistemden çekilen enerji oranlarıdır. Kurutma sistemi için geliştirilen modeller kullanılarak MATLAB programları hazırlanmıştır. İlk modeli kullanan TES'li SAHP kurutma sistemi için buğdayın kütlesel debisi ve Carnot verimi sırasıyla 50 kg/h ve % 40 olarak seçildiğinde, sistem beşinci yılda periyodik çalışma süresine ulaştığında kollektör alanı, TES tank hacmi, COP, COPs ve SMER değerleri sırasıyla 70 m^2, 300 m^3, 4.2, 4.1 ve 6 olarak elde edilmiştir. Yıllık enerji tasarrufu, aynı girdiler için HRU kullanmadan aynı sistemle karşılaştırıldığında % 21.4'tür. İkinci modeli kullanan HRU içeren ve içermeyen, TES tankı içeren SAHP kurutma sistemi için, sonuçlar buğdayda ilk ve son durumlardaki nem içeriğinin, buğdayın kütlesel debisinin sistem performans parametreleri üzerindeki etkilerinin yüksek olduğu ortaya çıkmaktadır. Sonuçlar ayrıca, HRU kullanımının sistem performans parametrelerini arttırdığını göstermektedir.

Anahtar Kelimeler: Isı Pompalı Kurutma, Enerji Depolama, Güneş Enerjisi, Isı Geri Kazanımı

I dedicate this thesis to

My Parents, my lovely wife Shaymaa,

My daughters Lana and Suma, and my son Ammar,

ACKNOWLEDGEMENTS

I would like to express my deepest gratitude to my supervisor Prof. Dr. Recep YUMRUTAŞ for his guidance, advice, criticism, encouragements and insight throughout the research. I am very grateful to him for his scientific advice and many insightful discussions and suggestions.

I would also like to thank my PhD Advisory Committee members, Prof. Dr. M. Sait SÖYLEMEZ and Prof. Dr. Hüsamettin BULUT for their continuous guidance and support.

I would like to express the highest appreciation to Duhok Polytechnic University and Bardarash Technical Institute for giving me the opportunity to complete my PhD study.

I would like to thank my mother, my wife, my daughters Lana and Suma, my son Ammar, my sisters, brothers, and everyone else for their endless support.

Finally, I would like to thank those who took part in the completion of this thesis.

TABLE OF CONTENTS

LIST OF TABLES

Page

LIST OF FIGURES

Page

LIST OF SYMBOLS

$\mathbf{A}$	tank surface area (m^2)
$\mathbf{A_i}$	inside heat transfer area for condenser (m^2)
$\mathbf{A_o}$	outside heat transfer area for condenser (m^2)
$\mathbf{A_f}$	fin area (m^2)
$\boldsymbol{A_{desup}}$	desuperheated heat transfer area for condenser (m^2)
$\boldsymbol{A_{cond}}$	condensation heat transfer area for condenser (m^2)
$\boldsymbol{A_c}$	free flow area (m^2)
$\boldsymbol{A_{col}}$	collector area (m^2)
$\boldsymbol{A_{fr}}$	front area (m^2)
$\mathbf{c}$	specific heat of earth (kJ kg^{-1} K^{-1})
$\mathbf{c_{pa}}$	specific heat of air (kJ kg^{-1} K^{-1})
$\mathbf{c_w}$	specific heat of water (kJ kg^{-1} K^{-1})
$\boldsymbol{C_{p_{wheat}}}$	specific heat of wheat (kJ kg^{-1} K^{-1})
$\boldsymbol{D_i}$	inside tube diameter for condenser (m)
$\boldsymbol{D_o}$	outside tube diameter for condenser (m)
$\boldsymbol{D_h}$	hydraulic diameter (m)
$\mathbf{E_S}$	energy saving by HRU (%)
$\boldsymbol{f}$	friction factor
$\mathbf{G}$	mass velocity for air across condenser (kg m^{-2} s^{-1})
$\mathbf{h}$	specific enthalpy of the moist air (kj kg^{-1})
$\mathbf{h_g}$	specific enthalpy of saturated water vapor (kj kg^{-1})
$\mathbf{h_a}$	specific enthalpy of dry air at the mixture temperature (kj kg^{-1})
$\mathbf{h_{fg}}$	latent heat of vaporization of water at the average temperature (kj kg^{-1})
$\boldsymbol{h_{p_4}}$	specific enthalpy of dry wheat pre drying for 1st case (kj kg^{-1})
$\boldsymbol{h_{p_5}}$	specific enthalpy of dry wheat after drying for 2nd case (kj kg^{-1})
$\boldsymbol{h_{p_5}}$	specific enthalpy of dry wheat pre drying for 1st case (kj kg^{-1})
$\boldsymbol{h_{p_6}}$	specific enthalpy of dry wheat after drying for 2nd case (kj kg^{-1})
$\boldsymbol{h_i}$	heat transfer coefficient of refrigerant side for condenser (W m^2 K^{-1})

$\boldsymbol{h_o}$	heat transfer coefficients of air side for condenser (W m^2 K^{-1})
$\mathbf{I_T}$	hourly solar radiation on tilted surface (W m^{-2})
I	hourly solar radiation on horizontal surface (W m^{-2})
$\mathbf{j_H}$	Colburn factor
$\boldsymbol{k_a}$	thermal conductivity for air (W m^{-1} K^{-1})
$\boldsymbol{k_w}$	thermal conductivity of tube wall for condenser (W m^{-1} K^{-1})
$\boldsymbol{k_f}$	fin conductivity (W m^{-1} K^{-1})
k	thermal conductivity of earth (W m^{-1} K^{-1})
$\boldsymbol{K_L}$	thermal conductivity of saturated liquid of refrigerant (W m^{-1} K^{-1})
$\mathbf{K_T}$	hourly clearness index
$\boldsymbol{l}$	length of fin (m)
$\mathbf{\dot{m}_a}$	mass flow rate of dry air (kg s^{-1})
$\mathbf{\dot{m}_w}$	amount of evaporated water from moist wheat (kg s^{-1})
$\mathbf{\dot{m}_{w_4}}$	mass flow rate of water in the product pre-drying for 1st case (kg s^{-1})
$\boldsymbol{\dot{m}_{w_5}}$	mass flow rate of water in the product after drying for 1nd case (kg s^{-1})
$\mathbf{\dot{m}_{w_5}}$	mass flow rate of water in the product pre-drying for 2st case (kg s^{-1})
$\boldsymbol{\dot{m}_{w_6}}$	mass flow rate of water in the product after drying for 2nd case (kg s^{-1})
$\boldsymbol{\dot{m}_p}$	mass flow rate of dry wheat (kg s^{-1})
$\boldsymbol{\dot{m}}$	equivalent mass velocity for two phase of refrigerant (kg m^{-2})
$\mathbf{\dot{M}}$	mass flow rate of the refrigerant (kg s^{-1})
$\mathbf{M_p}$	moisture content of wheat on a dry basis (kg water kg^{-1} solid)
$\boldsymbol{MC_4}$	moisture content pre drying for 1st case (%)
$\boldsymbol{MC_5}$	moisture content after drying for 1st case (%)
$\boldsymbol{MC_5}$	moisture content pre drying for 2st case (%)
$\boldsymbol{MC_6}$	moisture content after drying for 2st case (%)
$\boldsymbol{Nu_D}$	Nusselt number for refrigerant in superheated region
$\boldsymbol{Nu_a}$	Nusselt number for air
P	dimensionless, $P = \frac{\rho_w\, c_w}{3\rho\, c}$
$\boldsymbol{Pr}$	Prandtl number for refrigerant in desuperheated region
$\boldsymbol{Pr_a}$	Prandtl number for air
$\boldsymbol{Pr_L}$	Prandtl number for saturated liquid of refrigerant
q	dimensionless heat transfer to the tank

$\boldsymbol{Q}$	heat transfer to the tank (W)
$\dot{\mathbf{Q}}_{\mathbf{max}}$	maximum possible heat transfer rate for HRU (W)
$\dot{\mathbf{Q}}_{\mathbf{R}}$	recovered heat by HRU for 2nd case (W)
$\dot{\boldsymbol{Q}}_{\boldsymbol{H}}$	condenser heating load (W)
$\dot{\boldsymbol{Q}}_{\boldsymbol{evap}}$	latent heat of evaporation water from moist wheat (W)
$\dot{\mathbf{Q}}_{\mathbf{u}}$	solar energy rate (W)
$\dot{\mathbf{Q}}_{\mathbf{T}}$	The total heat transfer rate for 2nd case (W)
$\boldsymbol{q}_{\boldsymbol{u}}$	dimensionless useful solar energy charge rate to the tank, $q_u = \frac{\dot{Q}_u}{4\pi RKT_\infty}$
$\boldsymbol{q}_{\boldsymbol{H}}$	dimensionless condenser heat load, $q_H = \frac{\dot{Q}_H}{4\pi RKT_\infty}$
$\mathbf{r}$	radial distance from the tank centre (m)
$\mathbf{R}$	tank radius (m)
r_i	inside tube radius for condenser tubes (m)
$\boldsymbol{r}_{\boldsymbol{o}}$	outside tube radius for condenser tubes (m)
$\boldsymbol{Re}_{\boldsymbol{D}}$	Reynolds number for refrigerant in desuperheated region
$\mathbf{Re}_{\mathbf{a}}$	Reynolds number for air
$\boldsymbol{Re}_{\boldsymbol{e}}$	equivalent Reynolds number for two-phase flow of refrigerant
$\mathbf{r}_{\mathbf{h}}$	hydraulic radius for condenser (m)
$\mathbf{t}$	time (s)
$\mathbf{T}$	earth temperature (K)
$\mathbf{T}_{\mathbf{1}}$	condenser inlet temperature for 2nd case (K)
$\mathbf{T}_{\mathbf{2}}$	air temperature pre drying (K)
$\mathbf{T}_{\mathbf{3}}$	air temperature after drying (K)
$\mathbf{T}_{\mathbf{4}}$	wheat temperature pre drying for 1st case (K)
$\mathbf{T}_{\mathbf{4}}$	leaving air temperature from HRU for 2st case (K)
$\mathbf{T}_{\mathbf{5}}$	wheat temperature after drying for 1st case (K)
$\mathbf{T}_{\mathbf{5}}$	wheat temperature pre drying for 2st case (K)
$\mathbf{T}_{\mathbf{6}}$	wheat temperature after drying for 2st case (K)
$\mathbf{T}_{\mathbf{a}}$	ambient air temperature (K)
$\mathbf{T}_{\mathbf{o}}$	outside design air temperature (K)
$\mathbf{T}_{\mathbf{mo}}$	dry bulb temperature of moist air (K)
$\mathbf{T}_{\mathbf{w}}$	water temperature in the tank (K)
$\mathbf{T}_{\mathbf{wb,2}}$	wet bulb temperature in state 2 for 2nd case (K)

$\mathbf{T_{wb,3}}$ wet bulb temperature in state 3 for 2nd case (K)

$\mathbf{T_c}$ average temperature of air pre and after condenser (K)

$\mathbf{T_\infty}$ deep ground temperature (K)

u dimensionless parameter for design condition ,$(UA)_{he}/\dot{m}_a C_{p_a}$

$\mathbf{(UA)_{he}}$ product of heat transfer coefficient and area for heat pump condenser ($W\ K^{-1}$)

$\mathbf{U_o}$ overall heat transfer coefficient based on outside area of condenser ($Wm^{-2}\ K^{-1}$)

V volume of the tank (m^3)

$\dot{V}_a$ volume flow rate for air ($m^3\ kg^{-1}$)

V_{max} maximum velocity of air in free flow area ($m\ s^{-1}$)

V_{fr} front velocity of air in frontal area of condenser ($m\ s^{-1}$)

w dimensionless compressor work

$\dot{\mathbf{W}}_\mathbf{c}$ compressor input power (W)

$\dot{\mathbf{W}}_\mathbf{f}$ fan input power (W)

w_1 hour angle of the midpoint of the hour

$\mathbf{W_4}$ weight of wheat pre-drying for 1st case ($kg\ h^{-1}$)

$\mathbf{W_5}$ weight of wheat after drying ($kg\ h^{-1}$) for 1st case

$\mathbf{W_5}$ weight of wheat pre-drying for 2st case ($kg\ h^{-1}$)

$\mathbf{W_6}$ weight of wheat after drying ($kg\ h^{-1}$) for 2st case

x_v vapor quality for refrigerant

Greek letters

$\boldsymbol{\alpha}$ thermal diffusivity of earth ($m^2\ s^{-1}$)

$\boldsymbol{\varepsilon}$ effectiveness

$\boldsymbol{\eta_c}$ Carnot efficiency

$\boldsymbol{\eta_o}$ overall surface effectiveness (air side only) for the condenser

$\boldsymbol{\eta_f}$ fin efficiency

$\boldsymbol{\eta_{fc}}$ flat plate solar collector efficiency

$\emptyset$ latitude

$\boldsymbol{\beta}$ surface sloped (degree)

$\boldsymbol{\phi}$ dimensionless temperature for earth, $\frac{T-T_\infty}{T_\infty}$

$\boldsymbol{\phi_a}$ dimensionless ambient air temperature, $\frac{T_a-T_\infty}{T_\infty}$

$\boldsymbol{\phi_c}$ dimensionless average temperature for air pre and after condenser, $\frac{T_c - T_\infty}{T_\infty}$

$\boldsymbol{\phi_w}$ dimensionless water temperature in the tank, $\frac{T_w - T_\infty}{T_\infty}$

$\boldsymbol{\phi_1}$ dimensionless condenser inlet air temperature

$\boldsymbol{\phi_2}$ dimensionless air supply temperature pre-dryer, $\frac{T_2 - T_\infty}{T_\infty}$

$\boldsymbol{\varphi_3}$ relative humidity at state 3 for 2nd case

$\boldsymbol{\gamma}$ dimensionless parameter, $4\pi Rk/\dot{m}_a C_{p_a}$

$\boldsymbol{\rho_a}$ air density in air side of condenser (kg m^{-3})

$\boldsymbol{\rho}$ density of refrigerant in desuperheated region (kg m^{-3})

$\boldsymbol{\rho_w}$ water density (kg m^{-3})

$\boldsymbol{\rho_L}$ density of saturated liquid for refrigerant (kg m^{-3})

$\boldsymbol{\rho_G}$ density of saturated vapor for refrigerant (kg m^{-3})

$\boldsymbol{\tau}$ dimensionless time, $\tau = \frac{\alpha t}{R^2}$

$\boldsymbol{\Delta p}$ pressure drop of air across condenser (Pa)

$\boldsymbol{\Delta T_{ln}}$ log mean temperature difference (K)

$\boldsymbol{\sigma}$ free flow area/frontal area for condenser ($A_c\ A_{fr}^{-1}$)

$\boldsymbol{\mu_a}$ air viscosity (Pa. s)

$\boldsymbol{f}$ friction factor

$\boldsymbol{f_{cf}}$ parameter estimated from a figure

$\boldsymbol{v_1}$ specific volume for air pre-condenser ($m^3\ kg^{-1}$)

$\boldsymbol{v_2}$ specific volume for air after condenser ($m^3\ kg^{-1}$)

$\boldsymbol{v_m}$ average specific volume for air ($m^3\ kg^{-1}$)

$\boldsymbol{\omega}$ humidity ratio for moist air (kg water kg^{-1} dry air)

$\boldsymbol{\omega_2}$ humidity ratio for moist air pre drying process (kg water kg^{-1} dry air)

$\boldsymbol{\omega_3}$ humidity ratio for moist air after drying process (kg water kg^{-1} dry air)

$\boldsymbol{\delta_f}$ fin thickness (m)

$\boldsymbol{\delta}$ declination

LIST OF ABREVIATIONS

COP Coefficient Of Performance of heat pump

COPs Coefficient Of Performance of whole system

CE Carnot Efficiency

GSHP Ground Source Heat Pump

HPD Heat Pump Drying

HRU Heat Recovery Unit

HPD Heat Pump Drying

SMER Specific Moisture Evaporation Rate (kg kW^{-1} h^{-1})

SAHP Solar-Assisted Heat Pump

TES Thermal Energy Storage

CFFT Complex Finite Fourier Transform

CHAPTER 1

INTRODUCTION

Drying is commonly used for different purposes, like food and wood drying. In drying, heat and moisture transfer occur simultaneously. Various engineering domains rely on mass and heat transfer through the usage of different heat transfer media [1]. The drying process in the industrial applications consumes a great amount of energy. Drying of grains is a commonly known heat and mass transfer application. Grains have become a basic source of human food. This fact let researchers to be heavily oriented toward drying grains in order to preserve them for long periods. Grains can be divided into three groups; pulses, oil seeds and cereals, including wheat [2]. Due to the increased demand on wheat, it should be preserved throughout the year. There are many factors that contribute in preserving wheat for a long term such as maintaining the moisture content and the temperature of the crop in a convenient climate. The high moisture content and temperature encourage fungal and insect problems, respiration and germination. Therefore, reducing the harvest storage temperature and moisture eventually reduces the likelihood of respiration. The high temperatures of grains must be accompanied by reduced moisture content [2].

Decreasing moisture levels within stored crops is a requirement, and is attainable via drying processes [3]. A drying system can be designed for drying of the fresh and cooked wheat to secure continued production. In recent decades, the heat pump system has been used for drying applications because it is more efficient than the conventional drying systems. The main reasons for using Heat Pump Drying (HPD) system are the ability to control air humidity, drying temperature, and the potential of energy saving [4]. Energy saving by using HPD system reaches 40% in comparison with using the electrical heater dryers [5-6]. The drying efficiency may be enhanced by incorporating heat pump to a conventional hot air drying system [7]. The biggest amount gross energy (>60%) required for farm corn production goes to the drying process [8]. Drying consumes 9–25% of the overall energy in the industrial nations [9]. There are many kinds of HPD systems that are used for food or agricultural products drying.

Combining other mechanisms with HPD system has been investigated by many researchers, which includes solar-assisted heat pump dryer [10-13], air source heat pump dryer [14-15], ground source heat pump dryer [16-18], heat pump assisted (hybrid) microwave drying [19-21], chemical heat pump dryer [22], and other hybrid HPD systems [23-30].

A comparative review of HPD with other commonly used dryers as in Table 1.1 gives a clear indication of the validity, preference, and high efficiency of HPD used among all types. HPD can be classified into four main types, as in Figure 1.1.

Table 1.1 Comparison of HPD with other commonly used dryers [31].

Item	HPD	Hot air drying	Vacuum drying	Freeze drying
SMER (kg/kwh)	1.0-4.0	0.1-1.3	0.7-1.2	0.4 and lower
Operating temperature range (°C)	-10 to 80	40 to very high	30-60	-35 to >50
Operating % RH range	10-80	Varies depending on temperature	Low	Low
Drying efficiency (%)	Up to 95	35-40	Up to 70	Very low
Drying rate	Faster	Average	Very slow	Very slow
Capital cost	Moderate	Low	High	Very high
Running cost	Low	High	Very high	Very high
Control	Very good	Moderate	Good	Good

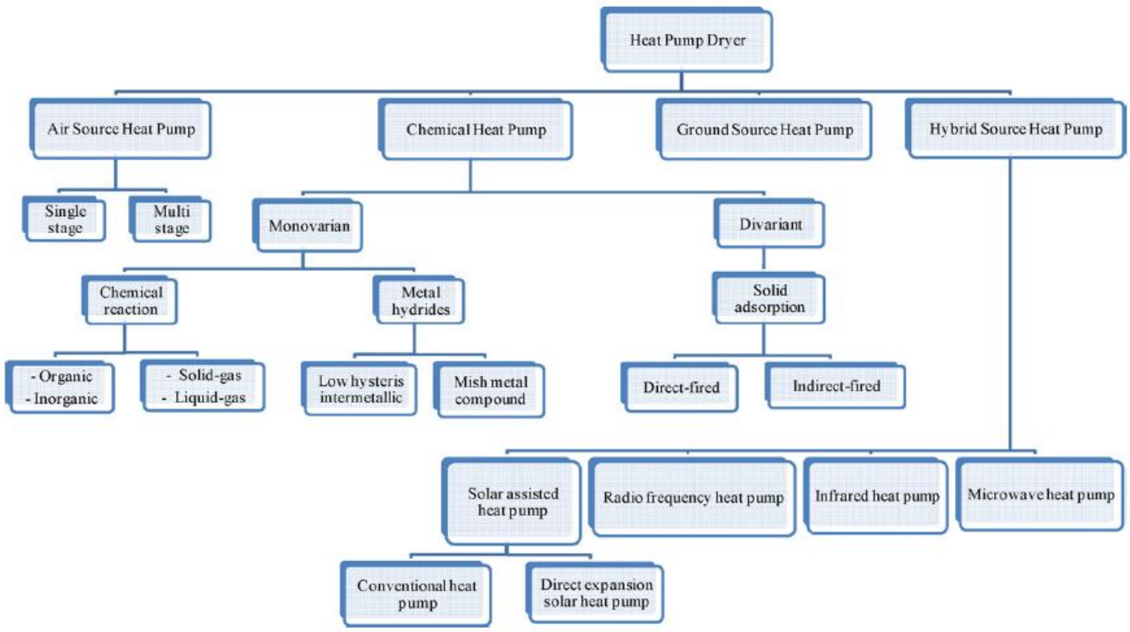

Figure 1.1 Classification of heat pump dryers [32, 33].

Systems that are more efficient in drying compared to conventional ones should be used to save energy and decrease pollution. Solar-Assisted Heat Pump (SAHP) drying systems are a more efficient drying system than the conventional drying systems. When both solar energy and heat pump are employed for food drying, performance of the system will be higher than the conventional drying systems. Underground TES application can be used to store energy acquired from the flat plate solar collectors. The utilization of the stored energy by the heat pump in drying applications should be considered a priority due to fluctuation of fossil fuels prices, environmental impacts, and anticipated depletion of conventional fossil fuels. Application of the SAHP drying system by storing of solar energy during the whole year in the form of thermal energy makes a greater system thermal performance than the other types of the systems.

Due to the multiple advantages of the proposed dryer system, a theoretical model for SAHP drying system with TES tank is developed in the first part of this study. The drying system is considered to work during the whole year. The ambient air temperature and useful solar energy will decline, especially in winter, then waste heat from the drying unit will increase and system performance go down; therefore a Heat Recovery Unit (HRU) is proposed to recover the waste heat from the dryer unit, especially throughout winter. Accordingly, a theoretical model for SAHP drying system with TES tank and HRU is developed as well, in the second and fourth cases of this study. The SAHP drying system considered in this study is an environmently friendly system.

The SAHP drying system comprises of a drying unit, solar collectors, a heat pump and a spherically-shaped underground TES tank with and without using HRU. Thermal analysis for all components of the drying system is obtained, and they are combined with each other to obtain a mathematical model for the new drying system with and without using HRU. A program prepared in MATLAB is executed by using different input data to find performance parameters for the drying system using multiple expressions for the components of the drying system. These parameters are water temperature in TES tank, Coefficient of Performance of the heat pump (COP) and system (COPs), Specific Moisture Evaporation Rate (SMER) and energy fractions. The input data that is used in the simulation model analysis are; wheat mass flow rate, Carnot efficiency, collector area, TES tank volume, and others.

The purposes of this study are:

- To find a mathematical model for SAHP drying system including spherical TES tank with and without HRU. Unsteady (hourly) heat transfer problem for TES tank is solved by applying Duhamel’s superposition and similarity transformation techniques. The model is obtained using energy expressions for each component of the drying system. The model is written in MATLAB program to find performance parameters and periodic operation situation of SAHP drying system for 10 years of operation.

- Unsteady (monthly) heat transfer problem for the tank is solved using Complex Finite Fourier Transform (CFFT) Technique. This model is obtained using energy expressions for each component of the drying system and written in MATLAB program to find performance parameters for periodic operation directly.

This thesis comprises of **eight chapters** which are arranged as follows:

In chapter two, comprehensive literature review of the research topic is summarized.

In chapter three, an analytical modeling procedure for SAHP drying system utilizing spherical TES tank with or without HRU is presented. The problem formulation consisting of a differential equation, boundary conditions and energy balance for the spherical storage is solved by applying similarity transformation and Duhamel's superposition techniques. Then the hourly water temperature in the tank after expression derivations of heat pump, drying unit, flat plate solar collectors, and HRU is solved.

In chapter four, an analytical modeling procedure is presented for predicting the periodic operation performance of SAHP drying system utilizing a spherical annual underground TES tank. The problem formulation consisting of a differential equation, boundary conditions and energy balance for the spherical storage is put into dimensionless form through incorporating dimensionless variables. Complex Finite Fourier Transform is applied to the dimensionless form of the problem, and the problem is solved assuming monthly heat input rates to the storage. By estimating the solar energy collection, the monthly solar heat gains by collectors is obtained using utizibility method $\bar{\phi}$.

In chapter five, validation results of SAHP drying system with TES tank for space heating application in the literature are presented in two sections. The first section is concerned with the validation results of the analysis employing SAHP drying system and spherical TES tank for space heating using Duhamel's superposition and similarity transformation techniques for TES tank for a study in literature. While the second section is concerned with the results of the analysis using Complex Finite Fourier

Transform (CFFT) Technique and the utizibility method, $\overline{\phi}$, to find monthly solar heat gains by flat plate solar collectors for another study in the literature.

Computational procedures for all parts of this study are performed in **chapter six**. Firstly, the procedures for mathematical modeling and thermal performance of SAHP drying system including TES tank with and without HRU using Duhamel's superposition and similarity transformation techniques are presented in two sections. Next, the same procedures for the SAHP drying system including TES tank with and without HRU are presented using Complex Finite Fourier Transform (CFFT) Technique and the utizibility method $\overline{\phi}$.

In chapter seven, results and discussions of this study are presented in four sections. The results and discussions of modeling and thermal performance of SAHP drying system including spherical TES tank with and without HRU using the models presented in chapter three are inserted in the first and second sections, while the results and discussions of modeling and thermal performance of SAHP drying system including spherical TES tank with and without HRU using the models presented in chapter four are inserted in sections three and four.

Conclusions of this simulation and recommendations for further study are presented in **chapter eight.**

CHAPTER 2

LITERATURE REVIEW

2.1 Introduction

A drying process consumes intensive energy in the industrial applications, so the alternative and clean energy should be used because of increase in unit price of fossil fuels, environmental effects, and human health protection. Storage of solar thermal energy is crucial in heating systems when an efficient and cost-effective solar energy utilization can be achieved. Therefore, the great amount of energy demand for drying process can be decreased by charging of solar energy into TES storage, and the stored energy being used via heat pump evaporator for drying of wheat in the drying unit. This chapter deals with comprehensive literature survey on utilization of solar energy and thermal energy storage with heat pump for heating, cooling, and drying processes applications.

2.2 Applications on Cooling and Heating Processes

A number of experimental and analytical works focusing on designing, analyzing, and optimizing TES tank and utilizing it for cooling and heating applications is presented in this section. Dincer [34, 35] addressed techniques and applications for the description, assessment, and usage of TES tank. Zogou and Stamatelos [36] analyzed how climate impacts heat pump system performance in cooling and heating applications for spaces and found that warmer Mediterranean climate best fits such applications. Petit and Meyer [37] compared technical and economic aspects for air conditioning systems between air-sourced and horizontal ground-sourced in South Africa. They indicated that the ground source system has a higher capital cost while the air source system has a higher running cost. Nikajima et al. [38] scrutinized the temperature field in the earth in the cylindrical coordinate system and forecasted the heat an earth tube can move from an indoor space. Hasegawa et al. [39] experimentally examined a full scale test house with an earth tube and showed the potential of enhancing interior thermal conditions in summer.

De Swardt and Meyer [40] conducted a comparative study between simulation and experimental results of reversible GSHP connected with a network of water pipes system with a traditional heat pump for cooling and heating. The study revealed that this is a feasible approach for the optimization of energy exploitation in air-conditioning purposes. Yumrutas and Unsal [41] developed a computational model for a heating system used for space heating using hemispherical tank to find periodic solution of the system. They studied the impacts of ground types around the storage, collector type, collector angle, collector surface area, and storage size on the heating system performance. They found that maximum water temperature is reached in September and November, while the minimum values can be observed during March and April. Sand earth gives the highest storage temperature and lowest collector efficiency, while granite gives minimum temperature of water.

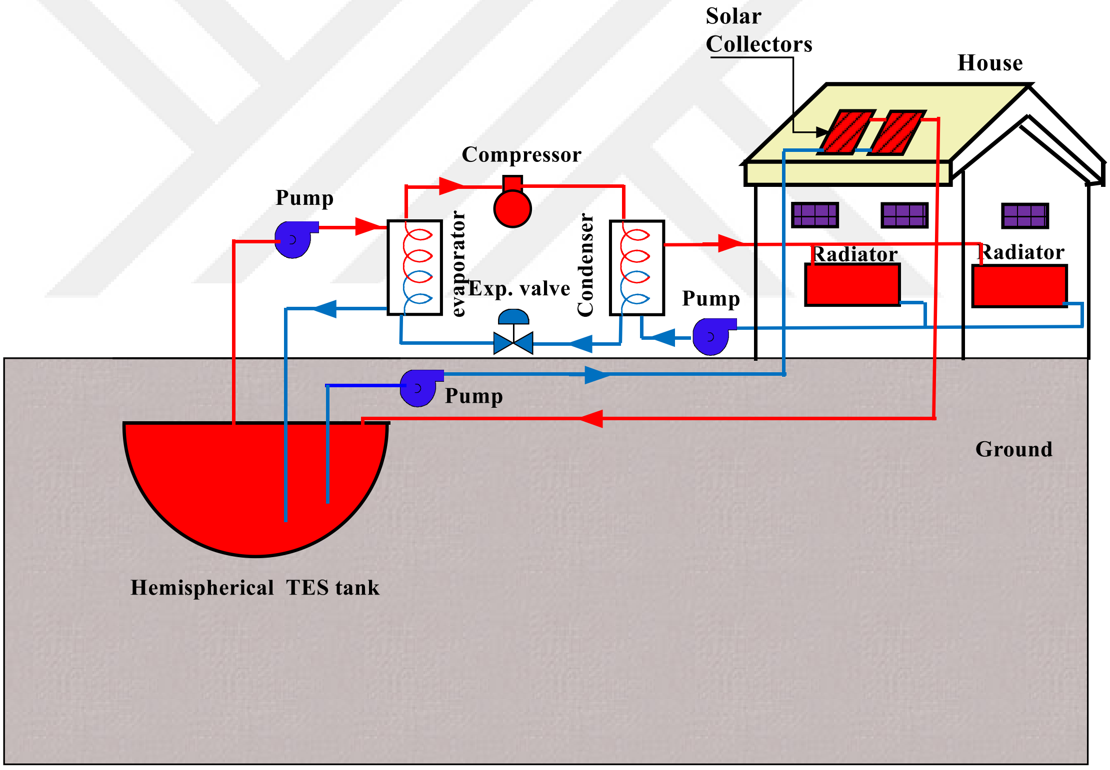

Figure 2.1 Heat pump system with a seasonal hemispherical surface tank type [41].

Yumrutas and Unsal [42] presented an analytical study utilizing thermal TES tank with a chiller for assessing yearly periodic temperature alteration in the tank and soil adjacent to the tank. They investigated the effects some parameters, such as water temperature in the tank, atmospheric temperature, CE ratio, soil kinds, and tank volume on the COP of chiller. It has been found that water temperature is below atmospheric temperature in summer. Higher chiller COP coincides with lower water and ambient air temperature. Tank volume has a significant impact on the chiller COP.

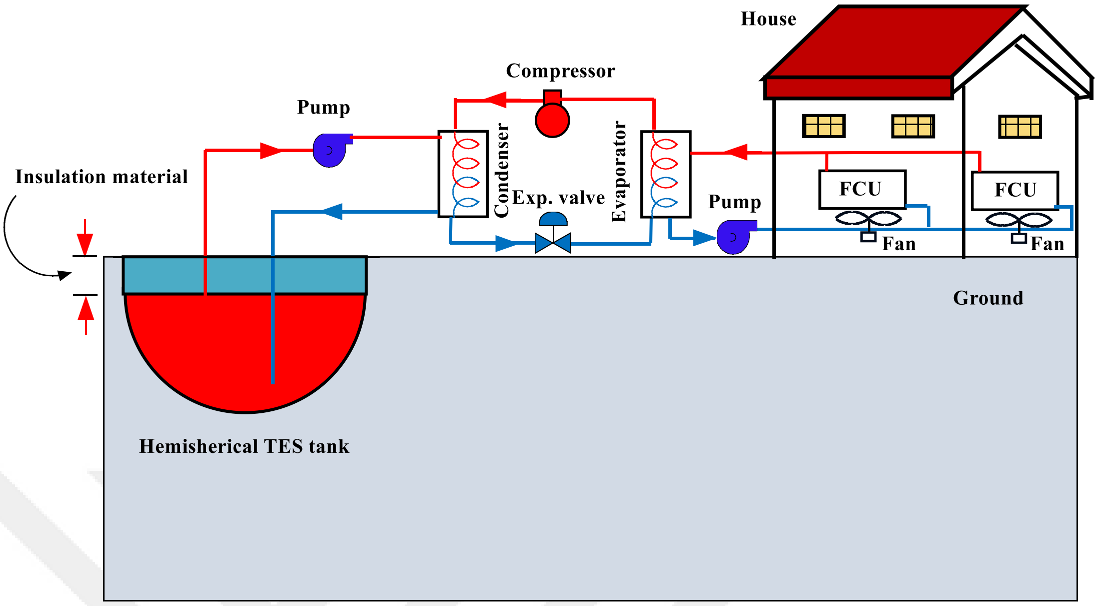

Figure 2.2 The cooling system with a hemispherical tank [42].

Hasnain and Alabbadi [43] examined a system that included TES techniques supplemented with a traditional air-conditioning unit. In this study, they made a comparison between ice storage and chilled water technologies in Saudi Arabia. They discovered that the ice storage technology may minimize about 20% of peak power demand in comparison with traditional systems.

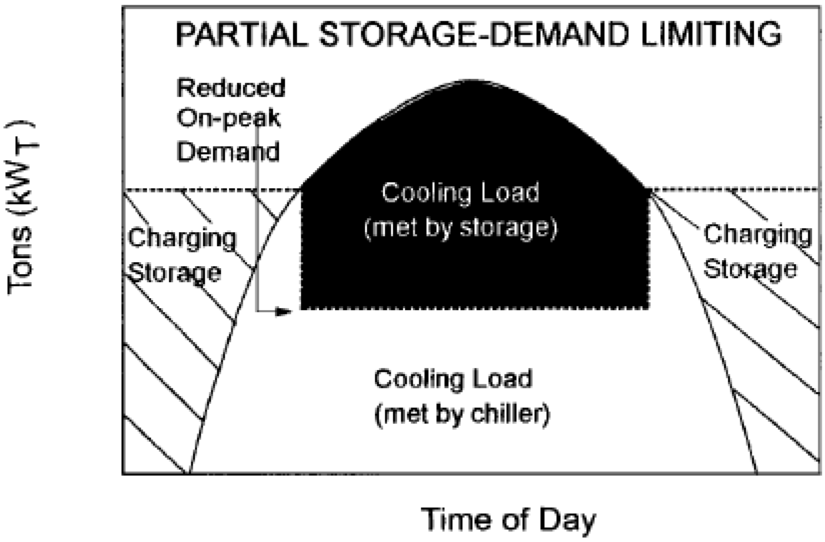

Figure 2.3 Basic thermal-storage operating strategies [43].

Yumrutas et al. [44] used Complex Finite Fourier Transform (CFFT) technique for resolving the problem of spherical underground TES tank. The heat pump-assisted TES tank is exploited in house cooling. They revealed that water temperature in the tank is below ambient air temperature in summer.

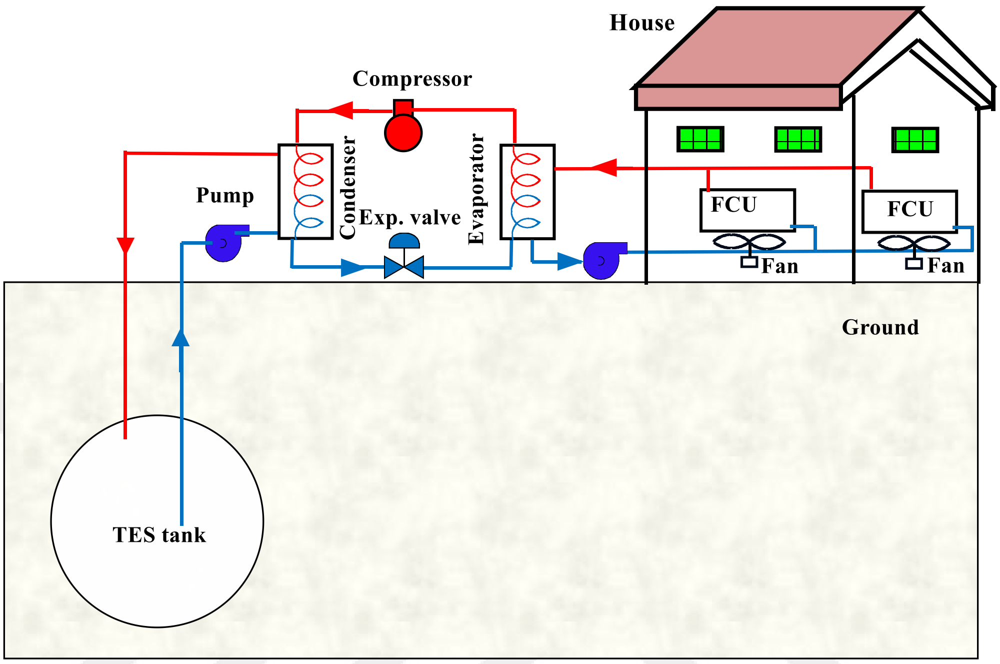

Figure 2.4 The cooling system with a spherical tank [44].

Papanicolaou and Belessiotis [45] conducted an experimental and numerical study of the flow and heat transport process occurring in a real-scale. For the numerical side of the study, charging of the tank at a constant flow rate and three various inlet-temperature histories were considered. The simulation of charging process has been performed by dynamic models based on the multinode and plug-flow methods in addition to two dimensional (2D) computational fluid dynamics (CFD). The impact of turbulence-model choice and water-surface heat losses found to be significant in the modeling. Wang and Qi [46] analyzed the performance of TES tank in a solar-assisted ground heat pump system for residential buildings. They indicated that the performance of such storage relies heavily on the intensity of solar radiation and the matching between the volume of water tank and solar collector's area. For the case of Tianjin, the efficiency of underground thermal storage based on the total solar radiation and absorbed solar energy may range from 40% and 70%, respectively. The range of 20–40 L/m^2 is a reasonable ratio between the volume of the tank and collector area.

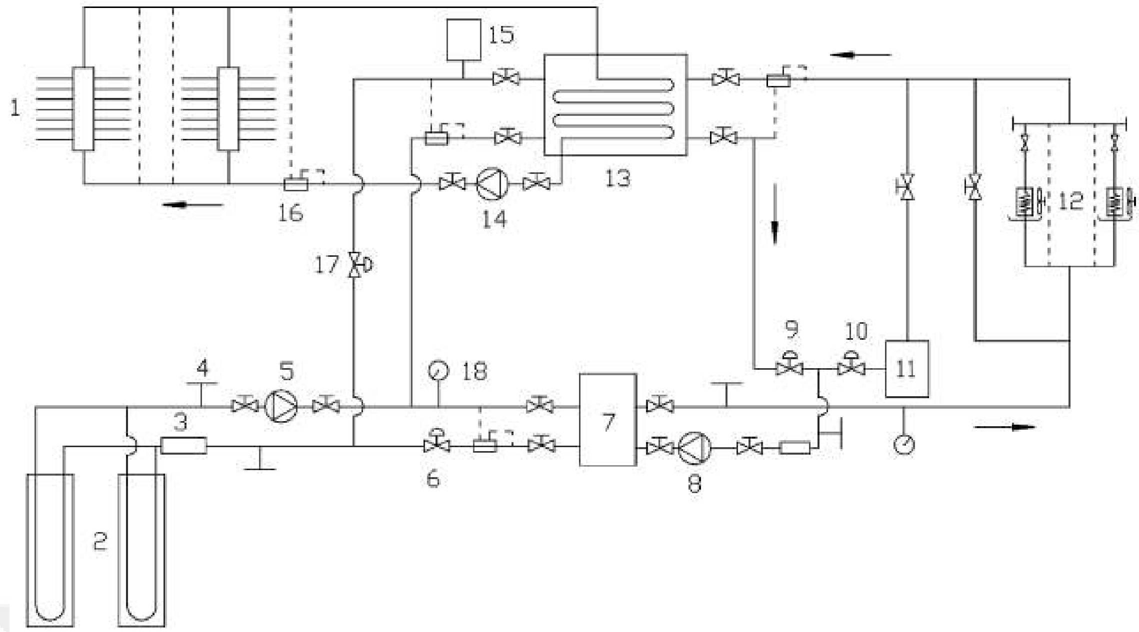

Figure 2.5 Principle diagram of SGCHPS [46].

Sarbu and Sebarchievici [47] reviewed GSHP systems for cooling and heating of buildings. The various hybrid ground-couplet heat pumps (GCHP) systems for cooling or heating, which are prevalent in buildings, are described. It is shown that the energy saving potential is significant by utilizing GSHP for both cold and hot weather areas. Xu et al. [48] reviewed available technologies in seasonal thermal energy storage. They focused on three technologies for seasonal heat storage: sensible, latent and chemical storage. Latent heat and chemical technologies store more energy than sensible ones. Navarro and Gracia [50] reviewed and integrated thermal storage systems in building designs to solve the problems of limited space for installations in these buildings. They classified them according to the thermal storage system location. Soni et al. [51] reviewed the current status of hybrid GCHE systems with passive renewable systems for space heating/cooling. The paper explains that earth air heat exchanger (EAHE), GSHP, and various passive techniques are commonly utilized in space heating/cooling.

Rui Fan et al. [52] studied cool injection and extraction performance of borehole cool energy storage for ground coupled heat pump system. For the purpose of addressing the low performance of GCHP system in summer in cooling-load dominated areas, BCES, that utilizes soil for storing and exchanging energy, was joined with hybrid GCHP systems to realize effective heating and cooling of constructions. When GHE is compared with BCES, it is found that more cool energy may be supplied for constructions peak hour demand due to injecting cooling energy. Based on the model of combined heat conduction and heat advection for BCES, a strategy for diurnal cool-injection and extraction for BCES in summer has been worked out for pinpointing the enhanced thermal functioning of the hybrid GCHP systems. The impact of borehole depth and spacing has been shown for hybrid BCES and GCHP systems to be helpful in minimizing the necessary borehole area, in extenuating peak power load, and enhancing operational efficiency.

Jongmin Choi et al. [53] contrasted the operation of R22 against R744 SGHH pumps based on heat source settings. The efficiency of solar collector in R744 SGHH pump is 4.1% greater than that in R22 one. Furthermore, the heating ability of the R22 was 10% greater than that of the R744. The efficiency of solar collector systems has been higher in the R744 hybrid heat pump in comparison with R22.

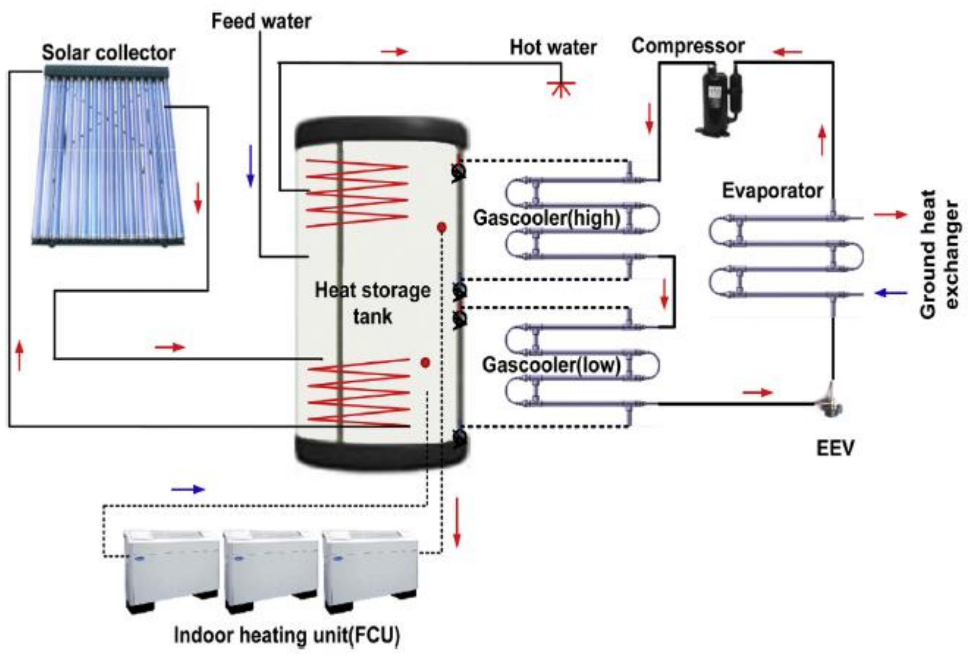

Figure 2.6 Schematic diagram of the hybrid solar-geothermal heat pump system [53].

Sebarchievici and Sarbu [54] developed an energy-operational optimization tool for a GCHP system through inserting a buffer tank between the heat pump and fan coil and consumer supply by relying upon quantitative adjustments with an adjustable speed circulating pump. After that, experimental calculations were employed for testing the functioning of GCHP system, in various operating settings. Energy efficiency and CO_2 emissions were both calculated for one operation month through utilizing both classical and optimized adjustments of the GCHP system, and a comparative account of these functioning with the assistance of TRNSYS software, two simulation models of thermal energy consumption in heating, cooling and domestic hot-water operation. The simulations were contrasted against experimental data, resulting in good agreement. Therefore, simulation models have been validated.

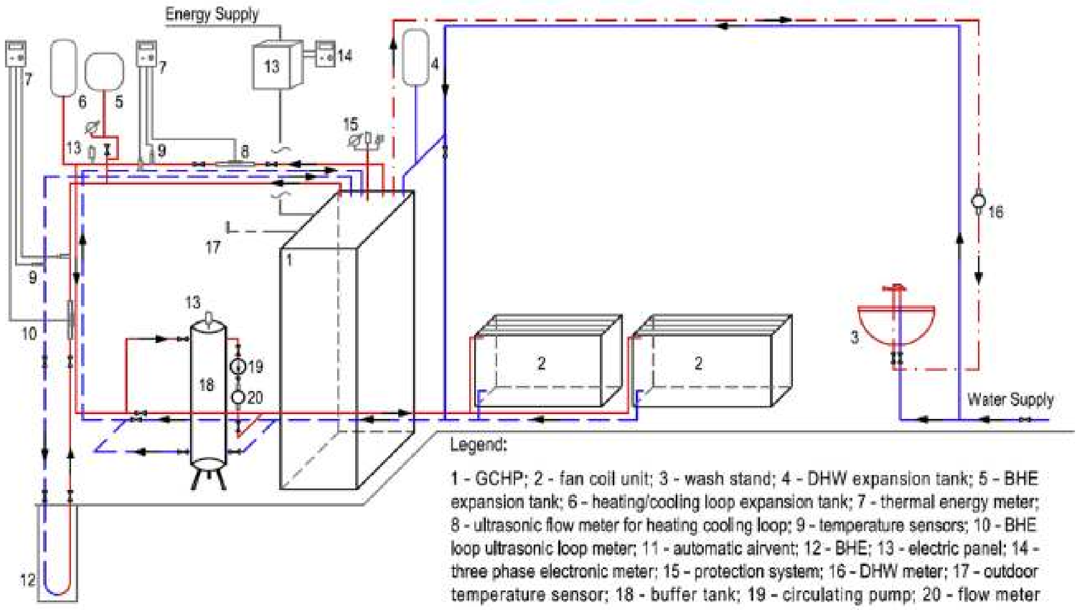

Figure 2.7 Schematic of the experimental GCHP system [54].

Chengchu Yan et al. [55] investigated seasonal cool storing systems according to separate type heat pipe for durable indoor cooling. Seasonal cold storing is very effective and environmentaly-friendly method that utilizes natural cold energy stored in winter (such as snow, ice or cold atmospheric air) for free-cooling in summer without utilizing any energy. This energy is converted as chilled water for cooling supply in summer that reduces chiller running time and the associated electricity load and gas emissions significantly. The impact of various factors, including weather data and the main parameters of heat pipes, on the charging of the cold storing systems are scrutinized. The success and sustainability of the proposed system are illustrated in a case study of a kindergarten building in Beijing.

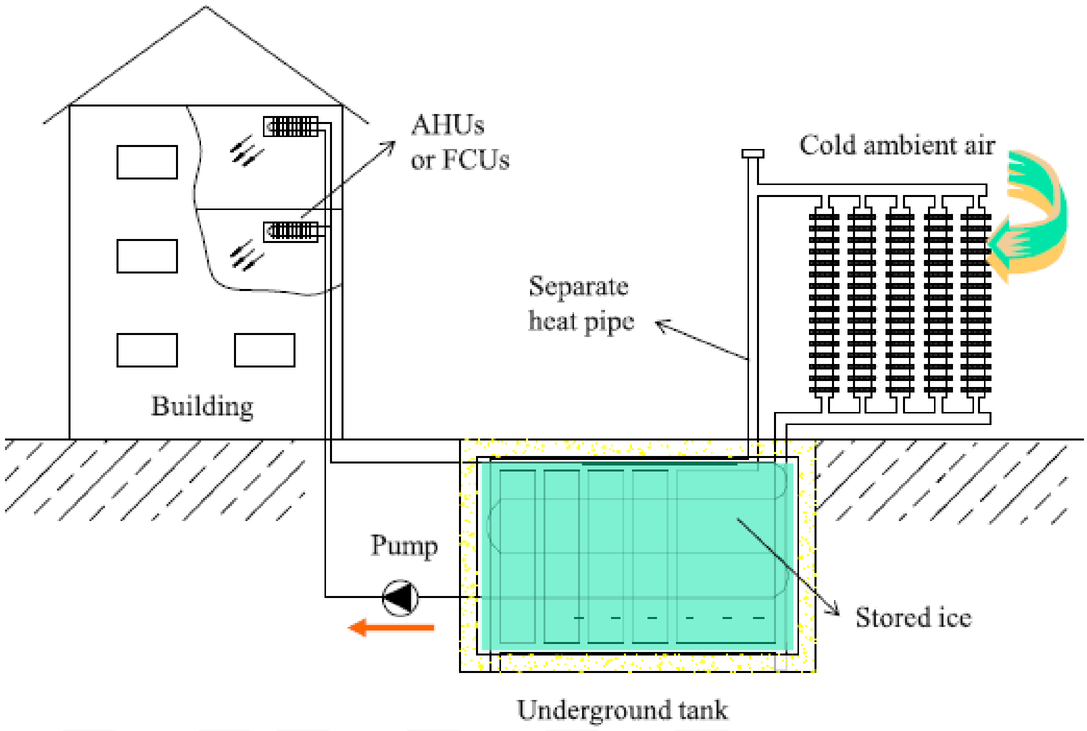

Figure 2.8 Schematic of the seasonal ice storage system using separate heat pipes [55].

Zhang et al. [56] studied operating functionality in cooling mode of a ground source heat pump of approximately-zero energy building in the cold area of China. Simulation results indicated that the heating, cooling, and lighting demands in this building may be minimized to 25 kWh/m^{2}yr through utilizing high-performance envelopes and hybrid renewable energy system. Heat pump COP may reach 5.0 in cooling operation strategy.

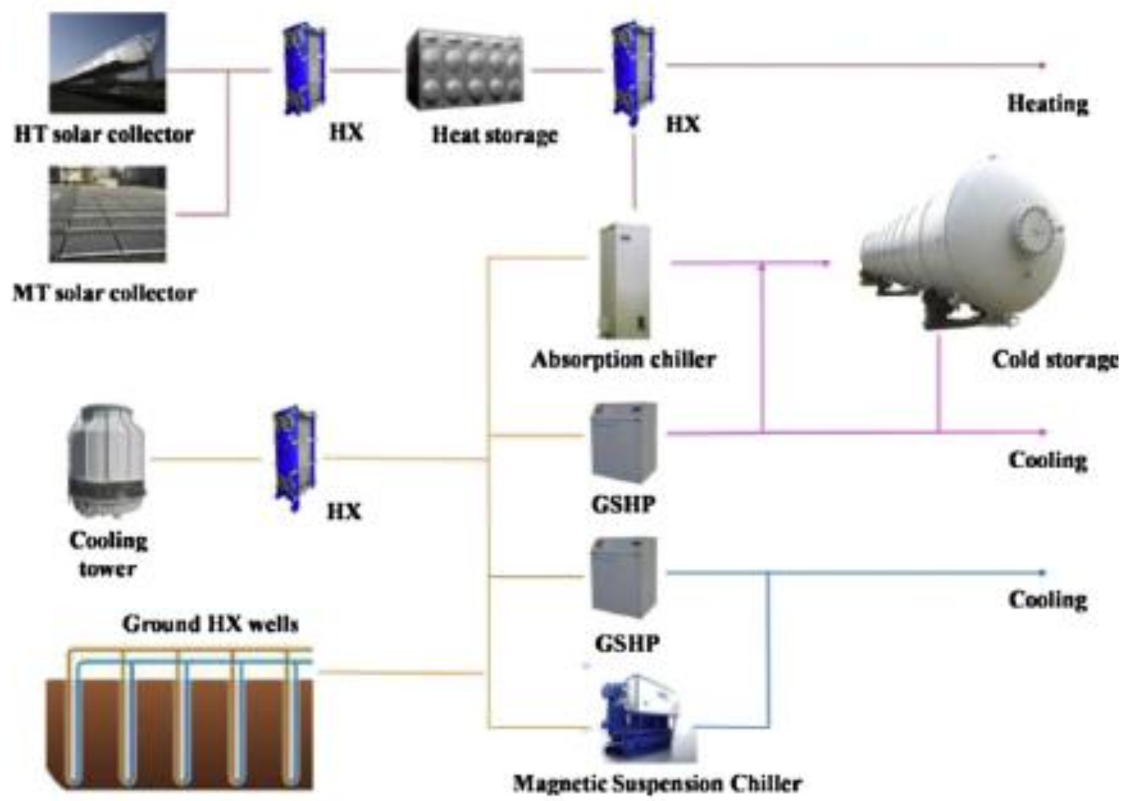

Figure 2.9 Schematic diagram of energy system [56].

Yanshun Yu et al. [57] developed a novel integrated system with a cooling storage in soil and ground-coupled heat pump. In such a system, the humid soil is used as a material for cooling storage, while pipes are used in cooling storage devices and geothermal heat exchangers at the same time. In seasons requiring cooling, the energy is stored in soil during the off-peak times and later extracted for indoor cooling during the on-peak times. In other seasons, however, the system functions as a ground-coupled heat pump for heating or cooling. It was revealed that the charging inlet temperature, tube diameter, moisture content of soil and pipe distance are crucial for illustrating cyclic performance of the integrated system.

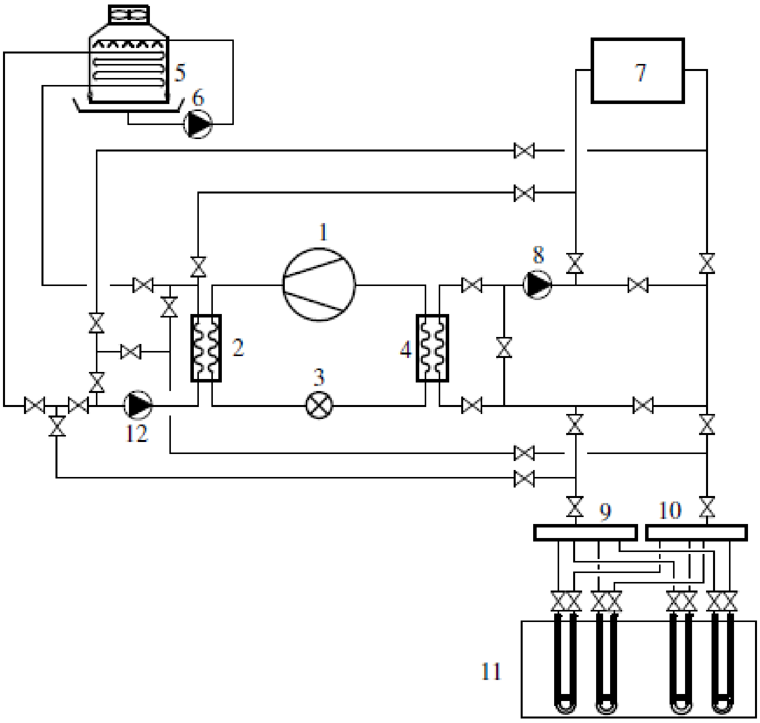

Figure 2.10 Schematic of the integrated system [57].

Pahud [58] & MeliB and Später [59] investigated systems combining a seasonal thermal storage with a solar assisted heat pump. Storing solar energy during summer and utilizing it for indoor heating purpases in the winter has been the subject of many investigations. Yumrutas et al. [60] used analytical and computational models to predict yearly periodic performance of solar-assisted GHPS for indoor heating with a cylindrical tank. They studied a tank immersed in various types of soil. It was indicated that the soil type has little impact on yearly energy ratios and there were bigger impacts on storing temperature and on yearly heat pump COP.

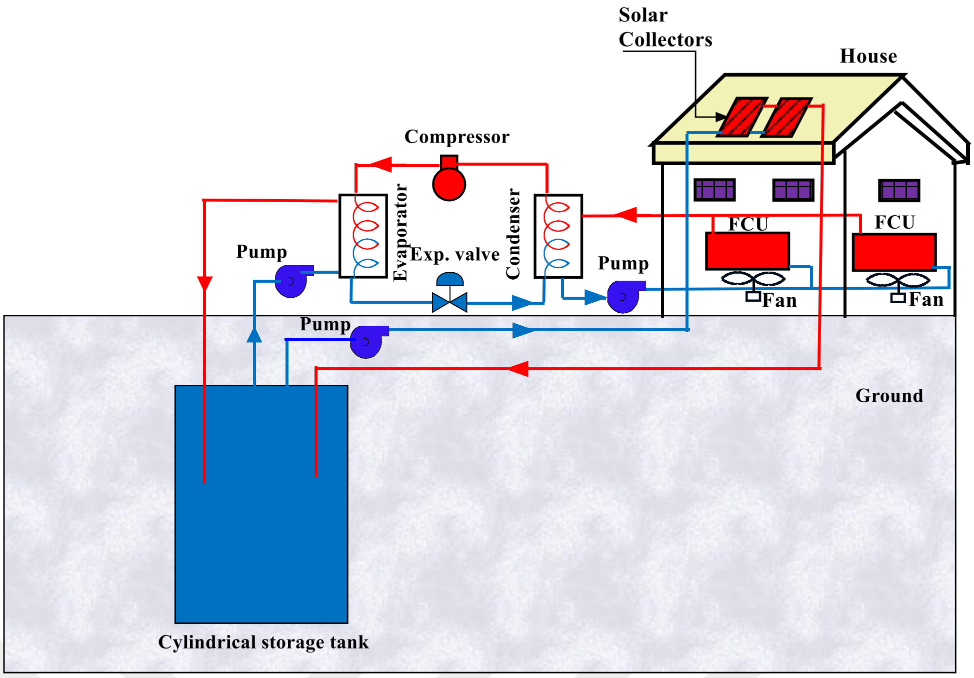

Figure 2.11 The cooling unit with spherical water tank [60].

Yumrutas and Kaska [61] experimentally analyzed indoor heating systems through exploiting a heat pump with daily storage of solar energy. They indicated that yearly COP ranged between 2.5 and 3.

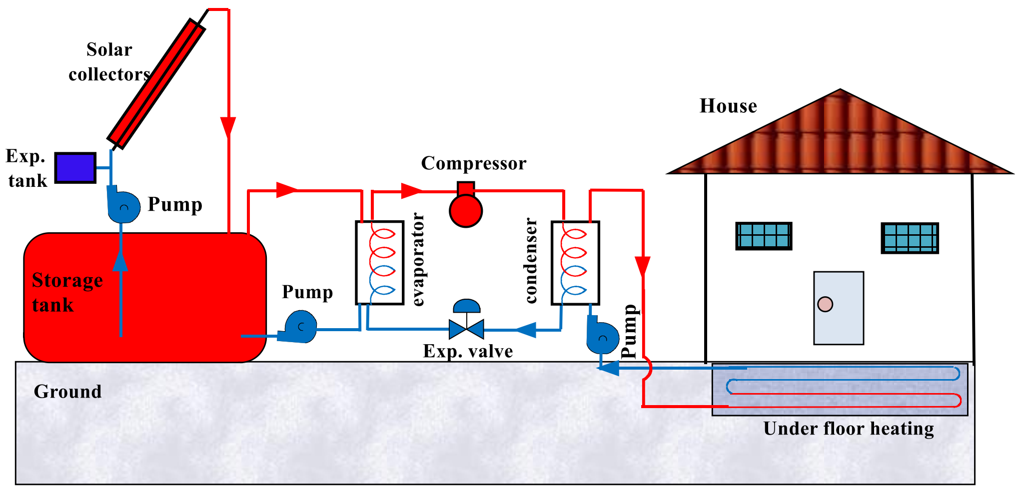

Figure 2.12 A heat pump, solar collectors, a storage tank, and a house heating [61].

Inalli et al. [62] proposed an analytical and computational model for gauging the yearly periodic functioning of a SAHP system with TES tank. Inalli [63] investigated a theoretical study of a SAHP system with spherical TES tank. He resolved the problem of unsteady heat transfer around TES tank through using a finite difference method and CFFT technique by taking into account the yearly periodic functioning. He indicated that the heat load, collector area, and tank volume were the extreme significant influencing factors. Ucar and Inalli [64, 65] employed the finite element method to analyze TES tank used with solar heating system using a MATLAB program. They observed an elevation in the water temperature when collector area was increased and storage volume decreased.

Chung et al. [66] adopted TRNSYS for forecasting thermal functioning and economic feasibility for central solar system to be work assisted seasonal storage. They found that the total heating load can be covered by a 39% solar energy with using 184 m^2 as collector area and 600 m^3 of storage volume for the system. Nordell and Hellström [67] obtained a solar fraction of 60% for a 90 single-family housing complex having a 1080 MW h total heat demand, a supply temperature of 30 °C, and 3000 m^2 of solar collector area. Wang and Qi [68] examined the functioning of a SAHP system with TES tank for a housing unit. It was found that the efficiency of the TES based on total solar radiation and absorbed solar energy by collectors may contribute to 40% and 70%, respectively. Wang et al. [69] experimentally investigated a SAHP system with seasonal TES tank used in housing units in Harbin. It was concluded that solar collectors contributed 49.7% of total heating output in the heating modem, and the average COP and COPs were 4.39 and 6.55, respectively. The system COP recorded 21.35, when starting of heat pump was not necessary, in the cooling mode. The heat pump extracted the stored heat from soil about 75.5%, following twelve months of operation. The rise in heat raises soil temperature, which in turn raises COP. Qu et al [70] approached the designing, installing, modeling and evaluating a solar thermal indoor heating and cooling system. It was revealed that such a system may contribute up to 20% of the heating and 39% of the cooling loads. Yumrutas and Unsal [71] developed an analytical model for a SAHP system with TES tank for space heating. They found that this type of heating system can reach periodic situation in 5-7 years. It was also found that water temperature has a proportional relation with collector area and tank volume.

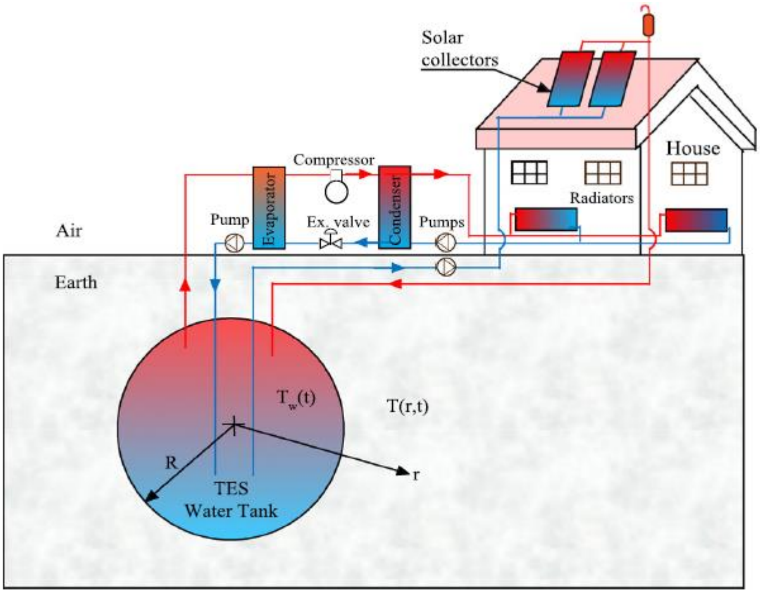

Figure 2.13 House heating with SAHP and TES tank [71].

Sweet and McLeskey [72] focused on an underground-fabricated SSTES bed. TRNSYS has been exploited for modeling and simulating the winter thermal load of a typical Richmond home, Virginia, USA. The optimization of the SSTES scheme showed that a 15 m^3 bed volume, 90% of the south facing roof, and a flow rate of 11.356 lpm through the solar collectors were optimal values. The total efficiency of the system was 50% to 70% in comparison with the total energy gain of the solar collectors. The total efficiency was between 6.1% and 7.6% in comparison with the total amount of solar radiation incident upon the solar collectors. Attar et al. [73] adopted TRNSYS simulation for assessing the functioning of SWHS for greenhouses for Tunisia weather. It has been found that, when tank volume is raised, the temperature at the collector outlet declines. Furthermore, high flow rate reduces the stratification and maximizes system effectiveness.

Calise et al. [74] developed a model for stimulating and optimizing a new solar trigeneration system. This model is developed to provide electricity, indoor heating or cooling and domestic hot water for small housing units. The study concluded that thermal and electrical efficiencies are up to 40% and 10%, respectively. The COP resulted above 4 for both heating and cooling modes. For the base case, a Simple Pay Back period of 5.36 years was found; such index decreases to 2.33 years in case a capital investment incentive of 30% is available. Chen and Yang [75] conducted a numerical simulation of SAGCHP system that can supply both indoor heating and domestic hot water. Optimization is carried out on the TRNSYS based platform through the simulation of the impact of solar collector area on the total borehole length and system performance. Results indicated that the optimized system under the particular load settings has a collector area of 40 m^2 and a borehole length of 264 m. Yearly overall heat extraction plus 75% of the hot water load may be supplied by solar energy in the optimized design. Chow et al. [76] developed a SAHP design for water-heating and indoor swimming pool space uses. It was concluded that the total system COP may record 4.5, and the fractional factor of energy saving is 79% in comparison with the traditional energy system. The economical payback period is less than 5 years. Xu et al. [77] indicated that 2304 m^2 solar-heated greenhouse supplied with a seasonal thermal energy storage system in Shanghai, east China. This system uses 4970 m^3 of underground soil to store the heat generated by a 500 m^2 solar collector in non-heating seasons through U-tube heat exchangers. It was found that in the first operation year, 331.9 GJ was charged, and 208.9 GJ was later extracted for greenhouse space heating.

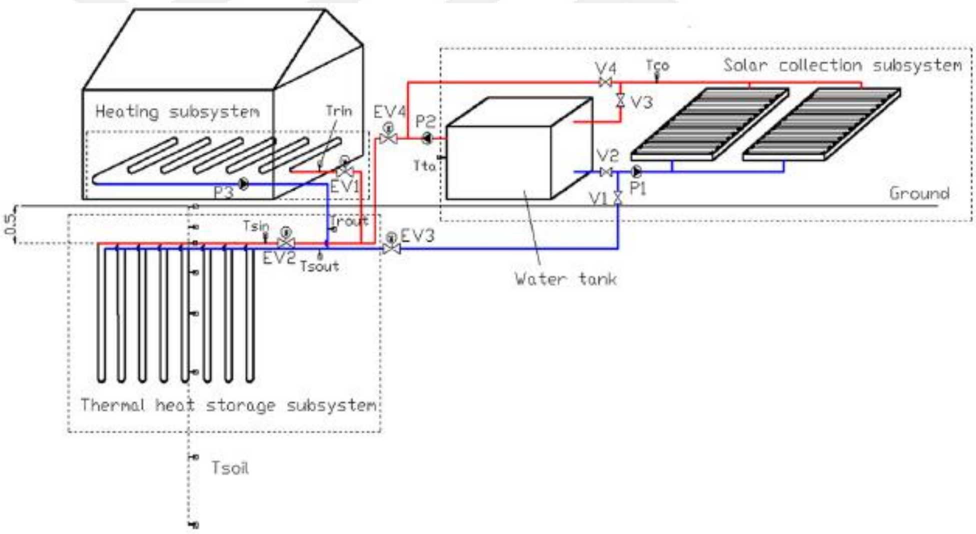

Figure 2.14 Schematic diagram of a solar heating system with seasonal TES [77].

Moon and Choi [78] in their study focused, on earth-contact concrete elements that are already required for structural reasons but that simultaneously work as heat exchangers. Pipes, energy-piles, and energy-slabs filled with a heat carrier fluid are installed under conventional structural elements, forming the primary circuit of a geothermal energy system. It has been found that the minimum COPs for the energy-pile and energy-slab system were 4.2 and 4.5, respectively. Karacavus and Can [79] investigated thermal and cost analysis of seasonal TES storage system in Thrace. Optimum collector area for the heating system has been determined. Total heat requirement of 69% has been met by means of heating system concerning the space heating and domestic water heating. The payback has been determined as 19-20 years.

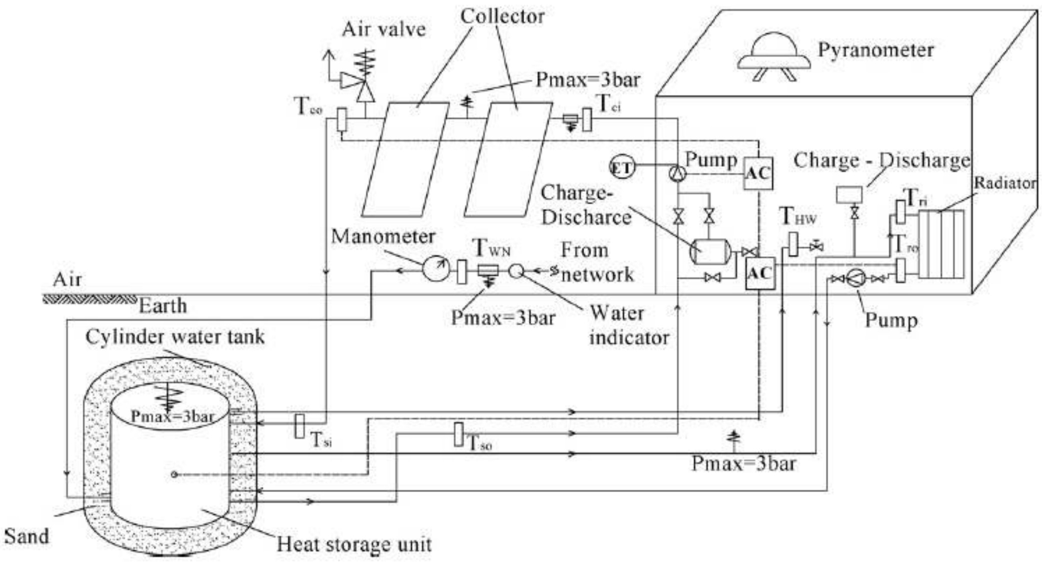

Figure 2.15 Installation scheme of the system [79].

Mahfuz et al. [80] experimentally studied; shell and tube TES system using paraffin wax was used in a water heating system to analyze its performance for solar water heating application. Life cycle costs were calculated for different flow rates of the Heat Transfer Fluid (HTF) with 0.033 kg/min and 0.167 kg/min flow rates of water as HTF, and energy efficiencies experienced were 63.88% and 77.41%, respectively, but in exergy analysis, efficiencies were observed to be about 9.58% and 6.02%, respectively. The total life cycle cost was predicted to be $ 654.61 for 0.033 kg/min flow rate, which could be reduced to $ 609.22 by increasing the flow rate to 0.167 kg/min. Therefore, the total life cycle cost decreases with the increase of flow rate.

Kuyumcu et al. [81] investigated the utilization of waste heat rejected from a chiller used for ice rink application and storing the gained energy in a spherical TES tank, which is used with a swimming pool heating system. They indicate that five to seven years are necessary for the swimming pool heating system to attain periodic operation. The results also reveal that, the performance of heating system reaches optimum at ice rink surface 475 m^2 with swimming pool 625 m^2.

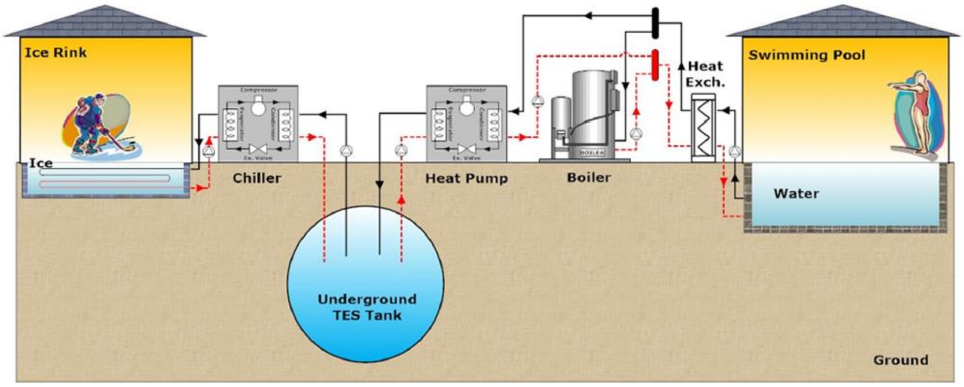

Figure 2.16 The swimming pool heating system with ice rink TES tank [81].

Tutumlu et al. [82] investigated thermal performance of an ice rink cooling system with underground TES tank. They found that five to seven years are enough for the system to attain periodic operation.

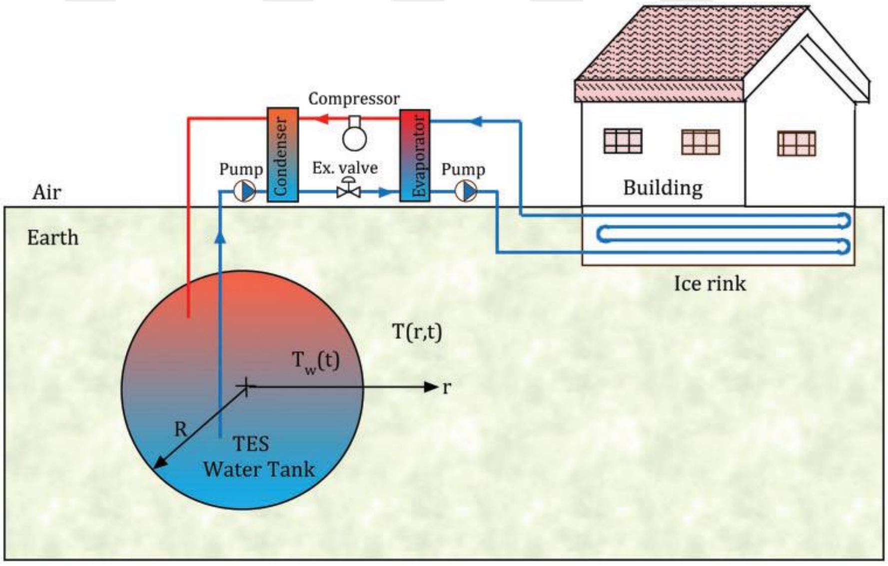

Figure 2.17 Ice rink cooling system with TES tank [82].

2.3 Drying Applications

There are many types of heat pump drying systems that are used for food or agricultural products drying. Combining other mechanisms with HPD system has been investigated by many researchers. Adapa et al [83] developed a simplified procedure for performance modeling of a low temperature heat pump coupled with a continuous cross flow bed dryer. Both outside heat and mass transfer coefficients at the evaporator and condenser coils have been taken into consideration as critical factors that regulate the transference of energy between the heat pump and dryer unit. A re-circulating heat pump continuous bed dryer system has been developed, built and tested in the field by

[84]. The results have shown that aerial plant products share drying properties, meanwhile root plant products vary in their drying rates as a result of the wide gap in their sizes, shapes and physical configurations. The re-circulation made by the heat pump dryer led to 22% energy saving and 65% less time required for drying in comparison with traditional dryers that have built-in electric coil heaters. A type of solar air collector and air-to-air heat recovery modules have been incorporated into the infrared dryer for the sake of minimizing specific energy load [85]. The heat recovery unit may contribute to 23–28% of the entire energy requirement. Exergy analysis approach has been employed to gauge system performance and the process [86]. The impacts of the temperature and velocity of drying air on the performance of the drying process have been reviewed. The real coefficient of performance was 2.37 for the HP unit and 2.31 for the whole system. The compressor has been shown as the key part of the system that enhances the efficiency. Exergetic efficiency of drying olive leaves ranged from 67.45 to 81.95%. It has been shown that they rise when the temperature of drying air falls and when the velocity of drying air rises. Moreover, during the operation of air-source heat pump in low temperatures, evaporator's surface temperature may drop to under 0 °C and lead to frost formation and accumulation, which might decrease performance. [15]. It also negatively affects air source heat pump. A solar energy system with a thermal storage has been developed by [13]. The solar energy may comprise up to 43% of the over-all drying load. Wang et al. [11] experimentally investigated the system of solar-assisted heat pump drying for mango in which a new drying system with a secondary heat restoring has been developed with the ability of operating autonomously in solar drying and heat pump drying method, or operating in a combined mode. A heat pump evaporator and a heat exchanger have been embraced to restore the heat lost from the exhaust moist air from the drying chamber to maximize energy efficiency. The efficiency of solar-assisted drying mode proved 6% greater than the heat pump drying mode and it saved 3.5kWh. Performance coefficients were 3.69 and 3.48 for solar-assisted heat pump mode and heat pump drying mode, respectively. The typical efficiency of heat exchanger for restoring lost heat may reach 41.7% throughout the entire operation.

Naemsai et al [12] inspected the performance of SAHP drying with heat restoring to minimize thermal energy required to dry chili peppers. The dryer assigned for the experimental part [12] is made up of a heat pump, multi trays, and a greenhouse cover.

The study has shown that the SAHP drying with restoring heat led to a better drying performance than conventional dying approaches. The dryer system may offer coefficient of performance, drying time, efficiency, and specific energy consumption of roughly 3.17, 24 h, 33.2%, and 2.21 kWh kg^{-1}, respectively. Moreover, the SAHP drying with heat restoration contributed to a better drying performance than the SAHP without heat restoration although there was alteration in the ambient condition. Drawing upon the economic indexes, the recovery period and net present value of the SAHP drying with heat recovery was roughly 1.9 years and 915.60 USD. The SAHP drying system is preferred for chili peppers because the rates of heat and mass transfer are high, and it is capable of working throughout nighttime and daytime [12]. A couple of heat pump cycles; multitemperature cascade cycle, and combined single-stage cycle, have been recommended to tackle the aforementioned shortcomings in drying process with large temperature lift [87]. The impact of various operation variables on heat pump cycles have been studied to develop an optimal cycle performance. Then, the aforementioned cycles in addition to a traditional cascade cycle, a bi-stage compression cycle, and a mono-stage compression cycle have compared to highlight cycle performance and drying performance in specific drying settings. The results have shown that the COPs of the multitemperature cascade cycle and combined mono-stage cycle are about 95% and 88% higher than that of the mono-stage compression cycle, respectively. Regarding the bi-cascade cycles (i.e., traditional cascade cycle and multitemperature cascade cycle), 49% more water evaporation with identical power may be produced through adding condenser and evaporator. Among the five cycles being examined, the multitemperature cascade cycle was found to be the optimal for retrofitting the drying equipment with large temperature lift [87]. Mohanraj and Chandrasekar [88] investigated chili drying via an experimental study on indirect forced convection solar dryer integrated with different sensible heat storage materials. Performance of a forced convection mixed mode solar dryer with thermal energy storage was experimentally analyzed by Baniasadi et al. [89]. During the experiments, they found that fresh apricot slices can be dried at different working conditions. Another experimental study was conducted by Şevik et al. [90] using a solar-assisted heat pump drying system with flat plate collectors for drying of mushroom. System coefficients performance (COP) were calculated as values in a range from 2.1 to 3.1 using experiment results. They also found that SMER values ranged between 0.26 and 0.92 kg kW^{-1} h^{-1}. Another experimental analysis using heat pump assisted solar air collector was carried out by Şevik [91] where four different vegetables were dried under different climatic conditions. He obtained COP of the drying system between 1.96 and 2.17 and SMER values between 0.03 kg kW^{-1} $h^{-1}$and 0.46 kg kW^{-1} h^{-1} for the vegetables.

Rahman et al. [92] studied economic optimization of evaporator and air collector area of a solar-assisted heat pump drying system. They revealed that this drying system has sufficient amount of savings during the life cycle with a minimum payback period of about 4 years. Şevik [93] designed and manufactured a new type of solar-heat pump dryer by using double-pass solar air collector, heat pump and photovoltaic unit. He indicated that the calculated thermal efficiency of double-pass collector ranged between 60%-78% based on experimental results. He observed that this system can be conveniently ran through skipping the heat pump under normal ambient air conditions. Aktas et al. [94] compared experimental results of a heat pump dryer and an infrared assisted-heat pump dryer to determine the energy and exergy efficiencies of dryers. They indicated several variations, including energy efficiency (5.3- 50%), COP of the system (2.11-2.96), and exergy efficiency (31.6% - 66.8%). Qiu et al. [95] performed an experimental study to obtain performance and operation mode analysis of a heat recovery and thermal storage solar-assisted heat pump drying system. They have shown that coefficient of performance of the drying system ranged from 3.21 to 3.49, and that payback periods for drying radish, pepper, and mushroom in the life span of the system were 6 years, 4 years, and 2 years, respectively. Ringeisen et al. [96] investigated the drying of tomatoes by adding a concave solar concentrator build from low cost to a typical Tanzanian solar crop dryer. They found the concentrator reduces the drying time by 21% in addition to reducing relative humidity and increasing internal dryer temperature. Singh et al. [97] used variable ambient and solar conditions in different months to investigate thermal performance of the packed bed solar heat storage system. They developed the packed bed and compared with packed bed filled with phase change material. They found the developed packed bed possesses a better efficiency. The solar collection and heat retrieval efficiency of heat storage system ranged between 36–51% and 75–77%, respectively. Mohanraj [98] studied the performance parameters such as COP, SMER and condenser heat capacity of a solar-ambient hybrid source heat pump drier for copra drying in hot-humid weather conditions. He used different heat capacities for condenser between 2900W and 3750W. The calculated value for SMER was 0.79 kg/kWh. The moisture content (on wet basis) of the copra was reduced from about 52% to about 9.2% and 9.8% in 40 h for trays at bottom and top, respectively.

However, searching the literature about the Solar Assisted Heat Pump (SAHP) drying system reveals that there are no previous studies related SAHP drying system with Thermal Energy Storage (TES) tank and Heat Recovery Unit (HRU) for long-term operation period. The SAHP drying system can be used in different industrial applications with the TES tank and HRU during all seasons. The first originality of the proposed drying system is the utilization of energy stored by solar collectors in underground TES tank with SAHP drying system. During all seasons, the heat pump extracts the solar energy stored in the TES tank. Incorporating higher heat supplies produced by solar collectors and stored in TES tank result in higher performance parameters such as coefficient of performance (COP) and Specific Moisture Extraction Rate (SMER). The second originality of this system is finding the performance parameters for the new drying system on hourly basis for long terms. Using HRU with SAHP drying system and TES tank increases performance parameters of the system.

Due to the multiple advantages of the proposed drying system, a theoretical model for SAHP drying system with underground TES tank and HRU is developed in the present study. The drying system comprises of a drying unit, HRU, solar collectors, a heat pump and an underground TES tank. Thermal analysis for each component of the drying system is obtained, and they are combined with each other to obtain a mathematical model for the new drying system. A computational model based on the mathematical model has been developed, and a program prepared in MATLAB is executed by using different input data to find performance parameters for the drying system. These parameters are temperature of water in the TES tank, Coefficient of Performance of the heat pump (COP) and system (COPs), Specific Moisture Evaporation Rate (SMER), and energy fractions.

CHAPTER 3

MATHEMATICAL MODELING OF A SOLAR-ASSISTED HEAT PUMP DRYING SYSTEM WITH UNDERGROUND THERMAL ENERGY STORAGE TANK AND HEAT RECOVERY UNIT

3.1 Introduction

This chapter presents the mathematical modeling of a Solar-Assisted Heat Pump (SAHP) drying system including TES tank with and without Heat Recovery Unit (HRU) to predict its long-term performance in both cases.

The cases are:

- Mathematical modeling of a SAHP drying system with TES tank.
- Mathematical modeling of a SAHP drying system with TES tank and HRU.

In order to find the hourly, monthly, and yearly performance parameters for 10 years of operation, a theoretical model using Duhamel's superposition method for TES tank and multiple expressions for other components of the drying system is developed to obtain the performance parameters.

3.2 Description of the Drying System (Case 1)

The wheat drying system under study is an environment-friendly drying system since it obtains a great amount of its energy from solar energy charged in the TES tank. The system is considered to be installed in Gaziantep (37.1^{o} N), Turkey. The scheme of the drying system is shown in Figure 3.1.

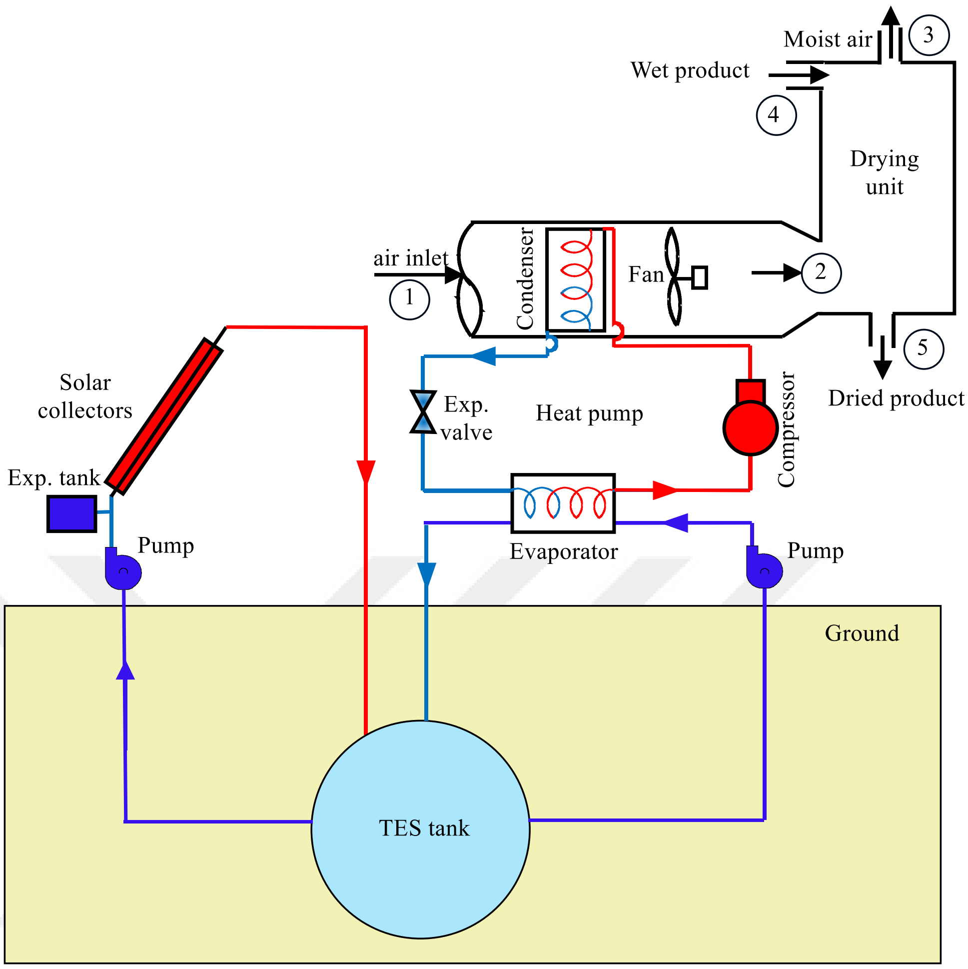

Figure 3.1 Schematic of the drying system with underground TES tank (1^{st} model).

The most important part of the drying system is the dryer unit since drying the wheat or evaporating the water in the wheat is performed in the dryer unit. It is considered to be in cylindrical in shape. Wet product enters the dryer unit from the top and moves slowly towards the bottom. At the same time, fresh air comes to a heating channel and is heated via condenser. The hot air is pumped by a blower from the bottom of the dryer unit, and moves toward the top of the unit by contacting the product. During this process, the water in the product is evaporated and exit with the air. The exiting hot air from the condenser passes over moist wheat in the drying chamber to evaporate undesired water available in the wheat and transfers it to the environment.

Heat pump is another essential part of the drying system. It works as a heat transformer from the TES tank to the dryer unit. It is known that heat pumps are energy efficient devices, and ground source heat pumps (GSHP) are much more efficient than the air source heat pumps. Therefore, GSHP is used in the drying system. Utilizing this type of heat pump in the drying system can supply much more energy for drying air than conventional drying air system since the GSHP coupled with the TES tank supplies higher energy for less temperature fluctuations. Heat is absorbed from the water in the TES tank by the refrigerant flowing through evaporator of the heat pump cycle. The energy extracted and transferred by the compressor is rejected from the condenser of the heat pump to the drying air. The heat pump operates in order to provide the heating requirement of the wheat and evaporate the water present in the wheat throughout the year.

The solar collectors are considered to be used in the drying system. They absorb solar energy and charge it to the TES tank throughout the entire year. They operate when exposed to useful solar energy. Otherwise, water in the cycle between collectors and the TES tank will not be circulated.

The TES tank is the heart of the drying system. Spherical tank is considered to store solar energy as sensible heat in the water present as a storage medium in the tank, and buried under the ground. It stores solar energy by circulating water between collectors and the tank during all seasons and gives the stored energy to the drying unit during the whole year by using the heat pump. Bigger volume is necessary for long term storage of solar energy, and to get benefit from it particularly in winter. Therefore, a large scale TES tank is used to collect more solar heat needed for the wheat drying process.

3.3 Mathematical Modeling of a SAHP Drying System with TES (Case 1)

The system consists of four main parts which are wheat dryer unit, a heat pump, flat plate solar collectors and an underground TES tank.

The expressions or energy models for the system components are defined to obtain mathematical modeling for the components. These models are for the drying unit, ground coupled heat pump, underground TES tank, and solar collectors. Mathematical modeling will be obtained by combining these expressions. In this chapter, the expressions will be given in detail.

3.3.1 Drying Unit

The dryer unit is used to evaporate moisture from wet wheat, which is shown in Figure 3.2. There are four main interactions in the drying unit; influx of drying air from condenser to drying chamber, exit of moist air after evaporation of moisture from the unit, input of wet wheat from top of the dryer and output of dried wheat with moisture lowered to the desired level.

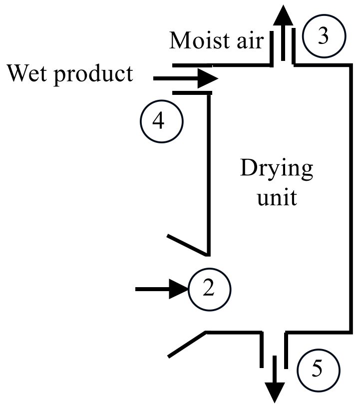

Figure 3.2 Drying unit.

Mass and energy balances may be formulated for the dryer unit by considering it as a control volume. Mass balances for the dryer unit may be expressed for product or wheat, dry air and water as:

$$\dot{m}_{p_4} = \dot{m}_{p_5} = \dot{m}_p \text{ for the product and } \dot{m}_{a_2} = \dot{m}_{a_3} = \dot{m}_a \text{ for the air}$$

$$\omega_2 \dot{m}_a + \dot{m}_{w_4} = \omega_3 \dot{m}_a + \dot{m}_{w_5} \quad \text{for the water} \tag{3.1}$$

or Eq. (3.1) can be rearranged as follows:

$$\dot{m}_w = \dot{m}_{w_4} - \dot{m}_{w_5} = \dot{m}_a(\omega_3 - \omega_2) \tag{3.2}$$

The dryer unit is assumed to be insulated. Under this assumption, an energy balance may be expressed for the drying chamber as follows:

$$\dot{m}_a\, h_2 + \dot{m}_p\, h_{p_4} + \dot{m}_{w_4} h_{w_4} = \dot{m}_a h_3 + \dot{m}_p\, h_{p_5} + \dot{m}_{w_5}\, h_{w_5} \tag{3.3}$$

Where $\dot{m}_w$, $\dot{m}_{w_4}, \dot{m}_{w_5}$, and ω are the mass flow rate for evaporated water from the product, mass flow rates of water in the product at states 4 and 5, and humidity ratio, respectively.

The enthalpy of the moist air is equal to total individual partial enthalpies of the dry air and water vapor. Thus, the moist air enthalpy may be formulated [99] as:

$$h = h_a + \omega\, h_g \tag{3.4}$$

Where h_g refers to the specific enthalpy of saturated water vapor, and h_a refers to the specific enthalpy of dry air at the mixture temperature. The specific enthalpy of the dry air is**:**

$$h_a = C_{p_a} T_{mo} \tag{3.5}$$

The enthalpy of the moist air may be given as follows [100].

$$h = 1.006\, T_{mo} + (2501 + 1.86\, T_{mo})\omega \tag{3.6}$$

Where T_{mo} is dry-bulb temperature of the moist air. The specific enthalpy of the product or wheat in the energy balance may be written as below:

$$\left(h_{p_5} - h_{p_4}\right) = C_{p\,wheat}(T_5 - T_4) \tag{3.7}$$

Therefore Eq. (3.3) can be written as the following expression:

$$\dot{m}_a(h_2 - h_3) = \dot{m}_p\, C_{p\,wheat}(T_5 - T_4) + \dot{Q}_{evap} \tag{3.8}$$

Heat transfer caused by phase change is:

$$\dot{Q}_{evap} = \dot{m}_w\, h_{fg} \tag{3.9}$$

Where h_{fg} refers to latent heat of water evaporation at the average temperature, $T_{av} = (T_4 + T_5)/2$, $\dot{m}_w$ is mass flow rate for evaporated water from moist wheat, $\dot{m}_p$ is mass flow rate for dry wheat, T_4 and T_5 are wheat temperatures before and after the drying process respectively.

The specific heat of wheat kernel offered by Kazarian and Hall [101] can be used:

$$C_{p_{wheat}} = 1398.3 + 4090.2\left(\frac{M_P}{1+M_P}\right) \tag{3.10}$$

Where, M_p refers to moisture content of wheat on a dry basis (kg water/kg solid), and $M_P = (\frac{W_4 - W_5}{W_5})$. W_4 refers to pre-drying weight, and W_5 refers to post-drying weight. Another equation is used to find the weight of the material after the drying process as follows [2]:

$$W_5 = W_4 - \left[W_4 \frac{(MC_4 - MC_5)}{100 - MC_5}\right] \tag{3.11}$$

Where MC_4 and MC_5 are moisture contents of the product on wet basis at states 4 and 5, respectively.

3.3.1.1 Fan Power Calculation

Fresh air is firstly is taken from atmosphere by a fan and is heated by the heat pump condenser, then sent to the dryer unit to evaporate water from the moist wheat. The fan is necessary for this operation. Pressure loss should be firstly calculated to find the energy requirement of the fan. For that reason, pressure loss of the air flowing over an air-cooled condenser is calculated. In the condenser, there may be heat transfer with three phases, which are desuperheating, condensing, and subcooling [102]. The condenser heat transfer area is:

$$\dot{Q}_H = U_o A_o \Delta T_{ln} \tag{3.12}$$

$$A_o = \frac{\dot{Q}_H}{U_o \Delta T_{ln}} \tag{3.13}$$

Where U_o is the overall heat transfer coefficient of the condenser. It is necessary to find overall heat transfer coefficients for refrigerant and air sides to obtain heat transfer area of the air cooled condenser.

The heat exchanger geometry is given in Table 3.3. There are two surface areas for the air-cooled condenser; desuperheated and condensation area.

$$A_o = A_{desup} + A_{cond} \tag{3.14}$$

The overall heat transfer coefficient, U_o is a function of air side, tube conductance, and refrigerant side resistances [103]:

$$\frac{1}{U_o} = \frac{1}{h_i\left(\frac{A_i}{A_o}\right)} + \frac{D_i \, ln\left(\frac{r_o}{r_i}\right)}{2k_w\left(\frac{A_i}{A_o}\right)} + \frac{1}{h_o \eta_o} \tag{3.15}$$

where D_i, D_o, r_i, r_o ,h_i, h_o, k_w and η_o are the inner and outer diameters, inner and outer radii of tubes, heat transfer coefficients of air and refrigerant, thermal conductivity of tubes wall, and overall surface effectiveness of air side, respectively.

$$\frac{A_i}{A_o} = \frac{D_i}{D_o}\left(1 - \frac{A_f}{A_o}\right) \tag{3.16}$$

$$\eta_o = \left[1 - \left(1 - \eta_f\right)\frac{A_f}{A_o}\right] \tag{3.17}$$

Where A_f is fin area, and η_f is fin efficiency. To evaluate efficiency for a rectangular fin, the following equations are used:

$$\eta_f = \frac{tanh\, ml}{ml} \tag{3.18}$$

$$m = \sqrt{\frac{2h_o}{k_f \delta_f}} \tag{3.19}$$

Where$l$, k_f, δ_f are length, thermal conductivity, and thickness of the fin respectively. Equation (3.15) may be applied to the air and refrigerant sides to find the U_o value for the condenser [104]. Accordingly, the outside area for the condenser is calculated at minimum temperature of Gaziantep city. The correlation obtained by Icropera and De Witt [105] is used for single-phase in the superheated and subcooled regions.

$$Nu_D = \frac{\left(\frac{f}{8}\right)\cdot(Re_D-1000)\cdot Pr}{1+12.7\left(\frac{f}{8}\right)^{0.5}\cdot\left(Pr^{\frac{2}{3}}-1\right)} \tag{3.20}$$

Where f is the friction factor, and it is calculated for smooth tubes by using the relation [105]:

$$f = (0.79\ lnRe_D - 1.64)^{-2} \tag{3.21}$$

Equation (3.21) is valid for $0.5 < \mathrm{Pr} < 2000$ and $10^4 < \mathrm{Re_D} < 5 \times 10^6$. There are many correlations in literature that can be used to find the condensation heat transfer coefficient. Correlation obtained by Akers et al. [106] is used in this work to find the condensation heat transfer coefficient in the tubes. They assumed complete condensation and used modified Reynolds number $\mathrm{Re_m}$. Local convection coefficient was given by [106]:

$$\frac{h_i(x)D_i}{K_L} = C\ Re_m^n\ Pr_L^{\frac{1}{3}} \tag{3.22}$$

The equivalent Reynolds number for two-phase flow $\mathrm{Re_e}$ is determined by using the following equations given in [106]:

$$Re_m = Re_e\left[1+\left(\frac{\rho_L}{\rho_G}\right)^{\frac{1}{2}}\right] = \frac{\dot{m}_e D_i}{\mu_L}\left[1+\left(\frac{\rho_L}{\rho_G}\right)^{\frac{1}{2}}\right] \tag{3.23}$$

$$\dot{m}_e = \dot{m}\left[(1-x_v)+x_v\left(\frac{\rho_L}{\rho_G}\right)^{\frac{1}{2}}\right] \tag{3.24}$$

The equivalent mass velocity is given as:

$$\dot{m} = \frac{\dot{M}}{\frac{\pi D_i^2}{4}} \tag{3.25}$$

Where $\dot{\mathrm{M}}$ is the mass flow rate of the working fluid. The empirical parameters C and n are:

$$\mathrm{C} = 0.0265, \quad \text{and } \mathrm{n} = 0.8 \text{ for } \mathrm{Re_e} > 50{,}000$$

$$C = 5.03, a \quad nd\ n = \frac{1}{3}\ for\ \ Re_e < 50{,}000$$

The heat transfer coefficient for air can be evaluated as:

$$\dot{Q}_H = \dot{m}_a c_{p_a} \Delta T \tag{3.26}$$

$$\dot{m}_a = \dot{V}_a\, \rho_a \tag{3.27}$$

$$\Delta T = T_2 - T_1(t) \tag{3.28}$$

$$V_{max} A_c \rho_a = V_{fr} A_{fr} \rho_a \tag{3.29}$$

$$\sigma = \frac{A_c}{A_{fr}} \tag{3.30}$$

$$V_{max} = \frac{V_{fr}}{\sigma} \tag{3.31}$$

where V_{fr} is front velocity, and should be selected carefully, $\dot{V}_a$ is volumetric flow rate for air, T_2 is the air temperature before drying, A_c and A_{fr} are free flow area, and frontal area for condenser respectively, V_{max} is the maximum velocity in free flow area.

$$G = \frac{\dot{m}_a}{A_c} = \rho_a V_{max} \tag{3.32}$$

$$Re_a = \frac{G \cdot D_h}{\mu_a} = \frac{V_{max} \rho_a D_h}{\mu_a} \tag{3.33}$$

$$Nu_a = \frac{h_o D_h}{k_a} \tag{3.34}$$

$$Pr_a = \frac{C_{p_a} \mu_a}{k_a} \tag{3.35}$$

$$Nu_a = 0.117\, Re_a^{0.65}\, Pr_a^{\frac{1}{3}} \tag{3.36}$$

where Re_a, Pr_a, Nu_a are Reynolds, Prandtl, Nusselt number of the air respectively, D_h is flow passage hydraulic diameter, and G is mass velocity of air. By neglecting entrance and exit losses, the pressure drop across the condenser for air side is computed [103],

$$\Delta P = G^2 \cdot \frac{v_1}{2} \left[(1 + \sigma^2) \left(\frac{v_2}{v_1} - 1 \right) + f_{cf} \cdot \frac{A_o}{A_c} \cdot \frac{v_m}{v_1} \right] \tag{3.37}$$

$$j_H = S_t \cdot Pr_{\mathrm{a}}^{\frac{2}{3}} \tag{3.38}$$

$$St = \frac{j_H}{Pr_a^{\frac{2}{3}}} \tag{3.39}$$

$$St = \frac{Nu_a}{Pr_a \cdot Re_a} = \frac{h_o}{G \cdot c_{p_a}} \tag{3.40}$$

where v_1 and v_2 are specific volumes of air before and after drying respectively, v_m is average specific volume for air, j_H and St are Calburn factor, and Stanton number respectively. j_H and f_{cf} are estimated from a figure adopted by Kays and London [103]. f_{cf} is used to find the air side pressure drop for the compact tube-fin heat exchanger. The hourly power input to the fan for the air cooled condenser can be calculated by:

$$\dot{W}_{fan}(t) = \Delta P(t)\, \dot{V}_a(t) \tag{3.41}$$

3.3.2 Modeling of the Heat Pump

Heat pumps are devices which extract heat from a source at low temperature, and transfer it to a hotter sink [99]. In the drying system, ground source heat pump extracts heat from ground, and uses for fresh air heating via heat pump condenser. The condenser heat load may be expressed as:

$$\dot{Q}_H(t) = (UA)_{he}[T_h(t) - T_c] \tag{3.42}$$

where $\mathrm{(UA)_{he}}$ and $\mathrm{T_h(t)}$ are the product of overall heat transfer and condenser area, and condenser temperature, and $\mathrm{T_c}$ represents the average of minimum air temperature entering and leaving condenser, $\mathrm{T_c} = (T_o + T_2)/2$.

The heat absorbed by the drying air is given as;

$$\dot{Q}_H(t) = \dot{m}_a C_{p_a}[T_2 - T_a(t)] \tag{3.43}$$

The heated air is used to dry the moist wheat or to evaporate the water present in the wheat, which is the dryer unit chamber. Therefore, energy requirement of the dryer unit can be expressed as;

$$\dot{Q}_H(t) = \dot{m}_p\, C_{pw}\, (T_5 - T_4) + \dot{m}_w\, h_{fg} \tag{3.44}$$

COP and COPs, work consumption of the compressor, and Specific Moisture Evaporation Rate (SMER) are very important for the heat pump drying system as they may serve as indicators for system performance. Therefore, expressions related with these parameters should be obtained. COP may be given as a function of Carnot efficiency, η_c:

$$COP = \eta_c \left(\frac{T_h(t)}{T_h(t) - T_w(t)}\right) \tag{3.45}$$

Then, Equations (3.42) and (3.43) can be combined, and solved for T_h as the following:

$$\frac{\dot{Q}_H(t)}{\dot{Q}_H(t)} = \frac{(UA)_{he}(T_h(t) - T_c)}{\dot{m}_a C_{p_a}(T_2 - T_a(t))} \tag{3.46}$$

The above equation can be simplified as follows:

$$u = \frac{(UA)_{he}}{\dot{m}_a C_{p_a}} = \frac{T_2 - T_a(t)}{T_h(t) - T_c} \tag{3.47}$$

where T_c in Eq. (3.42) can be calculated as follows:

$$T_c = \frac{T_2 + T_o}{2} = \frac{60 + (-9)}{2} = 25.5 \text{ °C} \tag{3.48}$$

and u value is calculated for the design conditions of the drying system for Gaziantep city, Turkey, as;

$$u = \frac{60 - (-9)}{66 - 25.5} = 1.7 \tag{3.49}$$

Then, $T_h(t)$ can be written in a simplified expression form as follows:

$$T_h(t) - T_c = \frac{T_2 - T_a(t)}{u} \tag{3.50}$$

$$T_h(t) = \frac{T_2 - T_a(t)}{u} + T_c \tag{3.51}$$

Combining Eq. (3.51) with Eq. (3.45) gives heat pump COP as below:

$$COP = \eta_c \left(\frac{\left(\frac{T_2 - T_a(t)}{u} + T_c\right)}{\left(\frac{T_2 - T_a(t)}{u} + T_c\right) - T_w(t)}\right) \tag{3.52}$$

Equation (3.52) can be simplified to the following expression form:

$$COP = \eta_c \left(\frac{T_2 - T_a(t) + uT_c}{T_2 - T_a(t) + uT_c - uT_w(t)}\right) \tag{3.53}$$

The following dimensionless forms can be used to simplify and find the final forms of COP and dimensionless compressor work, *w*, as follows:

$$\phi_2 = \frac{T_2 - T_\infty}{T_\infty}\ ,\ \phi_c = \frac{T_c - T_\infty}{T_\infty}\ ,\ \phi_a(t) = \frac{T_a(t) - T_\infty}{T_\infty}\ ,\ \phi_w(t) = \frac{T_w(t) - T_\infty}{T_\infty} \tag{3.54}$$

From Eq. (54) the values of T_2, T_c, $T_a(t)$, and $T_w(t)$ can be found in the dimensionless forms:

$$T_2 = \phi_2 T_\infty + T_\infty\ ,\ \ T_c = \phi_c T_\infty + T_\infty\ ,\ \ T_a = \phi_a T_\infty + T_\infty\ ,\ T_w = \phi_w T_\infty + T_\infty \quad (3.55)$$

Then, combining Equations (3.55) and (3.53) gives the following:

$$COP = \eta_c \left(\frac{\phi_2 T_\infty + T_\infty - [\phi_a(t) T_\infty + T_\infty] + u[\phi_c T_\infty + T_\infty]}{\phi_2 T_\infty + T_\infty - [\phi_a(t) T_\infty + T_\infty] + u[\phi_c T_\infty + T_\infty] - u[\phi_w(t) T_\infty + T_\infty]} \right) \quad (3.56)$$

Equation (3.56) can be simplified to easy form:

$$COP = \eta_c \left(\frac{u(\phi_c + 1) + \phi_2 - \phi_a(\tau)}{u\phi_c + \phi_2 - \phi_a(\tau) - u\phi_w(\tau)} \right) \quad (3.57)$$

where ϕ_c, ϕ_a, ϕ_2 and ϕ_w are dimensionless average air temperatures before and after condenser, ambient air temperature, air temperature pre-dryer, and water temperature in the TES tank respectively.

The following steps have been followed to obtain the formula of dimensionless compressor work, *w*, that is used in the analysis:

$$\dot{W}(t) = \frac{\dot{Q}_H(t)}{COP} \quad (3.58)$$

Equation (3.58) is represents the general form of heat pump COP in the case of desired output is the heating load. Substituting the condenser load formula Eq. (3.43) in the above equation gives the following form:

$$\dot{W}(t) = \frac{\left[\dot{m}_a C_{p_a}(T_2 - T_a(t))\right]}{COP} \quad (3.59)$$

The compressor work input formula in Eq. (3.59) can be transferred to dimensionless form, *w*, by inserting Eq. (3.57) in, as follows:

$$w = \frac{\dot{W}(t)}{\dot{m}_a C_{p_a} T_\infty} = \frac{(\emptyset_2 - \emptyset_a(\tau))}{\eta_c \left(\frac{u(\phi_c + 1) + \phi_2 - \phi_a(\tau)}{u\phi_c + \phi_2 - \phi_a(\tau) - u\phi_w(\tau)} \right)} \quad (3.60)$$

$$w(\tau) = \frac{[\phi_2 - \phi_a(\tau)][\, u\phi_c + \phi_2 - \phi_a(\tau) - u\phi_w(\tau)]}{\eta_c [u(\phi_c + 1) + \phi_2 - \phi_a(\tau)]} \quad (3.61)$$

COPs can be expressed as;

$$\mathrm{COP_s} = \frac{\dot{Q}_H(t)}{W_c(t) + W_f(t)} \quad (3.62)$$

For a drying system, the most suitable efficiency parameter is the Specific Moisture Evaporation Rate (SMER) [107], which is defined as the energy needed to take away 1 kg of water [100]. So, SMER is recorded as the heat pump dryer efficiency.

$$SMER = \frac{\dot{m}_w}{E_{in}} = \frac{\dot{m}_w}{\dot{W}_c(t)+\dot{W}_f} \quad (3.63)$$

Where E_{in}, $\dot{W}_c(t)$, and $\dot{W}_f$ are the total energy, hourly compressor work, and hourly fan power input to the ground heat pump drying system, respectively.

3.3.3 Solution of TES Tank Problem

TES tank is the drying system heart since solar energy will be stored in the tank during all seasons. The stored energy will be extracted and transferred to the drying air by the heat pump. At the same time, soil surrounding the tank is used as a storage medium. Therefore, the problem of the unsteady heat transfer by conduction around the tank should be solved to express the water temperature variation in the tank as a function of solar energy, condenser load and compressor work.

The selected TES tank located deep under earth is spherical. The water present in the TES tank is considered fully-mixed, and its temperature, $T_w(t)$, will change with respect to time, The water temperature is considered to be equal to the deep earth temperature T_∞ at initial time. It is assumed that the earth around the tank is homogeneous and thermally stable. Schematic representations of the TES tank and energy balance are shown in Figure 3.3.

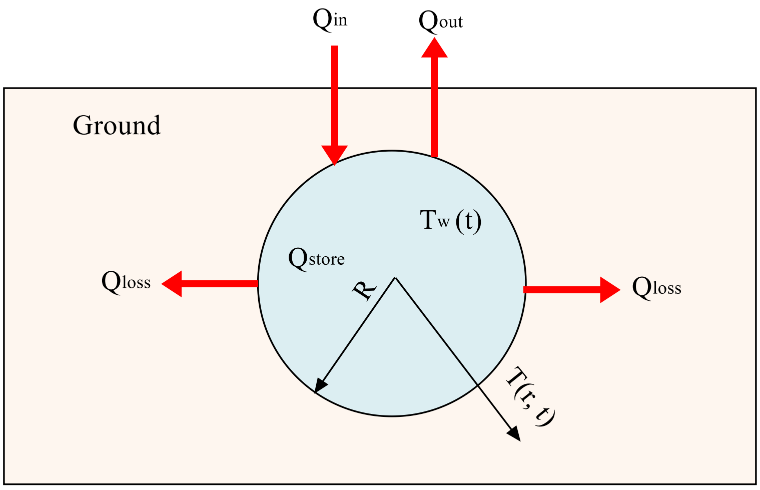

Figure 3.3 Schematic of the underground TES tank problem (1st model).

Unsteady heat transfer problem around the tank for a spherical coordinate is given by the following equations:

$$\frac{\partial^2 T}{\partial r^2} + \frac{2}{r}\frac{\partial T}{\partial r} = \frac{1}{\alpha}\frac{\partial T}{\partial t} \quad (3.64)$$

$$T(R,t) = T_w(t) \tag{3.65}$$

$$T(\infty,t) = T_\infty \tag{3.66}$$

$$T(r,0) = T_\infty \tag{3.67}$$

Some of the energy is charged to the storage tank as sensible heat

Some of the energy charged to the tank is stored in the tank as sensible heat, and the remaining will be transferred to the soil surrounding the tank by conduction heat loss. The energy balance for TES tank can be expressed as:

$$Q = \rho_w c_w V_w \frac{dT_w}{dt} - kA\frac{\partial T}{\partial r}(R,t) \tag{3.68}$$

Where V_w, ρ_w and c_w are volume, density and specific heat of the water in the tank. R, A and k are radius, surface area of the tank, and soil thermal conductivity.

The unsteady heat transfer by conduction expressed by Equations (3.64) - (3.68) has been converted into dimensionless equations as follows:

$$x = \frac{r}{R} \quad , \qquad \tau = \frac{\alpha t}{R^2} \ , \qquad q = \frac{Q}{4\pi RkT_\infty} \ , \qquad P = \frac{\rho_w c_w}{3\rho c} \ , \qquad \emptyset = \frac{T - T_\infty}{T_\infty} \ ,$$

$$\emptyset_w = \frac{T_w - T_\infty}{T_\infty}, \qquad \emptyset_a = \frac{T_a - T_\infty}{T_\infty} \tag{3.69}$$

Where *q is* the rate of net energy charging to the tank, ϕ is dimensionless temperature, τ is dimensionless time, *x* is the dimensionless radial distance, c is soil specific heat, ρ is soil density, and w represents water. When these equations were substituted in the problem raised in Eq. (3.64) - (3.68), the following formulations may be obtained:

$$\frac{\partial^2 \emptyset}{\partial x^2} + \frac{2}{x}\frac{\partial \emptyset}{\partial x} = \frac{\partial \emptyset}{\emptyset \tau} \tag{3.70}$$

$$\emptyset(x,\tau) = \emptyset_w(\tau) \tag{3.71}$$

$$\emptyset(\infty,\tau) = 0 \tag{3.72}$$

$$T(x,0) = 0 \tag{3.73}$$

$$q = P\frac{d\emptyset_w}{d\tau} - \frac{\partial \emptyset}{\partial x}(1,\tau) \tag{3.74}$$

This problem can be simplified using the transformation below:

$$\psi(x,\tau) = x\emptyset(x,\tau) \tag{3.75}$$

yielding:

$$\frac{\partial^2\psi}{\partial x^2} = \frac{\partial\psi}{\partial\tau} \tag{3.76}$$

$$\psi(1,\tau) = \emptyset_w(\tau) \tag{3.77}$$

$$\psi(\infty,\tau) = 0 \tag{3.78}$$

$$\psi(x,0) = 0 \tag{3.79}$$

$$q = p\frac{d\emptyset_w}{d\tau} - \frac{\partial\emptyset}{\partial x}(1,\tau) \tag{3.80}$$

Appling the following transformation $\boldsymbol{\eta}$

$$\eta = \frac{x-1}{2\sqrt{\tau}} \tag{3.81}$$

to the problem, a solution of constant $\emptyset$ can be obtained as:

$$\psi(x,\tau) = \emptyset_0\left[1 - erf\left(\frac{x-1}{2\sqrt{\tau}}\right)\right] \tag{3.82}$$

Unsteady temperature distribution in the earth around the TES tank is acquired using Duhamel's superposition technique as follows:

$$\psi(x,\tau) = \emptyset_w(0)\left\{1 - erf\left(\frac{x-1}{2\sqrt{\tau}}\right)\right\} + \int_0^\tau \frac{d\emptyset_w(\xi)}{d\xi}\left\{1 - erf\left(\frac{x-1}{2\sqrt{\tau}}\right)\right\}d\xi \tag{3.83}$$

Now, differentiation of $\emptyset$ with respect to x at x=1, and using Eq. (3.80) gives the following equation:

$$q = P\frac{d\emptyset_w}{d\tau} + \emptyset_w(\tau) + \int_0^\tau \frac{d\emptyset_w(\xi)}{d\xi}\frac{d\xi}{\sqrt{\pi(\tau-\xi)}} \tag{3.84}$$

Equation (3.84) can be discretized and solved for the water temperature in the tank in dimensionless form at the nth time increment to yield:

$$\phi_w(\tau_n) = \frac{q(\tau_n)+\left[\frac{P}{\Delta\tau}+\frac{1}{\sqrt{\pi\Delta\tau}}\right]\emptyset_w(\tau_{n-1})-\sum_{i=1}^{n-2}\frac{\emptyset_w(\tau_{i+1})-\emptyset_w(\tau_i)}{\sqrt{\pi\Delta\tau(n-i)}}}{1+\frac{P}{\Delta\tau}+\frac{1}{\sqrt{\pi\Delta\tau}}} \tag{3.85}$$

Equation (3.85) is used to find the hourly dimensionless water temperature. The term $q(\tau)$ in Eq. (3.85) refers to the net dimensionless heat input rate to the tank [71].The input heat rate, $q(\tau)$, is the difference between dimensionless useful solar energy and heat pump evaporator energy. It was expressed in [71, 108] as:

$$q(\tau) = q_u(\tau) - q_H(\tau) + \frac{w(\tau)}{\gamma} \tag{3.86}$$

Where $w(\tau)$ is dimensionless work input of compressor, γ is a dimensionless parameter obtained as $(4\pi Rk/\dot{m}_a(t)\, C_{p_a})$, $q_H(\tau)$ is dimensionless heat supplied by condenser for drying unit, and $q_u(\tau)$ is the useful solar energy rate in dimensionless form charged to the tank.

3.3.4 Flat Plate Solar Collectors

Solar collectors are used to absorb solar energy and to charge it to the tank. The solar energy charge rate, $\dot{Q}_u(t)$ is given by Duffie and Beckman [109] as;

$$\dot{Q}_u(t) = \eta_{fc}(t)\, A_{col}\, I_T(t) \tag{3.87}$$

Where η_{fc} is the collector efficiency, and A_{col} is the collector area. The following experimental correlation was obtained by [61] and is also used in the present study:

$$\eta_{fc}(t) = 0.72 - 6.4\left[\frac{T_w(t)-T_a(t)}{I_T(t)}\right] \tag{3.88}$$

Where $T_w(t)$ is the water temperature in the TES tank and $T_a(t)$ is the ambient air temperature. $I_T(t)$ in Equations (3.87-3.88) is the hourly solar radiation coming to the collector surface. Calculation procedure for finding $I_T(t)$ is given by Duffie and Beckman in [109] as follows:

$$I_T(t) = \dot{R} I(t) \tag{3.89}$$

Where $\dot{R}$ is the ratio of total radiation and can be calculated as [109]:

$$\dot{R} = \left(1 - \frac{I_d(t)}{I(t)}\right) R_b + \frac{I_d(t)}{I(t)}\left(\frac{1+\cos\beta}{2}\right) + \rho_{ref}\left(\frac{1-\cos\beta}{2}\right) \tag{3.90}$$

Calculation procedures for ratios $I_d(t)/I(t)$ and R_b are given by [109] as follows:

$$\frac{I_d(t)}{I(t)} = \begin{cases} 1.0 - 0.249k_T & for\ k_t \le 0.35 \\ 1.557 - 1.84k_T & for\ 0.35 < k_T \le 0.75 \\ 0.17 & for\ k_T > 0.75 \end{cases} \tag{3.91}$$

Where the hourly clearness index K_T can be defined

$$K_T = \frac{I}{I_0} \tag{3.92}$$

and I_0 is calculated as follows:

$$I_0 = \left[43200\frac{Gs}{\pi}\right] \times \left[1 + \frac{0.033 \times cos(2\pi n)}{365}\right] \times [cos\,\delta(sin w_2 - sin\, w_1) + (w_2 - w_1)\, sin\,\emptyset\, sin\,\delta] \tag{3.93}$$

R_b ratio can be calculated as in the following correlation:

$$R_b = \frac{[\cos(\emptyset-\beta)\cos\delta\cos w_1 + \sin(\emptyset-\beta)\sin\delta]}{[\cos\emptyset\cos\delta\cos w_1 + \sin\emptyset\sin\delta]} \tag{3.94}$$

The declination δ is calculated as in [116]:

$$\delta = 23.45\sin\left[360\,\frac{284+n_d}{365}\right] \tag{3.95}$$

$$w_1 = (t-12)\times 15 \tag{3.96}$$

$$w_2 = (t-11)\times 15 \tag{3.97}$$

$$W = \frac{w_1+w_2}{2} \tag{3.98}$$

where w_1 is hour angle of the midpoint of the hour

3.4 Input Data for the SAHP Drying System with TES Tank (Case 1)

A computer code in MATLAB has been developed for numerical calculations. In this section, the main input data for finding performance parameters for the drying system are outlined. The input data are for dryer unit, heat pump, TES tank, ground around the tank, and solar collectors. The data and information for the main components of the drying system are given in the following subsections.

Energy requirement of the dryer unit is necessary throughout all seasons on an hourly basis. Mass flow rate of the wet wheat is selected basically as 50 kg h^{-1}, which can be changed to find its effect on drying system performance. The inlet air temperature to dryer unit, T_2, and outside design air temperature for Gaziantep, T_o, are set as 60 ℃ depending on [110, 111] and -9 ℃, respectively. For design conditions, “u” value in Eq. (3.47) is 1.7. Ambient air temperature, $T_a(t)$, is heated up by the heat pump condenser to reach the design temperature (60 ºC), and is blown to the dryer unit by a fan to evaporate water existing in the wheat. The wet wheat temperature, T_4, and drying wheat temperature, T_5, are taken as 25 ℃ and 50 ℃, respectively. Moisture contents of moist wheat, MC_4, and drying wheat, MC_5, have been considered as 30% and 0% respectively, according to Sundaram et al. [110]**.** Hourly humidity ratio has been evaluated by using EES (Engineering Equation Solver) program depending on hourly ambient air temperature for Gaziantep at atmospheric pressure, while relative humidity of 30% is taken in this study based on [112, 113]. Pressure drop through the drying unit is neglected since it is very low in relation to the compressor work. EES program is also used to calculate hourly power input to the blower or fan.

Heat is absorbed by the heat pump evaporator from the underground TES tank, and some amount of energy is added to the refrigerant via the compressor. Heat is rejected to drying air to evaporate water in the wheat. Expressions for energy requirement and the heat pump COP are derived in Section 3.3. A practically reasonable Carnot efficiency (CE) value was used basically as 0.4 in the present study. Zogou and Stamatelos [36] expressed that CE values range between 0.30 and 0.50 for small electric heat pumps, so accordingly three CE values of 0.30, 0.40 and 0.50 were considered in this study. In the present study, the CE value was set at 0.4, and tank volume was set at 300 m^3 for all calculations unless stated otherwise.

Water in the TES tank is assumed to be fully mixed. Specific heat and density of the water are 4.18 kJ/kg°C, and 1000 kg/m^3, respectively. Temperature of the water at the beginning of operation is taken as equal to deep earth temperature of 15 ^oC. Solar energy is charged to the water if there is useful solar energy during the year. Some of the stored energy is absorbed by the heat pump, some is lost to the earth surrounding the tank, and the remaining part is stored as sensible heat in the TES tank. In this study, limestone is basically considered as an earth surrounding the tank since it is the prevalent geo-structure of Gaziantep. To investigate the effects of the earth type on the system performance, three types of soil are considered; limestone, granite and coarse graveled. Thermophysical properties of the earths (soils) are given in Ozisik [114], and illustrated in Table 3.4. Tank volume is selected as 300 m^3 in all calculations unless stated otherwise.

Table 3.1 Basic input parameters for case 1

Parameter item	Value
Wheat temperature at inlet, T_4 (°C)	25
Wheat temperature at outlet, T_5 (°C)	50
Wheat mass flow rate (kg/h)	50
Drying air temperature T_2 (°C)	60
Outside design temperature T_o (°C)	-9
Moisture content at inlet MC_4 (%)	30
Moisture content at outlet MC_5 (%)	0
Carnot efficiency CE (%)	40
Ground temperature, T_∞ (°C)	15
Tank volume (m^3)	300
Collector area (m^2)	70
Relative humidity, φ_a (%)	30

In this study, solar collectors are used to collect useful solar energy in TES tank. They are assumed to be directed toward the south, and their tilt angle is taken as latitude angle (37.1°N) of Gaziantep, Turkey since the highest solar energy is collected when the slope angle is equal to the latitude angle for yearly operation [115]. Useful solar energy charge to the underground TES tank given by Eq. (3.87) is calculated by using Equations (3.88-3.98). Hourly solar radiation values and ambient air temperatures are used in the numerical calculations. The values of the hourly solar radiation on a horizontal surface I(t) and ambient air temperature $T_a(t)$ were taken from Gaziantep Meteorological Station. Effect of solar energy collection rate on performance of the drying system is investigated. During the calculations of the model, collector area as an input data is set as 70 m^2 if another collector area is not used.

3.5 Description of the Drying System (Case 2)

The SAHP drying system in this study is considered to be located in Gaziantep (37.1° N), Turkey. The scheme of the drying system is shown in Figure 3.4. The whole system consists of five subsystems, which are dryer unit, HRU, heat pump, underground TES tank, and flat-plate solar collectors. They will be explained in detail in the following subsections.

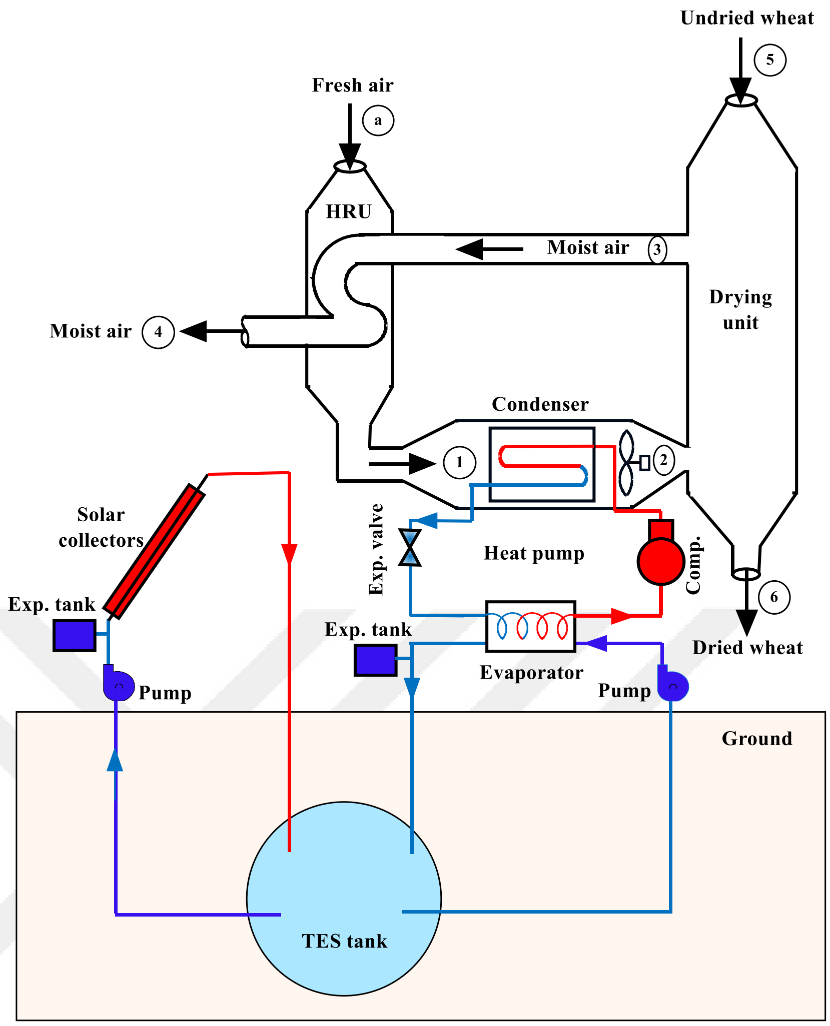

Figure 3.4 Schematic of the SAHP drying system with TES tank and HRU (2nd Case).

The dryer unit is the principal part of the SAHP drying system. The objective of the dryer unit is to evaporate undesired water in the wheat by supplying hot air in direct contact between hot air and wheat and releasing the evaporated water to the atmosphere. Wet product enters the dryer unit from the top, and moves slowly downward. At the same time, fresh air comes to the heating channel after passing through the heat recovery unit to gain the waste heat especially in the cold hours in winter, and to increase fresh air temperature. Later, the fresh air is heated more by the condenser, leaves the condenser pumped by a fan from bottom of the dryer unit, and finally moves toward the top of the unit by directly contacting with the product. During this process, undesired water present in the wheat is evaporated and transferred to the atmosphere with the air giving its energy to fresh air in the HRU.

A Heat Recovery Unit (HRU) is used in the drying system to gain an amount of waste energy and to reduce energy consumption of the drying system. The HRU is a type of heat exchanger that transfers heat from the hotter and moist air exhausted from the drying unit to fresh cold drying air. Since some of the wasted or exhausted heat will be absorbed by the fresh and cold air through the HRU, overall efficiency, COP, and SMER for the SAHP drying system increases or operation cost will decrease. Therefore, utilization of the HRU in the continuous SAHP drying system is one of the developments and originalities for this work.

Heat pump is an integral component of the drying system. It works as a heat transformer from the TES tank to the drier unit. It is known that heat pumps are energy efficient devices. GSHP are much more efficient than the air source heat pumps. Therefore, a GSHP is used in the present drying system. Utilizing this type of heat pump in the drying system can supply much more and cheaper energy to drying air than conventional drying systems, since the GSHP coupled with the TES tank supplies higher energy for less temperature fluctuations. As shown in Figure 3.4, there is a cycle between the heat pump evaporator and the TES tank, in which water is circulated through the cycle. The GSHP absorbs heat from the water in the cycle by the refrigerant flow through the evaporator of the heat pump cycle. The energy extracted and transferred by the compressor is rejected from the condenser of the heat pump to the drying air. The heat pump operates in order to evaporate water present in the wheat during all times of the year.

Solar energy is abundant in summer months. In summer, solar energy that has been deposited in underground TES tank for wheat drying is very useful especially in winter months. Flat-plate solar collectors have been considered for charging solar energy to the TES tank. Energy absorption is carried out by collectors, which is later stored in the TES tank throughout the entire year. Thus, water in the cycle between collectors and the TES tank will be circulated when there is useful solar energy.

The pivotal part of the drying system is the TES tank. Spherical tank is considered to store solar energy as sensible heat in the water present as a storage medium in the tank and is buried under the ground. The solar energy is stored by circulating water between solar collectors and the tank during all seasons and gives the stored energy to the drying unit during the whole year via the heat pump. Bigger volume is necessary for long-term storage of energy so that much more solar energy can be stored, and used particularly in low temperatures. Therefore, large-scale TES tank is used to collect more solar heat needed for the wheat drying process.

3.6 Mathematical Modeling of a SAHP Drying System with TES and HRU (Case 2)

The mathematical modeling of the drying system requires defining energy expressions or an energy model for each component of the system. These models are for the drying unit, ground coupled heat pump, underground TES tank, solar collectors, and HRU. Mathematical modeling will be obtained by combining these expressions. In this section, the expressions will be given in detail.

3.6.1 Drying Unit

The dryer unit is used to evaporate moisture from wet wheat. There are four main interactions; influx of drying air from condenser to drying chamber, exit of moist air after evaporation of moisture from the unit, input of wet wheat from top of the drier, and output of dried wheat with moisture lowered to the desired level. The schematic of the dryer unit is shown in Figure 3.5.

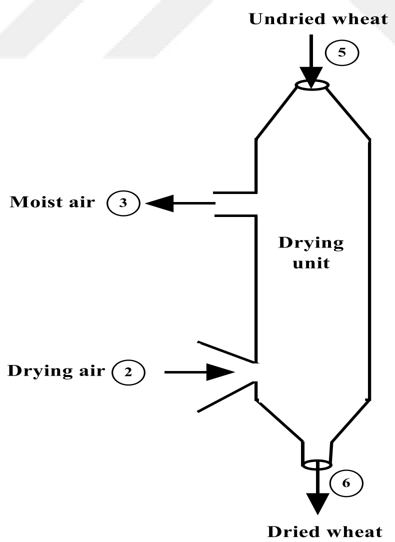

Figure 3.5 Schematic of the dryer unit.

Modeling details for the dryer unit is presented in previous case in this chapter, and only the subscript numbers for the symbols are changed from 4 and 5 to 5 and 6, respectively wherever found.

3.6.2 Heat Recovery Unit

Heat recovery unit device is a very important part of the drying system for energy saving, especially for ongoing the drying process in all seasons. The heat recovery unit (HRU) is used with ground source heat pump drying system to utilize waste heat from the drying chamber and increase fresh air temperature before entering the heat pump condenser. The scheme of the HRU is illustrated in Figure 3.6 Mass and energy balances may be formulated in this section to find a suitable model for the HRU.

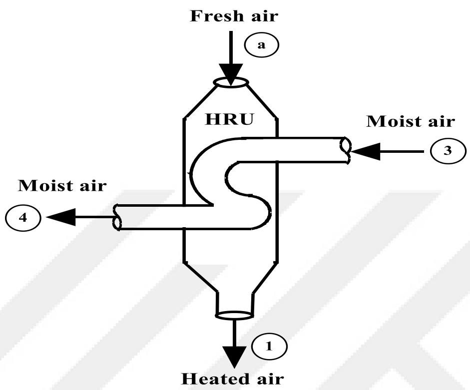

Figure 3.6 Schematic of Heat Recovery Unit (HRU).

Effectiveness (ε) is a dimensionless parameter which is defined as the ratio between actual heat transfer rates to maximum possible heat transfer rate from one stream to another [117]

$$\varepsilon = \frac{\text{Actual heat transfer rate}}{\text{Maximum possiable heat transfer rate}} = \frac{\dot{Q}}{\dot{Q}_{max}} \tag{3.99}$$

Energy balance for the HRU gives the actual heat transfer rate $\dot{Q}$ as follows:

$$\dot{Q} = \left(\dot{m}_a C_{p_a}\right)_{hot} (T_3 - T_4) = \left(\dot{m}_a C_{p_a}\right)_{cold} (T_1 - T_a) \tag{3.100}$$

The maximum possible heat transfer rate, $\dot{Q}_{max}$ is defined as

$$\dot{Q}_{max} = \left(\dot{m}_a C_{p_a}\right)_{min} (T_3 - T_a) \tag{3.101}$$

The value of $\left(\dot{m}_a \mathrm{C_{p_a}}\right)_{min}$ represents the minimum of $\left(\dot{m}_a \mathrm{C_{p_a}}\right)_{cold}$ and $\left(\dot{m}_a \mathrm{C_{p_a}}\right)_{hot}$ for cold and hot fluids.

Accordingly, the effectiveness can be expressed as follows:

$$\varepsilon = \frac{\left(\dot{m}_a \mathrm{C_{p_a}}\right)_{\mathrm{cold}} (T_1 - T_a)}{\left(\dot{m}_a \mathrm{C_{p_a}}\right)_{\mathrm{min}} (T_3 - T_a)} = \frac{\left(\dot{m}_a \mathrm{C_{p_a}}\right)_{\mathrm{hot}} (T_3 - T_4)}{\left(\dot{m}_a \mathrm{C_{p_a}}\right)_{\mathrm{min}} (T_3 - T_a)} \tag{3.102}$$

When the heat capacity for cold fluid $\left(\dot{m}_a C_{p_a}\right)_{cold}$ is equal to heat capacity for hot fluid $\left(\dot{m}_a C_{p_a}\right)_{hot}$, the effectiveness can be written as follows:

$$\varepsilon = \frac{(T_1 - T_a)}{(T_3 - T_a)} = \frac{(T_3 - T_4)}{(T_3 - T_a)} \tag{3.103}$$

Mass flow rate of air in the drying system can be calculated by using Eq. (3.2) as:

$$\dot{m}_a = \frac{\dot{m}_w}{(\omega_3 - \omega_2)} \tag{3.104}$$

The heat transfer rate from the heat pump condenser is determined as:

$$\dot{Q}_H(t) = \dot{m}_a C_{p_a}(T_2 - T_1(t)) \tag{3.105}$$

From effectiveness equation, the energy that recovered by HRU can be calculated as:

$$\dot{Q}_R(t) = \varepsilon \ (\dot{m}_a C_{p_a}) \ (T_3(t) - T_a(t)) \tag{3.106}$$

The total heat transfer rate in the drying system is computed as follows:

$$\dot{Q}_T = \dot{Q}_H + \dot{Q}_R \tag{3.107}$$

$$\dot{m}_a C_{p_a}(T_2 - T_a(t)) = \dot{m}_a C_{p_a}(T_2 - T_1(t)) + \varepsilon \, \dot{m}_a C_{p_a}(T_3(t) - T_a(t)) \tag{3.108}$$

The temperature of moist air discharged from the dryer unit is higher than that of the ambient air. The energy of moist air can be transferred to the cold drying air through the HRU. The energy saving for continuous heat pump drying system is very important and depends on recovered heat transfer rate by the HRU device from exhaust moist air [40]. Percentage of the energy saving by using HRU in the drying system can be determined as defined by [118]

$$E_S = \frac{\dot{Q}_R}{\dot{Q}_T} * 100 \tag{3.109}$$

As shown in Figure 3.4, a fan that is located after the condenser is used for blowing the drying air to the drying unit. Calculation procedure to find the pressure drop across the condenser for the air side is presented in section.

3.6.3 Modeling of the Heat Pump

Heat pumps are devices that extract heat from a source at low temperatures and transfer it to a hotter sink [99]. In the drying system, GSHP is used. The heat is extracted by GSHP via the heat pump evaporator, then the heat pump condenser supplies heat to cold drying air. The heat supplied by the condenser to the drying air can be written as a function of condenser temperature;

$$\dot{Q}_H(t) = (\mathrm{UA})_{\mathrm{he}}[T_h(t) - \mathrm{T_c}] \tag{3.110}$$

The heat absorbed by the drying air through the condenser can be calculated as follows:

$$\dot{Q}_H(t) = \dot{m}_a \mathrm{C_{p_a}}[\mathrm{T_2} - T_1(t)] \tag{3.111}$$

The heated air is used to dry the moist wheat or to evaporate the water present in the wheat. After heating of the drying air, it flows through the dryer unit. Then, the energy requirement of the dryer unit or the wheat and water can be expressed as;

$$\dot{\mathrm{Q}}_\mathrm{T} = \dot{\mathrm{m}}_\mathrm{p}\, \mathrm{C_{p_{wheat}}}(\mathrm{T_6} - \mathrm{T_5}) + \dot{\mathrm{m}}_\mathrm{w}\, \mathrm{h_{fg}} \tag{3.112}$$

COP and system COPs, work consumption of the compressor and Specific Moisture Evaporation Rate (SMER) are very important performance parameters for the SAHP drying system since they give information about whether the drying system operates efficiently or not. Therefore, expressions should be obtained related to these parameters. The COP may be given as a function of Carnot efficiency and it's given in Eq. (3.45) and mentioned here to build new model on:

$$COP = \eta_\mathrm{c}\left(\frac{T_h(t)}{T_h(t) - T_w(t)}\right) \tag{3.113}$$

Now, Equations (3.111) and (3.112) can be combined and solved for $\mathrm{T_h}$, then the result of $\mathrm{T_h}$ can be inserted in Eq. (3.113):

$$COP = \eta_\mathrm{c}\left(\frac{\mathrm{u}(\phi_\mathrm{c}+1)+\phi_2-\phi_1(\tau)}{\mathrm{u}\phi_\mathrm{c}+\phi_2-\phi_1(\tau)-\mathrm{u}\phi_w(\tau)}\right) \tag{3.114}$$

Where (u) in Eq. (3.114) is a parameter obtained when equating the heat transfer Equations (3.111) and (3.112); ϕ_c, ϕ_1, ϕ_2 and ϕ_w are dimensionless average air temperatures before and after condenser, inlet air temperature to condenser, air temperature pre-dryer, and water temperature in the TES tank respectively:

$$\mathrm{u} = \frac{(\mathrm{UA})_{\mathrm{he}}}{\dot{m}_a \mathrm{C_{p_a}}} = \frac{\mathrm{T_2} - T_1(t)}{T_h(t) - \mathrm{T_c}} \tag{3.115}$$

By using the definition of COP for the heat pump, work requirement of the compressor for the heat pump is known as:

$$W_c(t) = \frac{\dot{Q}_H(t)}{COP} \tag{3.116}$$

When the Equations (3.111) and (3.114) are inserted into Eq. (3.116), the dimensionless work for the compressor, w, can be derived as below:

$$w(\tau)=\frac{[\phi_2-\phi_1(\tau)][\,u\phi_c+\phi_2-\phi_1(\tau)-u\phi_w(\tau)]}{\eta_c[u(\phi_c+1)+\phi_2-\phi_1(\tau)]} \tag{3.117}$$

COPs can be expressed as;

$$COP_s=\frac{\dot{Q}_H(t)}{W_T(t)}=\frac{\dot{Q}_H(t)}{W_c(t)+W_f(t)} \tag{3.118}$$

In a HPD system, the most important performance parameter is the Specific Moisture Evaporation Rate (SMER) [107]. It is defined as the energy needed to take away 1 kg of water [100] In other words, the SMER is defined as the heat pump dryer efficiency, which is;

$$SMER=\frac{\dot{m}_w}{W_T(t)}=\frac{\dot{m}_w}{W_c(t)+W_f\,(t)} \tag{3.119}$$

The most significant performance parameters for the SAHP drying system are the SMER, heat pump COP, and system COPS. Two relations between these performance parameters can be expressed since all three of them are functions of the compressor power. Then, when the $W_c(t)$ given in Equation (3.119) is inserted into Equation (3.116), the following equation will be obtained;

$$SMER=\frac{\dot{m}_w\,COP}{\dot{Q}_H+W_f\,COP} \tag{3.120}$$

$W_T(t)$ is composed of $W_c(t)$ and $W_f(t)$ given in Equation (3.119) and is inserted in Equation (3.118), then the SMER will be obtained as a function of the system COPs.

$$SMER=\frac{\dot{m}_w}{\dot{Q}_H}\cdot COP_s \tag{3.121}$$

3.6.4 Solution of TES Tank Problem

TES tank is the main component of the drying system since solar energy will be stored in the tank during all seasons. The stored energy will be extracted and transferred to drying air by the heat pump. The selected TES tank located in deep earth is spherical. The water present in TES tank is considered fully-mixed and its temperature will change with respect to time, $T_w(t)$. It is assumed that the earth around the tank is homogeneous and thermally stable. Calculation procedures for solving unsteady conduction heat transfer problem around the TES tank presented in First Case in detail.

3.6.5 Flat Plate Solar Collectors

It has been considered that solar collectors are utilized for collecting solar energy and storing it in the tank. Calculation procedures for finding hourly charge rate, $\dot{Q}_u(t)$ and others parameters is presented in Case One in this chapter.

3.7 Input Data for the SAHP Drying System with TES tank and HRU (Case 2)

A computer code in MATLAB has been developed for numerical calculations. In this section, the main input data for finding performance parameters of water temperature, COP, COPs, SMER and energy fractions for the SAHP drying system are outlined. The input data belongs to the drier unit, heat pump, TES tank and ground around the tank, solar collectors, and HRU. The data for the main components of the drying system are given in the following subsections.

Energy requirement of the dryer unit is necessary throughout all seasons on an hourly basis. Mass flow rate of the wet wheat is selected as 100 kg h^{-1} unless another mass flow rate is used in the calculations. However, it can be changed to find effect of mass flow rate on the performance of the drying system. The inlet air temperature to dryer unit, T_2 and outside design air temperature for Gaziantep, T_o are used as 60 ℃ and -9 ℃, respectively. For the design conditions, the "u" value in Eq. (30) is calculated as 1.7. Ambient air at a temperature of $T_a(t)$ is heated up to design temperature of 60 ºC by the heat pump condenser and is blown to the dryer unit by a fan to evaporate water existing in the wheat. The undried wheat temperature, T_5 and dried wheat temperature T_6 are taken as 25 ℃ and 50 ℃, respectively. Moisture contents of undried wheat (MC_5) and dried wheat (MC_6) have been considered as 30% and 10% respectively, according to [2, 110]. Hourly humidity ratios have been evaluated by using EES (Engineering Equation Solver) program depending on hourly ambient air temperature for Gaziantep, for atmospheric pressure and relative humidity of 30% depending on [112-113]. The hourly power input to the blower or fan has been calculated by using EES program as well.

Heat is absorbed by the refrigerant flowing through the heat pump evaporator from the underground TES tank, and some amount of energy is added to the refrigerant by the compressor. Heat is rejected from the condenser of the heat pump to the drying air to evaporate water in the wheat. The heat pump is operated until the drying air temperature reaches 60 ºC. Correlations for energy demand and heat pump COP have been derived in Section 3.4. Carnot efficiency, CE, is the ratio of COP of heat pump to COP of Carnot. Actual COP relies on heat source and sink temperature of the heat pump. It also relies on the type and size of the actual heat pump. Carnot Efficiency (CE) values for small electric heat pumps have been expressed in the range of 0.30 to 0.50 [36]. Therefore, according to this reference, a CE value of as 0.4 used for all numerical calculations in the present study.

Water present in the TES tank was has been considered homogeneous. Specific heat and density of the water are 4.18 kJ $kg^{-1}°C^{-1}$ and 1000 kg m^{-3}, respectively. Temperature of the water at the beginning of operation is taken as equal to the deep earth temperature of 15 °C. Solar energy is charged to the water if there is useful solar energy during entire year. Some of the stored energy is absorbed by the heat pump, some is lost to the surrounding earth of the tank, and the remaining part is stored as sensible heat in the TES tank. To explore the impact of the earth type on system functioning, three types of earth are considered; limestone, granite and coarse graveled. Once other types of earth are not used in the calculations, limestone is considered as an earth surrounding the tank. Thermophysical properties of the earth types are given in [114], and illustrated in Table 3.4. Another input parameter is radius or volume of the TES tank, which affect performance parameters. Tank volume is selected as 300 m^3 in all calculations unless mentioned otherwise.

In this study, flat plate solar collectors are employed for collecting useful solar energy to the TES tank. They are assumed to be directed toward the south, and their tilt angle is taken as the latitude angle (37.1°N) of Gaziantep, Turkey because, the highest solar energy is collected when the slope angle is equal to the latitude angle for yearly operation [115]. Useful solar energy charge to the underground TES tank given by Eq. (3.87) is calculated by using Equations (3.88-3.98).

Useful solar energy that has been deposited in the underground TES tank given by Eq. (3.87) is calculated using Equations (3.88-3.98). Hourly solar energy values and ambient air temperatures are used in the numerical calculations. Hourly solar radiation readings on the horizontal surface and ambient air temperature were taken from Gaziantep Meteorological Station. Effect of solar energy collection rate will be investigated on performance of the drying system. The collection rate depends on the solar collector area. In the numerical calculations, collector area as an input data is used as 100 m^2 if another collector area is not used. Energy saving is very important for drying systems since the gain of waste energy increases performance parameters of the drying system. Therefore, Heat Recovery Unit (HRU) is proposed in this SAHP drying system. Some of the waste energy exhausted from the drying unit is gained by using the HRU. Equations (3.99-3.108) for the HRU can be solved together by considering some assumptions ($\varphi_3 = 60\%,\ T_{wb,3} = T_{wb,2}$) for all hours during the entire year. The assumed effectiveness value is (ε=0.7) according to [119].

Table 3.2 Basic input parameters for case 2

Parameter item	Value
Wheat temperature at inlet (T_5) (°C)	25
Wheat temperature at outlet (T_6) (°C)	50
Wheat mass flow rate (kg/h)	100
Drying air temperature T_2 (°C)	60
Outside design temperature T_o (°C)	-9
Moisture content at inlet MC_5 (%)	30
Moisture content at outlet MC_6 (%)	10
Carnot efficiency CE (%)	40
Ground temperature, T_∞ (°C)	15
Tank volume (m^3)	300
Collector area (m^2)	100
Relative humidity, φ_3 (%)	60
Relative humidity, φ_a (%)	30
Effectiveness, ε	0.7

Table 3.3 Input design parameters for condenser [103].

Parameter	Value
Tube outside diameter, D_o	17.17 (mm)
Fin pitch	305 (1/ m)
flow passage hydraulic diameter, D_h	3.48 (mm)
Fin thickness, t	0.4064 (mm)
Free flow area/frontal area, σ	0.481
Heat transfer area/total volume, α	554 m^2/m^3
Fin area/total area, A_f/A	0.95

Table 3.4 Characteristics of the ground structures [114].

Ground type	Conductivity (W/m K)	Diffusivity (m^2/s)	Specific heat (J/kg K)	Heat capacity (kJ/m^3K)
Limestone	1.3	5.75×10^{-7}	900	2250
Granite	3.0	14.00×10^{-7}	820	2164.8
Coarse	0.519	1.39×10^{-7}	1842	3772

Table 3.5 Monthly average reflectivity of earth [109]

Month	July	Aug	Sep	Oct	Nov	Dec	Jan	Feb	Mar	Apr	May	Jun
ρ_{ref}	0.1	0.1	0.1	0.1	0.1	0.1	0.3	0.7	0.5	0.3	0.1	0.1

CHAPTER 4

MODELING OF A SOLAR-ASSISTED HEAT PUMP DRYING SYSTEM WITH THERMAL ENERGY STORAGE TANK AND HEAT RECOVERY UNIT USING PERIODIC OPERATION

4.1 Introduction

In this chapter, annual periodic performance of a SAHP drying system including TES tank with and without Heat Recovery Unit (HRU) is investigated using analytical and computational procedures. This chapter presents other methods that are used for heat pump, TES tank and flat plate collector's analyses to predict annual periodic performance for the drying system in both cases.

These cases are:

- Mathematical modeling of a SAHP drying system with underground TES tank.
- Mathematical modeling of a SAHP drying system including TES tank and HRU.

4.2 Drying System Description (Case 3)

The heat pump extracts the stored energy that is used to dry of wheat in the drying unit. Schematic of the drying system is shown in Figure 4.1. The whole system consists of four subsystems, which are dryer unit, heat pump, underground TES tank, and flat-plate solar collectors. They will be explained in detail in the following subsections.

The total annual energy supplied to the drying system during the whole year is the sum of the solar energy extracted from the storage and heat pump work. A fraction of the solar energy will be lost into the earth surrounding the storage, and the remaining part will be used in the drying unit during all seasons. An analytical calculation procedure is given in the following sections. Temperature of the storage and geological structure surrounding the storage, heat pump work, available solar energy gain rate, and drying heat are to be determined from the analytical model for the heating system.

In order to find the periodic solution for the drying system, and analytical model is developed to obtain the performance parameters of the drying system using utilizability, $\bar{\phi}$, method to find the amount of charged energy for each month. The description of system components in detail was presented in chapter 3.

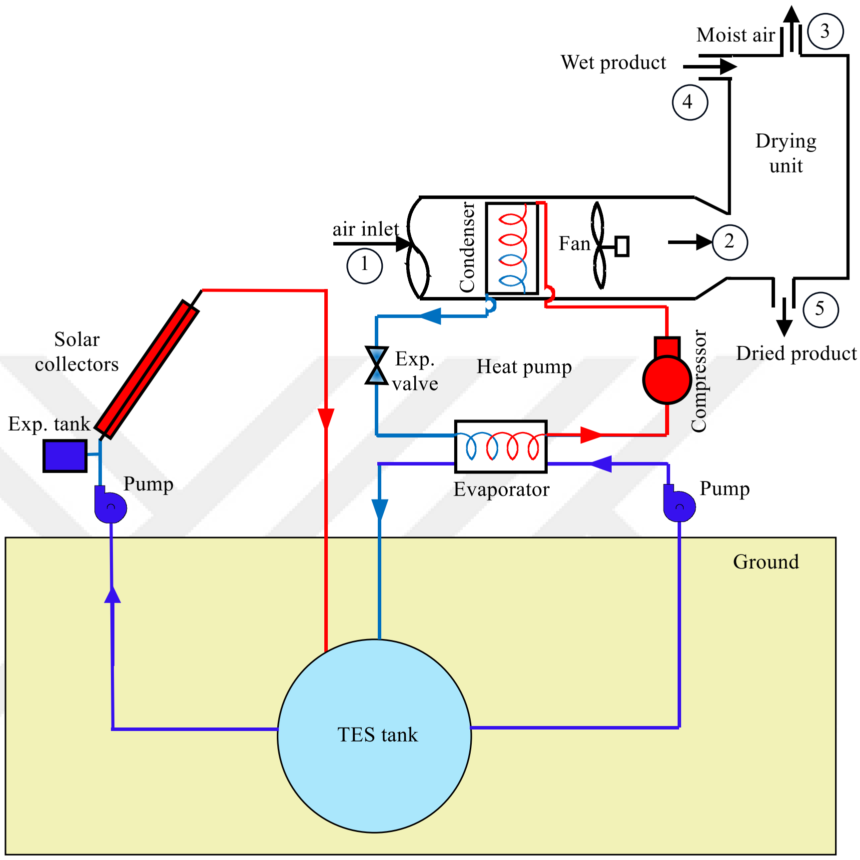

Figure 4.1 Schematic of the drying system with underground TES tank (2nd model).

4.3 Mathematical Modeling of a SAHP Drying System with TES Tank (Case 3)

The system consists of four main parts which are wheat dryer unit, a heat pump, flat plate solar collectors, and TES tank.

To obtain a mathematical modeling of the drying system, it is required to define energy expressions or energy model for each component of the system. These models are for the drying unit, ground coupled heat pump, underground TES tank, and solar collectors. Mathematical modeling will be obtained by combining these expressions. In this chapter, the expressions will be given in detail.

4.3.1 Drying Unit

There are four main interactions in the drying unit; influx of drying air from condenser to drying chamber, exit of moist air after evaporation of moisture from the drying unit, input of wet wheat from top of the dryer, and output of dried wheat with moisture lowered to the desired level. The modeling of drying unit detail was presented in chapter three.

4.3.1.1 Fan Power Calculation

Fresh air firstly is taken from the atmosphere by a fan and is heated by the condenser of the heat pump then sent to the dryer unit to evaporate water from the moist wheat. Accordingly, the fan is necessary for this operation. Calculation procedures to find the fan power input were presented in chapter three.

4.3.2 Modeling of the Heat Pump

In the drying system, ground source heat pump extracts heat from the TES tank, and supplies the heat to cold drying air. An algebraic expression for heat pump simulation is given in this section. It is used to calculate dimensionless heat pump work. Coefficient of performance of heat pump, COP is a function of condenser and evaporator temperatures. Characteristic heat pump performance curve was adapted from experimental data of an actual conventional heat pump in this study. A very good fit to the experimental data was obtained from the following expression [49] as follows:

$$COP = \beta_{hp}\left[\frac{T_w+100}{70} Ln\left(\frac{T_h}{T_h-T_w}\right) + \frac{35-T_h}{40}\right] \tag{4.1}$$

β_{hp} is a coefficient that may vary depending on model and manufacturer. It is assumed equal to unity in this study. T_h is the temperature of the water in the load side heat exchanger. Monthly average energy requirement of the drying system may be expressed as:

$$\dot{Q}_H(t) = (UA)_{he}[T_h(t) - T_c] \tag{4.2}$$

Where $(UA)_{he}$ and $T_h(t)$ are UA value and temperature for the condenser, and T_c represents the average temperature of air entering to condenser and that is leaving the condenser. The heat absorbed by the drying air is given as;

$$\dot{Q}_H(t) = \dot{m}_a C_{p_a}\left[T_2 - \overline{T}_a(t)\right] \tag{4.3}$$

Where $\overline{T}_a(t)$ represents monthly average ambient temperature. The heated air is used to evaporate the water present in the wheat. After heating the air, it is flowed through the dryer unit. Therefore, the energy requirement of the dryer unit as presented in chapter three can be expressed as;

$$\dot{Q}_H(t) = \dot{m}_p\, C_{pw}\,(T_5 - T_4) + \dot{m}_w\, h_{fg} \tag{4.4}$$

The following steps have been followed to obtain the formula of dimensionless compressor work, *w*, that is used in the analysis:

$$\dot{Q}_H(t) = \dot{W}_c(t)COP \tag{4.5}$$

Substituting Eq. (4.1) in Eq. (4.5) gives the following form for heating load:

$$\dot{Q}_H(t) = \dot{W}_c(t)\beta_{hp}\left(\frac{T_w+100}{70}Ln\left[\frac{T_h}{T_h-T_w}\right] + \frac{35-T_h}{40}\right) \tag{4.6}$$

The following dimensionless forms can be used to simplify and find the final forms of COP and dimensionless compressor work, *w*, as:

$$\phi_2 = \frac{T_2-T_\infty}{T_\infty},\quad \phi_c = \frac{T_c-T_\infty}{T_\infty},\quad \phi_a(t) = \frac{\overline{T}_a(t)-T_\infty}{T_\infty},\quad \phi_w(t) = \frac{T_w(t)-T_\infty}{T_\infty} \tag{4.7}$$

Combining Equations (4.2) and (4.3) giving the following:

$$u = \frac{(UA)_{he}}{\dot{m}_a C_{p_a}} = \frac{T_2-\overline{T}_a(t)}{T_h(t)-T_c} \tag{4.8}$$

Rearrange Eq. (4.1) using dimensionless forms in Eq. (4.7) and Eq. (4.8) gives the new formula of COP as follows:

$$COP = \beta_{hp}\left[\frac{T_\infty(\phi_w+1)+100}{70}Ln\left(\frac{T_\infty(\phi_2-\phi_a+\phi_c+u}{T_\infty((\phi_2-\phi_a)-u(\phi_c-\phi_w))}\right) + \frac{35u-T_\infty(\phi_2-\phi_a+u\phi_c+u)}{40u}\right] \tag{4.9}$$

Combining Equations (4.3) and (4.5) gives the following:

$$\dot{W}_c(t) = \frac{\dot{m}_a C_{p_a}\left[T_2-\overline{T}_a(t)\right]}{COP} \tag{4.10}$$

Then, inserting Eq. (4.9) in Eq. (4.10) to find the final form of dimensionless compressor work:

$$w = \frac{\dot{W}_c(t)}{\dot{m}_a C_{p_a} T_\infty} = \frac{(\phi_2-\phi_a)}{\beta_{hp}\left[\frac{T_\infty(\phi_w+1)+100}{70}Ln\left(\frac{T_\infty(\phi_2-\phi_a+\phi_c+u}{T_\infty((\phi_2-\phi_a)-u(\phi_c-\phi_w))}\right)+\frac{35u-T_\infty(\phi_2-\phi_a+u\phi_c+u)}{40u}\right]} \tag{4.11}$$

4.3.3 Periodic Solution of TES Tank Problem

Thermal energy storage tank was explained in detail in chapter three. The solution in this chapter is to find monthly water temperature in the tank using CFFT technique while the solution in chapter three was to find hourly water temperature in the tank using Duhamel's superposition and transformation techniques. Thus the used methodology here differs from the one used in chapter three in the energy analysis for TES tank. Schematic representations of the spherical TES tank and energy balance for the tank are shown in Figure 4.2.

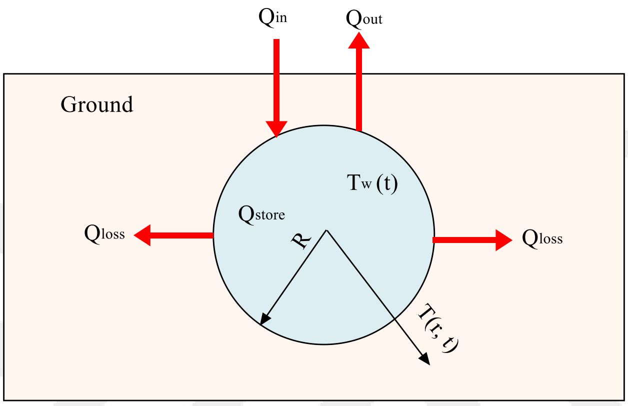

Figure 4.2 Schematic of the underground TES tank problem (2nd model).

The annually periodic transient heat transfer problem outside the spherical thermal energy storage may be expressed in the spherical coordinate system as follows:

$$\frac{\partial^2 T}{\partial r^2} + \frac{2}{r}\frac{\partial T}{\partial r} = \frac{1}{\alpha}\frac{dT}{dt} \tag{4.12}$$

$$T(R,t) = T_w(t) \tag{4.13}$$

$$T(\infty,t) = T_\infty \tag{4.14}$$

$$T(r,0) = T(r, one\ year) \tag{4.15}$$

where α in equation (4.12) is the thermal diffusivity of the earth surrounding the thermal energy storage. The energy balance relating energy charge rate, energy accumulation rate in the storage, and the conduction heat loss rate into the surrounding earth is expressed in the following form.

$$Q = \rho_w V_w C_w \frac{dT_w}{dt} - kA\frac{\partial T}{\partial r}(\alpha, t) \tag{4.16}$$

The above problem formulation will be put in dimensionless form using the following dimensionless variables.

$$x = \frac{r}{a} \;\; ; \;\; \tau = \frac{\alpha t}{a^2} \;\; , \qquad \phi = \frac{T - T_\infty}{T_\infty} \;\; , \qquad \phi_w = \frac{T_w - T_\infty}{T_\infty} \;\; , \;\; \phi_a = \frac{T_a - T_\infty}{T_\infty}$$

$$Y = \frac{\alpha(one\ year)}{a^2} \;, \qquad q = \frac{Q}{4\pi a k T_\infty} \;\; , \quad P = \frac{1}{3}\left(\frac{\rho_w C_w}{\rho C}\right) , \quad \psi(x,\tau) \; = x\phi(x,\tau) \quad (4.17)$$

Where, ρc given in equation (4.17) is the product of density and specific heat of soil surrounding the storage. Using dimensionless variables in Eq. (4.17) with Eq. (4.12) and taking 1st and 2nd derivations for x and r simplified gives the following form

The resulting dimensionless form of the problem formulation is given by:

$$\frac{\partial \phi}{\partial \tau} = \frac{\partial^2 \phi}{\partial x^2} + \frac{2}{x}\frac{\partial \phi}{\partial x} \tag{4.18}$$

$$\phi(1,\tau) = \phi_w(\tau) \tag{4.19}$$

$$\phi(\infty,\tau) = 0 \tag{4.20}$$

$$\phi(x,0) = \phi(x, one\ year) \tag{4.21}$$

The following transformation can be used for simplification:

$$\phi(x,\tau) = x^{-1}\,\psi(x,\tau) = \frac{\psi(x,\tau)}{x} \tag{4.22}$$

The result of derivation Eq. (4.22) with respect to τ gives the following:

$$\frac{\partial \phi}{\partial \tau} = \frac{1}{x}\frac{\partial \psi}{\partial \tau} \tag{4.23}$$

The differential equation and boundary conditions take place the following form:

$$\frac{\partial^2 \psi}{\partial x^2} = \frac{\partial \psi}{\partial \tau} \tag{4.24}$$

$$\psi(1,\tau) = \phi_w(\tau) \tag{4.25}$$

$$\psi(\infty,\tau) = 0 \tag{4.26}$$

$$\psi(x,0) = \psi(x,Y) \tag{4.27}$$

$$q = P\frac{d\phi_w}{d\tau} - \frac{\partial \psi}{\partial x}(1,\tau) + \psi(1,\tau) \tag{4.28}$$

The above problem formulation will be transformed using CFFT to omit time variable. CFFT is designed by

$$\psi(x,\tau) = \sum_{n=-\infty}^{\infty} \psi_n(x) e^{\frac{i2\pi n\tau}{y}} \tag{4.29}$$

$$\psi_n(x) = \frac{1}{y}\int_{-\frac{y}{2}}^{\frac{y}{2}} \psi(x,\tau)\, e^{\frac{-i2\pi n\tau}{y}}\, d\tau \tag{4.30}$$

If the CFFT technique is applied to the above problem formulation, the following form is obtained

$$\frac{\partial^2 \psi_n}{\partial x^2} - i\nu_n \psi_n = 0 \tag{4.31}$$

$$\psi_n(1) = \phi_{w_n} \tag{4.32}$$

$$\psi_n(\infty) = 0 \tag{4.33}$$

$$q = P\frac{-i2\pi n}{y}\phi_{w_n} - \frac{\partial \psi_n}{\partial x}(1) + \psi_n(1) \tag{4.34}$$

Then, the differential equation is solved as:

$$\psi_n(x) = Ae^{\sqrt{z}\,x} + Be^{-\sqrt{z}\,x} \tag{4.35}$$

where

$$z = \frac{i2\pi n}{y} = i\nu_n \tag{4.36}$$

Applying the first boundary condition for $(x = \infty)$ to the differential equation in Eq. (4.35) to find A constant:

$$\psi_n(x = \infty) = 0 = Ae^{\sqrt{z}\,\infty} + \frac{B}{e^{\sqrt{z}\,\infty}} \tag{4.37}$$

gives,

$$A = 0 \tag{4.38}$$

Again, applying the second boundary condition for $(x = 1)$ to the differential equation in Eq. (4.35) to find the value of B:

$$\psi_n(x = 1) = \phi_{w_n} = \frac{B}{e^{\sqrt{z}\cdot 1}} \tag{4.39}$$

$$B = \phi_{w_n} e^{\sqrt{z}} \tag{4.40}$$

The solution takes the following form

$$\psi_n(x) = \left[\phi_{w_n} e^{\sqrt{z}}\right] e^{-\sqrt{z}\,x} = \phi_{w_n} e^{(1-x)\sqrt{z}} \tag{4.41}$$

$$\psi_n(x) = \phi_{w_n} e^{-\sqrt{z}(x-1)} \tag{4.42}$$

$$\psi_n(x) = \phi_{w_n} e^{-\sqrt{\frac{i2\pi n}{y}}(x-1)} = \phi_{w_n} e^{-\sqrt{2i}\frac{\sqrt{n\pi}}{\sqrt{y}}(x-1)} \tag{4.43}$$

$$\psi_n(x) = \phi_{w_n} e^{-\left[\sqrt{(1+i)^2}\frac{\sqrt{n\pi}}{\sqrt{y}}(x-1)\right]} = \phi_{w_n} e^{-(1+i)\frac{\sqrt{n\pi}}{\sqrt{y}}(x-1)} \tag{4.44}$$

$$\psi_n(1) = \phi_{w_n} \tag{4.45}$$

$$\frac{d\psi_n}{dx} = -(1+i)\frac{\sqrt{n\pi}}{\sqrt{y}}\,\phi_{w_n}\,e^{-(1+i)\frac{\sqrt{n\pi}}{\sqrt{y}}(x-1)} \tag{4.46}$$

$$\frac{d\psi_n}{dx}(1) = -(1+i)\,\phi_{w_n}\frac{\sqrt{n\pi}}{\sqrt{y}} \tag{4.47}$$

Inserting these into the energy equation

$$q_n = P\,i\nu_n\,\phi_{w_n} + (1+i)\frac{\sqrt{n\pi}}{\sqrt{y}}\phi_{w_n} + \phi_{w_n} \tag{4.48}$$

$$q_n = \left[i\nu_n P + (1+i)\frac{\sqrt{n\pi}}{\sqrt{y}} + 1\right]\phi_{w_n} \tag{4.49}$$

$$\phi_{w_n} = \frac{q_n}{P\left(\frac{i2\pi n}{y}\right)+\frac{\sqrt{n\pi}}{\sqrt{y}}+i\frac{\sqrt{n\pi}}{\sqrt{y}}+1} = \frac{q_n}{\left(1+\frac{\sqrt{n\pi}}{\sqrt{y}}\right)+i\left(P\frac{2\pi n}{y}+\frac{\sqrt{n\pi}}{\sqrt{y}}\right)} \tag{4.50}$$

$$\phi_{w_n} = \frac{q_n}{\eta_1+i\eta_2} \tag{4.51}$$

where

$$\eta_1 = 1+\frac{\sqrt{n\pi}}{\sqrt{y}}\ ,\ \eta_2 = \frac{\sqrt{n\pi}}{\sqrt{y}} + P\frac{2\pi n}{y} \tag{4.52}$$

$$\phi_{w_n} = \frac{q_n}{\eta_1+i\eta_2}\times\frac{\eta_1-\eta_2}{\eta_1-\eta_2} \tag{4.53}$$

$$\phi_{w_n} = \frac{q_n(\eta_1-i\eta_2)}{\eta_1^2+\eta_2^2} \tag{4.54}$$

4.3.4 Complex Finite Fourier Transform of the Heat Input Rate

Available solar energy is charged by the flat plate solar collectors to the energy storage over the whole year. Part of the stored energy is supplied to the drying unit during the year by a heat pump. Dimensionless heat input rate into the energy storage $q(\tau)$ is equal to the difference between the charged energy to the storage and the energy extracted by the heat pump, which may be expressed as:

$$q(\tau) = q_u(\tau) - q_{hp}(\tau) \tag{4.55}$$

$q_{hp}(\tau)$ in Equation (4.55) is the energy extracted from the storage by the heat pump, which may be expressed as:

$$q_{hp}(\tau) = q_h(\tau) - \frac{w(\tau)}{\gamma} \tag{4.56}$$

When equation (4.56) is substituted into the Equation (4.55), the net energy input rate to the energy storage becomes:

$$q(\tau) = q_u(\tau) - q_h(\tau) + \frac{w(\tau)}{\gamma} \tag{4.57}$$

Where $q_h(\tau)$ and $w(\tau)$ are dimensionless house heat load and heat pump work respectively. $q_u(\tau)$ in Equation (4.57) is the dimensionless energy collection by the solar collectors. The method of calculation of available solar energy gain is based on the $\bar{\phi}$ method and is described in next section.

Annual dimensionless temperature distribution in earth given by Equation (4.29) depends on the complex Fourier coefficients of the dimensionless net heat input rate. $q(\tau)$ may be expressed by a Fourier series with a period of one year. Let g_i be the monthly components of the dimensionless energy input rate to the storage. The dimensionless heat input rate, $q(\tau)$ may be expressed by the following vector.

$$q(\tau) = (g_1, g_2, g_3, g_4, g_5, g_6, g_7, g_8, g_9, g_{10}, g_{11}, g_{12}) \tag{4.58}$$

The dimensionless heat input rate, $q(\tau)$ given by Equation (4.58) can be expressed by the following Fourier series with a period of one year.

$$q(\tau) = \sum_{n=-\infty}^{+\infty} q_k\, e^{i\nu_k \tau} \tag{4.59}$$

Complex Fourier coefficients of the dimensionless heat gain rate, q_k, in Equation (3.59) are given by:

$$q_0 = \frac{1}{12}\sum_{j=1}^{12} q_j \qquad \text{for } k = 0 \tag{4.60}$$

$$q_k = \frac{1}{2\pi k}\sum_{j=1}^{12} q_j(\eta_{3,j} + i\eta_{4,j}) \qquad \text{for } k \geq 1 \tag{4.61}$$

where

$$\eta_{3,j} = \sin(2\pi k r_j) - \sin(2\pi k r_{j-1}) \tag{4.62}$$

$$\eta_{4,j} = \cos(2\pi k r_j) - \cos(2\pi k r_{j-1}) \tag{4.63}$$

4.3.5 Calculation of Useful Energy by Utilizibility Method

The monthly average daily useful energy collection $\dot{Q}_u$, is equal to the monthly component of the daily energy input to the storage. It can be calculated from the following formula reported by Klein [120] and Mitchel et al. [121]:

$$\dot{Q}_u = A_{col} F_R \overline{(\tau\alpha)} \overline{H}_T \overline{\phi} \tag{4.64}$$

Where A_{col} is the collector surface area, and F_R is the collector heat removal factor. $\overline{(\tau\alpha)}$ is the monthly average transmittance absorbtance product for the collector. $\overline{H}_T$ is the monthly average daily total solar radiation on a tilted surface. $\overline{\phi}$ is the monthly average daily utilizability.

The concept of utilizability has been pioneered by Whillier [122], and later generalised by Lui and Jordan [123]. It has been simplified and extended by Klein and Beckman [124], who developed a general design method for solar systems involving flat plate collectors. The monthly average daily utilizability is defined as the sum for a month over all hours and days of the radiation on a tilted surface that is above a critical level divided by the monthly radiation.

The value of $\overline{\phi}$ for a monthly period depends upon the distribution of daily total solar radiation, collector orientation, location, and time of the year. A correlation for $\overline{\phi}$ was developed by Klein [120] as a function of the monthly clearness index $\overline{K}_T$, a dimensionless critical radiation level $\overline{X}_c$, and geometry factor, R_n/R. The resulting correlation is expressed as:

$$\overline{\phi} = \exp\left\{\left[A + B\left(\frac{R_n}{\overline{R}}\right)\right]\left(\overline{X}_c + C\overline{X}_c^2\right)\right\} \tag{4.65}$$

where

$$A = 2.943 - 9.271\overline{K}_T + 4.031\overline{K}_T^2 \tag{4.66}$$

$$B = -4.343 + 8.853\overline{K}_T - 3.602\overline{K}_T^2 \tag{4.67}$$

$$C = -0.17 - 0.306\overline{K}_T - 2.936\overline{K}_T^2 \tag{4.68}$$

The R_n given is the ratio of radiation on a tilted surface to that on a horizontal surface at noon for an average day of the month. It can be calculated by considering the beam, diffuse, and ground-reflected component of the radiation.

$$R_n = \left(1 - \frac{r_{d,n}}{r_{t,n}}\frac{H_d}{H}\right)R_{b,n} + \left(\frac{r_{d,n}}{r_{t,n}}\frac{H_d}{H}\right)\left(\frac{1+\cos\beta}{2}\right) + \rho_{ref}\left(\frac{1-\cos\beta}{2}\right) \tag{4.69}$$

where $r_{d,n}$ is the ratio of the diffuse radiation at noon to daily total radiation. The $r_{d,n}$ as suggested by Lui and Jordon [125] is given as:

$$r_{d,n} = \frac{\pi}{24}\frac{\cos w - \cos w_s}{\sin w_s - \left(\frac{2\pi w_s}{3600}\right)\cos w_s} \tag{4.70}$$

and $r_{t,n}$ is the ratio of the radiation at noon to daily total radiation which is given by the following equation given by Collares-Pereira and Rabl [126].

$$r_{t,n} = \frac{\pi}{24}(a_1 + b_1 \cos w)\frac{\cos w - \cos w_s}{\sin w_s - \left(\frac{2\pi w_s}{3600}\right)\cos w_s} \tag{4.71}$$

where a_1 and b_1 depend on the sunset hour angle and are given by:

$$a_1 = 0.409 + 0.5016 \sin(w_s - 60) \tag{4.72}$$

$$b_1 = 0.6609 + 0.4767 \sin(w_s - 60) \tag{4.73}$$

$R_{b,n}$ in Equation (4.69) is the ratio of beam radiation on a tilted surface to that on a horizontal surface at noon. For surfaces facing directly towards the equator, $R_{b,n}$ can be expressed as Klein [120]:

$$R_{b,n} = \frac{\cos(\theta_L - \beta)\cos\delta + \sin(\theta_L - \beta)\sin\delta}{cos\theta_L \cos\delta + \sin\theta_L \sin\delta} \tag{4.74}$$

where δ is the solar declination angle calculated from:

$$\delta = 23.45 \sin\left(360\,\frac{284+n}{365}\right) \tag{4.75}$$

H_d/H in Equation (4.69) is the daily diffuse radiation fraction. Collares-Pereira and Rabl [126] recommended a correlation for estimating H_d/H as a function of K_T, which is the ratio of the daily total radiation on a horizontal surface to the daily extraterrestrial radiation. For the average day considered in this analysis, K_T was taken to be the same value of $\overline{K}_T$. According to Duffie and Beckman [109]:

$$\frac{H_d}{H} = \begin{cases} = 0.99 & for\ K_T \leq 0.17 \\ = 1.188 - 2.272\mathrm{K_T} + 9.473K_T^2 - 21.863K_T^3 & \\ +14.648 & for\ 0.17 < K_T < 0.75 \\ = 0.54K_T - 0.632 & for\ 0.75 < K_T < 0.8 \\ = 0.2 & for\ K_T = 0.8 \end{cases} \tag{4.76}$$

$\overline{H}_T$ in Equation (4.64) is the monthly average daily total solar radiation on a tilted surface and is given by the following equation.

$$\overline{H}_T = \overline{R}\,\overline{H} \tag{4.77}$$

$\overline{\mathrm{R}}$ is the ratio of the monthly average daily total radiation on a tilted surface to that on a horizontal surface. $\overline{\mathrm{R}}$ can be estimated by considering the beam, diffuse, and ground-reflected components of radiation and is expressed as:

$$\overline{\mathrm{R}} = \left(1 - \frac{\overline{H}_d}{\overline{H}}\right)\overline{\mathrm{R}}_b + \left(\frac{\overline{H}_d}{\overline{H}}\right)\frac{1+\cos\beta}{2} + \rho_{\mathrm{ref}}\left(\frac{1-\cos\beta}{2}\right) \tag{4.78}$$

$\overline{\mathrm{R}}_b$ in Equation (4.78) is the monthly average daily beam radiation ratio. Lui and Jordan [127] suggested that it can be estimated from the ratio of extraterrestrial radiation on tilted surface to that on a horizontal surface for a month. For surfaces directed due south, Lui and Jordan give the following equation for $\overline{\mathrm{R}}_b$:

$$\overline{\mathrm{R}}_b = \frac{\cos(\theta_L-\beta)\cos\delta\sin w_s{}' + \left(\frac{\pi}{180}\right)w_s\sin(\theta_L-\beta)sin\delta}{\cos\theta_L\cos\delta\sin w_s + \left(\frac{\pi}{180}\right)w_s\sin\theta_L\sin\delta} \tag{4.79}$$

Where $w_s{}'$ is the sunset hour angle for a tilted surface given by:

$$w_s{}' = Min\begin{bmatrix}\cos^1(-\tan\theta_L\tan\delta)\\ \cos^1(-\tan(\theta_L-\beta)\tan\delta)\end{bmatrix} \tag{4.80}$$

$\overline{H}_d/\overline{H}$ in Equation (4.78) is the ratio of monthly average daily diffuse radiation to total daily radiation on a horizontal surface. Collares-Pereira and Rabl [126] developed the following correlation for calculation of $\overline{H}_d/\overline{H}$ as a function of monthly average clearness index, $\overline{K}_T$, and sunset hour angle, w_s:

$$\frac{\overline{H}_d}{\overline{H}} = 0.775 + 0.00653(w_s - 90) - [0.505 + 0.00455(w_s - 90)]\cos(115\overline{K}_T - 103) \tag{4.81}$$

$\overline{K}_T$ is monthly average clearness index

$$\overline{K}_T = \frac{\overline{H}}{\overline{H}_0} \tag{4.82}$$

$\overline{H}_0$, is the monthly average daily extraterrestrial radiation on a horizontal surface and is given by:

$$\overline{H}_0 = \frac{24*3600*G_S}{\pi}\left[1 + 0.033\cos\left(\frac{360n}{365}\right)\right]\left[\cos\theta_L\cos\delta\sin w_s + \left(\frac{2\pi w_S}{360}\right)\sin\theta_L\sin\delta\right] \tag{4.83}$$

where

$$w_s = \cos^{-1}(-\tan\theta_L\tan\delta) \tag{4.84}$$

The monthly average critical radiation ratio given, $\overline{X}_c$, in Equation (4.64) is expressed by:

$$\overline{X}_c = \frac{H_{T,c}}{r_{t,n} R_n \overline{H}} = \frac{H_{T,c}}{r_{t,n} R_n \overline{K}_T \overline{H}_0} \tag{4.85}$$

$$H_{T,c} = \frac{F_R U_c (\overline{T}_{ci} - \overline{T}_a)}{F_R (\overline{\tau\alpha})} \tag{4.86}$$

where the symbols are defined as; U_c, collector heat loss coefficient; $\overline{T}_{ci}$, inlet fluid temperature to collector; $\overline{T}_a$, monthly average outside air temperature; $(\overline{\tau\alpha})$, monthly average transmittance-absorbtance product.

4.3.5.1 Calculation of Transmittance-Absorptance Product

This method to find monthly average daily useful energy collection, which was mentioned in Eq. (4.64), is as a function of monthly average transmittance absorptance product. Therefore this section is focusing on the monthly average transmittance-absorptance product estimation. Transmittance of a transparent collector cover, τ, and absorptance of the collector plate, α, are functions of the material and the incidence angle of solar radiation. Beam, diffuse and ground-reflected components of the solar radiation are incident on the collector surface at different angles. The variation of incident angle of solar radiation with respect to the transmittance absorptance product, $(\tau\alpha)$, must be known to calculate monthly average transmittance absorptance product of flat plate collectors. Simon [128] presented performance test results for 23 different collector parameters. The four different collectors widely used at the applications are given in end of this chapter.

An expression for the transmittance absorptance product as given by Simon [128] (as a function of incident angle of beam radiation) is:

$$(\overline{\tau\alpha})_r = (\overline{\tau\alpha})_n \left[1 + B_0 \left(1 - \frac{1}{cos\vartheta_r}\right)\right] \tag{4.87}$$

where

$$\vartheta_r = 89.8 - 0.5788\beta + 0.002693\beta^2 \qquad (°) \tag{4.88}$$

and

$$B_0 = -0.17 \tag{4.89}$$

$$(\overline{\tau\alpha})_d = (\overline{\tau\alpha})_n \left[1 + B_0 \left(1 - \frac{1}{cos\vartheta_d}\right)\right] \tag{4.90}$$

$$\vartheta_d = \frac{\pi}{3} \quad \text{(Rad)} \tag{4.91}$$

$$(\overline{\tau\alpha})_b = (\overline{\tau\alpha})_n \left[1 + B_0 \left(1 - \frac{1}{cos\vartheta_b}\right)\right] \tag{4.92}$$

$$\vartheta_b = \cos^{-1}\left[\cos(\theta_L - \beta)\cos\delta\cos\left(\frac{5\pi}{24}\right) + \sin(\theta_L - \beta)\sin\delta\right] \tag{4.93}$$

Now, monthly average transmittance-absorptance product, $(\overline{\tau\alpha})$, can be expressed as:

$$(\overline{\tau\alpha}) = \frac{\left(1-\frac{\overline{H}_d}{\overline{H}}\right)\overline{R}_b(\overline{\tau\alpha})_b + \frac{\overline{H}_d}{\overline{H}}(\overline{\tau\alpha})_d\left(\frac{1+\cos\beta}{2}\right) + \rho_{\text{ref}}(\overline{\tau\alpha})_r\left(\frac{1-\cos\beta}{2}\right)}{\left(1-\frac{\overline{H}_d}{\overline{H}}\right)\overline{R}_b + \left(\frac{\overline{H}_d}{\overline{H}}\right)\frac{1+\cos\beta}{2} + \rho_{\text{ref}}\left(\frac{1-\cos\beta}{2}\right)} \tag{4.94}$$

4.4 Description of the Drying System (Case 4)

The SAHP drying system considered in this study is considered to be located in Gaziantep (37.1° N), Turkey. The scheme of the drying system is shown in Fig.4.3. The whole system consists of five subsystems which are dryer unit, HRU, heat pump, underground TES tank, and flat-plate solar collectors. The subsystems are explained in detail in chapter 3.

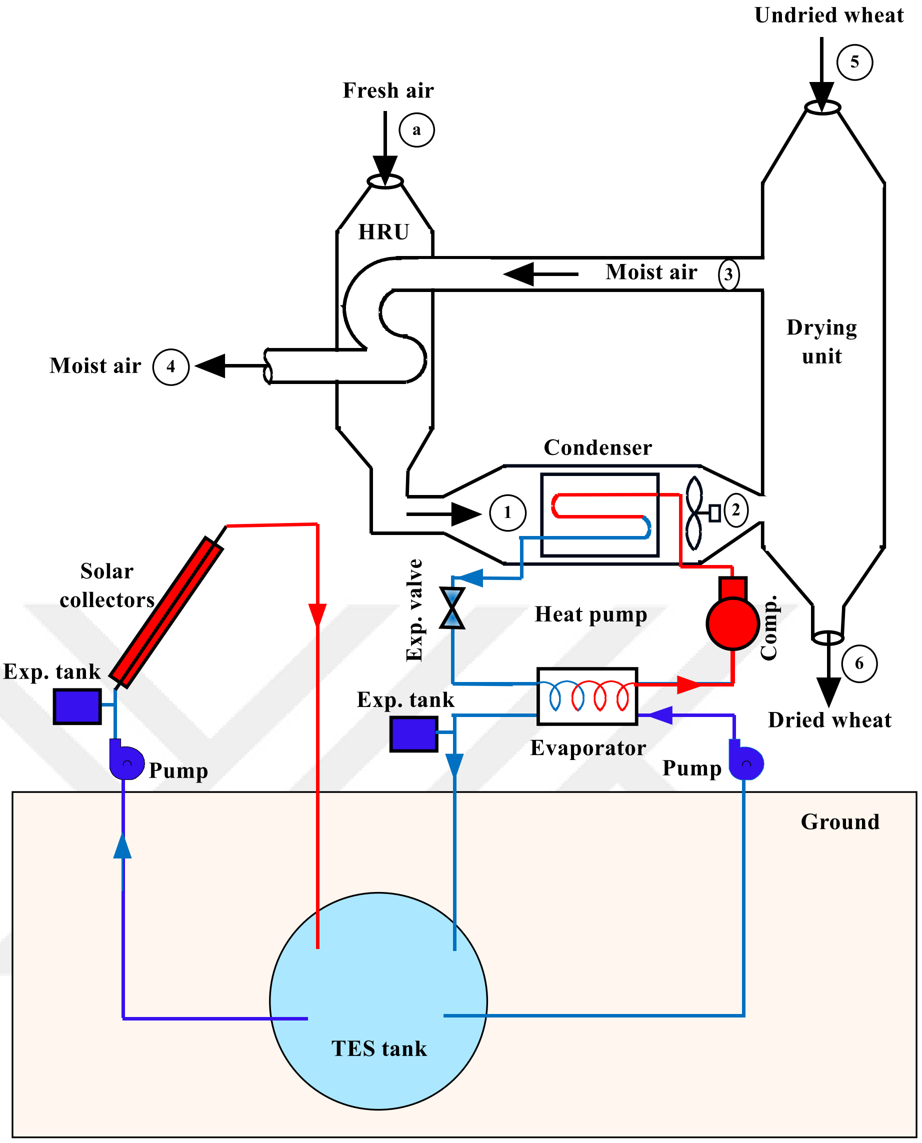

Figure 4.3 Schematic of the SAHP drying system with TES tank and HRU (4th Case).

4.5 Mathematical Modeling of a SAHP Drying System with TES Tank and HRU (Case 4)

The system consists of five main parts which are wheat dryer unit, a heat pump, flat plate solar collectors, an underground TES tank and HRU.

4.5.1 Modeling of the Heat Pump

The modeling of flat plate solar collectors, and underground thermal energy storage tank is presented in previous sections. While the modeling of drying unit and HRU was presented in chapter three. But heat pump model in the case of using HRU differs from the presented model for heat pump because different subscripts are used with some variables parameters. Rearranging equations (4.3-4.11) with referring to Fig. 4.3 gives the following equations:

$$\dot{Q}_H(t) = \dot{m}_a C_{p_a}\left[T_2 - \overline{T}_1(t)\right] \quad (4.95)$$

$$\phi_1(t) = \frac{\overline{T}_1(t) - T_\infty}{T_\infty} \quad (4.96)$$

$$u = \frac{(UA)_{he}}{\dot{m}_a C_{p_a}} = \frac{T_2 - \overline{T}_1(t)}{T_h(t) - T_c} \quad (4.97)$$

$$T_c = \frac{(T_1)_{min} + T_2}{2} \quad (4.98)$$

$$COP = \beta_{hp}\left(\frac{T_\infty(\phi_w+1)+100}{70} Ln\left[\frac{T_\infty(\phi_2-\phi_1+\phi_c+u}{T_\infty\{(\phi_2-\phi_1)-u(\phi_c-\phi_w)\}}\right] + \frac{35u - T_\infty(\phi_2-\phi_1+u\phi_c+u)}{40u}\right) \quad (4.99)$$

Combining Equations (4.3) and (4.5) gives the following:

$$\dot{W}_c(t) = \frac{\dot{m}_a C_{p_a}\left[T_2 - \overline{T}_1(t)\right]}{COP} \quad (4.100)$$

Then, inserting Eq. (4.99) in Eq. (4.100) to find final form of dimensionless compressor work:

$$w = \frac{(\phi_2-\phi_1)}{\beta_{hp}\left(\frac{T_\infty(\phi_w+1)+100}{70} Ln\left[\frac{T_\infty(\phi_2-\phi_1+\phi_c+u}{T_\infty\{(\phi_2-\phi_1)-u(\phi_c-\phi_w)\}}\right] + \frac{35u - T_\infty(\phi_2-\phi_1+u\phi_c+u)}{40u}\right)} \quad (4.101)$$

4.6 Input Parameters (Cases 3 and 4)

The present model for simulating the performance of a solar aided ground coupled heat pump system is used to study the effects of different parameters. A standard set of the parameters are defined and their effects on the system thermal performance are investigated. Some parameters are found to have a more dominant effect on the performance of the ground coupled heat pump heating system. These parameters are meteorological parameters, thermal and physical properties of the earth, collector parameters, ground reflectance, and storage system parameters. The parameters used in the calculations are briefly discussed in detail in the following sections while the input data for other components of the drying system such as drying unit are presented in chapter seven and given in Tables 4.1 and 4.2.

Table 4.1 Basic input parameters for case 3

Parameter item	Value
Wheat temperature at inlet, T_4 (°C)	25
Wheat temperature at outlet, T_5 (°C)	50
Wheat mass flow rate (kg/h)	30
Drying air temperature T_2 (°C)	55
Outside design temperature T_o (°C)	-9
Moisture content at inlet MC_4 (%)	25
Moisture content at outlet MC_5 (%)	10
Ground temperature, T_∞ (°C)	15
Tank radius (m)	3
Collector area (m^2)	45
Relative humidity, φ_a (%)	30

Table 4.2 Basic input parameters for case 4

Parameter item	Value
Wheat temperature at inlet, T_5 (°C)	25
Wheat temperature at outlet, T_6 (°C)	50
Wheat mass flow rate (kg/h)	50
Drying air temperature T_2 (°C)	55
Outside design temperature T_o (°C)	-9
Moisture content at inlet MC_5 (%)	22.5
Moisture content at outlet MC_6 (%)	12.5
Ground temperature, T_∞ (°C)	15
Tank radius (m)	3
Collector area (m^2)	50
Relative humidity, φ_a (%)	30
Relative humidity, φ_3 (%)	60
Effectiveness, ε	0.7

4.6.1 Meteorological Parameters

Temporal variation of temperature in the thermal energy storage and thermal performance of the drying system are functions of meteorological parameters. In this study, the parameters for five cities in Turkey are selected in the calculations. The selected cities are Ankara, Elazığ, Gaziantep, Istanbul, and Izmir.

The parameters consist of latitude angle θ_L, outside design air temperature T_o, monthly average outside air temperature $\overline{T}_a(t)$, and monthly average solar radiation on a horizontal surface $\overline{H}$. The outside design air temperature and the other parameters are taken respectively from Dağsöz [129] and Ünsal and Doğantan [130]. Values of these parameters for the cities under consideration are given in Table 4.3.

Table 4.3 Meteorological parameters

Months	Ankara ϑ_L = 40.0 ° T$_0$ =-12 °C		Elazığ ϑ_L = 38.7 ° T$_0$ = -12 °C		Gaziantep ϑ_L = 37.1 ° T$_0$ = -9 °C		Istanbul ϑ_L = 40.0 ° T$_0$ = -3 °C		Izmir ϑ_L = 38.5 ° T$_0$ = 0 °C	
	$\overline{T}_a$ (°C)	$\overline{H}$ Mj/m^2 day	$\overline{T}_a$ (°C)	$\overline{H}$ Mj/m^2 day	$\overline{T}_a$ (°C)	$\overline{H}$ Mj/m^2 day	$\overline{T}_a$ (°C)	$\overline{H}$ Mj/m^2 day	$\overline{T}_a$ (°C)	$\overline{H}$ Mj/m^2 day
Jul	23.1	23.7	27.2	20.9	27.1	22.1	23.2	21.5	27.5	19.0
Aug	23.3	22.3	27.0	19.9	26.9	21.1	19.7	19.8	27.0	17.6
Sep	18.4	17.6	22.0	15.6	22.2	16.8	15.5	14.9	22.7	13.9
Oct	12.9	12.5	14.8	10.2	15.3	11.7	11.9	10.0	18.3	10.1
Nov	7.7	7.4	7.8	5.9	9.4	7.9	8.0	6.7	13.9	6.4
Dec	2.5	4.9	1.5	4.6	4.5	5.7	5.1	4.5	10.4	4.4
Jan	0.3	6.0	-1.3	4.9	2.6	6.2	5.5	4.4	8.2	5.1
Feb	1.0	8.5	0.0	8.0	3.6	9.2	6.7	7.4	8.8	7.1
Mar	4.7	12.7	4.7	10.9	7.2	12.6	10.9	11.6	11.1	10.3
Apr	11.1	17.9	11.8	15.3	12.7	17.7	15.8	16.2	15.3	14.4
May	16.1	20.9	17.4	17.2	18.2	18.3	20.6	18.9	20.1	19.1
Jun	20.0	22.1	22.9	21.1	23.7	22.6	23.2	21.3	24.7	18.3

4.6.2 Thermophysical Properties of the Ground

Thermal and physical properties of the geological structure are the parameters affecting the temperature of the storage and the thermal performance of the drying system. Thermal and physical parameters of coarse gravelled earth, sand, granite and limestone were taken from Özisik [114], and given in Table 4.4.

Table 4.4 Characteristics of the ground structures [114].

Ground type	Conductivity (W/m K)	Diffusivity (m^2/s)	Specific heat (J/kg K)	Heat capacity (kJ/m^{3}K)
Limestone	1.3	5.75×10^{-7}	900	2250
Granite	3.0	1.40×10^{-7}	820	2164.8
Coarse	0.519	1.39×10^{-7}	1842	3772
Sand	0.3	2.5×10^{-7}	800	1500

4.6.3 Parameters of Solar Collectors

Solar collectors are special kinds of heat exchangers that transfer the radiant energy of incident sunlight to the thermal energy of a working fluid, usually liquid or air. Flat plate collectors are commonly used in low and medium temperature applications. They are useful in supplying thermal energy at moderate temperatures, up to the normal boiling point of water. The major applications of flat plate collectors are in domestic hot water, space heating, drying process and other applications in industrial processes.

Accordingly, the parameters corresponding to flat plate collectors are used in the study during the calculations. The solar collector construction, orientation, and operating temperature, combined with meteorological conditions: solar radiation level, air temperature, and wind speed and fluid flow rate through the collector are the primary factors affecting the performance.

There is a number of variable parameters that are important in the design of a residential active solar heating system. Those related to the collector are the collector area and the collector slope. Collector parameters have an effect on the useful solar energy gain. The water temperature in the energy storage and the thermal performance of the heat pump system is a function of the useful energy gain. Four different collectors are used in the present calculations. These collectors are one glass cover black paint, two glass cover black paint, one glass cover selective surface and two glass cover selective surface type collectors. Parameters of these collector types as given by Simon [128], are tabulated in Table 4.5.

Table 4.5 Collector parameters

Collector Type	b_o	$(\tau\alpha)_n$	α	ε	U_L,W/m^{2}C
Black paint-1 glass	0.078	0.89	0.97	0.97	7.4
Black paint-2 glass	0.15	0.76	0.97	0.97	4.5
Selective Surface-1 glass	0.11	0.80	0.90	0.1	5
Selective Surface-2 glass	0.16	0.74	0.95	0.07	3.2

In a solar system, collector orientation is also an important design consideration. Fixed position flat plate collectors are generally placed towards the south. In the present computer simulation, collectors are directed toward the south and the value of collector heat removal factor F_R, is taken as 0.75.

4.6.4 Monthly Average Reflectivity of Earth

Available solar energy gain by a solar collector depends upon the amount of radiation on a tilted surface. A tilted surface also receives solar radiation reflected from the ground and other surroundings. The ground and other surfaces seen by the tilted surface are assumed to have a diffuse reflectivity of ρ_{ref}. Lui and Jordan [127] suggested that monthly average ground reflectivity, ρ_{ref} varies from 0.2 to 0.7

depending upon the extent of snow cover. The monthly average ground reflectivity, ρ_{ref} values used in the present calculations are given in Table 4.6.

Table 4.6 Monthly average reflectivity of earth [131]

Month	July	Aug	Sep	Oct	Nov	Dec	Jan	Feb	Mar	Apr	May	Jun
ρ_{ref}	0.2	0.2	0.2	0.2	0.2	0.2	0.3	0.7	0.5	0.3	0.2	0.2

CHAPTER 5

VALIDATION PROCEDURES

5.1 Introduction

After examining the literature in chapter three, it was found that there was no published research related with SAHP drying system. However, there was utilization of flat plat solar collectors and underground spherical TES tank using Duhamel's superposition and transformation techniques for space heating, and the solar collectors and TES tank are components of drying system in this study. Accordingly, the study that done by [71] is selected for validation via preparing the new program in MATLAB. The results of the new program are inserted in figures in section 5.2 for comparison with results in [71].

Using the periodic solution for SAHP drying system in the literature as in chapter four has not been found. Fortunately, utilization of flat plate solar collectors and underground spherical TES tank using periodic solution as its modeling partially presented in chapter four for space heating was found. Therefore, the periodic performance of solar-assisted heat pump with TES for space heating study [131] is selected for validation via the preparation of the new program in MATLAB. The results of the new program are inserted in figures in section 5.3 for comparison with the results in [131].

5.2 Validation Procedure for the Study [71]

It is know that validation of any theoretical study is very important. If there is a similar experimental study with the theoretical study, results obtained from the experimental study should be compared with the theoretical results. However, if there are no similar theoretical or experimental studies in literature, the validation of some components such as solar collector and TES tank for space heating can be done [71]. Therefore the following comparisons are performed in order to check the results obtained by a program written in MATLAB using the same model in [71]. By using the MATLAB program prepared and used to find the results of modeling presented in [71], the hourly tilted solar and useful solar radiation charging to the underground TES tank are computed. The model of [71] is written in FORTRAN program while the same model is written in MATLAB program in this study to validate the same components such as solar collectors and TES tank which are used with SAHP drying system in the present study. MATLAB program for [71] was executed for the same input data, and some of the results are mentioned in the following figures along with the same figures concluded by [71] as follows:

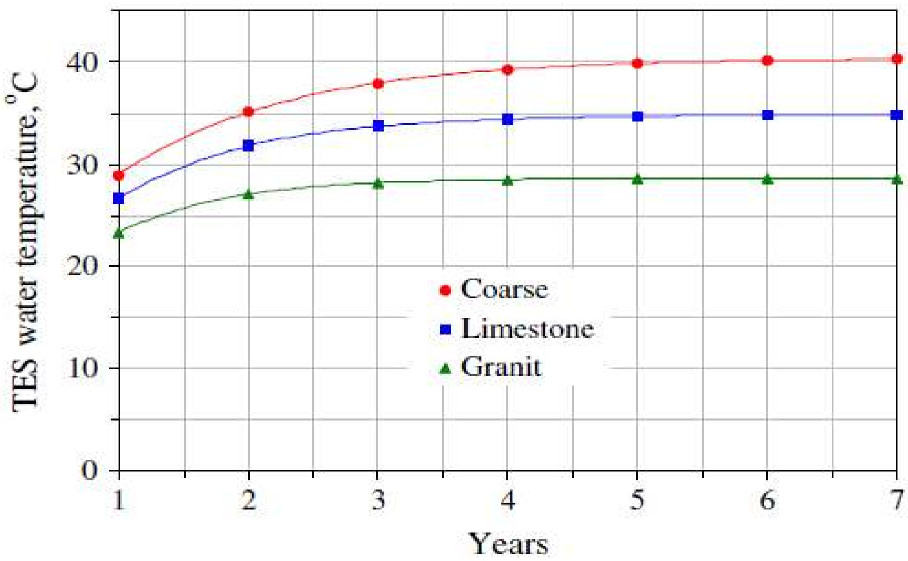

Figure 5.1 Annual T_w for September (Ac = 20 m^2, CE = 40%, V = 300 m^3) [71].

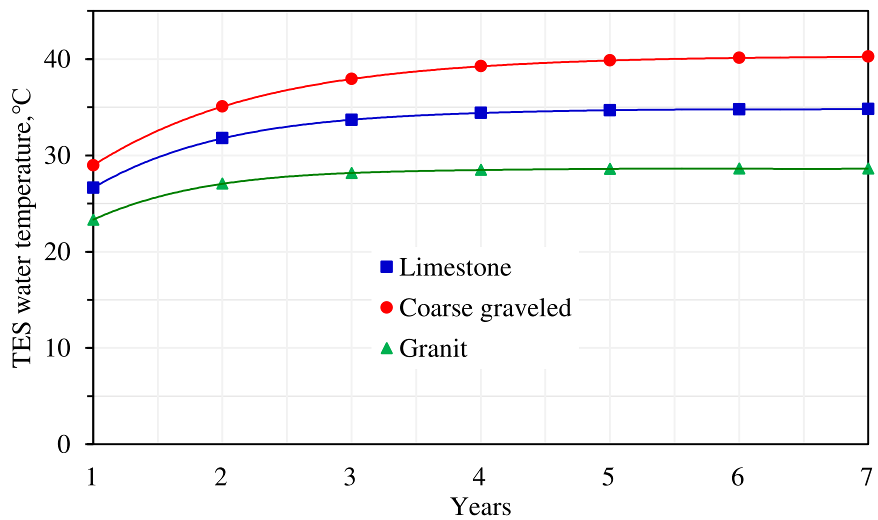

Figure 5.2 Annual T_w for September (Ac = 20 m^2, CE = 40%, V = 300 m^3) [Validated results].

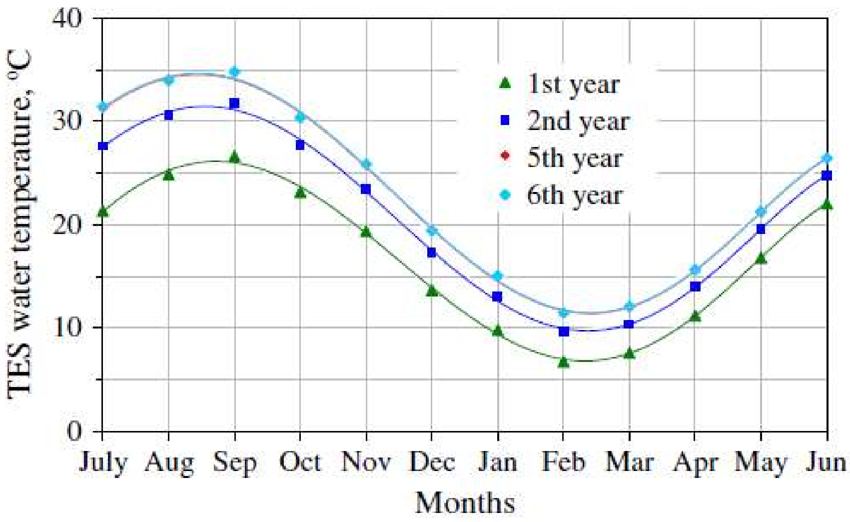

Figure 5.3 Annual T_w with number of operation years (limestone, Ac = 20 m^2, CE = 40%, V = 300 m^3) [71].

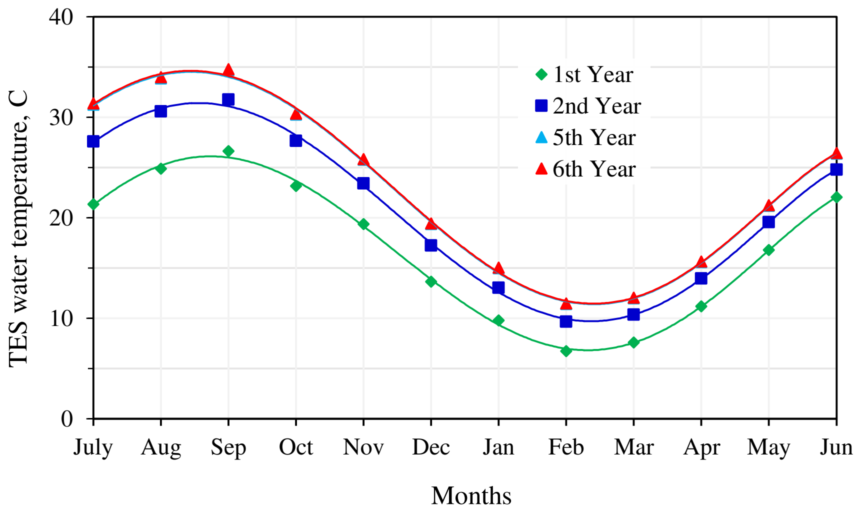

Figure 5.4 Annual T_w with number of operation years (limestone, Ac = 20 m^2, CE = 40%, V = 300 m^3) [Validated results].

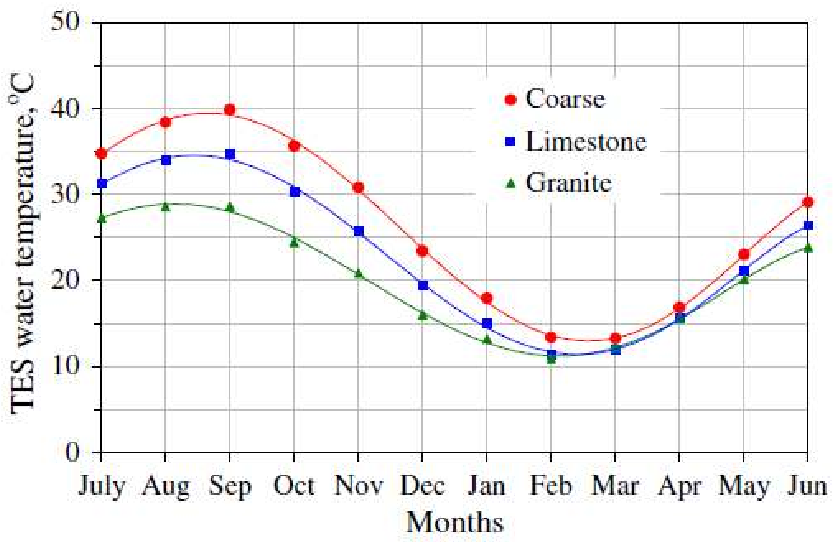

Figure 5.5 Effect of earth type on T_w during year 5 of operation (Ac = 20 m^2, CE = 40%, V = 300 m^3) [71].

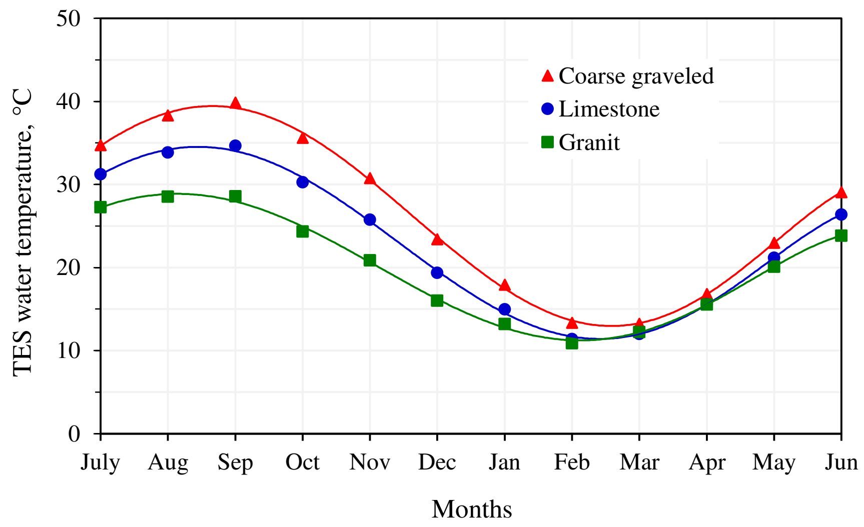

Figure 5.6 Effect of earth type on T_w during year 5 of operation (Ac = 20 m^2, CE = 40%, V = 300 m^3) [Validated results].

These figures (5.1-5.6) showed that the validation results which calculated from a MATLAB program of the model presented in [71] are correct. Accordingly, the models of solar collectors and TES tank, which were written in the MATLAB program can be used with SAHD drying system in this study. Inserting the new models for the remaining components of SAHP drying system in the prepared program in MATLAB gives the new results for the invented drying system in this research. The new results for this study are presented in sections 7.2 and 7.3 in chapter seven. There are some comments can be observed by comparison the concluded results from the MATLAB program prepared for the present study with the results presented in [71] for the same input data and model. These comments are listed in the following:

- The validated results in figures (5.2, 5.4, and 5.6) are identical to results in the figures (5.1, 5.3, and 5.5) presented in reference [71].
- The error in the results for the validation and literature [71] is not exceed 0.1%, accordingly the validation results are accurate and can be used in this study.
- The difference point between the model presented in [71] and the one presented in chapter three is that the heating load in the current study is considered to be constant while it is considered to be a variable in [71].
- The model in the present study is used for drying application while the model in

  [71] is used for space heating; accordingly, the models of the components such as heat pump, house, and drying unit will be different.
- The input data for reference [71] are different with the present study.
- For example, the amplitude for the water temperature curve in this study is different in comparison with [71] because of the mentioned reasons.

5.3 Validation Procedure for the Study [131]

Following the same principle that was introduced in section 5.2, it can be stated that there is no such a study in the literature related with periodic solution for SAHP drying system whose modeling is presented in chapter four. Therefore some figures from reference [131] were selected for comparison and validation. The following figures are the comparison of the results from [131] and validated results from a MATLAB program which prepared in this study:

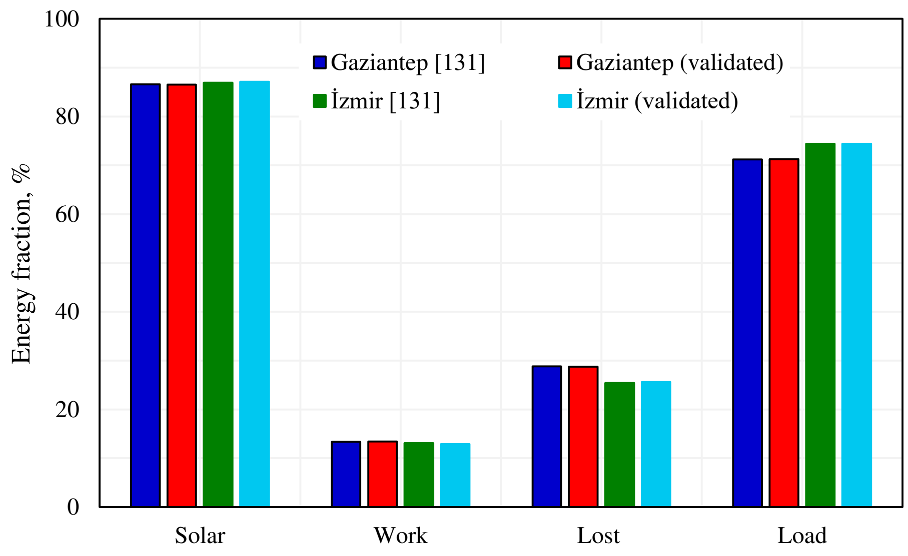

Figure 5.7 Annual energy fractions for 2 cities (one house, one glass-cover black surface, A_c = 30 m^2, $\beta = \theta_L$, a = 5 m, limestone) [Comparison].

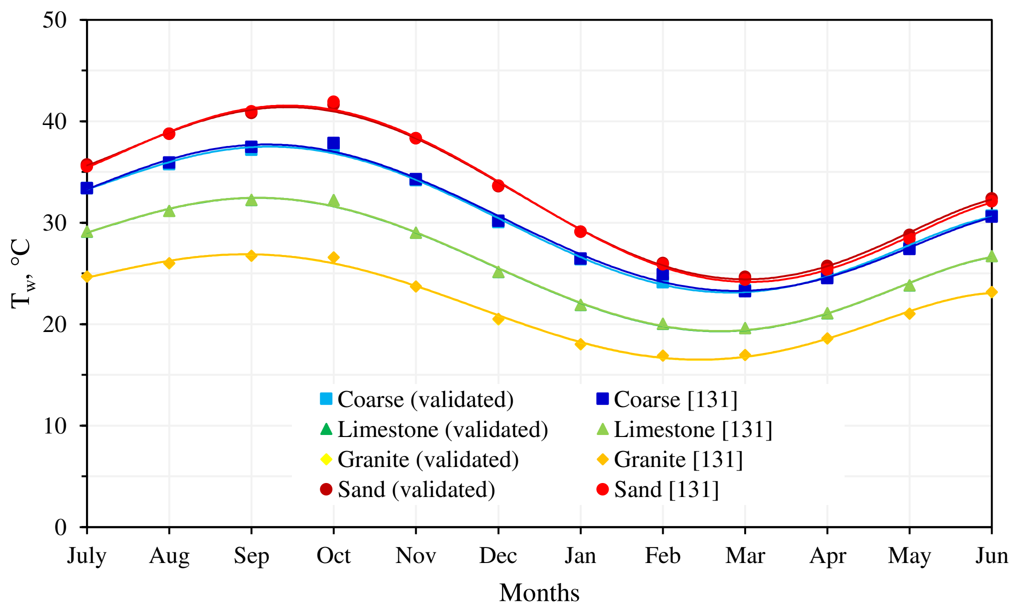

Figure 5.8 Annual variation of the water temperature in the storage for different geological structures (Gaziantep, one glass-cover black surface, A_c = 30 m^2, a = 5 m, β = 37.1°) [Comparison].

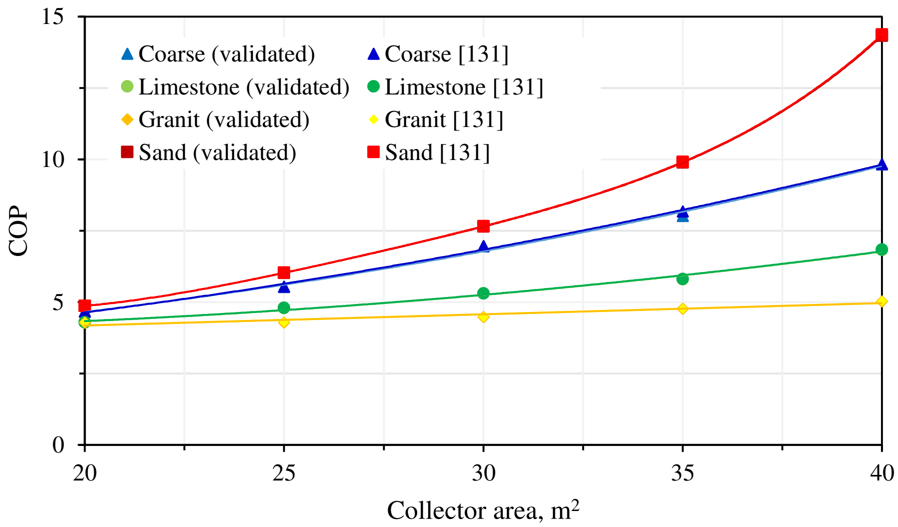

Figure 5.9 Annual COP versus collector area for four different earth types (Gaziantep, one house, one glass-cover black surface, β = 37.1 °, a = 5 m) [Comparison].

The validated results shows that the model for [131] written in MATLAB program is correct. Consequently, the models for the drying unit and heat pump in this study were inserted in MATLAB program in another new program for SAHP drying system, and the results are presented in sections 7.4 and 7.5 in chapter seven.

The following comments can be seen by comparison the validated results with the results presented in [131]:

- The results of the validation and literature [131] which are presented in figures (5.7, 5.8, and 5.9) are corresponded to each other.
- The results for the validation and literature [131] showed that the error between the two results cannot be mentioned because it is very low. Consequently, the validation program for the model presented in [131] and prepared in MATLAB can be used in this study, especially for solar collectors and spherical TES tank parts because they are the main components for the model presented in chapter four in this study.
- The heating load is considered to be constant in the present study while it is considered to be variable in reference [131].
- The model in the current study is used for drying application while the model in [131] is used for space heating, therefore the models of the components such as heat pump, house, and drying unit will be different.

- The input data for this study are different with those presented in [131].
- For example the amplitude for the water temperature curve which presented in chapter seven in several figures, is different in comparison with that presented in [71] because of the previous reasons.

CHAPTER 6

COMPUTATIONAL PROCEDURES

6.1 Introduction

This chapter presents computational procedures for the SAHP drying system with TES tank and HRU or without HRU using different methods and input data for load, flat plate solar collectors, and TES tank etc. Accordingly, the computational procedures for the system modeling analysis are presented in four sections. The details of the system modeling for all cases are introduced in chapters three and four. The same model that was presented in chapter three is used for both cases but HRU is considered to be operated with the drying system for energy saving in the second case. Also, the same model that was presented in chapter four is used for both cases but HRU is considered to be used with the drying system for energy saving in the second case. Computational procedures in sections 6.2 and 6.3 are related with drying system modeling presented in chapter three while sections 6.3 and 6.4 are related with system modeling presented in chapter four. All computational precedures for the study cases are represented in flow charts in Appendix A.

6.2 Computational Procedure for the SAHP Drying System with TES Tank

In order to examine the performance of wheat drying system, a computational procedure is developed by using interrelated analytical models and expressions for each system component. The drying system consists of four main components: drying unit, heat pump, solar collectors, and TES tank. The current drying system is a solar-assisted heat pump drying system with the TES tank. The numerical computation was prepared by using MATLAB, and is explained in this section.

The computation procedure passes through several stages. Firstly, heating load for the drying unit has been calculated through Equations (3.1-3.11). Hourly heating requirement of the drying unit and wheat mass flow rate are considered to be constant in this calculation. Secondly, since ambient air temperature changes hourly, the mass or volume flow rate of the air will change. The power input required by the fan is calculated by using Equations (3.12) to (3.41). Thirdly, hourly useful solar energy, $\dot{Q}_u$(t), is computed by using Eq. (3.87) in addition to Eq. (3.88), which was recommended by Yumrutas, and Kaska [61]. Collector efficiency in Eq. (3.88) is computed by using hourly solar radiation rates on tilted surfaces, TES tank temperature, and outside air temperature. Solar energy gain is later transformed into dimensionless form using dimensionless expressions in Eq. (3.69), which is referred to in [71]. Next, new hourly water temperature in TES tank is estimated through Eq. (3.85) by utilizing net energy charge rate to TES tank expressed in Eq. (3.86). Finally, hourly, monthly and annual values of water temperature in TES tank, COP, COPs, SMER and energy fractions are computed. These computations were done on an hourly basis for sufficient number of years until the annual temperature distribution of the water in the TES tank reached annually periodic operating conditions for 10 years of operation.

6.3 Computational Procedure for the SAHP Drying System with TES Tank and HRU

In order to examine the performance of a wheat drying system, a computational model is developed by using analytical models and expressions for each component of the system. The drying system consists of five main components, which are drying unit, heat recovery unit (HRU), heat pump, TES tank, and solar collectors. The drying system is defined as solar assisted heat pump (SAHP) drying system with the HRU and TES tank. A program in MATLAB was prepared for the numerical computations. This section has an additional part which is HRU to be operated with the drying system to recover the waste energy from the drying unit. Accordingly, the model of HRU is added to SAHP drying with TES tank model. Therefor HRU model will be considered during the calculation procedure.

Procedure of the computational model was explained in this section. Firstly, heating load for drying unit has been calculated through Equations (3.1-3.11) with using subscript (1) instead of (a). Hourly heating requirement of the drying unit is constant with constant mass flow rate of the wheat. Secondly, since hourly ambient air temperature changes hourly, mass or volume flow rate of the air will change, then its capacity that enters the condenser is calculated by using Eq. (3.12) through (3.41). Thirdly, useful solar energy per hour (Q_u(t)) has been computed by employing Eq. (3.87) and the appropriate correlation for collector efficiency suggested by [61].

Collector efficiency in Eq. (3.88) has been computed through utilizing hourly solar energy rates on tilted surfaces, temperature of TES tank, and temperature of fresh air. Gain in solar energy has been later transformed into dimensionless form using dimensionless expressions (3.69) given in [71]. In the next step, new hourly water temperature in TES tank has been estimated through Eq. (3.85) by utilizing the rate of net energy charged to the tank expressed in Eq. (3.86) with noticing that, $q_H(\tau)$ in Eq. (3.86) is the energy supplied by condenser to the drying unit. The heat gain of the fresh air from the HRU may be available when moist exhaust air temperature, $T_3(t)$ from drying chamber is higher than fresh air temperature, $T_1(t)$. Therefore, when $T_1(t) \geq T_3(t)$, the total load for drying process is supplied by heat pump condenser only, and this situation occurs only in summer season. This situation can be analyzed by using equations (3.99-3.109), which are used to find all necessary parameters related with HRU in the calculations. Finally, hourly, monthly and annual values of water temperature in TES tank, COP, COPs, SMER and energy fractions have been computed. These computations were done for the drying system hourly throughout adequate years until the distribution of yearly water temperature in the tank reached annual periodic operational status for 10 years of operation.

6.4 Computational Procedure for the SAHP Drying System with TES tank for Periodic Operation

A computational model is developed by using analytical models and expressions for system components in order to examine performance of drying system. The drying system comprises of drying unit, heat pump, solar collectors and TES tank. The current drying system is a solar-assisted heat pump drying system with the TES tank.

The computation procedure passes through several stages as previously explained. Firstly, heating load for drying unit has been calculated through Equations. (3.1-3.11). Monthly heating requirement of the drying unit and wheat mass flow rate are considered constant in this study. Secondly, since ambient air temperature changes monthly, mass or volume flow rate of the air will change. The power input required by the fan is calculated by using Equations (3.12) through (3.41). Thirdly, the power required for compressor and heat pump COP are calculated using Eqn. (4.5) through (4.11). Fourthly, monthly useful solar energy, $\dot{Q}_u$(t), and other parameters related are computed by using Equations (4.64-4.94). Solar energy gain is later transformed into dimensionless form using dimensionless expressions in Eq. (4.17). Next, new monthly water temperature in TES tank using CFFT technique has been estimated through Equations (4.50-4.54) by utilizing the net energy charge rate to TES tank expressed in Equations (4.57-4.63). Finally, monthly and annual values of water temperature in TES tank, COP, COPs, SMER and energy fractions have been computed. These computations were done on a monthly basis for one year of operation to find the periodic operating conditions directly without need to several years of operation.

6.5 Computational procedure for the SAHP drying system with TES tank and HRU for periodic operation

A computational model is developed by using analytical models and expressions for system components in order to examine the performance of the drying system. The drying system comprised of drying unit, a heat recovery unit (HRU), a heat pump, solar collectors and TES tank. The drying system is defined as solar assisted heat pump (SAHP) drying system with the HRU and TES tank. A program in MATLAB was prepared for the numerical computations. The different point in this section is that HRU is considered to work with drying system.

The computation procedure passes through several stages. Firstly, heating load for drying unit has been calculated through Equations (3.1-3.11). Hourly heating requirement of the drying unit and wheat mass flow rate are considered to be constant in this study. Secondly, since ambient air temperature changes hourly, mass or volume flow rate of the air will change accordingly. The power input required by the fan is calculated by using Equations (3.12) through (3.41). Thirdly, the power required for compressor and heat pump COP are calculated using Eqn. (4.5) through (4.11). Fourthly, monthly useful solar energy, $\dot{Q}_u$(t), and other parameters related with it are computed by using Equations (4.64-4.94). Solar energy gain is later transformed into dimensionless form using dimensionless expressions in Eq. (4.17). Next, new monthly water temperature in TES tank using CFFT technique is estimated through Equations (4.50-4.54) by utilizing net energy charge rate to TES tank expressed in Equations (4.57-4.63). Equations (3.95-3.101) are used to find all necessary parameters related with HRU in calculations. Finally, monthly and annual values of water temperature in TES tank, COP, COPs, SMER and energy fractions are computed. These computations were done on a monthly basis for one year of operation to find the periodic operating condition directly without the need of several years of operation as in sections (6.2 and 6.3).

CHAPTER 7

RESULTS AND DISCUSIONS

7.1 Introduction

This chapter presents and discusses the simulation results of Solar-Assisted Heat Pump (SAHP) drying system with Thermal Energy Storage (TES) tank and Heat Recovery Unit (HRU) or without HRU. The drying system comprises of four main components which are; a drying unit, a heat pump, an underground TES tank, and solar collectors for the case one in both chapters 3 and 4. While the drying system comprises of five main components which are; a drying unit, a heat pump, an underground TES tank, solar collectors, and HRU for the case two in both chapters 3 and 4. In fact, the results of four cases are presented in this chapter. The cases are as follows:

- The results of mathematical modeling of a SAHP drying system with underground TES tank are described in this chapter. In this case, Duhamel's superposition technique is used to solve TES tank problem and its model and others system components models in addition to input data are mentioned in chapter three. The computational procedure for this case is explained and presented in chapter five. Consequently, only the results of this case are presented in section 8.2.

- The results of mathematical modeling of a SAHP drying system with underground TES tank and HRU are described in this chapter. In this case, Duhamel's superposition technique is used to solve TES tank problem and its model and others system components models in addition to input data are mentioned in chapter three. Also, the model of HRU and its input data are presented in chapter three. The computational procedure for this case which considered HRU to be used with drying system is explained and presented in chapter five. Therefore, only the results of this case are presented in section 8.3.

- The results of mathematical modeling of a SAHP drying system with underground TES tank are described in this chapter. In this case, CFFT technique is used to Solve TES tank problem. The system components models of this case and input data are presented in chapter four. The computational procedure for this case is explained and presented in chapter five. Accordingly, only the results of this case are presented in section 8.4.

- The results of mathematical modeling of a SAHP drying system with underground TES tank and HRU are described in this chapter. In this case, Duhamel's superposition technique is used to solve TES tank problem and its model and others system components models in addition to input data are mentioned in chapter three. Also, the model of HRU and its input data are presented in chapter three. The computational procedure for this case which considered HRU to be used with drying system is explained and presented in chapter five. Consequently, only the results of this case are presented in section 8.5.

7.2 Results for SAHP Drying System with Underground TES Tank (Case 1)

This section presents the results of the drying system without using HRU which its model is explained in chapter 3. It is necessary to find performance parameters for the drying system in order to know whether the system within which the parameters operate are efficient or not. The performance parameters are: temperature of water in TES tank, coefficient of performance for the heat pump (COP) and system (COPs), energy ratios, and specific moisture evaporation ratio (SMER). They have been computed by executing a computer program in MATLAB and using drying system parameters such as Carnot efficiency, type of ground, collector area, and TES tank volume. In the calculations, limestone is used as a geological structure, and Carnot efficiency (CE), collector area, volume of TES tank are set as, 0.4, 70 m^2 and 300 m^3, respectively, unless other values of these input parameters are used. Results obtained from the simulation computations for the first case of the system modeling in chapter 3 are presented in figures, and discussed in this section. This case is to investigate the drying system performance without using HRU to find periodic situation for 10 years of operation.

Each earth surrounding TES tank gives different performance parameters because of different thermophysical properties. Variation of water temperature in the TES tank is a type of performance parameter. Hence, every performance parameter depends on storage temperature. For that reason, Fig. 7.1 depicts the individual effects of the three selected types of ground on temperature variation of water in TES tank during fifth year of operation by using these input parameters; collector area (70 m^2), Carnot efficiency factor (40%), storage volume (300 m^3), and mass flow rate of cooked wheat (50 kg h^{-1}). The reasons behind selecting these parameters are discussed in the following figures. It is observed from Fig. 7.1 that water temperatures have higher values during summer months and lower values during winter season when the TES tank is surrounded by the coarse graveled earth. But, water temperatures for granite have lower values in summer and higher values in winter. Limestone gives medium temperature values that are between coarse graveled and granite, which accordingly give medium performance parameters. Granite and coarse graveled earth types do not present widely as a geological structure around Gaziantep City, Turkey. All figures depict limestone ground since it is widely present in Gaziantep, unless another type is given in this section.

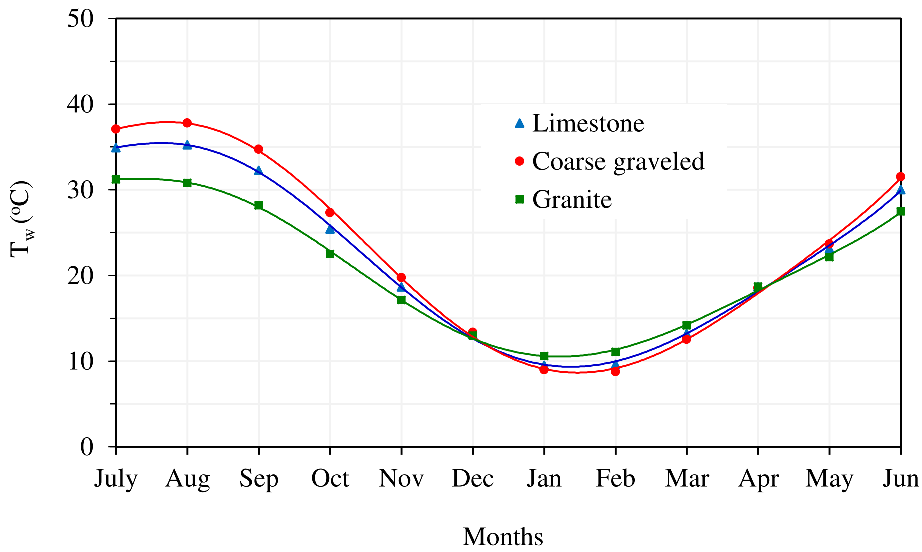

Figure 7.1 Effect of earth type on annual temperature variation of water in the TES tank during fifth year.

Figure 7.2 shows long term temperature variations of water in TES tank surrounded by three different kinds of earth; coarse graveled earth, limestone, and granite for September. It is seen from Fig. 7.2 that coarse graveled earth gives greater TES tank temperatures than the limestone and granite. Such a variation may be attributed to three thermophysical properties for the ground, which are thermal conductivity, specific heat and density. Heat capacity ($C=\rho C_p$) is a property, and depends on density and specific heat. Thermal diffusivity ($\alpha=k/\rho C_p$) is another property and depends on thermal conductivity, density and specific heat. From Table 3.2 which includes the thermophysical properties, it can be seen that thermal conductivity and diffusivity for the coarse graveled earth are lower than the corresponding properties of other two types, while specific heat and heat capacity are higher than the granite and limestone. It is observed from these properties that lower thermal conductivity and diffusivity decrease heat transfer and propagation from the TES tank to the surrounding earth. While, higher specific heat or heat capacity increases heat absorption capability. Variation of water temperature during the first few years and after fifth year is another observation. Water temperature in TES tank increases rapidly until the fifth year of operation. This indicates that the drying system reaches periodic operation in the fifth year for the given input system parameters, which adds more significance to the drying system.

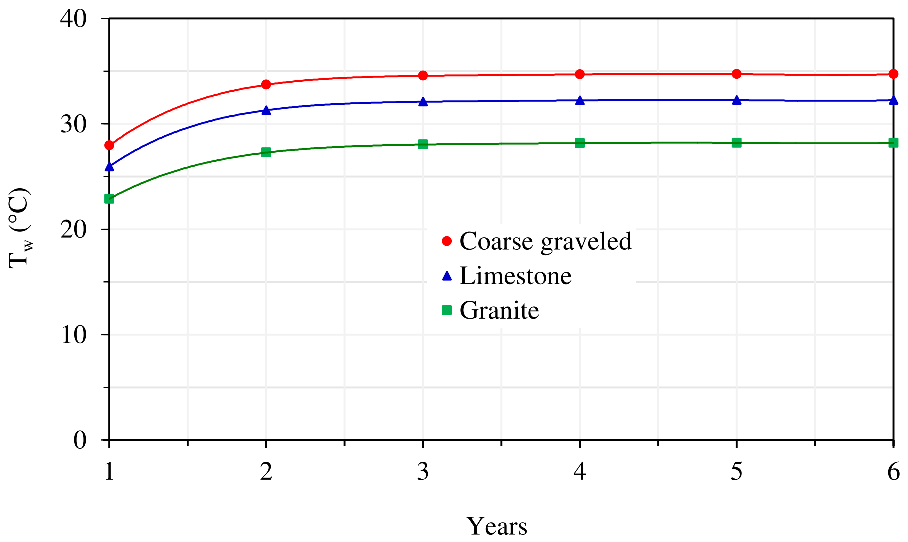

Figure 7.2 Effect of earth type on annual temperature variation of water in the TES tank for September.

Figures 7.3 and 7.4 show effects of three different kinds of earth; coarse graveled earth, limestone, and granite for several years. It is seen from Figs. 7.3 and 7.4 that coarse graveled earth gives greater COP and SMER than the limestone and granite. Such a variation may be attributed to three thermophysical properties for the ground, which are thermal conductivity, specific heat and density in Table 3.2. It is observed from these properties that lower thermal conductivity and diffusivity such as coarse graveled earth decrease heat transfer and propagation from the TES tank to the surrounding earth. Accordingly, COP and SMER increase as shown in Figures 7.3 and 7.4. While, higher specific heat or heat capacity as in coarse graveled earth increases heat absorption capability. COP and SMER increase rapidly until the fifth year of operation. This indicates that the drying system reaches periodic operation in the fifth year onwards for the given input system parameters, which adds more significance to the drying system.

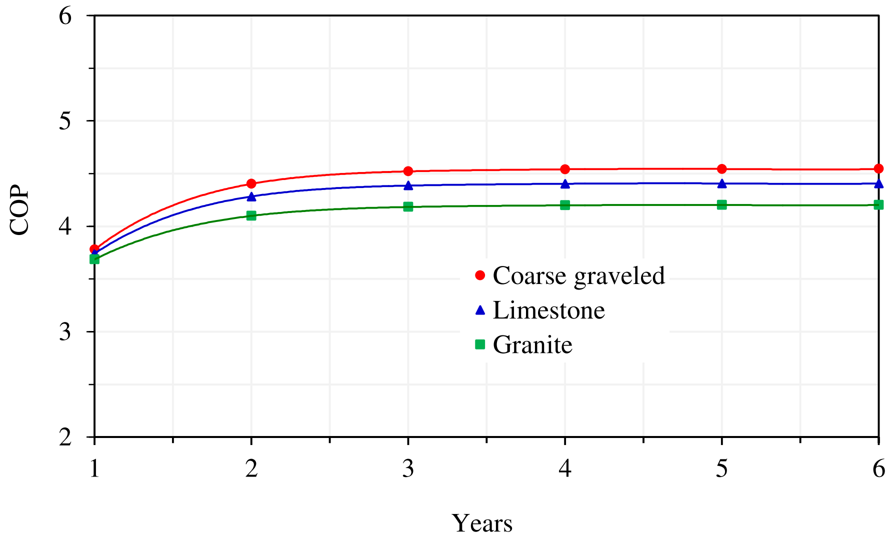

Figure 7.3 Effect of earth type on COP.

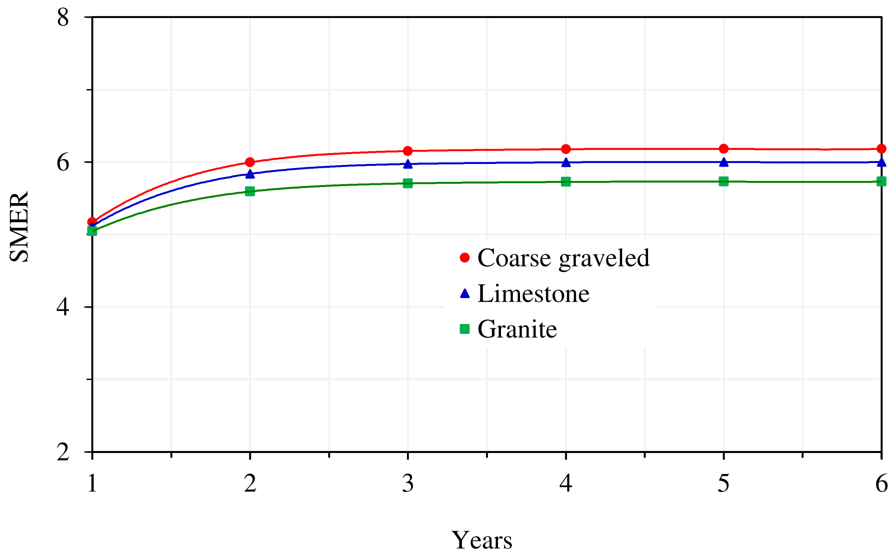

Figure 7.4 Effect of earth type on SMER.

Annual temperature variation of water in the TES tank for the first, second, third and fifth year of operation is shown in Fig. 7.5. It is seen from the figure that water temperature varies rapidly during the first few years. After that this variation decreases, and the drying system reaches the annual periodic operation in fifth year of operation onwards. It can be concluded that the number of periodical operation is equal to 5 years. That is, energy input to the TES tank is equal to heat loss from the tank, and energy balance takes place from fifth year of operation.

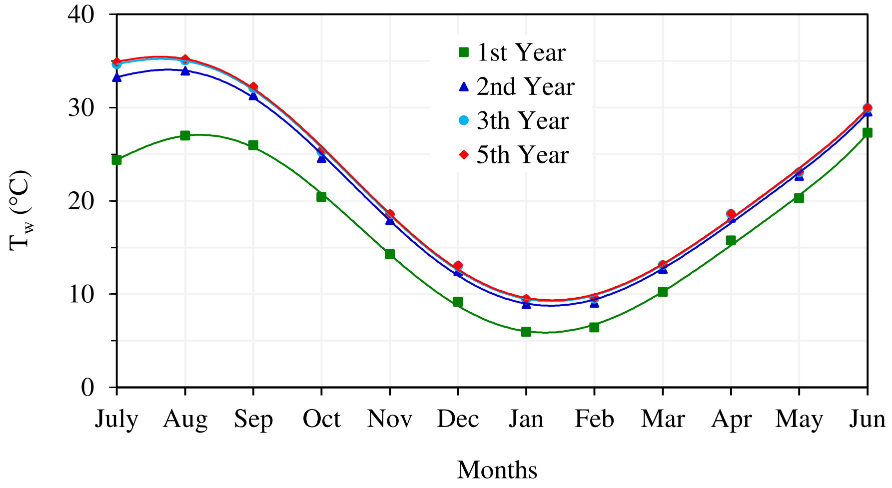

Figure 7.5 Annual temperature variation of water in the TES tank with number of operation years.

In order to define collector area for selected load or mass flow rate of cooked wheat, Fig.7.6 illustrates three different collector areas which are 65, 70 and 75 m^2. It is known that higher collector area gives higher water temperature. This indicates that there is a proportional relationship between collector area and water temperature in TES tank. An important point is that the selection of collector area should provide reasonable temperature for the water in TES tank. It is known that minimum collector area should be selected for reasonable performance parameters and three selected areas were suitable. When the collector area decreases below 65 m^2, water temperature approaches 0 °C especially for the first year of operation, and consequently gives lower performance parameters of COP, COPs and SMER such as in Figs. 7.7 and 7.8. Therefore, the suitable collector area is 70 m^2.

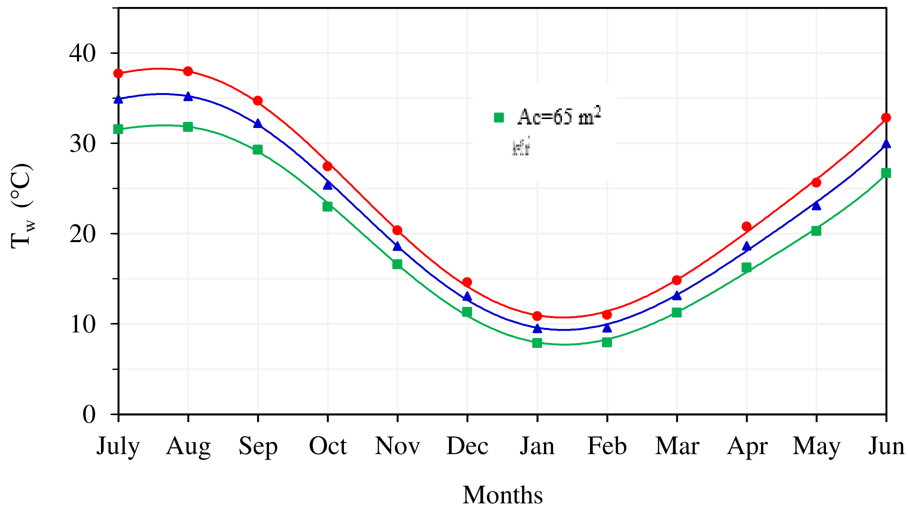

Figure 7.6 Effect of collector area on annual temperature of water in the TES tank during fifth year.

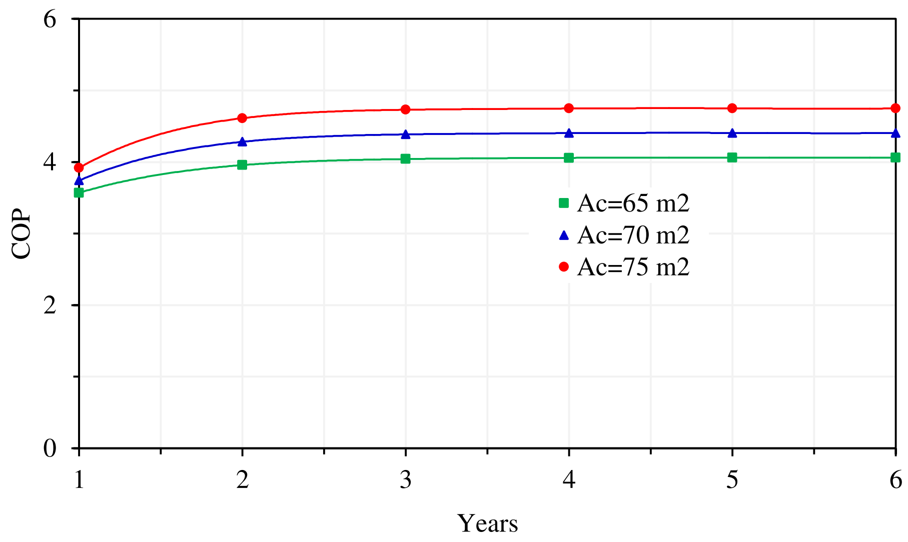

Figure 7.7 Effect of collector area on heat pump COP.

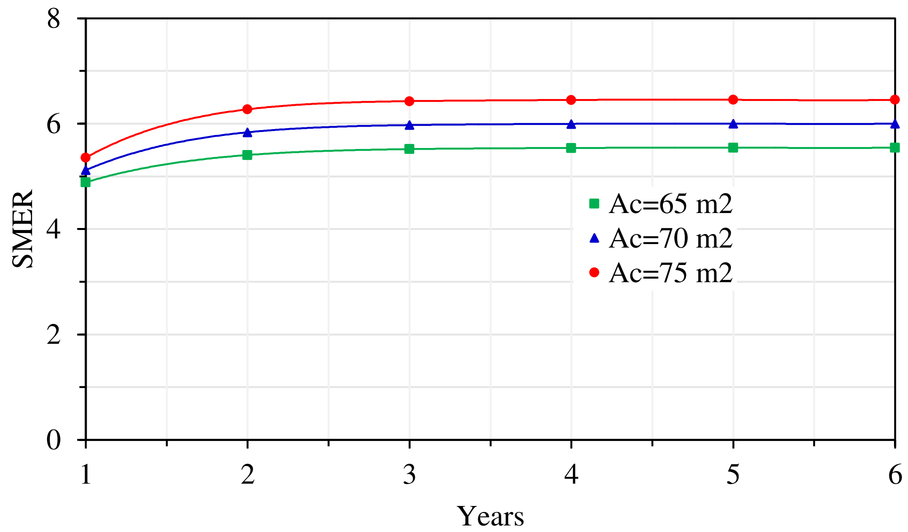

Figure 7.8 Effect of collector area on SMER.

Storage volume should be minimized to offer reasonable performance parameters. Fig. 7.9 determines the storage volume for the selected wet wheat mass flow rate of 50 kg h^{-1}. It is observed from the figure that lower TES tank volume gives higher water temperature during summer and lower water temperature during winter. That is, lower tank volume gives higher water temperature amplitude. Once the tank volume is 200 m^3, water temperature approaches 5 ^oC and then, performance parameters decrease to unreasonable values. For that reason, tank volume is selected as 300 m^3, and used to examine the effect of other parameters on the drying system performance.

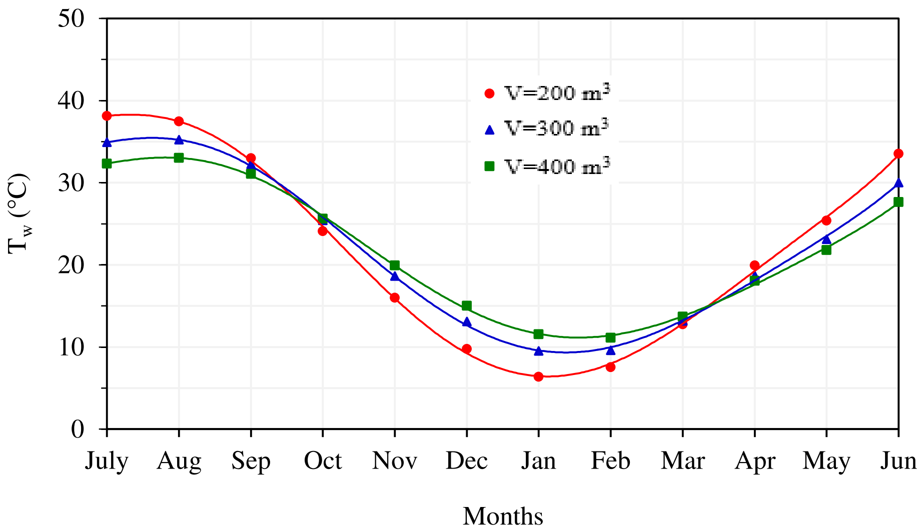

Figure 7.9 Effect of TES tank volume on T_w.

The effect of moisture content existing in wet wheat at final state MC_5 on SMER is depicted in Figure 7.10. Three different moisture contents with values of 0, 5, and 10 % for the wet wheat at final state are selected in the analysis for comparison of SMER. As it is clear from the figure, when the moisture content, MC_5 increase to 10%, SMER increases since latent heat requirement decreases with moisture content of wheat. Consequently, the drying heating load and power input to compressor are decrease.

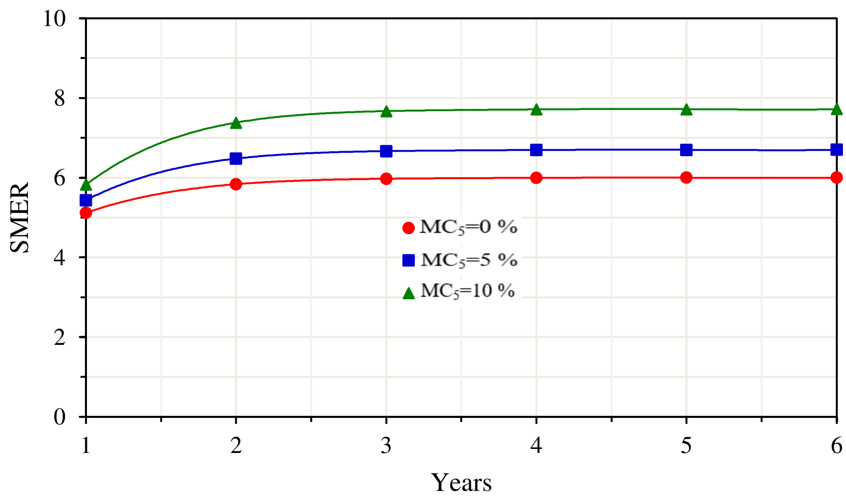

Figure 7.10 Effect of moisture content in wheat at final state on SMER.

Figure 7.11 depicts yearly variations of COP, COPs and SMER in order to see the effect of fan power on COP and periodic operation year. It is seen from the figure that COP and COPs are reasonably closer to each other for several years. Its reason is that power consumption of the fan is very low with respect to compressor power. Yearly fan power required is about 3 % of compressor load. Another point can be drawn from the figure that the performance parameters do not change or stay constant after fifth year. It means that the drying system reaches periodic operation at fifth year. This type of heating system requires periodic operation time from 5 to 7 years [71].

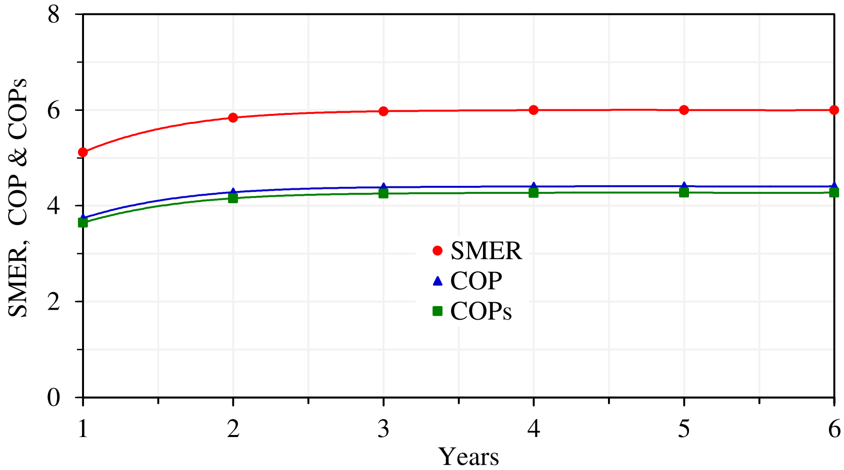

Figure 7.11 Yearly COP, COPs and SMER.

Carnot efficiency (CE) is defined as the ratio of Carnot COP to the actual COP. Actual COP depends on the types and size of a real heat pump. Zogou and Stamatelos [36] reported in their study that CE values in the ranges from 0.30 to 0.50 for small electric heat pumps. Therefore, three CE values of 0.30, 0.40 and 0.50 were selected in this study. Annual variation of water temperature in the TES tank is shown in Fig. 7.12. When CE increases, water temperature decreases, and COP of the heat pump and SMER increase. Annual variation of COP and SMER with three different Carnot Efficiencies are shown in Figs. 7.13 and 7.14, respectively. They increase with the number of operation years, and reach periodic operation during fifth year, and they remain constant after periodic condition.

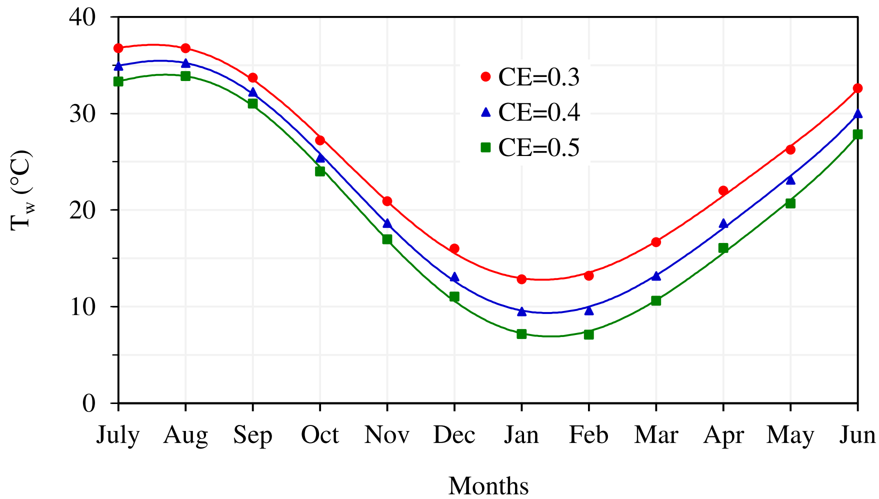

Figure 7.12 Effect of CE on annual T_w in TES tank during fifth year of operation.

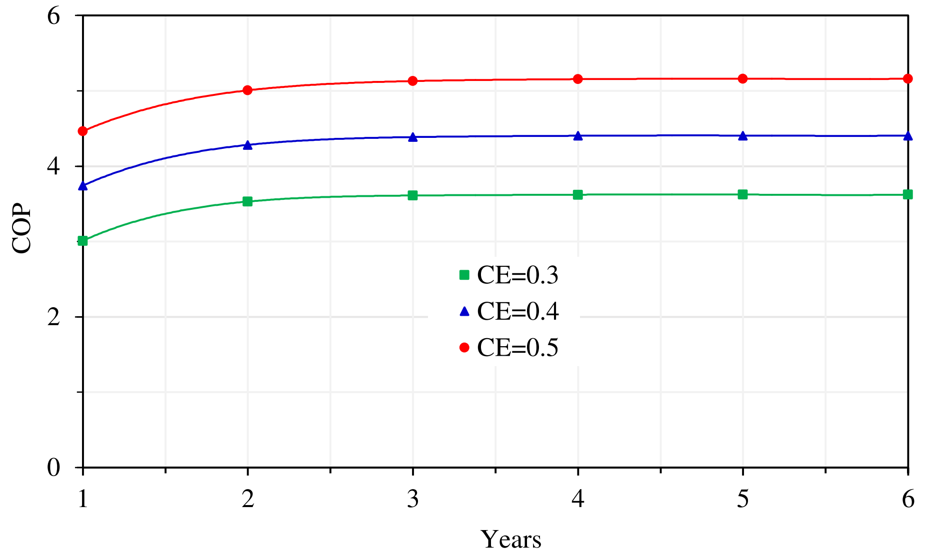

Figure 7.13 Annual variation of COP with different CE.

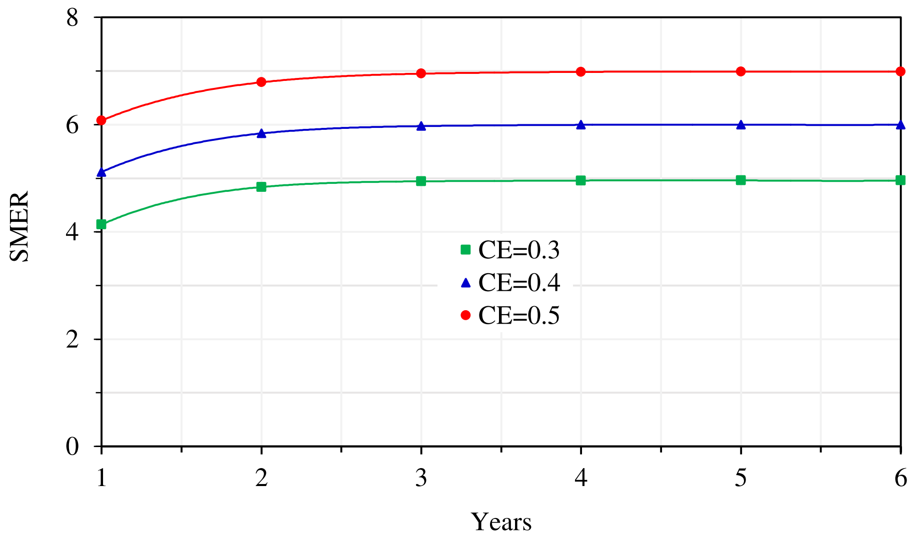

Figure 7.14 Annual variation of SMER with different CE.

It is important to make annual energy balance for the drying system. The energy supplied to the drying system consists of solar energy, heat pump work and fan power. The energy supplied to the system should be equal to total useful energy or load for the dryer unit, partially stored energy in the TES tank, energy lost to the surrounding earth. Energy fractions are defined as the ratio of each energy component to the total energy supplied to the system. Figure 7.15 shows energy fractions during the fifth year of operation for the first, second and fifth year of operation. It is seen from the figure that solar energy increases, compressor work decreases, and fan power stays constant throughout years. At the same time, both stored and lost energy decrease, and load increases with the years. It is observed that there is no stored energy during the fifth year operation, that is, the system operates periodically during and after fifth year.

Total energy input to the drying system supplied by solar energy, compressor work and fan power are 76.63 %, 22.68 %, and 0.7 % respectively during the fifth year of operation. It is observed from the figure that fan power is below 1 % of total energy input.

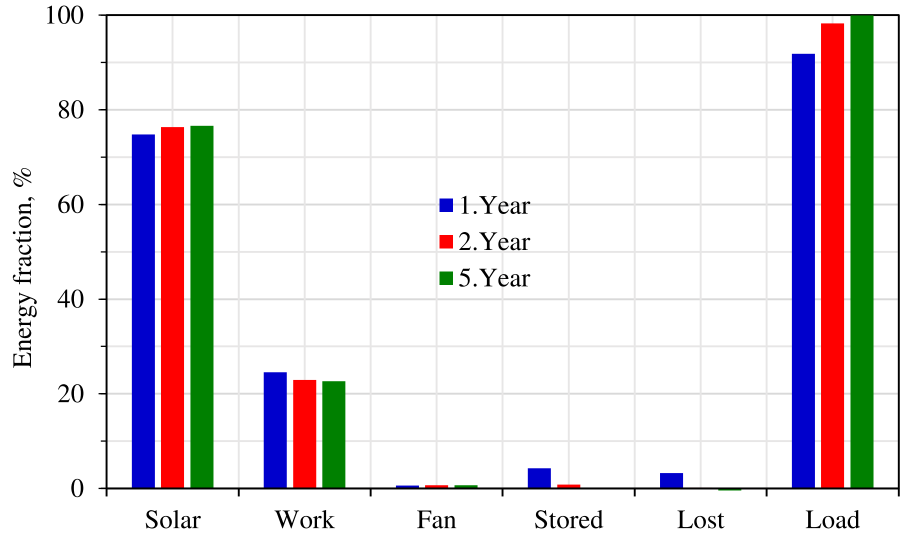

Figure 7.15 Variation of energy fractions with years of operation.

Mass flow rate of wheat affects performance parameters such as water temperature in TES tank, SMER, COP and COPs. Heating requirement of the wheat drying is calculated when wheat mass flow rate is selected. Then, collector area and storage tank volume are determined to get reasonable performance parameters. For that reason, the effect of wet wheat mass flow rate on COP during the fifth year or periodic operation is shown in Fig. 7.16. As it is shown in the figure, three different wheat flow rates (45, 50 and 55 kg h^{-1}) are selected to determine suitable flow rate under the given input data. The figure also shows that when the wheat mass flow rate is increased, the COP decreases. However, COP of heat pump range from 3 to 4 for mass flow rate of 55 kg h^{-1}. While, COP values varied from 4 to 5 for the mass flow rates of 45 ad 50 kg h^{-1} during the periodic operation year. Thus, these values are reasonable for the solar-assisted heat pump drying system. When mass rate of wheat is higher than 55 kg $h^{-1}$for TES tank volume of 300 m^3 and collector area of 70 m^2, water temperature will go under 5 °C, and consequently COP will go under 3 during the first year, which makes this value unreasonable. Consequently, W_4 or mass rate of wheat is taken as 50 kg h^{-1}

for all calculations since it is suitable for all performance parameters of the drying system.

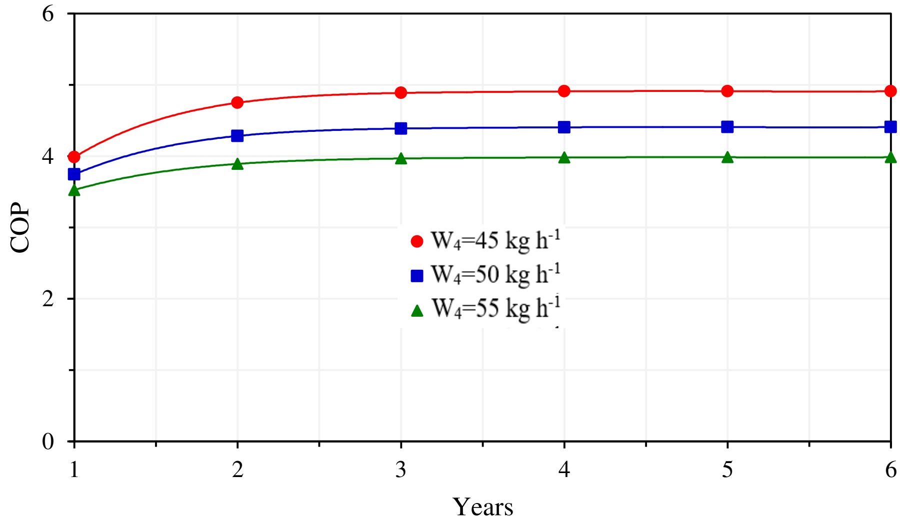

Figure 7.16 Effect of wheat mass flow rate variation on COP.

Heating load for the drying unit that must be provided hourly during the year is considered constant and that load is divided into two parts; sensible and latent heat. The biggest part of the load of wet wheat is the latent. In order to evaporate the moisture present in the wet wheat, more heat is required. There are some factors such as moisture content of wheat at inlet and outlet states of wheat. Moisture content of inlet state of wheat should be considered to be within reasonable values. Therefore, the effect of moisture content existing in wet wheat on performance parameters of water temperature in TES tank, and SMER is shown in Figs. 7.17 and 7.18, respectively. Three different moisture contents with values of 27.5, 30, and 32.5 % for the wet wheat are selected in the analysis for comparison of water temperature, SMER and COP. As it is clear from those figures, when the moisture content, MC_4 decrease to 27.5%, the all performance parameters of T_w, SMER, and COP increase since latent heat requirement decreases with moisture content of wheat. For that reason, heating load will decrease, and higher performance parameters of T_w, SMER, and COP are obtained. These three different moisture contents with values of 27.5, 30, and 32.5 % are selected according to [110]. The intermediate value which is 30% is selected for all other calculations in this case study.

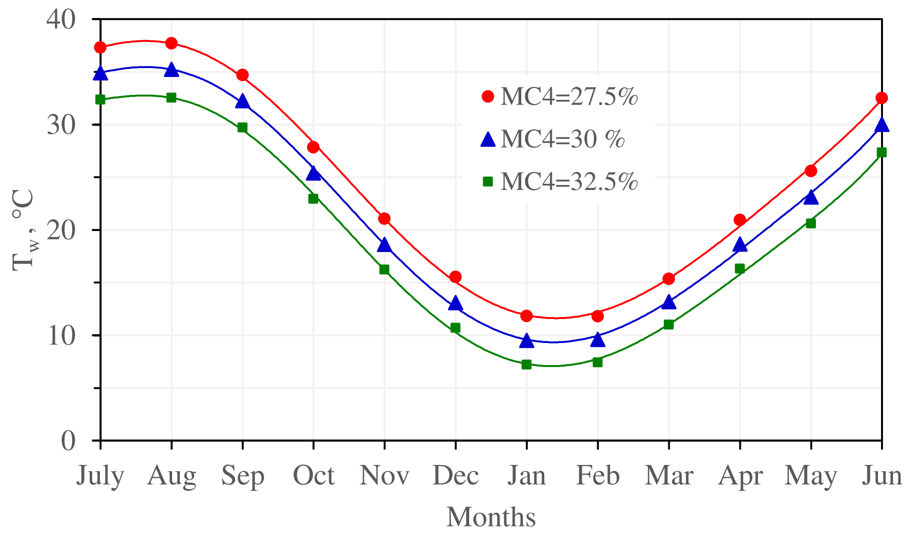

Figure 7.17 Effect of entering moisture content of wheat on T_w.

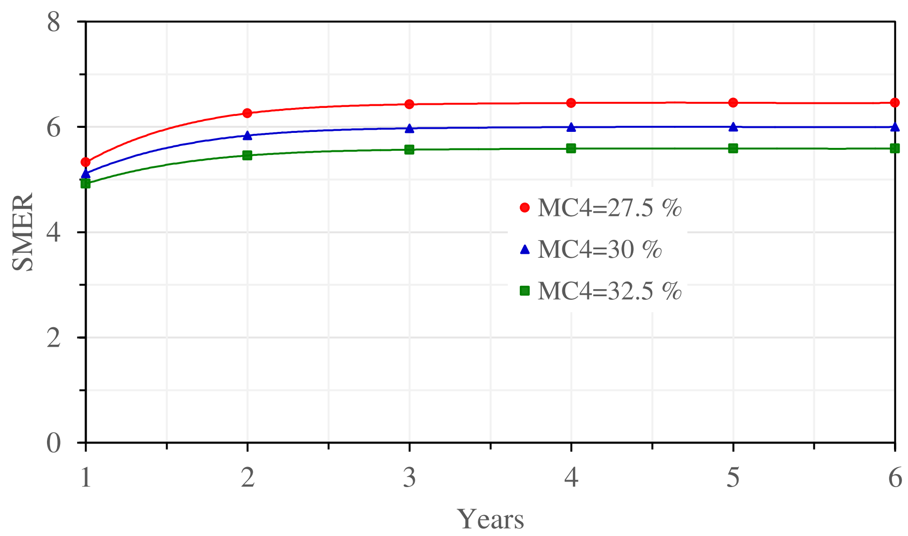

Figure 7.18 Effect of entering moisture content of wheat on SMER

7.3 Results for SAHP Drying System with Underground TES Tank and HRU (Case 2).

This case investigates thermal performance of SAHP drying system with and without Heat Recovery Unit (HRU) in order to know whether the system operates efficiently or not by finding performance parameters. These parameters are: temperature of water in the TES tank, coefficient of performance for the heat pump (COP) and system (COP_s), Specific Moisture Evaporation Ratio (SMER), energy fractions and energy saving in the HRU. They have been computed by executing a computer program in

MATLAB and using drying system parameters such as hourly solar energy on horizontal surfaces and temperatures of fresh air and other input parameters. In this case, same input data presented in chapter three are used for both drying system with HRU and without HRU in the referred figures otherwise, the figures for drying system with HRU are used. In this section, effect of each input parameter on the performance parameters will be discussed. These input parameters are type of geological structure, use of the HRU, collector area, TES tank volume, wheat mass flow rate and moisture content in dried wheat at final state. They will be discussed in the following subsections.

The different geological structures present around TES tank gives different performance parameters since each of them has different thermophysical properties. Water temperature in the tank comes under performance parameters since it affects all performance parameters for the SAHP drying system. Therefore, thermophysical properties for three commonly used earth types, which are coarse graveled earth, granite and limestone, are used to show the effect of soil type on water temperature in the tank in year 5 of operation, as shown in Fig. 7.19. The figure illustrates that water temperatures have higher values during summer months and lower values during winter months for all types of earth since energy charged in the tank has been extracted by heat pump evaporator during all seasons. During winter months, solar energy charging to the TES tank declines to the minimum values. Water temperature reaches the higher values when there is coarse graveled earth around the tank; while water temperatures for granite have lower values, and limestone gives medium temperature values that are between coarse graveled and granite. This is the case because values of thermal conductivity and diffusivity, specific heat and heat capacity of the limestone are between those values of the coarse graveled and granite. The medium temperature values give medium performance parameters. Sequencing of the water temperature distributions for these type of earths are in line with the studies [71; 108]. Granite and coarse graveled earth types do not exist widely as a geological structure around the Gaziantep City, Turkey. Therefore, all figures will illustrate limestone unless another type is given in the present study.

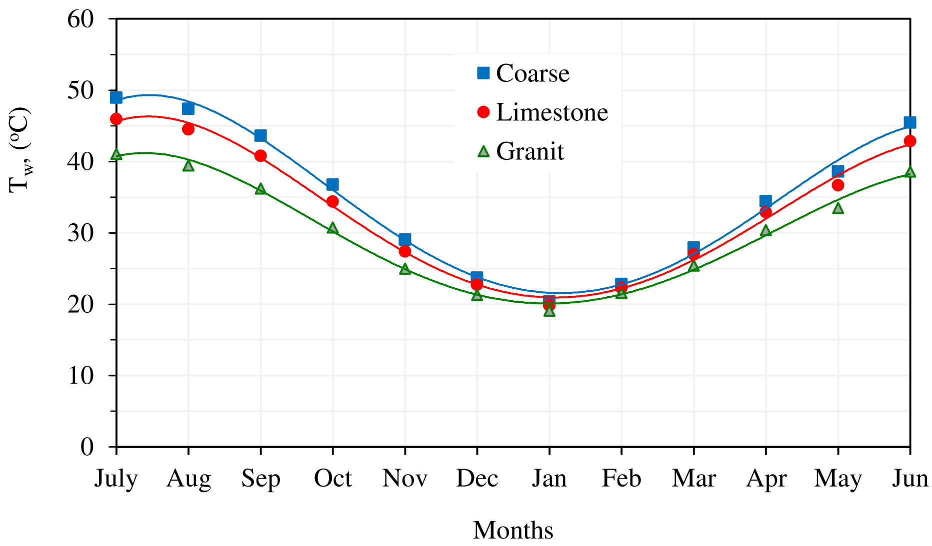

Figure 7.19 Effect of geological structure on yearly water temperature in the tank in fifth year.

Figure 7.20 shows long-term temperature variations of water in the tank which is surrounded by three various kinds of earth in September with and without HRU. The figure indicates the impact of various earth types and HRU on temperature of water in the tank. Coarse graveled earth has been shown to give greater tank temperatures than the limestone and granite type of ground for the system with and without HRU. It is possible to explain this situation by using three thermophysical properties for the ground, which are thermal conductivity, specific heat and density. Heat capacity ($C = \rho\ C_p$) is a property, and depends on density and specific heat. Thermal diffusivity ($\alpha = k/\rho C_p$) is another property and depends on thermal conductivity, density and specific heat. Table 1 shows that all these properties for the coarse graveled earth existing between those corresponding properties for the granite and limestone. It is observed from these properties that lower thermal conductivity and diffusivity lead to lower heat transfer and propagation from the TES tank to the surrounding earth. Higher specific heat or heat capacity lead to higher capability of heat absorption.

Second observation from the Fig. 7.20 is that using HRU increases water temperature. There is about 10 ºC increment in water temperature for each type of earths when the HRU is employed since some of the waste heat rejected from the drying unit is gained by the HRU, and the heat gain will lower the use of energy extracted from the TES tank. At this situation, temperature of water increases, and as a result, this increment will increase performance parameters of COP, COPs and SMER.

Fluctuation of water temperature during the first few years and fifth year onwards has also been observed. Water temperature inside the tank increases rapidly until year 5 of operation. This indicates that the drying system reaches periodic operation on the fifth year for the given input system parameters, which is also an important point for the SAHP drying system.

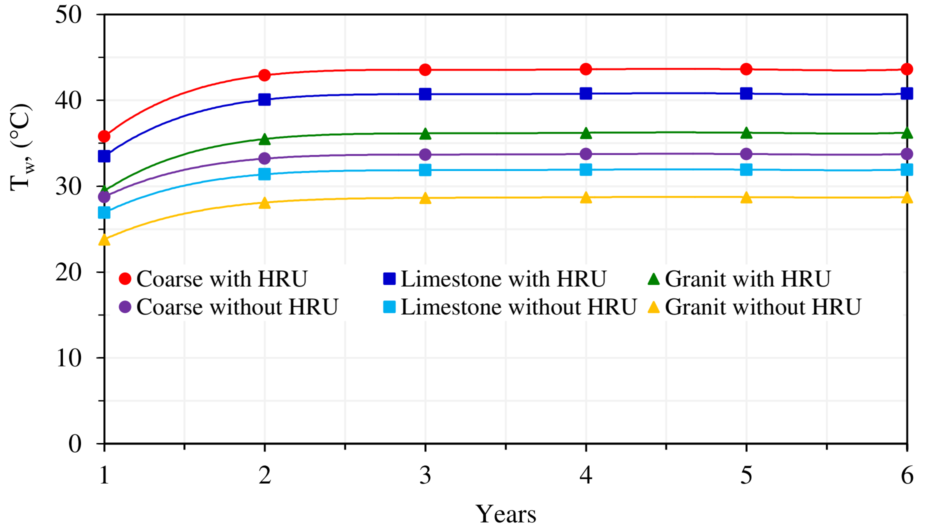

Figure 7.20 Effect of geological structure and HRU on yearly water temperature in the tank in September.

Heat gain from a waste energy is very important regarding energy saving and cost. In the SAHP drying system, some of the waste heat is gained by using a HRU. Figure 7.21 demonstrates the impact of the HRU upon the temperature of water in TES tank in the drying system operated with and without HRU. The variation of water temperature is explained during first, fifth and seventh year of operation. The figure shows that the water temperature approaches 0 °C in winter particularly in January and February because of low ambient air temperature and available solar energy charged to the TES tank for the system working without using HRU. The lower water temperature gives lower system performance parameters. When water temperature approaches 0 °C, it will be necessary to use auxiliary heating system such as electric heater. When the HRU is used, water temperature increases to about 15 °C for the winter months and 45 °C for summer months. This temperature range gives higher or reasonable performance parameters. It is clearly understood from the figure that the auxiliary heating will not be used. The figure also indicates that use of the HRU will have strong effect on the system performance. The following figure shows to extent the use of HRU will effect performance parameters of COP and SMER values

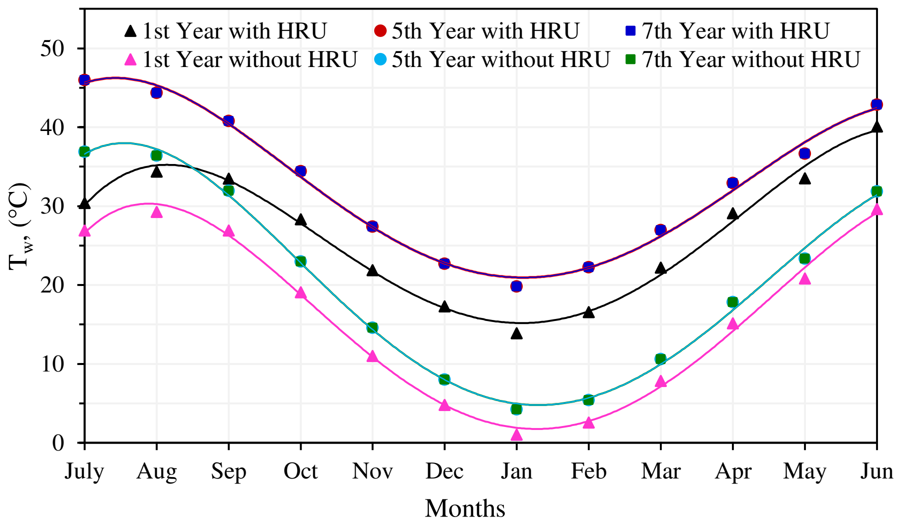

Figure 7.21 Yearly variation in water temperature in the TES tank for number of operation years with and without using HRU.

It is known that adding HRU to the drying system increases performance parameters of the drying system due to increased water temperature. In order to know the effect of the HRU on the drying system performance, it is possible to compare performance parameters of SMER and COP for the drying system with and without HRU. Yearly variations of SMER and COP are shown in Fig.7.22, which explains the parameters increase gradually depending on years. The system reaches periodic operation during fifth year for given input parameters and distributions of both parameters are similar. This is normal since the SMER is a function of the COP. Yearly variation of the COP is in line with the variation of COP given in the study [71]. However, values of the COP are different since loads of the heating systems are different.

It is noted that yearly COP of heat pump increases from 4.20 to 5.55 (32.14%), and yearly SMER for the drying system increases from 5.69 to 9.25 (62.56%) by using HRU for fifth year of operation. Variation of SMER is approximately double the COP variation when the HRU is applied to the drying system. The maximum upsurge in COP is (32.14%) and for SMER is (62.56%) because compressor work input decreases basically by using HRU or heat gaining from the HRU since the SMER is directly proportional with a value of $\dot{m}_w/\dot{Q}_H$ given in Eq. (3.121).

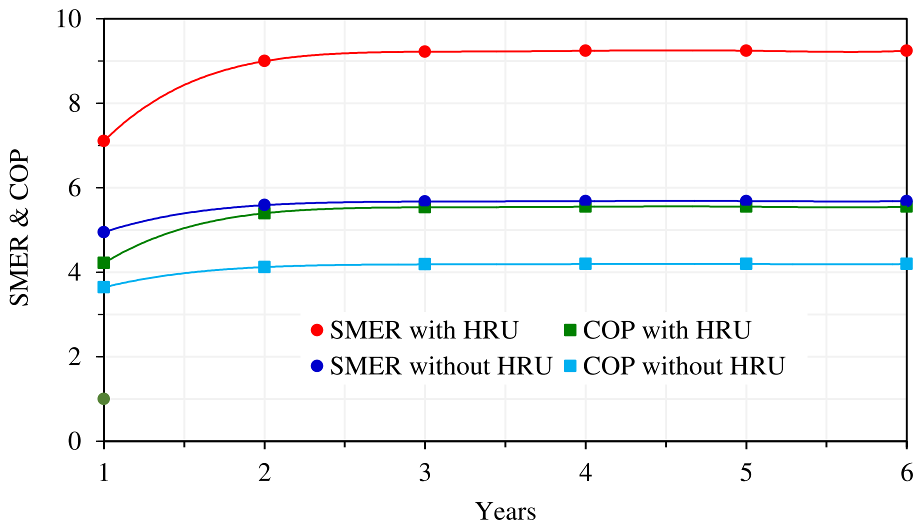

Figure 7.22 Comparison of yearly COP and SMER for number of operation years with and without using HRU.

Solar energy is the most important parameter for the performance of the SAHP drying system since the amount of stored solar energy depends on the collector area. For that reason, it is necessary to examine the influence of collector surface area on water temperature in the tank for selected mass flow rate of 100 kg h^{-1} cooked wheat. Monthly temperature variation of water in the TES tank is shown in Fig. 7.23 for three collector areas of 75, 100 and 125 m^2. It is known that higher collector area gives higher solar energy charging to water in TES tank, and lower collector area gives lower solar energy. Considering all that, the selection of the collector area should provide reasonable temperature for the water in the TES tank since reasonable temperature gives reasonable performance parameters. As it is seen from the figure, the three temperatures are suitable. When the collector area is selected as 75 m^2, water temperature approaches 0 °C during first year, and performance parameters will be lower than reasonable value. There is a criterion based on which, water temperature shall not approach 0 °C especially for the first year of operation. Collector area is set as 100 m^2 since it is suitable.

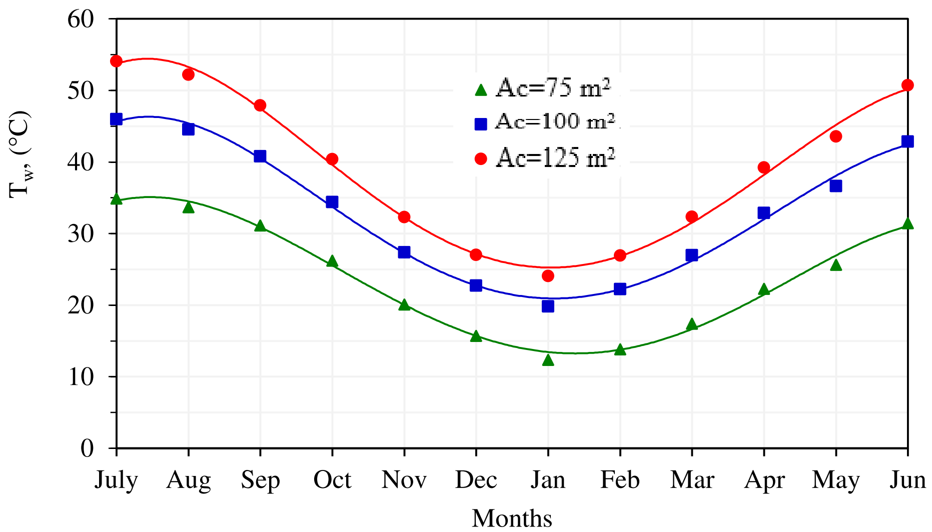

Figure 7.23 Effect of collector area on yearly water temperature in the tank in year 5.

Performance parameters are important for the drying system. The parameters are water temperature in the tank, SMER and COP. Impact of collector area upon variation in water temperature during fifth year is discussed in Fig.7.24. The effects of collector area on SMER and COP for the drying system with HRU are illustrated in Fig.7.24 for three different collector areas which are 75, 100 and 125 m^2 for year 5 of operation. It can be noticed that the COP and SMER increases with the collector area because of increasing energy charging to the TES tank. It is important to select a reasonable collector area in order to have a reasonable SMER and COP. It is seen from the figure that SMER ranged between 5 and 7, and COP ranged between 3 and 4 for the collector area 75 m^2 during fifth year of operation. These are not reasonable values for the periodic operation. When collector area is selected as 100 m^2, COP takes reasonable values between 4 and 6, and the values of SMER are between 7 and 10. The results for the COP are in agreement with [71]. Because of these reasonable values of COP and SMER, collector area is selected as 100 m^2 for the other input data used in this study.

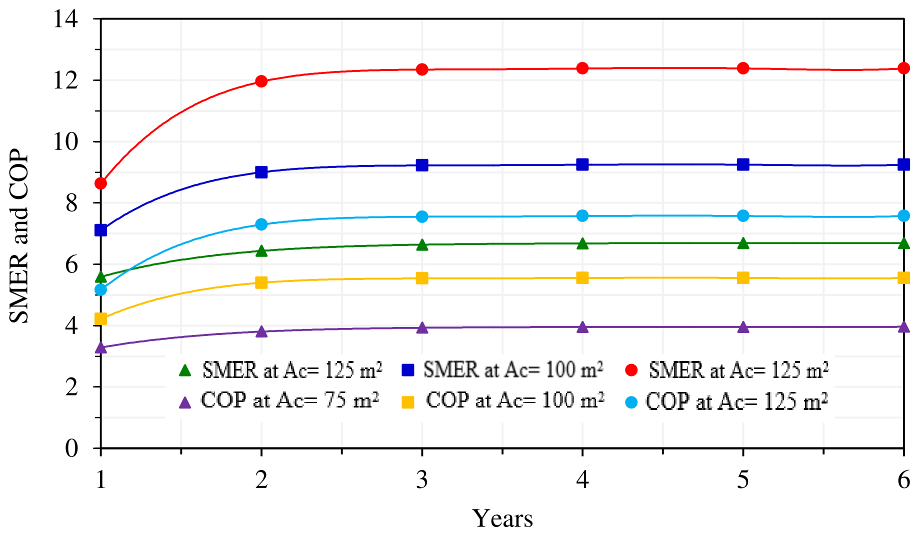

Figure 7.24 Effect of collector area on yearly SMER and COP.

The heating load of the drying unit is energy required to remove moisture from the wheat. The load is corresponds to heat pump condenser and HRU. Utilizing of HRU offers an opportunity to use the waste heat from drying unit for energy saving. The heating requirement depends on mass flow rate of wheat. That is, source of energy need is the wheat mass flow rate. When it changes, heating requirement will change. The effects of wet wheat mass flow rate on performance parameters of water temperature in the tank, and SMER and COP are depicted in Figs. 7.25 in year 5 of operation, while Fig. 7.26 shows these data for several years of operation. Three different wheat flow rates, which are 75, 100 and 125 kg h^{-1}, used in the analysis will be compared to select suitable flow rate under the given input data. It can be seen from those figures when the wheat mass flow rate is increased, the all performance parameters, $T_w(t)$, COP, and SMER will decrease. It is clearly observed from the Fig.7.25 that the performance parameters changes in suitable ranges if wheat flow rates, W_5 are selected as 100 kg h^{-1} and 125 kg h^{-1}. However, when the W_5 is selected as 75 kg h^{-1}, values of the COP and SMER will be around 4 and 7 during fifth year, respectively. These values are not reasonable values for the SAHP drying system. Consequently, W_5 is selected as 100 kg h^{-1} since it is suitable for all performance parameters of the drying system.

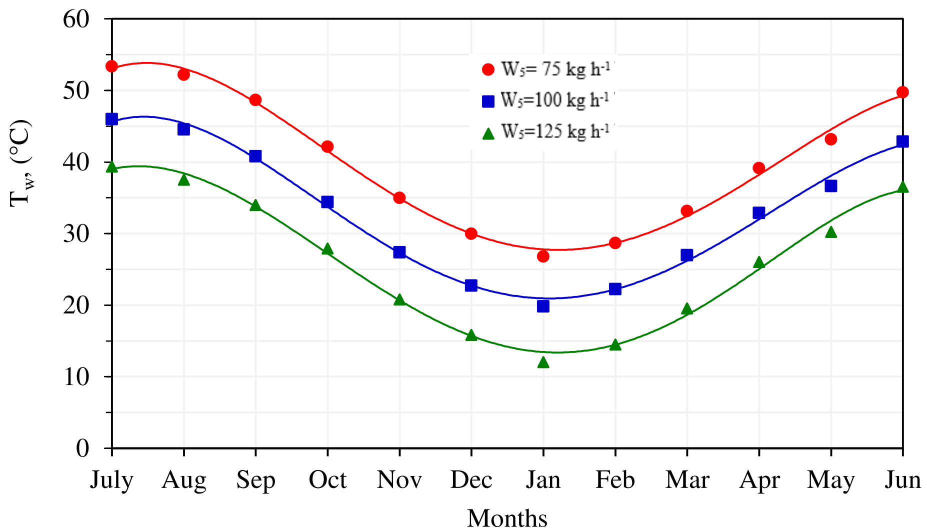

Figure 7.25 Effect of wheat mass flow rate on hourly water temperature in the tank in fifth year.

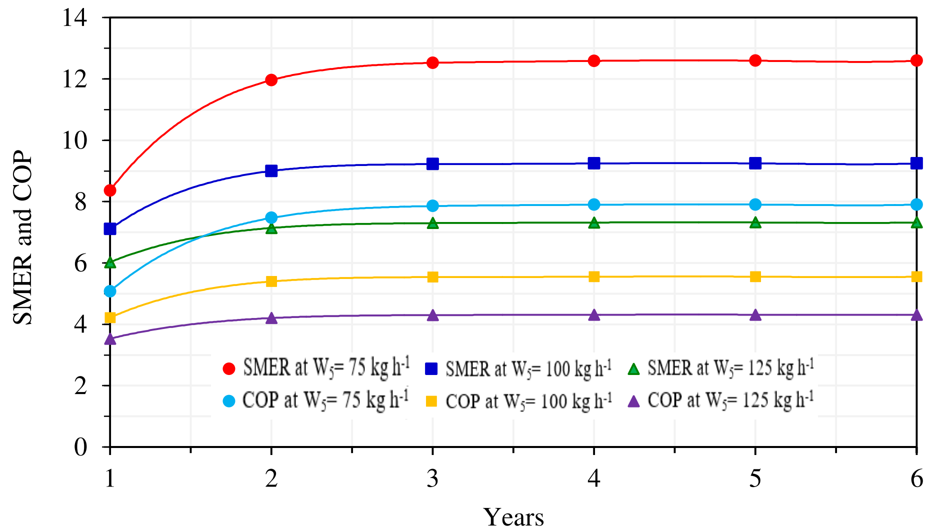

Figure 7.26 Effect of wheat mass flow rate on yearly SMER and COP.

Heating load for the drying unit that must be provided hourly during the year is considered constant and that load is divided into two parts; sensible and latent heat. The biggest part of the load of wet wheat is the latent. In order to evaporate the moisture present in the wet wheat, more heat is required. There are some factors such as moisture content of wheat at inlet and outlet states of wheat. Moisture content of final state of wheat should be considered to be within reasonable values. Therefore, the effect of moisture content existing in dried wheat on performance parameters of water temperature in TES tank, and SMER and COP is shown in Figs. 7.27 and 7.28, respectively. Three different moisture contents with values of 0, 5, and 10 % for the dried wheat are selected in the analysis for comparison of water temperature, SMER and COP. As it is clear from those figures, when the moisture content, MC_6 decrease to 0%, the all performance parameters of T_w, SMER, and COP decrease since latent heat requirement increases with moisture content of wheat. For that reason, heating load will increase, and lower performance parameters of T_w, SMER, and COP are obtained. It is seen from Fig. 7.28 that COP ranges between 3 and 4 for moisture content of 0 %, and between 3.73 and 4.66 for 5 % of moisture content. At the same time, the 0% and 5 % of moisture content of the wheat at the exit state elevate energy demand for the drying unit. However, moisture content of 10 % is suitable for energy saving for the drying system. Storing the dried wheat at this moisture content 10 % can be accepted, and it can be stored in a safe climatic condition, that is below room temperature [2]. Moisture content with 10 % gives higher performance parameters for the SAHP drying system. Therefore, moisture content at exit state of wheat is selected as 10 % for all calculations in this study.

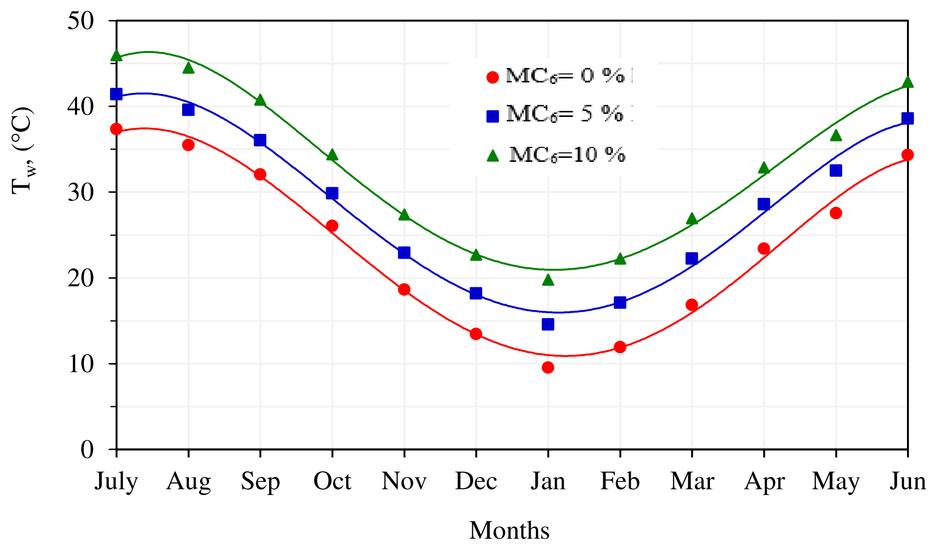

Figure 7.27 Monthly variation in the temperature of water with respect to wheat moisture content at the exit during fifth year.

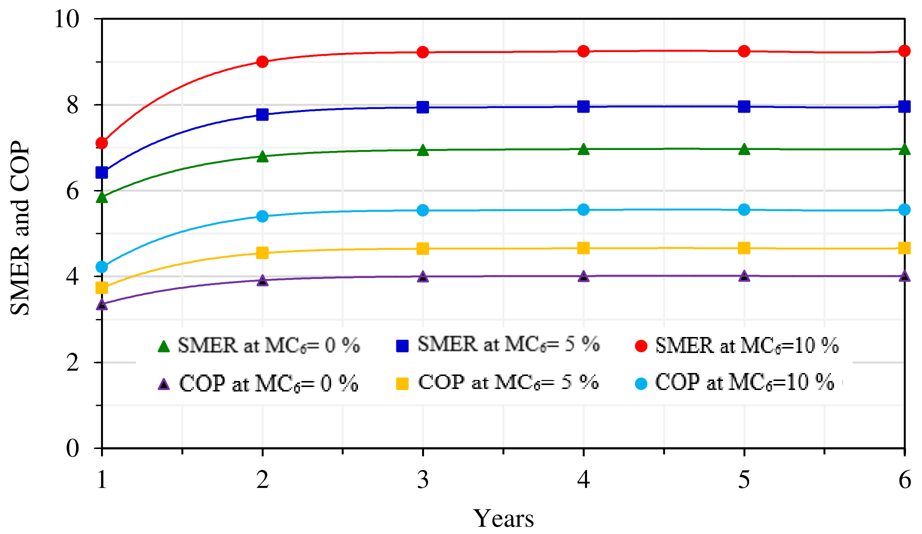

Figure 7.28 Yearly variation of SMER and COP with respect to wheat moisture content at exit state.

There are three important performance parameters for the drying system, which are COP, COPs and SMER. These indicate the convenience of the drying system. Figure 7.29 presents the effect of selected parameters for the drying system on the COP, COPs and SMER. They increase starting from July, and reach the maximum values in August due to the high ambient air temperature and available solar energy stored in the tank.

Ambient air having high temperature requires lower energy absorbed from the condenser and lower compressor work. At the same time, high solar energy raises water temperature in the tank. Heat pump evaporator has extracted more energy from the tank. Due to the higher absorbed energy by the refrigerant in the evaporator and lower energy rejected from the condenser, the compressor work of the heat pump lowers. Consequently, COP, COPs and SMER will increase during the summer months. Another point is that COP of the heat pump and SMER are parallel to each other throughout the year. The physical mentalities of the COP and SMER are similar since COP is heat rejected from the condenser for one kilowatt energy consumption of the compressor, and SMER is mass of evaporated moisture for one kilowatt of energy requirement. The other important result shown in the figure is that the COPs for the drying system is lower than COP for the heat pump in June, July, August and September which considered local summer months, but closer to each other in remaining months. These conditions can be explained as; load of drying unit and supply air temperature T_2 are constant, and pre-condenser air temperature in addition to air mass flow rate are variables. The total load supplied by the system which equal to drying load is composed of condenser and HRU loads. Accordingly, pre-condenser air temperature has inverse relation with air mass flow rate. During June, July, August and September, ambient air temperature increases then temperature difference between the ambient air and supply air temperatures decreases. As a result, fan capacity and its power should be increased. For that reason, fan power increases and COPs for the system decreases during June, July, August and September. Using the HRU in this study raises monthly COP, COPs, and SMER particularly from October to May because the HRU recovers the waste heat from drying unit and increases the ambient air temperature before entering the condenser. As a result, COP, COPs, and SMER will increase.

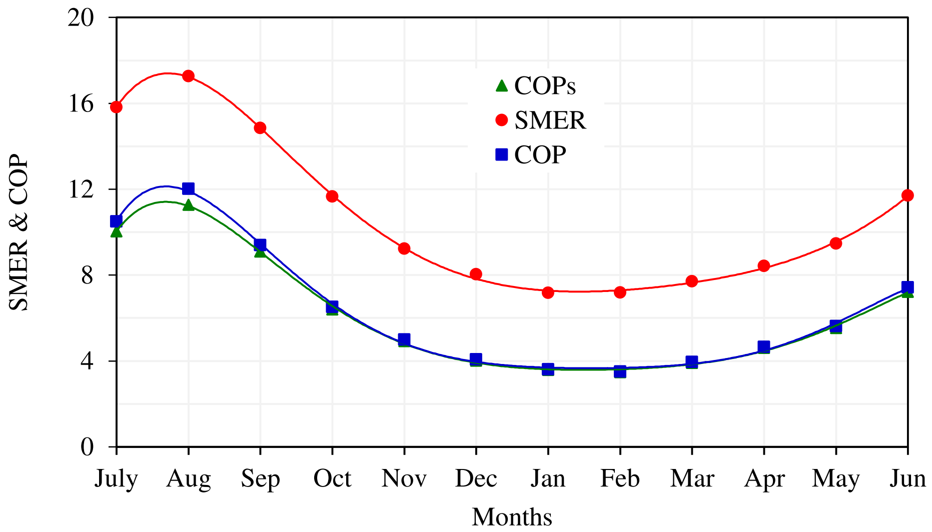

Figure 7.29 Average monthly variation of COP, COPs and SMER.

The SAHP drying system has input energies, which are solar energy, compressor and fan works. All of these energies constitute the total energy provided to the drying system for long-term period. Part of the charging energy to the TES tank is stored in the tank while the remaining part is lost to the ground. Remaining part of the input energy lost to the ground when temperature of the ground surrounding the tank is less than stored temperature of water. Annual input and output energies for the drying system may be represented as the ratio of individual energy component to the overall yearly energy. Yearly energy fractions for the drying system for the first year of operation with different TES tank volumes of 200, 250, and 300 m^3 are depicted in Fig. 7.30. It is seen from the figure that 80% of the energy input consists of solar energy, about 19% from the compressor work, and only 1 % is charged by the fan.

Fractions of stored energy in the tank and energy lost increase while heat gain by the HRU and compressor work decrease when tank volume increases. The figure indicates that increasing the stored energy and decreasing compressor work will increase performance parameters of SMER and COP for the SAHP drying system.

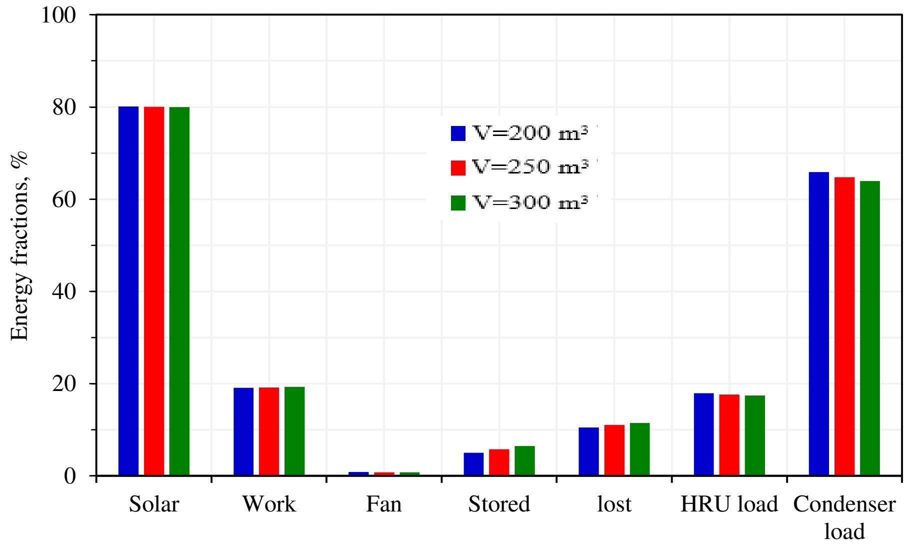

Figure 7.30 Effect of TES tank volume on energy fraction for 1st year of operation.

The SAHP drying system operates as unsteady state annually. Therefore, performance parameters change hourly. Figure 7.31 depicts time effect on energy for first, second, and fifth year of operation. This figure indicates that solar energy fraction goes up while the compressor work fraction goes down depending on operating years. Energy fraction for fan is very low and slightly increases with time when the drying system is operating for second and fifth years. It can be observed from the figure that stored and lost fractions decrease, while heat gain by the HRU condenser load fractions increase with time. Since energy is charged to the TES tank, temperature of water in the tank increases. The tank loses energy to the ground since its temperature is higher than that of the geological structure. The ground absorbs heat and its temperature increases by time. After long time, heat lost will decrease by over years.

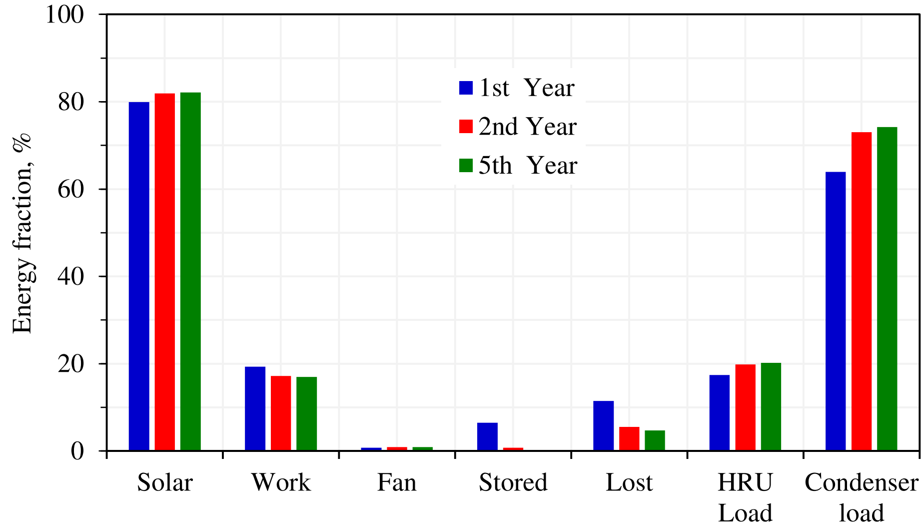

Figure 7.31 Effect of years of operation on energy fractions.

7.4 Results for SAHP Drying System with Underground TES Tank (Case 3)

This section presents the results of the drying system without using HRU which its model is explained in chapter 4. In the calculations, limestone is used as a geological structure as default for Gaziantep and may be used for other selected cities. The collector area, TES tank radius, wheat mass flow rate, moisture contents of wheat at inlet and outlet, and T_2 are set as, 45 m^2, 3 m, 30 kg h^{-1}, 25%, 10%, 55 °C, respectively. The default input data for city, collector parameters, latitude, ground type are Gaziantep, one glass-cover black surface, β = 37.1°, and Limestone, respectively unless other values of these input parameters are used. Results obtained from the simulation computations for the first case of the system modeling in chapter 4 are presented in figures, and discussed in this section. This case is to investigate the drying system performance without using HRU to find periodic situation by 1 year of operation.

Each earth surrounding TES tank gives different performance parameters because of different thermophysical properties. Also different cities give different performance parameters. Variation of water temperature in the TES tank is a type of performance parameter. Hence, every performance parameter depends on storage temperature. For that reason, Fig. 7.32 depicts the individual effects of the four selected types of ground on temperature variation of water in TES tank. Figure 7.32 shows the annually periodic variation of water temperature in the storage buried in four different earth types. Figure 7.32 shows the annually periodic variation of water temperature in the storage buried in four different earth types. The highest temperature occurs at the end of the summer season while the lowest temperature occurs at the end of the winter season. Energy charged to the storage by solar collectors throughout the summer season results in an increase in the temperature of the storage. Extraction of energy from the storage through the winter season results in a decrease in the storage temperature. It is seen also from the figure that highest temperatures occur in the storage surrounded with sand in most months which has the lowest thermal conductivity while lowest temperatures occur in the storage surrounded with granite which has the highest thermal conductivity.

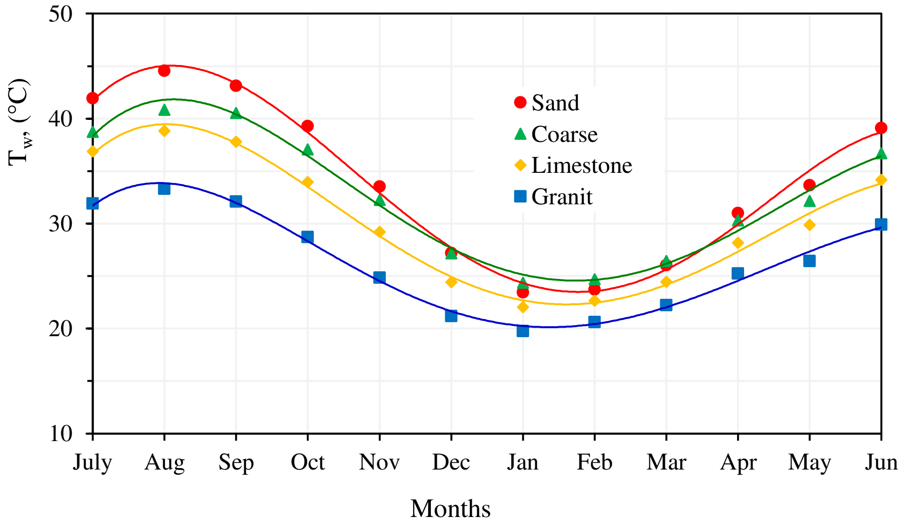

Figure 7.32 Effect of different geological structures on water temperature in TES tank.

The effects of different cities on annually periodic variation of water temperature for limestone ground are illustrated in Fig. 7.33. The highest water temperature in the tank can be observed for Gaziantep and Ankara while the minimum water temperature is recorded for Elazig in winter months and Izmir in July, August, and September. The different meteorological data for cities gives this different in water temperature in TES tank.

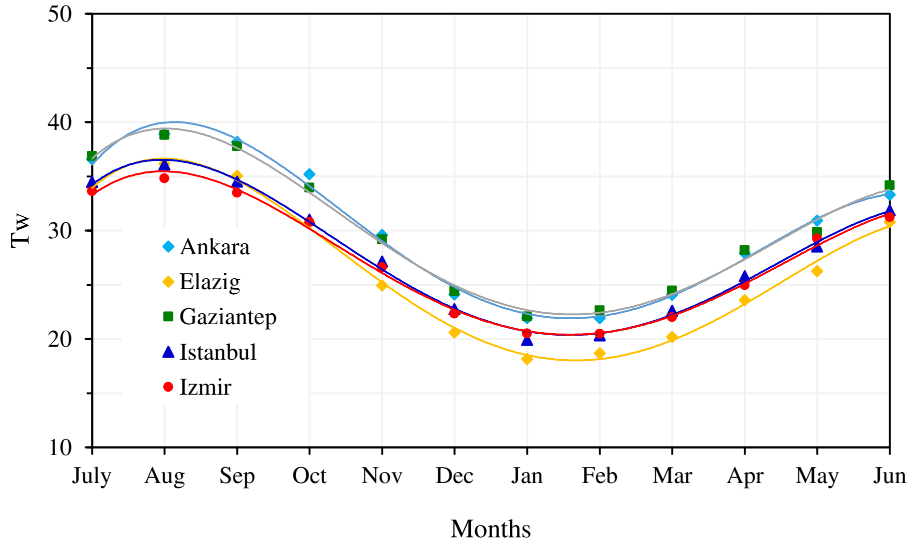

Figure 7.33 Effect of selected cities on water temperature in TES tank.

Figure 7.34 shows the effect of collector types on the water temperature in the storage embedded in limestone. It is observed that the lowest storage temperature takes place when the collector type is selected for black paint-two glass cover. But the other collectors give approximately the same temperature for a month. So, the collector parameters corresponding to a black paint-1 glass cover collector, which is widely used in applications, was used in all calculation results for this section and section 8.5.

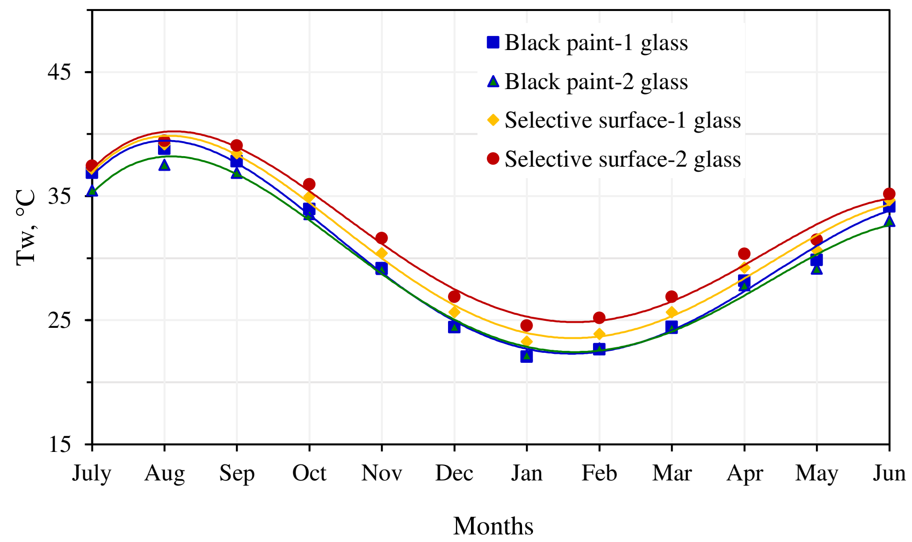

Figure 7.34 Effect of collector parameters on water temperature (limestone, Gaziantep).

Figures 7.35 illustrates variation of collector efficiency for different earth types. It is seen from this figure that collector efficiency is high for granite for all months while sand has the minimum values among selected ground types.

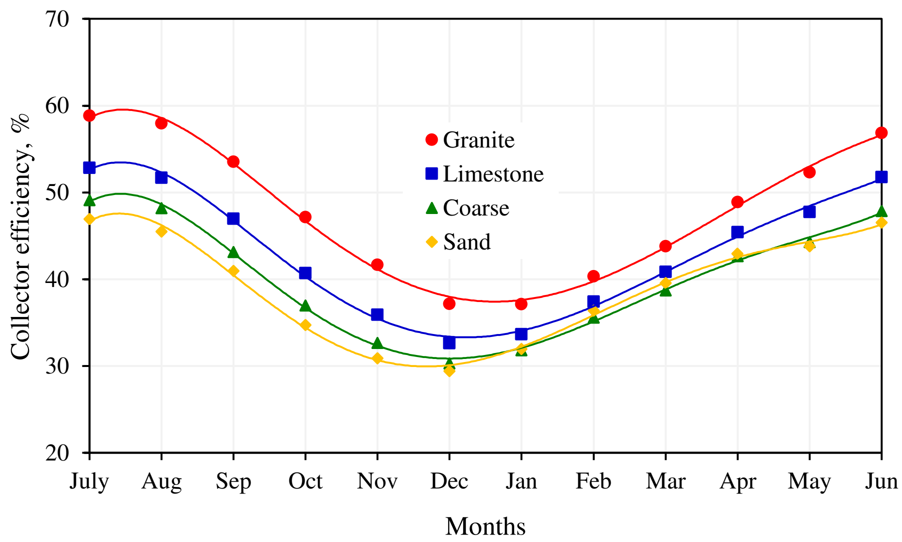

Figure 7.35 Annual variation of the collector efficiency for different geological structures.

Figures 7.36 and 7.37 illustrate variation of annual COP and SMER with collector surface area for different earth types. It's observed from the Fig. 7.36 that all earth tapes are increase linearly with increasing collector area. Sand earth type has higher COP while granite earth has the lowest values among selected earth types.

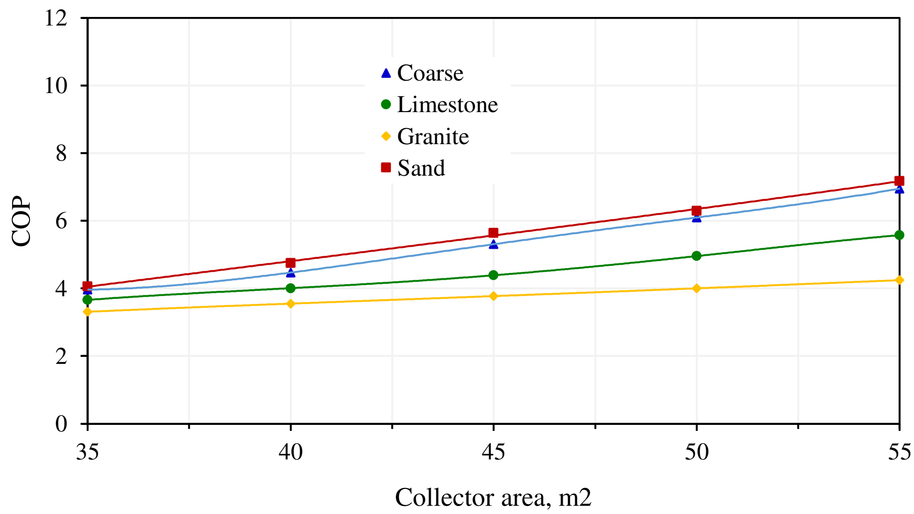

Figure 7.36 Annual COP versus collector area for four different collector area.

Figure 7.37 shows linearly increasing of SMER by increasing collector area. There is a proportional relation between collector area and SMER. The highest values can be seen with sand ground while the lowest value is recorded with granite as its clear from the figure.

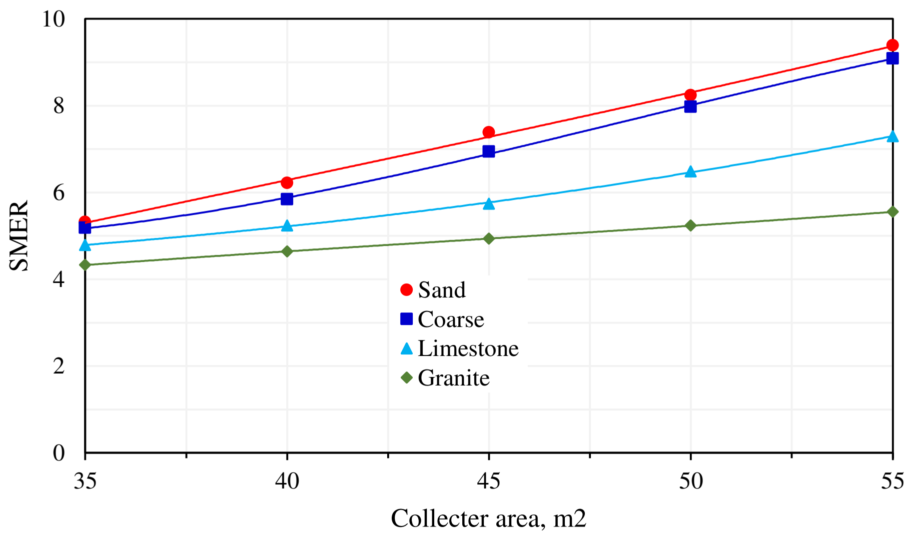

Figure 7.37 Effect of collector area on SMER.

The input data for wheat to the drying unit are important to take into account to know their effects on system performance parameters. The effects of the values 20, 22.5, 25, 27.5, and 30 % for moisture content in wheat at initial state on system performance parameters are investigated and depicted in Figs. 7.38, 7.39, and 7.40. Figure 7.38 shows that when the moisture content in wheat at initial state is increased the annual periodic variation of water temperature in tank is decreases. Its mean that there is an inversely relation between moisture content percentage and water temperature in tank. The minimum value of annual water temperature is recorded at maximum value (30%) of moisture content and the maximum value of annual water temperature can be seen at minimum value (20%) of moisture content among selected values. Figures 7.39 and 7.40 illustrate the effects of moisture content in wheat on COP and SMER, respectively. These figures show that the increasing in moisture content leads to decreasing of COP and SMER. There is also an inversely relation between moisture content percentage and COP and SMER. Another observation from the figures is that COP and SMER for sand ground (in comparison with other types) are decline steeply while for granite they decrease linearly and gradually with increasing in moisture content and it has the minimum values of COP and SMER among selected earth types.

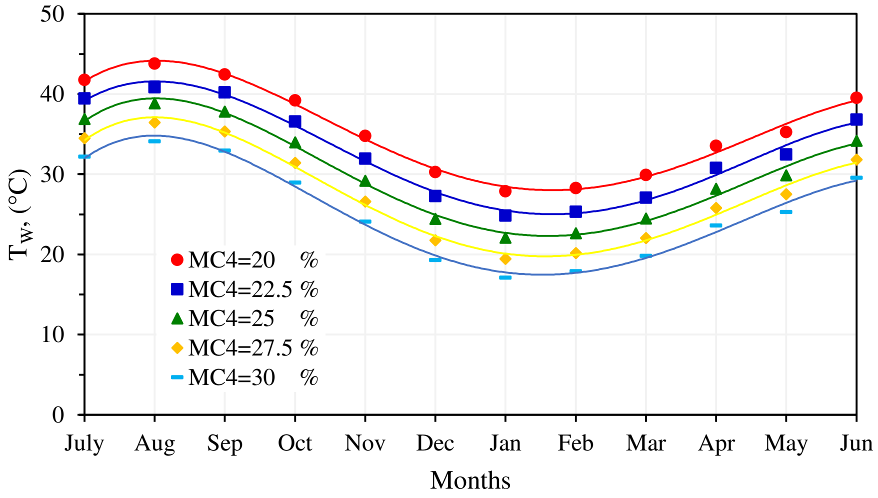

Figure 7.38 Effect of moisture content in wheat at initial state on water temperature.

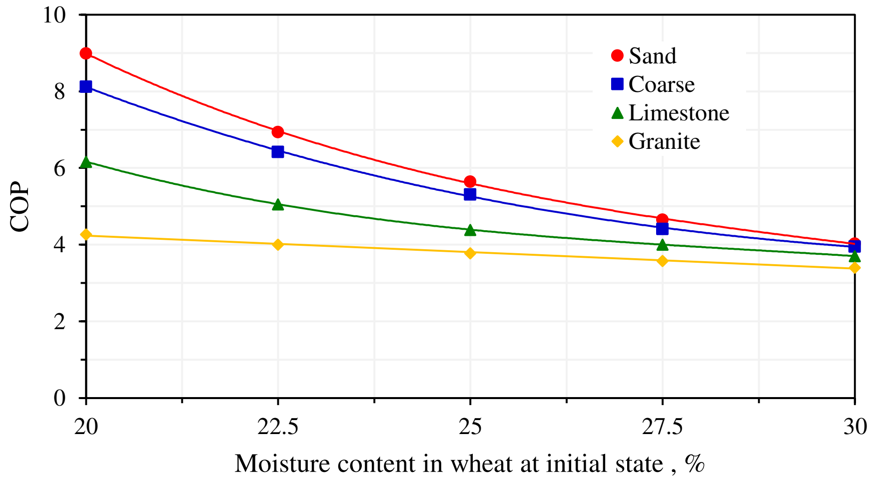

Figure 7.39 Effect of moisture content in wheat at initial state for different ground types on COP.

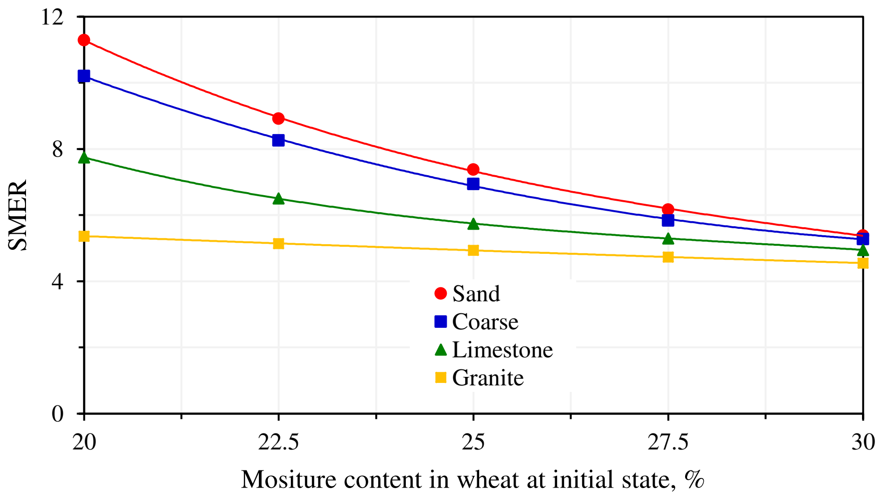

Figure 7.40 Effect of moisture content percentage in wheat at initial state for different ground types on SMER.

The effects of the values 5, 7.5, 10, 12.5, and 15 % for moisture content in wheat at final state on system performance parameters are showed in Figs. 7.41, 7.42, and 7.43. The highest value of annual water temperature can be seen at (MC_5=5%) while the lowest value is recorded at (MC_5=15%) as it's clear from Fig. 7.41. The maximum values of water temperature for all selected moisture content values are recorded in summer months such as July, August, and September however minimum values can be observed in winter months such as January and February. Figures 7.42 and 7.43 showed the effects of moisture content percentage on COP and SMER respectively. COP and SMER for sand ground are more affected than other ground types by increasing the moisture content of wheat, while the granite has the least affected by moisture increasing. The minimum values of COP and SMER for all ground types are showed from Figs. 7.42 and 7.43 at minimum value (MC_5=5%) however the maximum values of COP and SMER can be observed at maximum value of moisture content (MC_5=15%). Another observation from these figures can be clarified that there is proportional relation between performance parameters and moisture content percentage in wheat at final state.

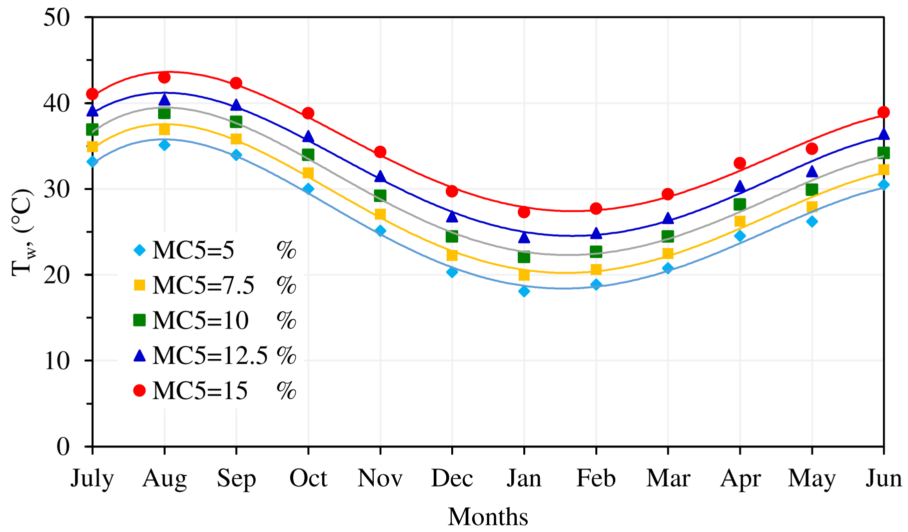

Figure 7.41 Effect of moisture content in wheat at final state on water temperature.

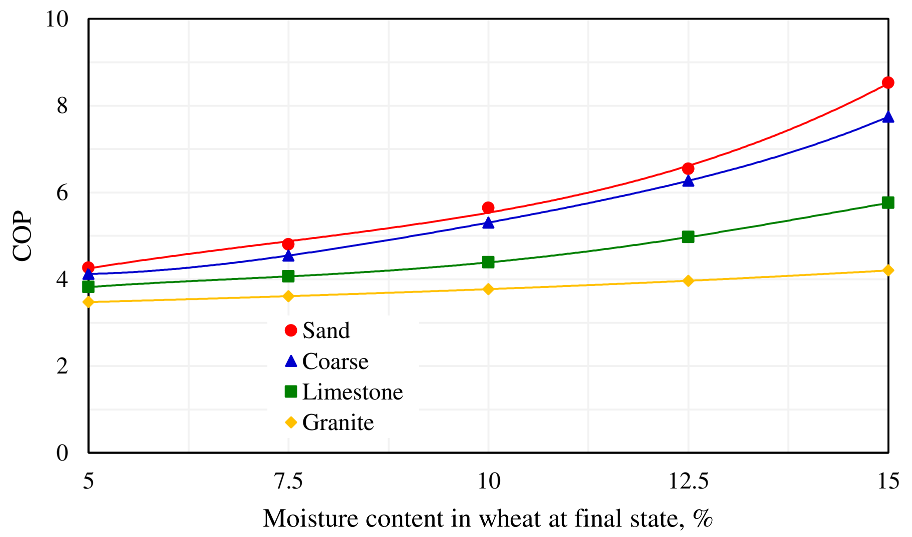

Figure 7.42 Effect of moisture content in wheat at final state for different ground types on COP.

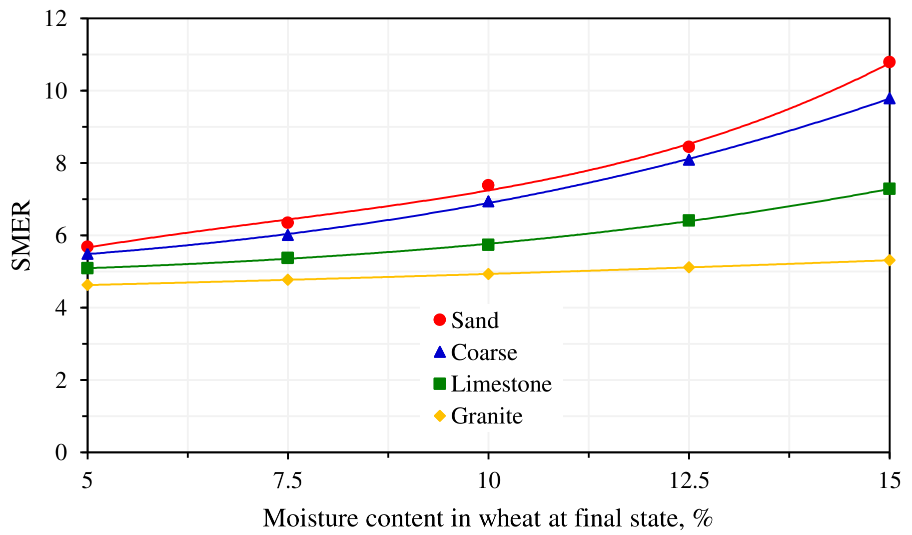

Figure 7.43 Effect of moisture content in wheat at final state for different ground types on SMER.

Any change in mass flow rate of wet wheat affects performance parameters such as COP and SMER. Accordingly, the effects of five different mass flow rate of wheat on COP and SMER for four different ground types are depicted in Figs. 7.44 and 7.45 respectively. Five different wheat flow rates (20, 25, 30, 35 and 45 kg h^{-1}) are selected for four ground types to determine suitable flow rate under the given input data. The selected ground types are sand, coarse, limestone, and granite. Both figures are showed that when mass flow rate of wet wheat is decreases the COP and SMER are increases and vice versa. Its mean there is an inversely relation between them. It can be seen that the maximum values for COP and SMER for all ground types are at minimum values for mass flow rate. The figures indicate that sand ground has the maximum value while granite has the minimum value among selected ground types.

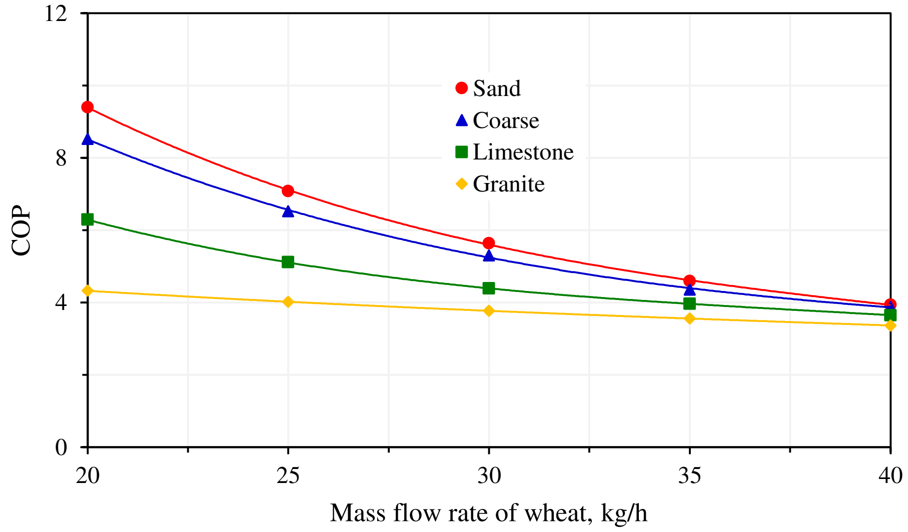

Figure 7.44 Effect of mass flow rate of wheat on COP.

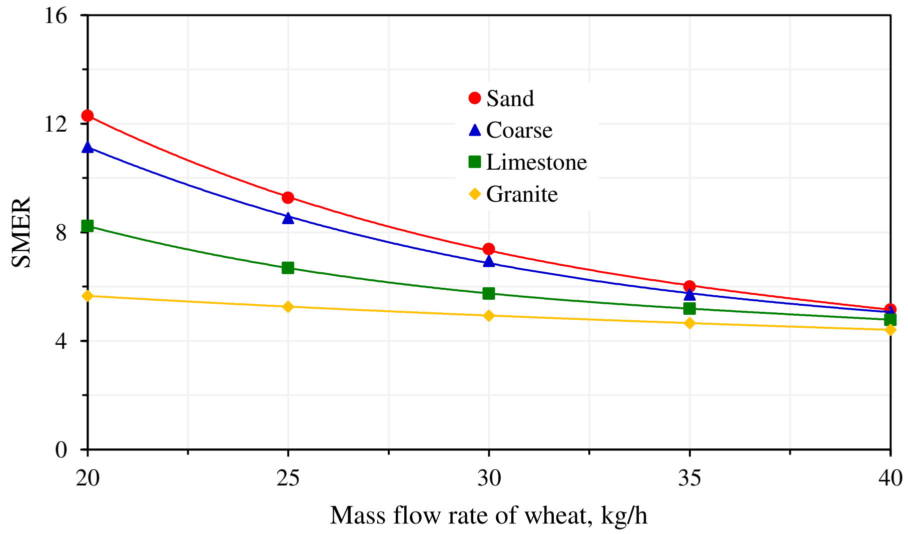

Figure 7.45 Effect of mass flow rate of wheat on SMER.

7.5 Results for SAHP-TES-HRU (Case 4).

This section presents the results of the drying system without using HRU which its model is explained also in chapter 4. But here the effect of using Heat Recovery Unit (HRU) is considered in the analysis. In other word the drying system for this case comprises of a drying unit, a heat pump, TES tank, solar collectors, and HRU. The collector area, TES tank radius, wheat mass flow rate, moisture contents of wheat at inlet and outlet, and T_2 are set as, 50 m^2, 3 m, 50 kg h^{-1}, 22.5%, 12.5%, 55 °C, respectively. The default input data for city, collector parameters, latitude, ground type are Gaziantep, one glass-cover black surface, β = 37.1°, and Limestone, respectively unless other values of these input parameters are used.

Figure 7.46 shows the annually periodic variation of water temperature in the storage buried in four different earth types. The maximum water temperature in summer months such as July and August while the minimum water temperature can be seen in winter months such as January and February for all ground types. It can be seen from the figure that sand and coarse ground are affected by the using HRU more than other types because of thermophysical properties.

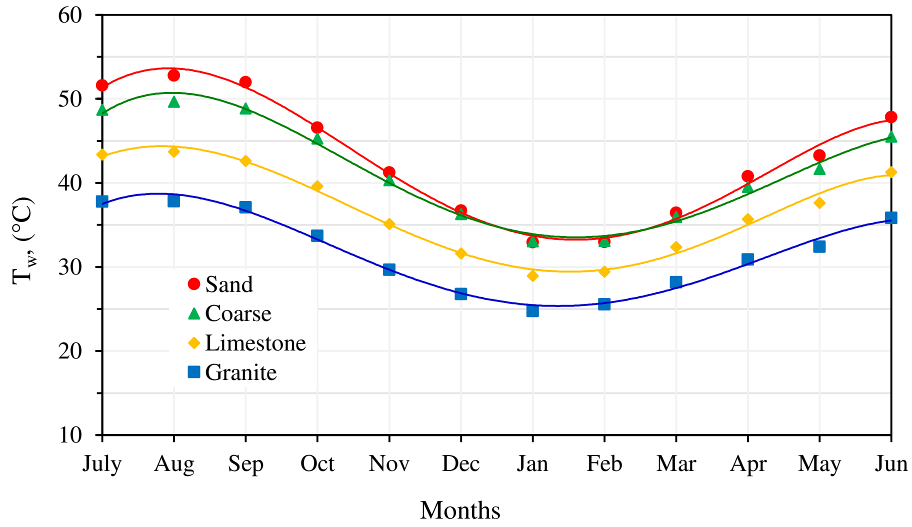

Figure 7.46 Effect of different geological structures on water temperature in TES tank with HRU.

Figure 7.47 is illustrated to show the effect of using HRU on water temperature in TES tank for coarse gravelled earth and limestone. The water temperature in tank increases with using HRU for same input data as shown in the figure. This figure indicates that water temperature for both limestone and coarse gravelled earths are affect in summer months by low values in comparison with recorded values in winter months because HRU will be active in the winter more than summer. This figure reveals that coarse gravelled earth is affected by using HRU more than limestone because they have different themophysical properties.

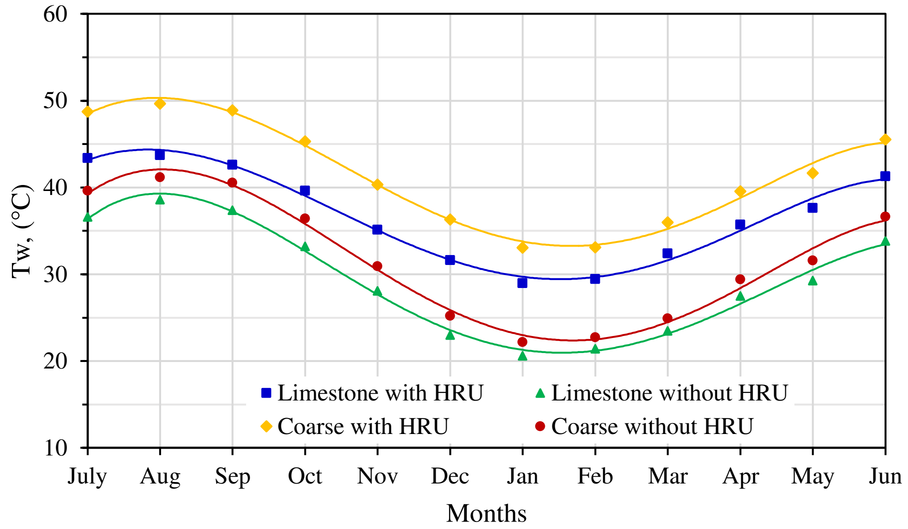

Figure 7.47 Comparison of water temperature with different geological structures with and without HRU.

Figure 7.48 shows approximately linearly increasing of SMER by increasing collector area. There is a proportional relation between collector area and SMER. The highest values can be seen with coarse gravelled ground while the lowest value is recorded with limestone as its clear from the figure. Another observation from this figure is that coarse earth increased more than 25% at collector area 50 m^2, while the limestone increased less than this value because it has different thermophysical properties.

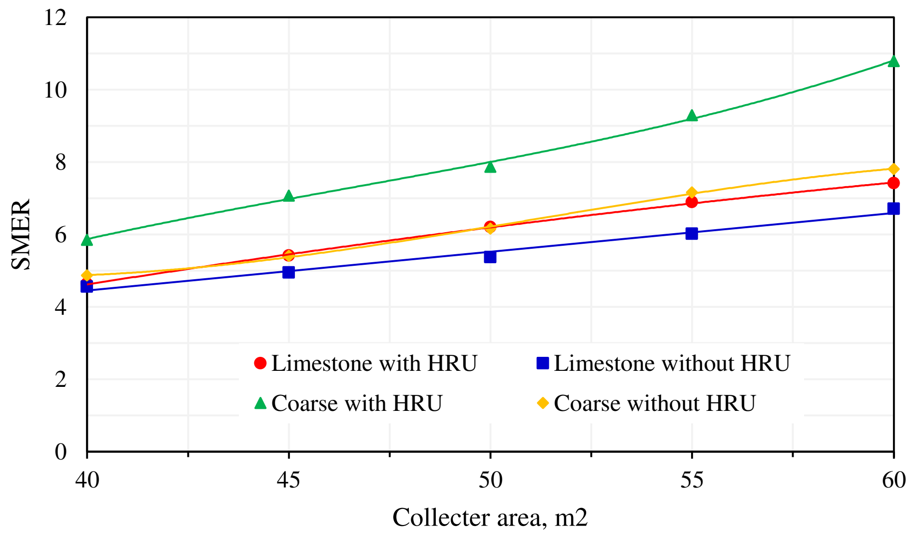

Figure 7.48 Comparison of SMER with different geological structures with and without HRU.

The effect of moisture contents (MC_5=20, 22.5%) in wheat at initial state on water temperature in the tank is illustrated in Fig. 7.49. This figure indicates that when the moisture content in wheat at initial state increases the water temperature decreases.

Water temperature is increased about 7.5 °C at (MC_5=20%) and 7.5 °C at (MC_5=22.5%) for July with using HRU. These values fluctuate during the reaming months of the year as it is evident in the figure.

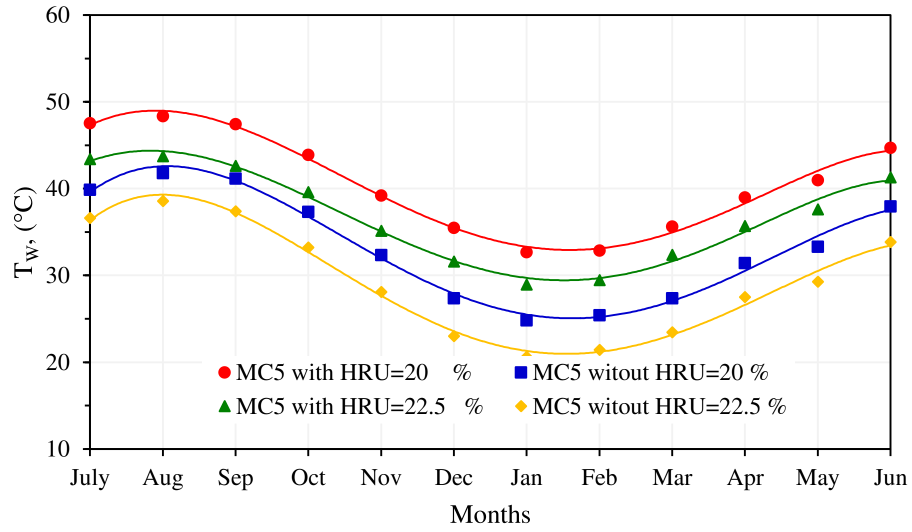

Figure 7.49 Effect of moisture content in wheat at initial state on water temperature with and without HRU.

The final state of moisture content in wheat is important to be known when designing the drying system. Therefore, Fig. 7.50 shows the effects of different moisture contents in wheat at final state on water temperature with and without using HRU. Water temperature in the tank increased about 7 °C at (MC6=10 %) and (MC6=12.5%) for July with using HRU, and the maximum values can be noted in January for both cases.

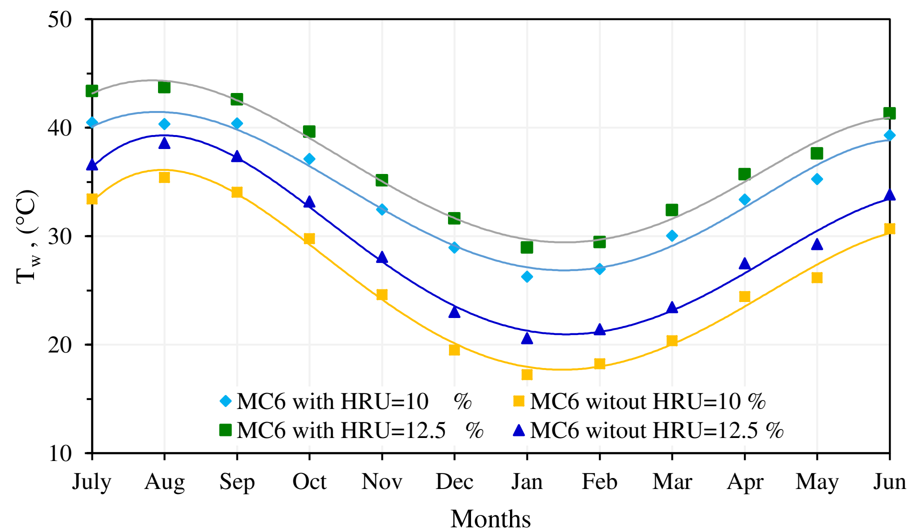

Figure 7.50 Effect of moisture content in wheat at final state on water temperature with and without HRU.

CHAPTER 8

CONCLUSIONS AND RECOMMENDATIONS

8.1 Conclusions

Thermal performance analysis of a SAHP drying system including TES tank with and without HRU is performed in the present study. Mathematical expressions for each individual component of the system (drying unit, HRU, solar collectors, heat pump and TES tank) are derived to find a mathematical modeling for the drying system and its performance parameters. Two different models (long-term and periodic operation) are used for SAHP drying system with TES tank, and each model is performed with and without using HRU. Consequently, four cases are investigated in this study. Many important input parameters, such as collector area, type of earth, TES tank volume, Carnot Efficiency (CE), mass flow rate of product, collector area, moisture content in wheat are considered in the analysis. A MATLAB program is prepared to compute the effects of those input parameters on system performance parameters such as water temperature in the TES tank, SMER, heat pump COP, system COPs, and energy fractions. The most important results obtained from this study are outlined below:

1- It is observed that all performance parameters, such as water temperature in TES tank, COP of the heat pump (COP) and system (COPs), SMER, and energy fraction for the load increase gradually from the beginning of drying operation until fifth year of operation. The system works as a periodic operation from fifth year onwards.

2- Earth type or thermophysical characteristics of the geological structure around the underground TES tank have a great effect on the drying system performance. Thus, it is recommended that suitable region should be selected for installing such a drying system.

3- When wheat mass flow rate and Carnot Efficiency are selected as 50 kg h^{-1} and 40% more suitable collector area and TES tank volume are obtained as 70 m^2 and 300 m^3 respectively. For these values, the performance parameters of the COP, COPs and SMER are obtained as 4.2, 4.1 and 6 respectively, when the drying system reaches periodic operation from fifth year onwards for the Case One (SAHP drying system with TES tank using long-term operation).

4- Total energy input to the drying system supplied by solar energy, compressor work and fan power are 76.63 %, 22.68 %, and 0.7 % respectively during the fifth year of operation. Condenser fan power is below 1 % of total energy input to the drying system for the Case One of this study.
5- When mass flow rate of wet wheat and moisture content of dried wheat are selected as 100 kg h^{-1} and 10 %, the volume of TES tank and collector area are obtained as 300 m^3 and 100 m^2. Accordingly, annual COP and SMER variety from 4 to 6 and 6 to 10, respectively for the Case Two in this study
6- Moisture content of wheat at initial state and solar collector area have a proportional relation with COP, COPs, SMER, and temperature of water in TES tank. While, wheat mass flow rate has inverse relation with them.
7- Using HRU saves 21.4 % of energy of the total heat load of the drying unit for Case Two in this research.
8- It is observed that the drying system reaches periodic operation in fifth year onwards.
9- System COPs is obtained as approximately 5% lower than heat pump COP for Case Two (SAHP drying system including TES tank and HRU using long term operation) in this study.
10- The collector efficiency is recorded the maximum value throughout months for granite earth among selected types while the minimum value can be seen for sand, this observation can be found in Case Three (SAHP drying system with TES tank using periodic operation).
11- Solar collector area has a proportional relation with performance parameters such as water temperature in TES tank, heat pump COP, and SMER. This finding is shown for Case Three and in line with results of Cases One and Two.
12- Moisture content in wheat for initial and final states has a strong effect on system performance parameters. This conclusion drawn from Cases Three and Four analyses are in line with results of Cases One and Two.
13- Using HRU unit with the drying system for Case Four gives higher performance parameters in comparison with using the same input data and system without HRU. This result is in line with the findings of Case Two.

8.2. Recommendations for Future Research

The following recommendations have been suggested in this study for further study:

1- The optimal value per hour for each parameter do not necessarily mean that it is considered the optimal value for other parameters in the same hour. Accordingly, the optimization of the drying system is separate study and may be involved in further studies.

2- Exergy analysis is another suggested study to assess the exergy destruction in the system components and possibility of development for energy saving.

3- This study did not addressed cost analysis for the drying system because it is out of this study's scope.

4- There are some assumptions in this study that can be studied later in depth such as; soil is assumed to have constant thermal properties and homogeneous structures. Thermal properties are dependent on the soil composition and moisture content. Energy transport in the soil occurs by means of both conduction and convection. Convection heat transfer and phase change of moisture in the soil may be also involved in a further study.

5- Thermal performance of a solar-assisted heat pump drying system can be studied experimentally for several years of operation. The experimental study gives the validity of this work. Then the study will become more comprehensive and realistic. Experimental study can be done by taking a prototype of the system.

REFERENCES

[1] Inaba, H., Aoyama, S., Haruki, N., Horibe, A., Nagayoshi, K. (2002). Heat and Mass Transfer Characteristics of Air Bubbles and Hot Water by Direct Contact, *Heat and Mass Transfer.* **38**, 449-457.

[2] Mrema, G. C., Gumbe, L. O., Chepete, H. J., Agullo, J. O. (2012). *Rural structures in the tropics, design and development*. Food and Agriculture Organization of the United Nations.

[3] Leon, M. A., Kumar, S., Bhattacharya, S. C. (2002). A Comprehensive Procedure for Performance Evaluation of Solar Food Dryers, *Renewable and Sustainable Energy Reviews.* **6**, 367-393.

[4] Goh, L. J., Othman M. Y., Mat, S., Ruslan, H., Sopian, K. (2011). Review of Heat Pump Systems for Drying Application, *Renewable and Sustainable Energy Reviews.* **15**, 4788-4796.

[5] Rossi, S. J., Neues, L. C., Kicokbusch, T. G. (1992). Thermodynamic and Energetic Evaluation of a Heat Pump Applied to the Drying of Vegetables, *Drying.* **92**, 475-478.

[6] Queiroz, R., Gabas, A. L., Telis, V. R.N. (2004). Drying Kinetics of Tomato by Using Electric Resistance and Heat Pump Dryers, *Drying Technology.* **22**, 1603-1620.

[7] Jolly, P., Jia, X., Clements, S. (1990). Heat Pump Assisted Continuous Drying Part 1: Simulation Model, *International Journal of Energy Research.* **14**, 757-770.

[8] Mujumdar, A. S. (1987). *Handbook of industrial drying*. 2nd Ed. New York, USA: Marcel Dekker Inc.

[9] Mujumdar, A. S. (2014). *Handbook of industrial drying*. CRC press.

[10] Ji, J., He, H., Chow, T., Pei, G., He, W., Liu, K. (2009). Distributed Dynamic Modeling and Experimental Study of PV Evaporator in a PV/T Solar-Assisted Heat Pump, *International Journal of Heat and Mass Transfer.* **52**, 1365-1373.

[11] Wang, Y., Li, M., Qiu, Y., Yu, Q., Luo, X., Li, G., Ma, X. (2019). Performance Analysis of a Secondary Heat Recovery Solar-Assisted Heat Pump Drying System for Mango, *Energy Exploration & Exploitation.* p.0144598718823937.

[12] Naemsai, T., Jareanjit, J., Thongkaew, K. (2019). Experimental Investigation of Solar-Assisted Heat Pump Dryer with Heat Recovery for the Drying Of Chili Peppers, *Journal of Food Process Engineering*. **25**, 13193.

[13] Büyükakın, M. K., Öztuna, S., Demir, H. (2017). Design and Thermodynamic Analysis of a Solar-Assisted Cini Ceramic Drying System, *Renewable Energy.* **111**, 147-156.

[14] Pal, U. S., Khan M. K., Mohanty S.N. (2008). Heat Pump Drying of Green Sweet Pepper, *Drying Technology.* **26**, 1584-1590.

[15] Song, M., Deng, S., Dang, C., Mao, N., Wang, Z. (2018). Review on Improvement for Air Source Heat Pump Units During Frosting and Defrosting, *Applied Energy.* **211**, 1150–1170.

[16] Colak, N, Hepbasli, A. (2005). Exergy Analysis of Drying of Apple in a Heat Pump Dryer. Second International Conference of the Food Industries & Nutrition Division on Future Trends in Food Science and Nutrition. 145–158.

[17] Kuzgunkaya, E. H., Hepbasli, A. (2007). Exergetic Evaluation of Drying of Laurel Leaves in a Vertical Ground-Source Heat Pump Drying Cabinet, *International Journal of Energy Research.* **31**, 245-258.

[18] Kuzgunkaya, E. H., Hepbasli, A. (2007). Exergetic Performance Assessment of a Ground-Source Heat Pump Drying System, *International Journal of Energy Research.* **31**, 760-777.

[19] Sanga, E. C. (2002). Microwave assisted drying of composite materials: Modelling and experimental validation (Doctoral dissertation, McGill University Libraries).

[20] Zhi-qiang, G., Li-jing, Z., Min, L., Sheng-lan, G. (2012). Optimization of a Combined Heat Pump–Microwave Drying Process of Tilapia Fillets Using a

Comprehensive Weighted Scoring Method, *Journal of Nutrition Food Sciences.* **2** (168), 2.

[21] Zielinska, M., Zapotoczny, P., Alves-Filho, O., Eikevik, T. M., Blaszczak, W. (2013). Microwave Vacuum–Assisted Drying of Green Peas Using Heat Pump and Fluidized Bed: A Comparative Study Between Atmospheric Freeze Drying and Hot Air Convective Drying, *Drying Technology.* **31**, 633-642.

[22] Fadhel, M. I., Sopian, K., Daud, W. R. W. (2010). Performance Analysis of Solar-Assisted Chemical Heat-Pump Dryer, *Solar Energy*. **84**, 1920-1928.

[23] Ceylan, I. (2009). Energy Analysis of PID Controlled Heat Pump Dryer, *Engineering.* **1** (03), 188.

[24] Fadhel, M. I., Sopian, K., Daud, W. R. (2010). Performance Analysis of Solar-Assisted Chemical Heat-Pump Dryer, *Solar Energy.* **84**, 1920-1928.

[25] Fatouh, M., Metwally, M. N., Helali A. B., Shedid M. H. (2006). Herbs Drying Using a Heat Pump Dryer, *Energy Conversion and Management*. **47**, 2629-2643.

[26] Xu, C., Xu, G., Zhao, S., Dong, W., Zhou, L., Yang, Y. (2016). A Theoretical Investigation of Energy Efficiency Improvement by Coal Pre-Drying in Coal Fired Power Plants, *Energy conversion and management.* **122**, 580-588.

[27] Erbay, Z., Hepbasli, A. (2014). Advanced Exergoeconomic Evaluation of a Heat Pump Food Dryer, Biosystems engineering. **124**, 29-39.

[28] Nowak, D., Lewicki, P. P. (2004). Infrared Drying of Apple Slices, *Innovative Food Science & Emerging Technologies*. **5**, 353-360.

[29] Wang, Y., Zhang, M., Mujumdar, A. S., Chen, H. (2014). Drying and Quality Characteristics of Shredded Squid in an Infrared-Assisted Convective Dryer, *Drying technology*. **32**, 1828-1839.

[30] Aktaş, M., Şevik, S., Aktekeli, B. (2016). Development of Heat Pump and Infrared-Convective Dryer and Performance Analysis for Stale Bread Drying, *Energy Conversion and Management*. **113**, 82-94.

[31] Mujumdar, A. S., Jangam, S. V. (2011). Energy Issues and Use of Renewable Source of Energy for Drying of Foods, *Proceedings of the International Workshop on Drying of Food and Biomaterials,* June, Bangkok, Thailand.

[32] Wongsuwan, W., Kumar, S., Neveu, P., Meunier, F. (2001). A Review of Chemical Heat Pump Technology and Applications, *Applied Thermal Engineering*. **21**, 1489–1519.

[33] Daghigh, R., Ruslan, M. H., Sulaiman, M. Y., Sopian, K. (2010). Review of Solar Assisted Heat Pump Drying Systems for Agricultural and Marine Products, *Renewable and Sustainable Energy Reviews*. **14**, 2564–2579.

[34] Dincer, I. (2002). Thermal Energy Storage Systems as a Key Technology in Energy Conservation, *International Journal of Energy Research*. **26**, 567-588.

[35] Dincer, I. (2002). On Thermal Energy Storage Systems and Applications in Buildings, *Energy and Buildings*. **34**, 377-388.

[36] Zogou, O., Stamatelos, A. (1998). Effect of Climatic Conditions on the Design Optimization of Heat Pump Systems for Space Heating and Cooling, *Energy Conversion and Management*. **39**, 609-622.

[37] Petit, P. J., Meyer, J. P. (1997). A Techno-Economic Analytical Comparison of the Performance of Air-Source and Horizontal Ground-Source Air-Conditioners in South Africa, *International Journal of Energy Research*, **21**, 1011-1021.

[38] Nikajima, Y., Ito, Y., Suziki, K. (1982). Study on Cooling Tubes by Simulations, *Technical papers of annual meeting of the Society of Heating, Air Conditioning and Sanitary Engineers of Japan.* 189-192.

[39] Hasegawa, F., Kimura, K. I., Yoshino, H., Ishikawa, Y. (1988). Experimental Study on Cooling Performance of the Earth Tube Connected to Passive Solar Test House, Part 1 Performance Three Tubes Embedded in the Earth Under the Floor, *Journal of ISES*. **14**, 23-30.

[40] Swardt, C. A., Meyer, J. P. (2001). A Performance Comparison between an Air-Source and a Ground-Source Reversible Heat Pump, *International Journal of Energy Research*. **25**, 899-910.

[41] Yumrutas, R., Unsal, M. (2000). Analysis of Solar Aided Heat Pump Systems with Seasonal Thermal Energy Storage in Surface Tanks, *Energy*. **25**, 1231-1243.

[42] Yumrutas, R., Unsal, M. (2005). Modeling of a Space Cooling System with Underground Storage, *Applied Thermal Engineering*. **25**, 227-239.

[43] Hasnain, S. M., Alabbadi, N. M. (2000). Need for Thermal-Storage Air-Conditioning in Saudi Arabia, *Applied Energy*. **65**, 153–164.

[44] Yumrutas, R., Kanoglu, M., Bolatturk, A., Bedir, M. (2005). Computational Model for a Ground Coupled Space Cooling System with an Underground Energy Storage Tank, *Energy and Buildings*. **37**, 353–360.

[45] Papanicolaou, E., Belessiotis, V. (2009). Transient Development of Flow and Temperature Fields in an Underground Thermal Storage Tank under Various Charging Modes, *Solar Energy*. **83**, 1161-1176.

[46] Wang, H., Qi, C. (2008). Performance Study of Underground Thermal Storage in a Solar-Ground Coupled Heat Pump System for Residential Buildings, *Energy and Buildings*, **40**. 1278-1286.

[47] Sarbu, I., Sebarchievici, C. (2014). General Review of Ground-Source Heat Pump Systems for Heating and Cooling of Buildings, *Energy and buildings*. **70**, 441-454.

[48] Xu, J., Wang, R. Z., Li, Y. (2014). A Review of Available Technologies for Seasonal Thermal Energy Storage, *Solar energy*. **103**, 610-638.

[49] Yumrutaş, R., Ünsal, M. (2000). A Computational Model of a Heat Pump System with a Hemispherical Surface Tank as the Ground Heat Source, *Energy*. **25**(4), 371-388.

[50] Navarro, L., De Gracia, A., Colclough, S., Browne, M., McCormack, S. J., Griffiths, P., Cabeza, L. F. (2016). Thermal Energy Storage in Building Integrated Thermal Systems: A Review. Part 1. Active Storage Systems, *Renewable Energy*. **88**, 526-547.

[51] Soni, S. K., Pandey, M., Bartaria, V. N. (2016). Hybrid Ground Coupled Heat Exchanger Systems for Space Heating/Cooling Applications: A Review, *Renewable and Sustainable Energy Reviews*. **60**, 724-738.

[52] Fan, R., Gao, Y., Pan, Y., Zhang, Y. (2015). Research on Cool Injection and Extraction Performance of Borehole Cool Energy Storage for Ground Coupled Heat Pump System, *Energy and Buildings*. **101**, 35-44.

[53] Choi, J., Kang, B., Cho, H. (2014). Performance Comparison between R22 and R744 Solar-Geothermal Hybrid Heat Pumps According to Heat Source Conditions, *Renewable energy*. **71**, 414-424.

[54] Sebarchievici, C., Sarbu, I. (2015). Performance Of An Experimental Ground-coupled Heat Pump System for Heating, Cooling and Domestic Hot-Water Operation, *Renewable energy*. **76**, 148-159.

[55] Yan, C., Shi, W., Li, X., Wang, S. (2016). A Seasonal Cold Storage System Based on Separate Type Heat Pipe for Sustainable Building Cooling, *Renewable energy*. **85**, 880-889.

[56] Zhang, S., Jiang, Y., Xu, W., Li, H., Yu, Z. (2016). Operating Performance in Cooling Mode of a Ground Source Heat Pump of a Nearly-Zero Energy Building in the Cold Region of China, *Renewable energy*. **87**, 1045-1052.

[57] Yu, Y., Ma, Z., Li, X. (2008). A New Integrated System with Cooling Storage in Soil and Ground-Coupled Heat Pump, *Applied Thermal Engineering*. **28**, 1450-1462.

[58] Pahud, D. (2000). Central Solar Heating Plants with Seasonal Duct Storage and Short-Term Water Storage: Design Guidelines Obtained by Dynamic System Simulations, *Solar Energy*. **69**, 495-509.

[59] Meliß, M., Späte, F. (2000). The Solar Heating System with Seasonal Storage at the Solar-Campus Jülich, *Solar Energy*. *69*, 525-533.

[60] Yumrutaş, R., Kunduz, M., Ayhan, T. (2003). Investigation of Thermal Performance of a Ground Coupled Heat Pump System with a Cylindrical Energy Storage Tank, *International Journal of Energy Research*. **27**, 1051-1066.

[61] Yumrutaş, R., Kaska, Ö. (2004). Experimental Investigation of Thermal Performance of a Solar Assisted Heat Pump System with an Energy Storage, *International Journal of Energy Research*. **28**, 163-175.

[62] Inalli, M., Ünsal, M., Tanyildizi, V. (1997). A Computational Model of a Domestic Solar Heating System with Underground Spherical Thermal Storage, *Energy*. **22**, 1163-1172.

[63] Inallı, M. (1998). Design Parameters for a Solar Heating System with an Underground Cylindrical Tank, *Energy*. **23**, 1015-1027.

[64] Ucar, A., Inalli, M. (2007). A Thermo-Economical Optimization of a Domestic Solar Heating Plant with Seasonal Storage, *Applied Thermal Engineering*. **27**, 450-456.

[65] Ucar, A., Inalli, M. (2008). Thermal and Economic Comparisons of Solar Heating Systems with Seasonal Storage Used in Building Heating, *Renewable Energy*. **33**, 2531-2539.

[66] Chung, M., Park, J., Yoon, H. K. (1998). Simulation of a Central Solar Heating System with Seasonal Storage in Korea, *Solar Energy*. **64**, 163-178.

[67] Nordell, B. O., Hellström, G. (2000). High Temperature Solar Heated Seasonal Storage System for Low Temperature Heating of Buildings, *Solar energy*. **69**, 511-523.

[68] Wang, H., Qi, C. (2008). Performance Study of Underground Thermal Storage in a Solar-Ground Coupled Heat Pump System for Residential Buildings, *Energy and Buildings*. **40**, 1278-1286.

[69] Wang, X., Zheng, M., Zhang, W., Zhang, S., Yang, T. (2010). Experimental Study of a Solar-Assisted Ground-Coupled Heat Pump System with Solar Seasonal Thermal Storage in Severe Cold Areas, *Energy and Buildings*. **42**, 2104-2110.

[70] Qu, M., Yin, H., Archer, D. H. (2010). A Solar Thermal Cooling and Heating System for a Building: Experimental and Model Based Performance Analysis and Design, *Solar Energy*. **84**, 166-182.

[71] Yumrutaş, R., Ünsal, M. (2012). Energy Analysis and Modeling of a Solar Assisted House Heating System with a Heat Pump and an Underground Energy Storage Tank, *Solar Energy*. **86**, 983-993.

[72] Sweet, M., McLeskey, J. (2012). Numerical Simulation of Underground Seasonal Solar Thermal Energy Storage (SSTES) for a Single Family Dwelling Using TRNSYS, *Solar Energy*. **86**, 289-300.

[73] Attar, I., Naili, N., Khalifa, N., Hazami, M., Farhat, A. (2013). Parametric and Numerical Study of a Solar System for Heating a Greenhouse Equipped with a Buried Exchanger, *Energy Conversion and Management*. **70**, 163-173.

[74] Calise, F., Accadia, M. D., Figaj, R. D., Vanoli, L. (2016). Thermoeconomic Optimization of a Solar-Assisted Heat Pump Based on Transient Simulations and Computer Design of Experiments, *Energy Conversion and Management*. **125**, 166-184.

[75] Chen, X., Yang, H. (2012). Performance Analysis of a Proposed Solar Assisted Ground Coupled Heat Pump System, *Applied Energy*. **97**, 888‑896.

[76] Chow, T. T., Bai, Y., Fong, K. F., Lin, Z. (2012). Analysis of a Solar Assisted Heat Pump System for Indoor Swimming Pool Water and Space Heating, *Applied Energy*. **100**, 309‑317.

[77] Xu, J., Li, Y., Wang, R .Z., Liu, W. (2014). Performance Investigation of a Solar Heating System with Underground Seasonal Energy Storage for Greenhouse Application. *Energy*, **67**, 63-73.

[78] Moon, C. E., Choi, J. M. (2015). Heating Performance Characteristics of the Ground Source Heat Pump System with Energy-Piles and Energy-Slabs, *Energy*. **81**, 27-32.

[79] Karacavus, B., Can, A. (2009). Thermal and Economical Analysis of an Underground Seasonal Storage Heating System in Thrace, *Energy and Buildings*. **41**, 1‑10.

[80] Mahfuz, M. H. Anisur, M. R., Kibria, M. A., Saidur, R., Metselaar, I. H. S. C. (2014). Performance Investigation of Thermal Energy Storage System with Phase Change Material (PCM) for Solar Water Heating Application, *International Communications in Heat and Mass* Transfer. **57**, 132–139.

[81] Kuyumcu, M. E., Tutumlu, H., Yumrutaş, R. (2016). Performance of a Swimming Pool Heating System by Utilizing Waste Energy Rejected from an Ice Rink with an Energy Storage Tank, *Energy Conversion and Management*. **121**, 349-357.

[82] Tutumlu, H., Yumrutas, R., Yildirim, M. (2017). Investigating Thermal Performance of an Ice Rink Cooling System with an Underground Thermal Storage Tank, *Energy Exploration & Exploitation*. **0**, 1–21.

[83] Adapa, P. K., Schoenau, G. J., Sokhansanj, S. (2002). Performance Study of a Heat Pump Dryer System for Specialty Crops—Part 1: Development of a Simulation Model, *International Journal of Energy Research*. **26**, 1001-1019.

[84] Adapa, P. K., Schoenau G. J. (2005). Re-Circulating Heat Pump Assisted Continuous Bed Drying and Energy Analysis, *International Journal of Energy Research*. **29**, 961-972.

[85] Aktaş, M., Şevik, S., Amini, A., Khanlari, A. (2016). Analysis of Drying of Melon in a Solar-Heat Recovery Assisted Infrared Dryer, *Solar Energy.* **137**, 500-515.

[86] Erbay, Z., Icier, F., Hepbasli, A. (2010). Exergetic Performance Assessment of a Pilot-Scale Heat Pump Belt Conveyor Dryer, *International Journal of Energy Research.* **34**, 249-264.

[87] Peng, Z. R., Wang, G. B., Zhang, X. R. (2019). Thermodynamic Analysis of Novel Heat Pump Cycles for Drying Process with Large Temperature Lift, *International Journal of Energy Research*. **43**, 3201-3222

[88] Mohanraj, M., Chandrasekar, P. (2009). Performance of a Forced Convection Solar Dryer Integrated with Gravel as Heat Storage Material for Chili Drying, *Journal of Engineering Science and Technology*, *School of Engineering, Taylor's University College*. **4**, 305–314.

[89] Baniasadi, E., Ranjbar, S., Boostanipour, O. (2017). Experimental Investigation of the Performance of a Mixed-Mode Solar Dryer with Thermal Energy Storage, *Renewable Energy*. **112**, 143- 150.

[90] Şevik, S., Aktaş, M., Doğan, H., Koçak, S. (2013). Mushroom Drying with Solar Assisted Heat Pump System, *Energy Conversion and Management*. **72**, 171–178.

[91] Şevik, S. (2014). Experimental Investigation of a New Design Solar-Heat Pump Dryer Under the Different Climatic Conditions and Drying Behavior of Selected Products, *Solar Energy*. **105**, 190–205.

[92] Rahman, S. M., Saidur, R., Hawlader, M. N. (2013). An Economic Optimization of Evaporator and Air Collector Area in a Solar Assisted Heat Pump Drying System, *Energy Conversion and Management*. **76**, 377-384.

[93] Şevik, S. (2013). Design, Experimental Investigation and Analysis of a Solar Drying System, *Energy Conversion and Management*. **68**, 227-234.

[94] Aktaş, M., Khanlari, A., Amini, A., Şevik, S. (2017). Performance Analysis of Heat Pump and Infrared–Heat Pump Drying of Grated Carrot Using Energy-Exergy Methodology, *Energy Conversion and Management*. **132**, 327-338.

[95] Qiu, Y., Li, M., Hassanien, R. H., Wang, Y., Luo, X., Yu, Q. (2016). Performance and Operation Mode Analysis of a Heat Recovery and Thermal Storage Solar-Assisted Heat Pump Drying System, *Solar Energy*. **137**, 225-235.

[96] Ringeisen, B., Barrett, D. M., Stroeve, P. (2014). Concentrated Solar Drying of Tomatoes, *Energy for sustainable development*. **19**, 47-55.

[97] Singh, P. L., Deshpandey, S. D., Jena, P. C. (2015). Thermal Performance of Packed Bed Heat Storage System for Solar Air Heaters, *Energy for Sustainable Development*. **29**, 112-117.

[98] Mohanraj, M. (2014). Performance of a Solar-Ambient Hybrid Source Heat Pump Drier for Copra Drying Under Hot-Humid Weather Conditions, *Energy for Sustainable Development*. **23**, 165-169.

[99] ASHRAE, ASHRAE Handbook Fundamentals. (1997). American Society of Heating, Refrigerating and Air Conditioning Engineers. Atlanta, USA.

[100] Alves-Filho, O. (2015). *Heat pump dryers: Theory, design and industrial applications*. CRC Press, Taylor & Francis Group. https://doi.org/10.1201/b18783.

[101] Kazarian, E. A., Hall, C. W. (1962). *Thermal properties of grain* (Doctoral dissertation, Michigan State University of Agriculture and Applied Science. Dept. of Agricultural Engineering).

[102] ASHRAE, ASHRAE Handbook Systems and Equipment. American Society of Heating, Refrigerating, and Air- Conditioning Engineers. Atlanta, USA, 2000.

[103] Kays, W. M., London A. L. (1984). Compact heat exchangers. 3rd ed. Blacklick, Ohio, USA, McGraw Hill.

[104] Cavallaro, A. R., Bullard, C. W. (1994). Effects of Varying Fan Speed on a Refrigerator/Freezer System, *Air Conditioning and Refrigeration Center, College of Engineering, University of Illinois at Urbana Champaign*.

[105] Icropera, F. P., De Witt, D. P. (2006). *Fundamentals of Heat and Mass Transfer*. Sixth Edition, John Wiley and Sons, Inc. USA.

[106] Akers, W. W., Deans, H. A., Crosser, O. K. (1958). Condensing Heat Transfer within Horizontal Tubes, *Chemical Engineering Program*. **54**,

[107] ASHRAE, ASHRAE Handbook Applications. American Society of Heating, Refrigerating and Air Conditioning Engineers, Atlanta, USA, 1999.

[108] Yumrutaş, R., Ünsal, M. (2000). Analysis of Solar Aided Heat Pump Systems with Seasonal Thermal Energy Storage in Surface Tanks, *Energy*. **25**, 1231-1243.

[109] Duffie, J. A., Beckman, W. A. (1991). *Solar Engineering of thermal process*. WA, New York.

[110] Sundaram, P., Sudhakar, P., Yogeshwaran, R. (2016). Experimental Studies and Mathematical Modelling of Drying Wheat in Fluidized Bed Dryer, *Indian Journal of Science and Technology*. **9**(36).

[111] KCD dryer continuo's mixed flow. Operation manual, www.kongskilde.com, kcd-mk4_man-gb_117012512., 25.07.2019.

[112] Strommen, I. (1980). *Drying of heavily salted codfish*. Ph.D. Thesis, the Norwegian Institute of Technology, Division of Refrigeration Engineering, and Trondheim, Norway (in Norwegian).

[113] Magnussen, O. M., Strommen, I. (1981). Heat pump drying of heavily salted codfish. Nordic Refrigeration Meeting, Copenhagen, May 21–23 (in Norwegian).

[114] Ozisik, M. N. (1985). *Heat Transfer: A Basic Approach*. McGraw-Hill, New York.

[115] Elminir, H. K., Ghitas, A. E., El-Hussainy, F., Hamid, R., Beheary, M. M., Abdel-Moneim, K. M. (2006). Optimum Solar Flat-Plate Collector Slope: Case Study for Helwan, Egypt, *Energy Conversion Management*. **47**, 624–637.

[116] Cooper PI. (1969). The Absorption of Radiation in Solar Stills, *Solar energy*. **12**, 333-346.

[117] Cengel, Y. A., Ghajar, A. J. (2011). *Heat and mass transfer (a practical approach, SI version)*. McGraw-700 Hill Education. 701-752.

[118] Oğulata. R. T. (2004). Utilization of Waste-Heat Recovery in Textile Drying, *Applied energy*. **79**, 41-49.

[119] Söylemez, M. S. (2006). Optimum Heat Pump in Drying Systems with Waste Heat Recovery, *Journal of Food Engineering*. **74**, 292-298.

[120] Klein, S. A. (1978). Calculation of Flat-Plate Collector Utilizability, *Solar energy*. **21**, 393-402.

[121] Mitchell, J. C., Theilacker, J. C., Klein, S. A. (1981). Calculation of Monthly Average Collector Operating Time and Parasitic Energy Requirements, *Solar Energy*. **26**, 555-558.

[122] Whillier, A. (1953). *Solar energy collection and its utilization for house heating* (Doctoral dissertation, Massachusetts Institute of Technology).

[123] Liu, B. Y., Jordan, R. C. (1963). A Rational Procedure for Predicting the Long-Term Average Performance of Flat-Plate Solar-Energy Collectors, *Solar Energy*. **7**, 53.

[124] Klein, S. A., Beckman, W. A. (1979). A General Design Method for Closed-Loop Solar Energy Systems, *Solar energy*. **22**(3), 269-282.

[125] Liu, B. Y., Jordan, R. C. (1960). The Interrelationship and Characteristic Distribution of Direct, Diffuse and Total Solar Radiation, *Solar energy*. **4**, 1-19.

[126] Collares-Pereira, M., Rabl, A. (1979). The Average Distribution of Solar Radiation-Correlations between Diffuse and Hemispherical and between Daily and Hourly Insolation Values, *Solar energy*. **22**, 155-164.

[127] Liu, B. Y., Jordan, R. C. (1977). Availability of Solar Energy for Flat Plate Solar Heat Collectors. Application of Solar Energy for Heating and Cooling of Buildings. ASHRAE, Atlanta.

[128] Simon, F. F. (1976). Flat-Plate Solar-Collector Performance Evaluation with a Solar Simulator as a Basis for Collector Selection and Performance Prediction, *Solar Energy*. **18**, 451-466.

[129] Dağsöz, A. K. (1995). Türkiye'de Derece Gün Sayıları, Ulusal Enerji Tasarruf Politikası Yapılarda Isı Yalıtımı. İTÜ Makine Fakültesi Isı Geçişi ve Ekonomisi Birimi, Alp Teknik Yayınları, İstanbul.

[130] Ünsal, M., Doğantan, Z. S. (1981). "Güneş Enerjisi Takviyeli Isıtma Sistemleri İçin Aylık Ortalama Geçiş-yutma Sayısı", Isı Bilimi ve Tekniği Dergisi, **4** (1), 35-44.

[131] Yumrutaş, R. (1998). *Simulation of solar assisted heat pump space heating systems with seasonal thermal energy tank*. Ph.D. Thesis, University of Gaziantep, Gaziantep, Turkey

APPENDICES

APPENDIX A

FLOW CHARTS OF COMPUTATIONAL PROCEDURES FOR ALL STUDY CASES

Figure A. 1 Flow chart of first model (case 1)

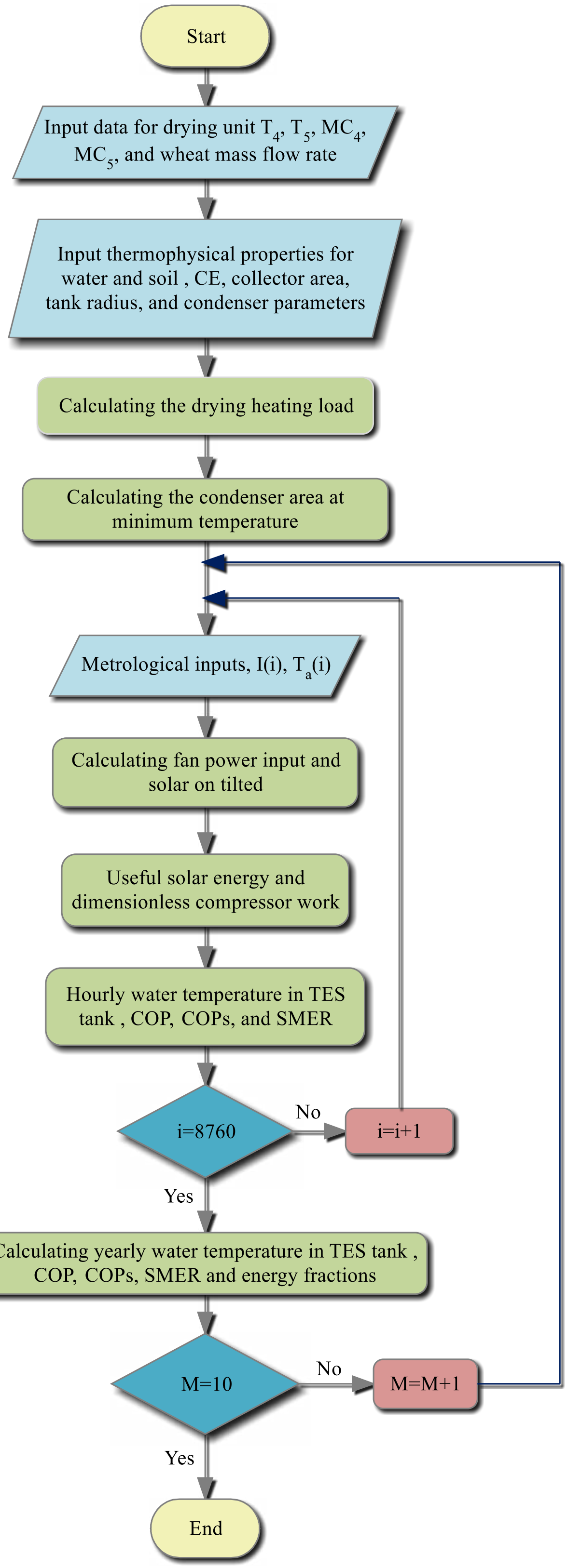

Figure A. 2 Flow chart of first model (case 2)

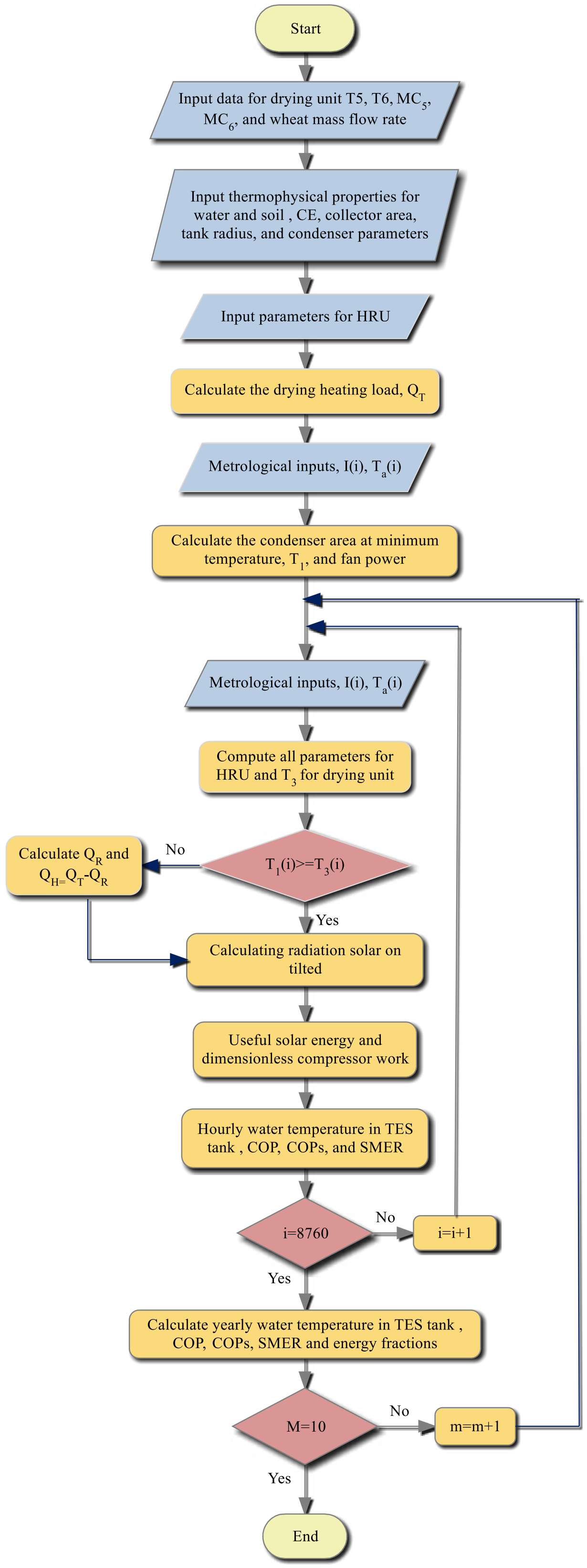

Figure A. 3 Flow chart of second model (case 3)

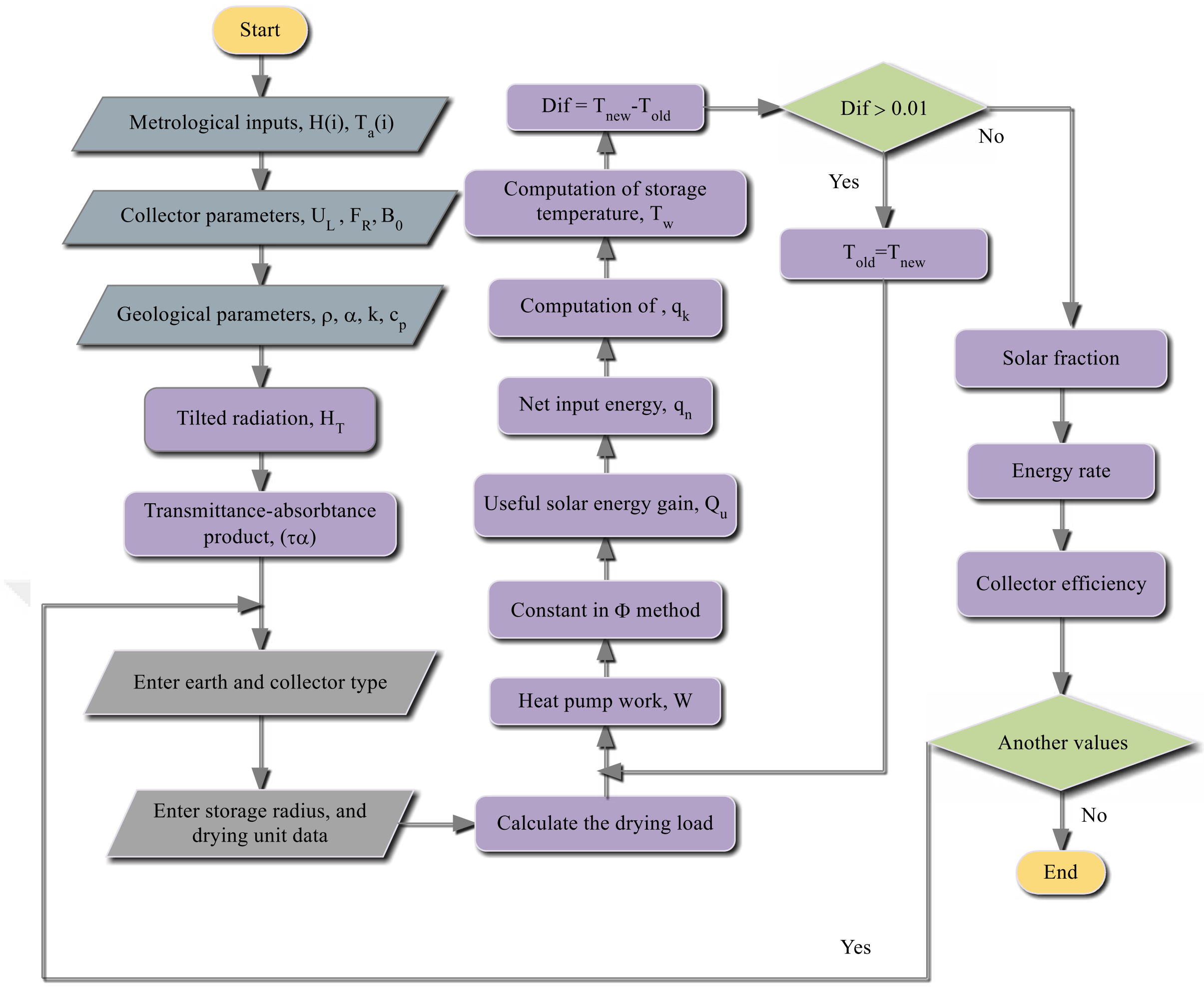

Figure A. 4 Flow chart of second model (case 4)

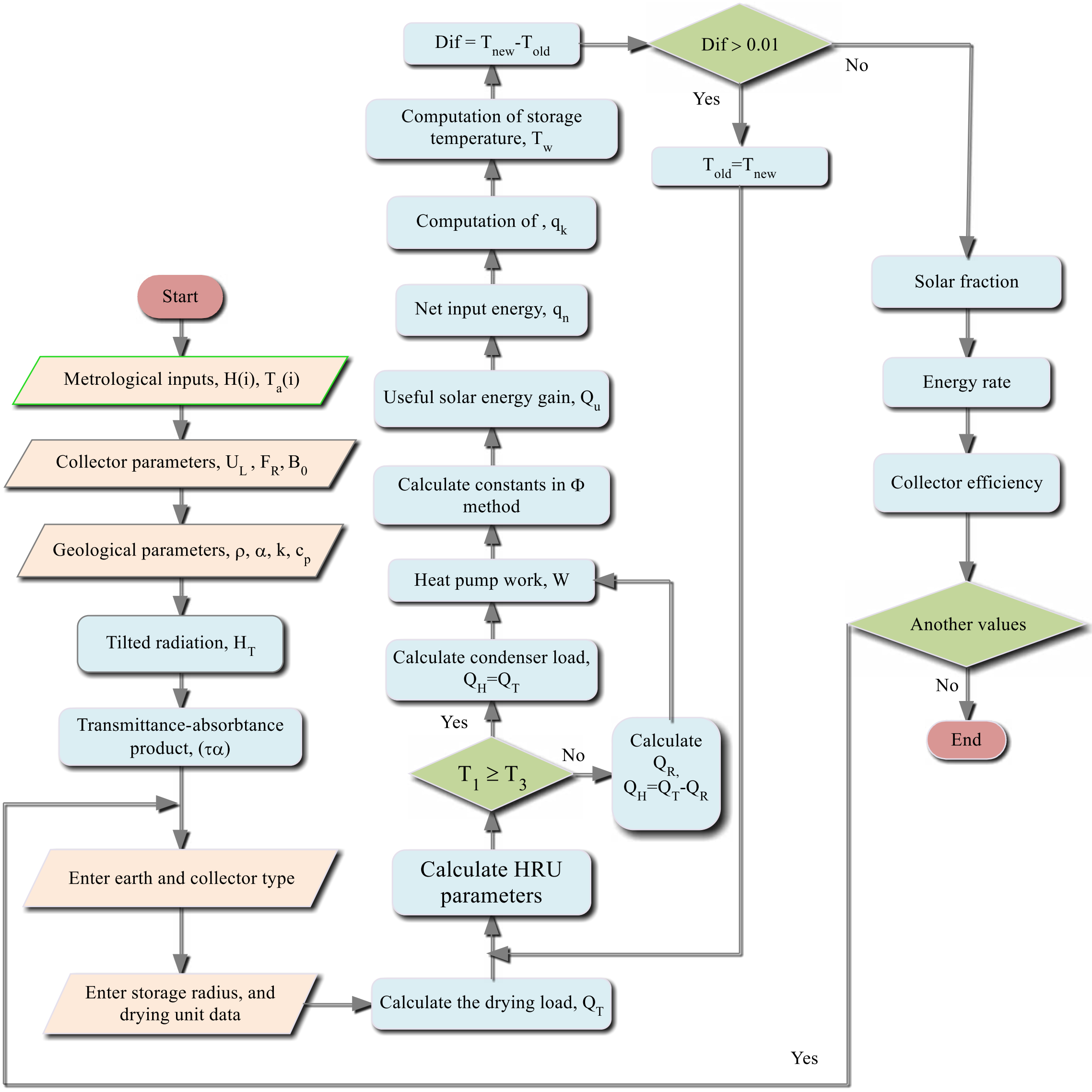

Start
Metrological inputs, H(i), T_a(i)
Collector parameters, U_L, F_R, B_0
Geological parameters, ρ, α, k, c_p
Tilted radiation, H_T
Transmittance-absorbtance product, (τα)
Enter earth and collector type
Enter storage radius, and drying unit data
Calculate the drying load, Q_T
Calculate HRU parameters
$T_1 \geq T_3$
No
Yes
Calculate Q_R, Q_H=Q_T-Q_R
Calculate condenser load, Q_H=Q_T
Heat pump work, W
Calculate constants in Φ method
Useful solar energy gain, Q_u
Net input energy, q_n
Computation of , q_k
Computation of storage temperature, T_w
Dif = T_{new}-T_{old}
Dif > 0.01
Yes
No
T_{old}=T_{new}
Solar fraction
Energy rate
Collector efficiency
Another values
No
Yes
End

APPENDIX B

MATLAB PROGRAMS FOR ALL STUDY CASES

Appendix B. 1 MATLAB program for Case 1

```
clc
clear
close all
%load('toit','ii','to');
load('IITO','ii','to');
load('omega2','omega2');
load('wf','wfan');
rhow = 1000;
cpw = 4.187;
tinf = 288;
t2=60;
tc=(-9+t2)/2;
fi =((273+t2) - 288) / 288;
fc=((273+tc) - 288) / 288;
ac =70;
ce=0.4;
nodryer = 1;
r = 4.1528;
v = 4/3 * pi * r^3;
rhos = 2500;
cps = 0.9;
con = 1.3;
alpha = 5.75e-7;
cpa=1006;
t5=25;
t6=50;
mc5=30;
mc6=0;
W5=50;
W6=W5-((W5*(mc5-mc6))/(100-mc6));
mw5=W5*mc5/100;
mw6=W6*mc6/100;
mevap=mw5-mw6;
mp=W5-mevap;
mpw=mp/3600;
mcp=(W5-W6)/W6;
cpwt=1398.3+(4090.2*(mcp/(1+mcp)));
mw=mevap/3600;
hfg=2412
qevap=mw*hfg*1000;
qdp=mpw*(cpwt)*(t6-t5);
qcond=qdp+qevap;
```

```
u=1.7;
fr=0.9;
taln=0.8;
tgalf=taln;
ul=8;
p= rhow * cpw / (3 * rhos *cps);
dt = 3600 * alpha / r^2;
p1=p/dt;
rt=1/(sqrt(pi*dt));
sbt1=(nodryer * ac) / (4 * pi * r * con * 288);
crp = [1 1 1 1 1 1 1 1 1 1 1 1];
ido = [31 31 30 31 30 31 31 28 31 30 31 30];
ef=[0.56 0.55 0.49 0.39 0.32 0.27 0.29 0.35 0.40 0.47 0.5
0.55];
re=[0.1 0.1 0.1 0.1 0.1 0.1 0.3 0.7 0.5 0.3 0.1 0.1];
day=0;
ihr = zeros(1,12);
tay=zeros(10,8760);
lg=zeros(1,12);
del=zeros(1,365);
n=zeros(1,12);
n(1)=ido(1);
lg(1)=ido(1);
for i=2:12
lg(i)=n(i-1)+ido(i);
n(i)=lg(i);
end
cr1=2*pi/365;
cr2=pi/180;
pir = zeros(1,365);
delta=zeros(1,365);
for i=1:365
    pir(i)=cr1*(284+i);
    delta(i)=23.45*sin(pir(i));
    del(i)=cr2*delta(i);
end
bt=37.1;
fai=37;
fii=fai*pi/180;
btt=bt*pi/180;
j1=1;
dec=2;
n=182;
tem=0;
tsum=0;
gs=1353;
nn=n-182;
for i=1:8760
    if (n==365),n=0; end
        n=n+1;
        if (nn==365),nn=0; end
```

```
        nn=nn+1;
        l=floor(((i-1)/24)+1);
        w1(i)=15*(t-12)*pi/180;
        w2(i)=15*(t-11)*pi/180;
        w(i)=(w1(i)+w2(i))/2;
        rin(nn)=2*pi*n/365;
rq(nn)=(43200.*(gs./pi)).*(1+(0.033.*cos(rin(nn)))).*(cos
(fii).*cos(del(n)).*(sin(w2(i))-sin(w1(i)))+((w2(i)-
w1(i)).*sin(fii).*sin(del(n))));
        iio(i)=abs(rq(nn));
        kt(i)=ii(i)/iio(i)*41870;
    if (kt(i)<=0.35)
        idi(i)=1-0.249*kt(i);
    elseif (kt(i)<=0.75)
        idi(i)=1.557-1.84*kt(i);
    else
        idi(i)=0.177;
    end
    rbc(i)=((cos(fii-
btt)*cos(del(n))*cos(w1(i)))+(sin(fii-
btt)*sin(del(n))))/((cos(fii)*cos(del(n))*cos(w1(i)))+(si
n(fii)*sin(del(n))));
    bs(i)=abs(rbc(i));
    if(bs(i)>=2)
        rb(i)=0.4;
    else
        rb(i)=bs(i);
    end
    ar1(i)=(1-idi(i))*rb(i);
    ar2(i)=idi(i)*((1+cos(btt))/2);
    ar3(i)=re(j1)*((1-cos(btt))/2);
    rcf(i)=ar1(i)+ar2(i)+ar3(i);
    it(i)=rcf(i)*ii(i)*41870/3600;

    %%%%%%%%%%%%%%%%%%%%%%%%%%%%%%%%
    k1=floor(i/24);
    k2=24*k1;
    if (i==k2),t=-1;end
    t=t+1;
    ihd=ihd+ii(i);
    itd=itd+it(i);
    tem=tem+to(i);
    m1=i/24;
    m2=24*m1;
    if (i~=m2), continue; end
    ihdav(l)=ihd/24*41870/3600;
    itdav(l)=itd/24;
    ihm=ihm+ihd;
    itm=itm+itd;
    ihd=0;
    itd=0;
```

```
    km=lg(j1)*24;
    kl=ido(j1)*24;
    if (i~=km), continue; end
    ihmav(j1)=ihm/kl*41870/3600;
    itmav(j1)=itm/kl;
    tam(j1)=tem/kl;
    ihy=ihy+ihm;
    ity=ity+itm;
    tsum=tsum+tam(j1);
    tdif=20-tam(j1);
    j1=j1+1;
    ihm=0;
    itm=0;
    tem=0;
end
ihory=ihy*41870/(8760*3600);
itily=ity/8760;

for i = 1:12
    day = day + ido(i);
    ihr(i)= day * 24;
end
k=1;
fa = zeros(1,8760);
c1 = zeros(1,8760);
h = zeros(1,8760);
t1= zeros(1,8760);
omega3=zeros(1,8760);
qhru=zeros(1,8760);
hh=zeros(1,8760);
ma=zeros(1,8760);
uah=zeros(1,8760);
gama=zeros(1,8760);
sbt2=zeros(1,8760);
t3=zeros(1,8760);
for i = 1: 8760
    ma(i)=(qcond)/(cpa*(t2-to(i)));
    omega3(i)=(mw/ma(i))+ omega2(i);
    uah(i)=ma(i)*cpa;
    gama(i) = 4 * pi *r* con / (nodryer * uah(i));
    sbt2(i)=(nodryer * uah(i)) / (4 * pi * r * con *
288);
    h(i) = crp(k) * sbt2(i)*(t2 - to(i));
    hh(i)=uah(i)*(t2 - to(i));
    fa(i) = ((to(i) + 273) /288)-1;
    c1(i) = (u * fc)+fi-fa(i);
    if (h(i) <= 0)
        h(i) =0;
    end
    if (i == ihr(k)), k=k+1; end
end
```

```
fw= zeros(10,8760);
tdg= zeros(10,8760);
del=zeros(365);
fw(1,1) = 0;
tdg(1,1) = 15; k=1;
cop=zeros(1,10);
cop1=zeros(1,10);
cop2=zeros(1,10);
smer=zeros(1,10);
qls = zeros(1,8760);
e =zeros(1,8760);
winhr=zeros(1,8760);
xsol=zeros(1,8760);
smerhr=zeros(1,8760);
for m=1:10
    fw(m,1) = fw(1,1);
    tdg(m,1) = ((fw(m,1) + 1) * 288) - 273;
    wo(1) = (fi - fa(1)) * (c1(1) - (u*fw(m,1))) / (ce*
(c1(1) +u) * gama(1));
   if (u*fw(m,1) >= c1(1)), wo(1) =0; end
    if ( it(1) <= 0)
        e(1)=0;
    else
        qls = (tdg(m,1) - to(1)) / it(1);
        if(qls >= 0.72)
            e(1) = 0;
        else
            e(1) = 0.72 - 6.4 * qls;
            if(e(1) <= 0 )
                e(1) = 0;
            elseif (e(1) > 0.72 )
                e(1) = 0.72;
            end
        end
    end
    s(1) = sbt1 * e(1) * it(1);
    qn(1) = s(1) - h(1) + wo(1);
    winhr(1)=wo(1)*gama(1)*uah(1)*288;
    xsol(1)=(s(1)/sbt1);
    fw(m,2)=(qn(1)+((p1+rt)*fw(m,1)))/(1+p1+rt);
    tdg(m,2)=((fw(m,2)+1)*288)-273;
    wo(2) = (fi - fa(2)) * (c1(2) - (u*fw(m,1))) / (ce*
(c1(2) +u) * gama(2));
    if (u*fw(m,2)>=c1(2)),wo(2)=0;end
    if(it(2)<=0)
        e(2)=0;
    else qls = (tdg(m,1) - to(2)) / it(2);
        if(qls >= 0.72)
            e(2) = 0;
        else
            e(2) = 0.72 - 6.4 * qls;
```

```
                if(e(2) <= 0 )
                    e(2) = 0;
                elseif (e(2) > 0.72)
                    e(2) = 0.72;
                end
            end
        end
        s(2) = sbt1 * e(2) * it(2);
        qn(2) = s(2) - h(2) + wo(2);
        winhr(2)=wo(2)*gama(2)*uah(2)*288;
        xsol(2)=(s(2)/sbt1);
        for i=3:8760
            s1=0;
            for n=1:i-2;
                s1=s1+(fw(m,n+1)-fw(m,n))/(sqrt(pi*dt*(i-
n)));
            end
             wo(i) = (fi - fa(i)) * (c1(i) - (u*fw(m,i-1))) /
(ce* (c1(i) +u) * gama(i));
            if (u*fw(m,2)>=c1(2)),wo(2)=0;end
            if(it(i)<=0)
                e(i)=0;
            else
                qls(i) = (tdg(m,i-1) - to(i)) / it(i);
                if(qls(i) > 0.72)
                    e(i) = 0;
                else     e(i) = 0.72 - (6.4 * qls(i));
                    if(e(i) <= 0 )
                        e(i) = 0;
                    elseif (e(i) > 0.72)
                        e(i) = 0.72;
                    end
                end
            end
            s(i) = sbt1 * e(i) * it(i);
            qn(i) = s(i) - h(i) + wo(i);
            fw(m,i)=(qn(i)+((p1+rt)*fw(m,i-1))-s1)/(1+p1+rt);
            tdg(m,i)=((fw(m,i)+1)*288)-273;
            qsy=qsy+s(i)*dt;
            qsol=qsol+(s(i)/sbt1);
            xsol(i)=(s(i)/sbt1);
            wy=wy+wo(i)*dt;
winput=winput+(wo(1)*gama(1)*uah(1)*288)+(wo(2)*gama(2)*u
ah(2)*288)+(wo(i)*gama(i)*uah(i)*288);
            wf=wf+wfan(i);
            winhr(i)=wo(i)*gama(i)*uah(i)*288;
            qly=qly+h(i)*dt;
            qy=qy+qn(i)*dt;
            qhh=qhh+hh(i);

smerhr(i)=mevap/((xsol(i)/1000)+((winhr(i)/1000)*1.1));
```

```
        if (i~=ihr(k)), continue; end
        efc=efc/(ido(k)*24);
        tay(m,k)=tdg(m,i);
        k=k+1;
        if (i==8760),fw(1,1)=fw(m,8760); end
    end
    if (m~=1)
        qst=p*(fw(m,8760)-fw(m,1));
    else
        qst=p*(fw(m,8760)-0);
    end
        cop(m)=qly/wy;
        workinp=qhh/cop(m);
        cops(m)=qhh/(workinp+wf);
        wr=wf/workinp;
        qtt=qsy+(wy*(1+wr));
        r1(m)=qsy*100/qtt;
        r2(m)=wy*100/qtt;
        r3(m)=qst*100/qtt;
        r4(m)=qly*100/qtt;
        r5(m)=(qy-qst)*100/qtt;
        r6(m)=(wy*wr)*100/qtt;

smer(m)=(mevap*8760)/(((workinp/1000)+(wf/1000)));
    k=1;
end
```

Appendix B. 2 MATLAB program for Case 2

```
clc
clear
close all
load('IITO','ii','to');
load('omega2','omega2');
load('wfhru','wfhru');
load('t1','t1');
load('t3','t3');

rhow = 1000;
cpw = 4.187;
tinf = 288;
t2=60;
tc=(16.55+t2)/2;
fi =((273+t2) - 288) / 288;
fc=((273+tc) - 288) / 288;
ac =100;
ce=0.4;
nodryer = 1;
r = 4.1528;
v = 4/3 * pi * r^3;
 rhos = 2500;
 cps = 0.9;
 con = 1.3;
 alpha = 5.75e-7;
cpa=1006;
t5=25;
t6=50;
mc5=30 ;
mc6=10;
W5=100;
W6=W5-((W5*(mc5-mc6))/(100-mc6));
mw5=W5*mc5/100;
mw6=W6*mc6/100;
mevap=mw5-mw6;
mp=W5-mevap;
mpw=mp/3600;
mcp=(W5-W6)/W6;
cpwt=1398.3+(4090.2*(mcp/(1+mcp)));
mw=mevap/3600;
hfg=2412;
qevap=mw*hfg*1000;
qdp=mpw*(cpwt)*(t6-t5);
```

```
q23=qdp+qevap;
u=1.7;
fr=0.9;
taln=0.8;
tgalf=taln;
ul=8;
p= rhow * cpw / (3 * rhos *cps);
dt = 3600 * alpha / r^2;
p1=p/dt;
rt=1/(sqrt(pi*dt));
sbt1=(nodryer * ac) / (4 * pi * r * con * 288);
crp = [1 1 1 1 1 1 1 1 1 1 1 1];
ido = [31 31 30 31 30 31 31 28 31 30 31 30];
ef=[0.56 0.55 0.49 0.39 0.32 0.27 0.29 0.35 0.40 0.47 0.5
0.55];
re=[0.1 0.1 0.1 0.1 0.1 0.1 0.3 0.7 0.5 0.3 0.1 0.1];
day=0;
ihr = zeros(1,12);
tay=zeros(10,8760);
lg=zeros(1,12);
del=zeros(1,365);
n=zeros(1,12);
n(1)=ido(1);
lg(1)=ido(1);
for i=2:12
    lg(i)=n(i-1)+ido(i);
    n(i)=lg(i);
end
cr1=2*pi/365;
cr2=pi/180;
 pir = zeros(1,365);
 delta=zeros(1,365);
for i=1:365
    pir(i)=cr1*(284+i);
    delta(i)=23.45*sin(pir(i));
    del(i)=cr2*delta(i);
end
bt=37.1;
fai=37;
fii=fai*pi/180;
btt=bt*pi/180;
j1=1;
dec=2;
ihd=0;
itd=0;
ihm=0;
itm=0;
ihy=0;
ity=0;
n=182;
t=0;
```

```
tem=0;
tsum=0;
gs=1353;
nn=n-182;
for i=1:8760
    if (n==365),n=0; end
        n=n+1;
        if (nn==365),nn=0; end
        nn=nn+1;
        l=floor(((i-1)/24)+1);
        w1(i)=15*(t-12)*pi/180;
        w2(i)=15*(t-11)*pi/180;
        w(i)=(w1(i)+w2(i))/2;
        rin(nn)=2*pi*n/365;

rq(nn)=(43200.*(gs./pi)).*(1+(0.033.*cos(rin(nn)))).*(cos
(fii).*cos(del(n)).*(sin(w2(i))-sin(w1(i)))+((w2(i)-
w1(i)).*sin(fii).*sin(del(n)))); %iq represent I_0 in the
equations
        iio(i)=abs(rq(nn));
        kt(i)=ii(i)/iio(i)*41870;
    if (kt(i)<=0.35)
        idi(i)=1-0.249*kt(i);
    elseif (kt(i)<=0.75)
        idi(i)=1.557-1.84*kt(i);
    else
        idi(i)=0.177;
    end
    rbc(i)=((cos(fii-
btt)*cos(del(n))*cos(w1(i)))+(sin(fii-
btt)*sin(del(n))))/((cos(fii)*cos(del(n))*cos(w1(i)))+(si
n(fii)*sin(del(n))));
    bs(i)=abs(rbc(i));
    if(bs(i)>=2)
        rb(i)=0.4;
    else
        rb(i)=bs(i);
    end
    ar1(i)=(1-idi(i))*rb(i);
    ar2(i)=idi(i)*((1+cos(btt))/2);
    ar3(i)=re(j1)*((1-cos(btt))/2);
    rcf(i)=ar1(i)+ar2(i)+ar3(i);
    it(i)=rcf(i)*ii(i)*41870/3600;
tetaz=acos(sin(fii)*sin(del(n))+cos(fii)*cos(del(n))*cos(
w(i)));
    tq=abs(rb(i)*cos(tetaz));
    if (tq>1)
        tal(i)=taln;
    else
       teta=acos(tq);
    end
```

```
    if (dec==1)
       bo=-0.10;
    else
       bo=-0.17;
    end
        amod=1+bo*(1/cos(teta)-1);
    if (amod<=0.2)
       amod=0.9-0.01*teta*180/pi;
   end
    if (amod>=1), tal(i)=taln;
    else
       tal(i)=taln*amod;
    end

    k1=floor(i/24);
    k2=24*k1;
    if (i==k2),t=-1;end
    t=t+1;
    ihd=ihd+ii(i);
    itd=itd+it(i);
    tem=tem+to(i);
    m1=i/24;
    m2=24*m1;
    if (i~=m2), continue; end
    ihdav(l)=ihd/24*41870/3600;
    itdav(l)=itd/24;
    ihm=ihm+ihd;
    itm=itm+itd;
    ihd=0;
    itd=0;
    km=lg(j1)*24;
    kl=ido(j1)*24;
    if (i~=km), continue; end
    ihmav(j1)=ihm/kl*41870/3600;
    itmav(j1)=itm/kl;
    tam(j1)=tem/kl;
    ihy=ihy+ihm;
    ity=ity+itm;
    tsum=tsum+tam(j1);
    tdif=20-tam(j1);
    j1=j1+1;
    ihm=0;
    itm=0;
    tem=0;
end
ihory=ihy*41870/(8760*3600);
itily=ity/8760;

for i = 1:12
    day = day + ido(i);
    ihr(i)= day * 24;
```

```
end
k=1;
fa = zeros(1,8760);
c1 = zeros(1,8760);
h = zeros(1,8760);
t11= zeros(1,8760);
omega3=zeros(1,8760);
qhru=zeros(1,8760);
hh=zeros(1,8760);
ma=zeros(1,8760);
uah=zeros(1,8760);
gama=zeros(1,8760);
sbt2=zeros(1,8760);
sbt3=zeros(1,8760);
qh=zeros(1,8760);
qrec=zeros(1,8760);
qrecov=zeros(1,1);

for i = 1:8760

    if (t1(i)>=t3(i))
       t11(i)=to(i);
       qrec(i)=0;
       qh(i)=q23;
       ma(i)=q23/(cpa*(t2-to(i)));
    else
       t11(i)=t1(i);
       ma(i)=q23/((0.7*cpa*(t3(i)-to(i)))+(cpa*(t2-
t11(i))));
       qrec(i)=0.7*ma(i)*cpa*(t3(i)-to(i));
       qh(i)=q23- qrec(i);
    end

  qrecov=qrecov+qrec(i);

    omega3(i)=(mw/ma(i))+omega2(i);
    uah(i)=ma(i)*cpa;
    gama(i) = 4 * pi *r* con / (nodryer * uah(i));
    sbt2(i)=(nodryer * uah(i)) / (4 * pi * r * con *
288);
    sbt3(i)=(nodryer)/ (4 * pi * r * con * 288);
    h(i)=crp(k)*sbt3(i)*qh(i);
    hh(i)=uah(i)*(t2 - t11(i));
    fa(i) = ((t11(i) + 273) /288)-1;
    c1(i) = (u * fc)+fi-fa(i);

    if (h(i) <= 0)
       h(i) =0;
    end
    if (i == ihr(k)), k=k+1; end
end
```

```
es=(qrecov/(q23*8760))*100;

fw= zeros(10,8760);
tdg= zeros(10,8760);
del=zeros(365);
fw(1,1) = 0;
tdg(1,1) = 15;
k=1;
cop=zeros(1,10);
cop1=zeros(1,10);
cop2=zeros(1,10);
cop3=zeros(1,10);
smer=zeros(1,10);
qhpp=zeros(1,10);
qrecu=zeros(1,10);
r1=zeros(1,10);
r2=zeros(1,10);
r3=zeros(1,10);
r4=zeros(1,10);
r5=zeros(1,10);
r6=zeros(1,10);
r7=zeros(1,10);
qht=zeros(1,10);
qls = zeros(1,8760);
e =zeros(1,8760);
winhr=zeros(1,8760);
xsol=zeros(1,8760);
smerhr=zeros(1,8760);
for m=1:10
    fw(m,1) = fw(1,1);
    tdg(m,1) = ((fw(m,1) + 1) * 288) - 273;
    wo(1) = (fi - fa(1)) * (c1(1) - (u*fw(m,1))) / (ce*
(c1(1) +u) * gama(1));
   if (u*fw(m,1) >= c1(1)), wo(1) =0; end
    if ( it(1) <= 0)
        e(1)=0;
    else
        qls = (tdg(m,1) - t11(1)) / it(1);
        if(qls >= 0.72)
            e(1) = 0;
        else
            e(1) = 0.72 - 6.4 * qls;
            if(e(1) <= 0 )
                e(1) = 0;
            elseif (e(1) > 0.72 )
                e(1) = 0.72;
            end
        end
    end
    s(1) = sbt1 * e(1) * it(1);
```

```
    qn(1) = s(1) - h(1) + wo(1);
    winhr(1)=wo(1)*gama(1)*uah(1)*288;
    xsol(1)=(s(1)/sbt1);
    qhpc(1)=ma(1)*cpa*(t2-t11(1));
    fw(m,2)=(qn(1)+((p1+rt)*fw(m,1)))/(1+p1+rt);
    tdg(m,2)=((fw(m,2)+1)*288)-273;
    wo(2) = (fi - fa(2)) * (c1(2) - (u*fw(m,1))) / (ce*
(c1(2) +u) * gama(2));
    if (u*fw(m,2)>=c1(2)),wo(2)=0;end
    if(it(2)<=0)
        e(2)=0;
    else qls = (tdg(m,1) - t11(2)) / it(2);
        if(qls >= 0.72)
            e(2) = 0;
        else
            e(2) = 0.72 - 6.4 * qls;
            if(e(2) <= 0 )
                e(2) = 0;
            elseif (e(2) > 0.72)
                e(2) = 0.72;
            end
        end
    end
    s(2) = sbt1 * e(2) * it(2);
    qn(2) = s(2) - h(2) + wo(2);
    winhr(2)=wo(2)*gama(2)*uah(2)*288;
    xsol(2)=(s(2)/sbt1);
     qhpc(2)=ma(2)*cpa*(t2-t11(2));
    for i=3:8760
        s1=0;
        for n=1:i-2;
            s1=s1+(fw(m,n+1)-fw(m,n))/(sqrt(pi*dt*(i-
n)));
        end
         wo(i) = (fi - fa(i)) * (c1(i) - (u*fw(m,i-1))) /
(ce* (c1(i) +u) * gama(i));
        if (u*fw(m,2)>=c1(2)),wo(2)=0;end
        if(it(i)<=0)
            e(i)=0;
        else
            qls(i) = (tdg(m,i-1) - t11(i)) / it(i);
            if(qls(i) > 0.72)
                e(i) = 0;
            else     e(i) = 0.72 - (6.4 * qls(i));
                if(e(i) <= 0 )
                    e(i) = 0;
                elseif (e(i) > 0.72)
                    e(i) = 0.72;
                end
            end
        end
```

```
        s(i) = sbt1 * e(i) * it(i);
        qn(i) = s(i) - h(i) + wo(i);
        fw(m,i)=(qn(i)+((p1+rt)*fw(m,i-1))-s1)/(1+p1+rt);
        tdg(m,i)=((fw(m,i)+1)*288)-273;
        qsy=qsy+s(i)*dt;
        qsol=qsol+(s(i)/sbt1);
        qhpc(i)=ma(i)*cpa*(t2-t11(i));
        xsol(i)=(s(i)/sbt1);
        wy=wy+wo(i)*dt;
winput=winput+(wo(1)*gama(1)*uah(1)*288)+(wo(2)*gama(2)*u
ah(2)*288)+(wo(i)*gama(i)*uah(i)*288);
        qht=qht+qhpc(i)+(ma(1)*cpa*(t2-
t11(1)))+(ma(2)*cpa*(t2-t11(2)));
        wf=wf+wfhru(i);
        winhr(i)=wo(i)*gama(i)*uah(i)*288;
        qly=qly+h(i)*dt;
        qy=qy+qn(i)*dt;
        qhh=qhh+hh(i);
        qhrut=qhrut+qrec(i);
  smerhr(i)=mevap/((xsol(i)/1000)+((winhr(i)/1000)*1.1));
        if (i~=ihr(k)), continue; end
        efc=efc/(ido(k)*24);
        tay(m,k)=tdg(m,i);
        k=k+1;
        if (i==8760),fw(1,1)=fw(m,8760); end
    end
    if (m~=1)
        qst=p*(fw(m,8760)-fw(m,1));
    else
        qst=p*(fw(m,8760)-0);
    end
        cop(m)=qly/wy;
        workinp=qhh/cop(m);
        qhpp(m)=qhh/(q23*8760);
        qrecu(m)=qhrut/(q23*8760);
        cop2(m)=qhh/(workinp+wf);
        wr=wf/workinp;
        qt=qsy+(wy*(1+wr));
        r11(m)=qsy*100/qt;
        r22(m)=wy*100/qt;
        r33(m)=(wy*wr)*100/qt;
        r44(m)=qst*100/qt;
        r55(m)=(qy-qst)*100/qt;
        r66(m)=(qly*100*(1-(es/100)))/qt;
        r77(m)=(qly*100*(es/100))/qt;
       smer(m)=(mevap*8760)/(((workinp/1000)+(wf/1000)));
    k=1;
end
```

Appendix B. 3 MATLAB program for Case 3

```
clc
clear
close all
r=3;
ac=45;
nod1=1;
ri=0.01;
tia=55;
ti=15;
tinf=15;
t2=tia;
tb=37.1;
td=-9;
hrad=[22.1 21.1 16.8 11.7 7.9 5.7 6.2 9.2 12.6 17.7 18.3
22.6];
tair=[27.1 26.9 22.2 15.3 9.4 4.5 2.6 3.8 7.2 12.7 18.2
23.7];
tc=(td+t2)/2;
fb=tb;
ta=tair;
ihm=hrad;
ref=[0.2 0.2 0.2 0.2 0.2 0.2 0.3 0.7 0.5 0.3 0.2 0.2];
sbt=[1 1 1 1 1 1 1 1 1 1 1 1];
imo=[31 31 30 31 30 31 31 28 31 30 31 30];

%%%% Black paint-1 glass %%%
ul=7.4;
taln=0.89;
b0=0.078;

%%%%%%limstone
ro = 2500;
cp = 0.9;
con = 1.3;
alfa = 5.75e-7;

nabd=[198 228 258 288 318 334 17 47 75 105 135 162];
ww=0;
fib=fb*pi/180;
btb=tb*pi/180;
```

```
for i=1:12
dlta(i)=23.45*sin(2*pi/365*(284+nabd(i)))*pi/180;
ws(i)=acos(-1*tan(fib)*tan(dlta(i)));
hq=(24*3600*1353/pi)*(1+0.033*cos(2*pi*nabd(i)/365))*((co
s(fib)*cos(dlta(i))*sin(ws(i)))+(ws(i)*sin(fib)*sin(dlta(
i))));
ho(i)=abs(hq)/10^6;
ktm(i)=ihm(i)/ho(i);
hdh(i)=0.775+(0.00653*(ws(i)*180/pi-
90))(0.505+0.00455*(ws(i)*180/pi-90))*cos((115*ktm(i)
103)*pi/180);
wsp1(i)=acos(-1*tan(fib)*tan(dlta(i)));
    wsp2(i)=acos(-1*tan(fib-btb)*tan(dlta(i)));
    if (wsp1(i)>=wsp2(i))
        wsp(i)=wsp2(i);
    else
        wsp(i)=wsp1(i);
    end
    ra=(cos(fib-
btb)*cos(dlta(i))*sin(wsp(i))+wsp(i)*sin(fib-
btb)*sin(dlta(i)))/(cos(fib)*cos(dlta(i))*sin(ws(i))+ws(i
)*sin(fib)*sin(dlta(i)));
    rba(i)=abs(ra);
    rr(i)=((1-
hdh(i))*rba(i))+(hdh(i)*((1+cos(btb))/2))+(ref(i)*((1-
cos(btb))/2));
    ht(i)=rr(i)*ihm(i);
    a1(i)=0.409+0.5016*sin(ws(i)-(pi/3));
    b1(i)=0.6609-0.4767*sin(ws(i)-(pi/3));
    rd(i)=pi/24*(cos(ww)-cos(ws(i)))/(sin(ws(i))-
ws(i)*cos(ws(i)));
    rt(i)=pi/24*(a1(i)+b1(i)*cos(ww))*(cos(ww)-
cos(ws(i)))/(sin(ws(i))-ws(i)*cos(ws(i)));
    hh(i)=1.188-2.272*ktm(i)+(9.473*ktm(i)^2)-
(21.865*ktm(i)^3)+(14.648*ktm(i)^4);
    if (ktm(i)>=0.8),hh(i)=0.2;end
    if (ktm(i)<=0.17),hh(i)=0.99;end

    rbb(i)=abs((cos(fib-btb)*cos(dlta(i))+sin(fib-
btb)*sin(dlta(i)))/(cos(fib)*cos(dlta(i))+sin(fib)*sin(dl
ta(i))));
    rn(i)=(1-
rd(i)*hh(i)/rt(i))*rbb(i)+(rd(i)/rt(i)*hh(i)*(1+cos(btb))
/2)+(ref(i)*(1-cos(btb)))/2;
    aa(i)=2.943-(9.271*ktm(i))+(4.031*(ktm(i)^2));
    bb(i)=-4.345+(8.853*ktm(i))-(3.602*(ktm(i)^2));
    cc(i)=-0.170-(0.306*ktm(i))+(2.936*(ktm(i)^2));
end

md=0.01;
w=0.088;
```

```
dlt=0.0005;
ds=0.01;
cpc=3300;
hc=300;
fib=fb*pi/180;
btb=tb*pi/180;
tr=89.8-(0.5788*tb)+(0.002693*(tb^2));
tetr=tr*pi/180;
talr=taln*(1+b0*(1-(1/cos(tetr))));
tetd=pi/3;
tald=taln*(1+b0*(1-(1/cos(tetd))));
for i=1:12
    tb1=acos(cos(fib-
btb)*cos(dlta(i))*cos(5*pi/24)+sin(fib-
btb)*sin(dlta(i)));
    talb(i)=taln*(1+b0*(1-1/cos(tb1)));
    tal1=(1-
hh(i))*rba(i)*talb(i)+hh(i)*tald*(1+cos(btb))/2+ref(i)*ta
lr*(1-cos(btb))/2;

    tal2=(1-hh(i))*rba(i)+hh(i)*(1+cos(btb))/2+ref(i)*(1-
cos(btb))/2;
    talf(i)=tal1/tal2;

end
mdc=md*ac;
qm=sqrt(ul/(pk*dlt));
fl=tanh(qm*(w-ds)/2)/(qm*(w-ds)/2);
fp=1/(ul*w*(1/(ul*(ds+(w-ds)*fl))+1/cb+1/(pi*ds*hc)));
fr=mdc*cpc/(ac*ul)*(1-exp(-1*ac*ul*fp/(mdc*cpc)));
cpa=1006;
t5=25;
t6=50;
mc5=25;
mc6=10;
W5=30;
W6=W5-((W5*(mc5-mc6))/(100-mc6));
mw5=W5*mc5/100;
mw6=W6*mc6/100;
mevap=mw5-mw6;
mp=W5-mevap;
mpw=mp/3600;
mcp=(W5-W6)/W6;
cpwt=1398.3+(4090.2*(mcp/(1+mcp)));
mw=mevap/3600;
hfg=2412;
qevap=mw*hfg*1000;
qdp=mpw*(cpwt)*(t6-t5);
qcond=qdp+qevap;
u=1.7;
fi2=tia/tinf-1;
```

```
fc=tc/tinf-1;
p=1000*4.187/(3*ro*cp);
y=alfa*31536000/r^2;
scons=nod1/(24*3600*4*pi*r*con*tinf);
for i=1:12
    ma(i)=qcond/(cpa*(tia-ta(i)));
    ua(i)=ma(i)*cpa;
    gama(i)=4*pi*r*con/(nod1*ua(i));
    hcons(i)=nod1*ua(i)/(4*pi*r*con*(tinf));
end

for i=1:12
    h(i)=sbt(i)*hcons(i)*(tia-ta(i));
    if(h(i)<=0),h(i)=0;end
    tag(i)=(-1/2)+(i/12);
    dtt(i)=alfa*3600*24*imo(i)/(r^2);
    tin(i)=ti;
    told(i)=ti;
end
for j=1:13
    rj(j)=(j-7)/12;
end

for m=1:1000

    for i=1:12
        fw(i)=tin(i)/tinf-1;
        fa=ta(i)/tinf-1;
        c1=(tinf*(fw(i)+1)+100)/70;
        th=tinf*(u*(fc+1)+fi2-fa);
        c2=tinf*((u*fc)+fi2-fa-(u*fw(i)));
        c3=((35*u)-(tinf*(u*(fc+1)+fi2-fa)))/(40*u);

        if(c2<=0),wo(i)=0;
        else
        wo(i)=sbt(i)*(fi2-fa)/(c1*log((th+273)/c2)+c3);
        end
        wo(i)=wo(i)/gama(i);
    end

    q0=0;
    for i=1:12
        itc(i)=ul*(tin(i)-ta(i))/talf(i);
        if (itc(i)<=0),itc(i)=0;end
        xcb(i)=itc(i)/(rt(i)*rn(i)*ho(i)*ktm(i))*0.0036;

fbar(i)=exp((aa(i)+bb(i)*rn(i)/rr(i))*(xcb(i)+cc(i)*xcb(i
)^2));
        qum(i)=ac*fr*talf(i)*ht(i)*fbar(i)*10^6;
        ef(i)=qum(i)*100/(ac*ht(i)*10^6);
        htt(i)=ht(i)*10^6/(24*3600);
```

```
        s(i)=scons*qum(i);
        qn(i)=s(i)-h(i)+wo(i);
        q0=q0+qn(i);
    end
    a0=q0/12;

    for i=1:12
        sumg=0;
        for n=1:40
            eta1=1+sqrt(n*pi/y);
            eta2=sqrt(n*pi/y)+p*2*pi*n/y;
            acns=1/(pi*n*(eta1^2+eta2^2));
            suma=0;
            sumb=0;
            for j=1:12
                eta3=sin(2*pi*n*rj(j+1))-
sin(2*pi*n*rj(j));
                eta4=cos(2*pi*n*rj(j+1))-
cos(2*pi*n*rj(j));
                suma=suma+qn(j)*(eta1*eta3+eta2*eta4);
                sumb=sumb+qn(j)*(eta2*eta3-eta1*eta4);
            end

sumg=sumg+acns*(suma*cos(2*pi*n*tag(i))+sumb*sin(2*pi*n*t
ag(i)));
        end
        tnew(i)=(fw(i)+1)*tinf;
    end
    flag = 0;
    for i=1:12
        frk(i)=abs(tnew(i)-told(i));
        if (frk(i)>0.01)
            for j=1:12
                tin(j)=tin(j)+ri*(tnew(j)-tin(j));
                told(j)=tnew(j);
            end
            disp([num2str(m) '    ' num2str(i)]);
            flag=1;
            break;
        end
    end
    if(flag==0)
        break;
    end
end

qy=0;
wy=0;
qsy=0;
qly=0;
tmn=0;
```

```
for i=1:12
    tmn=tmn+tnew(i);
    qy=qy+qn(i)*dtt(i);
    qsy=qsy+s(i)*dtt(i);
    qly=qly+h(i)*dtt(i);
    wy=wy+wo(i)*dtt(i);
end

cop=qly/wy;
workin=(qcond*8760)/cop;
wr=wf/workin;
cops=qly/(wy+wr);
SMER=(mevap*8760)/((workin*1.03)/1000);
qlt=qy;
f=(qsy-qlt)*100/qly;
tmn=tmn/12;
rtot=qsy+(wy*(1+wr));
r11=(qsy/rtot)*100;
r22=(wy/rtot)*100;
r33=(qlt/rtot)*100;
r44=(qly/rtot)*100;
r55=((wy*wr)/rtot)*100;
```

Appendix B. 4 MATLAB program for Case 4

```
clc
clear
close all
r=3;
ac=50;
noh=1;
ri=0.01;
tia=55;
ti=15;
tinf=15;
t2=tia;
tb=37.1;
td=-9;
hrad=[25.3 21.6 17.8 12.2 7.6 6.1 5.4 8.8 13.7 18.1 20.1
25.1];
to=[26.6 28.9 23.6 14.3 11.6 4.5 4.4 0.4 5.9 13.9 20.0
24.4];
t1=[30.5 31.7 29.1 25.0 23.9 21.2 21.2 19.8 21.8 24.8
27.5 29.5];
t3=[32.2 32.9 31.5 29.6 29.2 28.4 28.4 28.1 28.6 29.5
30.6 31.6];
ihm=hrad;
ref=[0.2 0.2 0.2 0.2 0.2 0.2 0.3 0.7 0.5 0.3 0.2 0.2];
sbt=[1 1 1 1 1 1 1 1 1 1 1 1];
imo=[31 31 30 31 30 31 31 28 31 30 31 30];
ul=7.4;
taln=0.89;
b0=0.078;
ro = 2500;
cp = 0.9;
con = 1.3;
alfa = 5.75e-7;
nav=[198 228 258 288 318 334 17 47 75 105 135 162];
ww=0;
fib=fb*pi/180;
btb=tb*pi/180;
for i=1:12
alfa = 5.75e-7;
nav=[198 228 258 288 318 334 17 47 75 105 135 162];
ww=0;
fib=fb*pi/180;
btb=tb*pi/180;
```

```
for i=1:12
    dlta(i)=23.45*sin(2*pi/365*(284+nav(i)))*pi/180;
    ws(i)=acos(-1*tan(fib)*tan(dlta(i)));

hq=(24*3600*1353/pi)*(1+0.033*cos(2*pi*nav(i)/365))*((cos
(fib)*cos(dlta(i))*sin(ws(i)))+(ws(i)*sin(fib)*sin(dlta(i
)));
    ho(i)=abs(hq)/10^6;
    ktm(i)=ihm(i)/ho(i);

    hdh(i)=0.775+(0.00653*(ws(i)*180/pi-90))-
(0.505+0.00455*(ws(i)*180/pi-90))*cos((115*ktm(i)-
103)*pi/180);
    wsp1(i)=acos(-1*tan(fib)*tan(dlta(i)));
    wsp2(i)=acos(-1*tan(fib-btb)*tan(dlta(i)));
    if (wsp1(i)>=wsp2(i))
        wsp(i)=wsp2(i);
    else
        wsp(i)=wsp1(i);
    end

    ra=(cos(fib-
btb)*cos(dlta(i))*sin(wsp(i))+wsp(i)*sin(fib-
btb)*sin(dlta(i)))...

/(cos(fib)*cos(dlta(i))*sin(ws(i))+ws(i)*sin(fib)*sin(dlt
a(i)));
    rba(i)=abs(ra);
    rr(i)=((1-
hdh(i))*rba(i))+(hdh(i)*((1+cos(btb))/2))+(ref(i)*((1-
cos(btb))/2));
    ht(i)=rr(i)*ihm(i);
    a1(i)=0.409+0.5016*sin(ws(i)-(pi/3));
    b1(i)=0.6609-0.4767*sin(ws(i)-(pi/3));
    rd(i)=pi/24*(cos(ww)-cos(ws(i)))/(sin(ws(i))-
ws(i)*cos(ws(i)));
    rt(i)=pi/24*(a1(i)+b1(i)*cos(ww))*(cos(ww)-
cos(ws(i)))/(sin(ws(i))-ws(i)*cos(ws(i)));
        hh(i)=1.188-2.272*ktm(i)+(9.473*ktm(i)^2)-
(21.865*ktm(i)^3)+(14.648*ktm(i)^4);
    if (ktm(i)>=0.8),hh(i)=0.2;end
    if (ktm(i)<=0.17),hh(i)=0.99;end

    rbb(i)=abs((cos(fib-btb)*cos(dlta(i))+sin(fib-
btb)*sin(dlta(i)))/(cos(fib)*cos(dlta(i))+sin(fib)*sin(dl
ta(i))));
    rn(i)=(1-
rd(i)*hh(i)/rt(i))*rbb(i)+(rd(i)/rt(i)*hh(i)*(1+cos(btb))
/2)+(ref(i)*(1-cos(btb)))/2;
    aa(i)=2.943-(9.271*ktm(i))+(4.031*(ktm(i)^2));
    bb(i)=-4.345+(8.853*ktm(i))-(3.602*(ktm(i)^2));
```

```
    cc(i)=-0.170-(0.306*ktm(i))+(2.936*(ktm(i)^2));
end

md=0.01;
pk=45;
w=0.088;
dlt=0.0005;
ds=0.01;
cb=300;
cpc=3300;
hc=300;
fib=fb*pi/180;
btb=tb*pi/180;
tr=89.8-(0.5788*tb)+(0.002693*(tb^2));
tetr=tr*pi/180;
talr=taln*(1+b0*(1-(1/cos(tetr))));
tetd=pi/3;
tald=taln*(1+b0*(1-(1/cos(tetd))));
for i=1:12
    tb1=acos(cos(fib-
btb)*cos(dlta(i))*cos(5*pi/24)+sin(fib-
btb)*sin(dlta(i)));
    ttld(i)=taln*(1+b0*(1-1/cos(tb1)));
    taall=(1-
hh(i))*rba(i)*ttld(i)+hh(i)*tald*(1+cos(btb))/2+ref(i)*ta
lr*(1-cos(btb))/2;
    ttbb=(1-hh(i))*rba(i)+hh(i)*(1+cos(btb))/2+ref(i)*(1-
cos(btb))/2;
    twdf(i)=taall/ttbb;
end
mmdc=md*ac;
qm=sqrt(ul/(pk*dlt));
fl=tanh(qm*(w-ds)/2)/(qm*(w-ds)/2);
fp=1/(ul*w*(1/(ul*(ds+(w-ds)*fl))+1/cb+1/(pi*ds*hc)));
fr=mdc*cpc/(ac*ul)*(1-exp(-1*ac*ul*fp/(mdc*cpc)));

cpa=1006;
t5=25;
t6=50;
mc5=22.5 ;
mc6=12.5;
W5=50;
W6=W5-((W5*(mc5-mc6))/(100-mc6));
mw5=W5*mc5/100;
mw6=W6*mc6/100;
mevap=mw5-mw6;
mp=W5-mevap;
mpw=mp/3600;
mcp=(W5-W6)/W6;
cpwt=1398.3+(4090.2*(mcp/(1+mcp)));
mw=mevap/3600;
```

```
hfg=2412;
qevap=mw*hfg*1000;
qdp=mpw*(cpwt)*(t6-t5);
qcond=qdp+qevap;
u=1.7;
fi2=tia/tinf-1;
fc=tc/tinf-1;
p=1000*4.187/(3*ro*cp);
y=alfa*31536000/r^2;
scons=noh/(24*3600*4*pi*r*con*tinf);
qrecov=0;
for i=1:12

    if (t1(i)>=t3(i))
       t11(i)=to(i);
       qrec(i)=0;
       qh(i)=qcond;
       ma(i)=qcond/(cpa*(t2-to(i)));
    else
       t11(i)=t1(i);
       ma(i)=qcond/((0.7*cpa*(t3(i)-to(i)))+(cpa*(t2-
t11(i))));
       qrec(i)=0.7*ma(i)*cpa*(t3(i)-to(i));
       qh(i)=qcond- qrec(i);
    end

    ua(i)=ma(i)*cpa;
    gama(i)=4*pi*r*con/(noh*ua(i));
    hcons(i)=noh*ua(i)/(4*pi*r*con*(tinf));
    qrec(i)=0.7*ma(i)*cpa*(t3(i)-to(i));
    qrecov=qrecov+qrec(i);
end

es=(qrecov/(qcond*12))*100;

for i=1:12
    h(i)=sbt(i)*hcons(i)*(t2-t11(i));
    if(h(i)<=0),h(i)=0;end
    tag(i)=(-1/2)+(i/12);
    dtt(i)=alfa*3600*24*imo(i)/(r^2);
    tin(i)=ti;
    told(i)=ti;
end
for j=1:13
    rj(j)=(j-7)/12;
end

for m=1:1000

    for i=1:12
        fw(i)=tin(i)/tinf-1;
```

```
        fa=ta(i)/tinf-1;
        c1=(tinf*(fw(i)+1)+100)/70;
        th=tinf*(u*(fc+1)+fi2-fa);
        c2=tinf*((u*fc)+fi2-fa-(u*fw(i)));
        c3=((35*u)-(tinf*(u*(fc+1)+fi2-fa)))/(40*u);

        if(c2<=0),wo(i)=0;
        else
        wo(i)=sbt(i)*(fi2-fa)/(c1*log((th+273)/c2)+c3);
        end

        wo(i)=wo(i)/gama(i);
    end

    q0=0;
    for i=1:12
        ccaa(i)=ul*(tin(i)-ta(i))/twdf(i);
        if (ccaa(i)<=0),ccaa(i)=0;end
        xcb(i)=ccaa(i)/(rt(i)*rn(i)*ho(i)*ktm(i))*0.0036;

fbar(i)=exp((aa(i)+bb(i)*rn(i)/rr(i))*(xcb(i)+cc(i)*xcb(i
)^2));
        qac(i)=ac*fr*twdf(i)*ht(i)*fbar(i)*10^6;
        ef(i)=qac(i)*100/(ac*ht(i)*10^6);
        htt(i)=ht(i)*10^6/(24*3600);
        s(i)=scons*qac(i);
        qn(i)=s(i)-h(i)+wo(i);
        q0=q0+qn(i);
    end
    a0=q0/12;


    for i=1:12
        sumg=0;
        for n=1:40
            ee11=1+sqrt(n*pi/y);
            ee22=sqrt(n*pi/y)+p*2*pi*n/y;
            acns=1/(pi*n*(ee11^2+ee22^2));
            suma=0;
            sumb=0;
            for j=1:12
                eta3=sin(2*pi*n*rj(j+1))-
sin(2*pi*n*rj(j));
                eta4=cos(2*pi*n*rj(j+1))-
cos(2*pi*n*rj(j));
                suma=suma+qn(j)*(ee11*eta3+ee22*eta4);
                sumb=sumb+qn(j)*(ee22*eta3-ee11*eta4);
            end

sumg=sumg+acns*(suma*cos(2*pi*n*tag(i))+sumb*sin(2*pi*n*t
ag(i)));
```

```
        end
        fw(i)=a0+sumg;
        tnew(i)=(fw(i)+1)*tinf;
    end
    flag = 0;
    for i=1:12
        frk(i)=abs(tnew(i)-told(i));
        if (frk(i)>0.01)
            for j=1:12
                tin(j)=tin(j)+ri*(tnew(j)-tin(j));
                told(j)=tnew(j);
            end
            disp([num2str(m) '    ' num2str(i)]);
            flag=1;
            break;
        end
    end
    if(flag==0)
        break;
    end
end
qy=0;
wy=0;
qsy=0;
qly=0;
tmn=0;
for i=1:12
    tmn=tmn+tnew(i);
    qy=qy+qn(i)*dtt(i);
    qsy=qsy+s(i)*dtt(i);
    qly=qly+h(i)*dtt(i);
    wy=wy+wo(i)*dtt(i);
end

cop=qly/wy;
workin=(qcond*8760)/cop;
wf=0.05*workin;
wr=wf/workin;
SMER=(mevap*8760)/((workin*1.05)/1000);
qlt=qy;
f=(qsy-qlt)*100/qly;
tmn=tmn/12;
rtot=qsy+(wy*(1+wr));
r1=qsy/rtot;
r2=wy/rtot;
r3=qlt/rtot;
r4=qly/rtot;
r5=(wy*wr)/rtot;
r6=(qly*(1-(es/100)))/rtot;
r7=(qly*100*(es/100))/rtot;
```

CURRICULUM VITAE

PERSONAL DETAILS

Name Surname: Hatem Hasan ISMAEEL

Birth Date: 01.01.1976

Marital Status: Married

Mobile: +90 5375400186

E-mail: bardarashi77@gmail.com

EDUCATION

2015 Febraury-2019 November: Gaziantep University, Gaziantep / Turkey, Faculty of Engineering/ Mechanical Department/ Ph.D. in Energy program.

2010 – 2012: Gaziantep University, Gaziantep / Turkey, Faculty of Engineering / Mechanical Department / Master of Science in Thermodynamics program.

1998-2003: University of Mosul, Mosul/ Iraq, College of Engineering/ Mechanical Department/ General branch.

LANGUAGE SKILLS

Kurdish: Mother Tongue

Arabic: Excellent

English: Very Good

Turkish: Intermediate

PAPARES

ISMAEEL, H.H., Yumrutas, R. (2019). Thermal performance of a solar-assisted heat pump drying system with thermal energy storage tank and heat recovery unit. International journal of energy research. In production, DOI: 10.1002/er.4966.

ISMAEEL, H.H., Yumrutas, R. (2019). Investigation of a solar-assisted heat pump wheat drying system with underground thermal energy storage tank. Solar energy, under revising.

ATTENDED CONFERENCES

Yumrutas. R., ISMAEEL, H.H. (2018). Mathematical modeling and performance analysis of solar assisted heat pump wheat drying system with energy storage tank. ICOEST, 19-23 September 2018 Kiev, Ukraine.

ISMAEEL, H.H., Yumrutas, R. (2019). Energy analysis of a solar-assisted heat pump drying system with energy storage tank. UEMK 2019, 24-25 October 2019 Gaziantep University, Gaziantep, TURKEY.